THE JOURNAL OF

PHYSICAL CHEMISTRY

Volume 74, Number 13 June 25, 1970

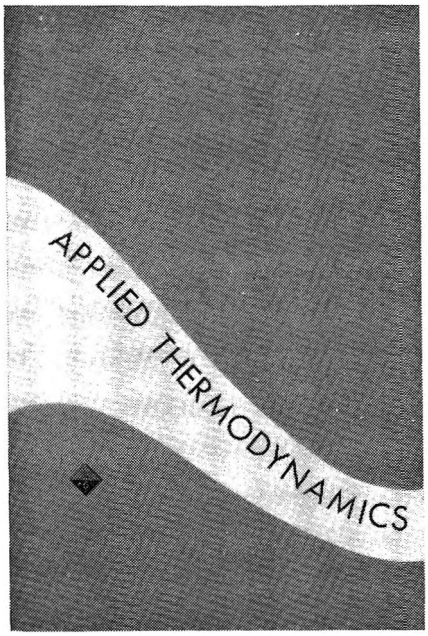

APPLIED THERMODYNAMICS

Based on the Symposium on Applied Thermodynamics sponsored by INDUSTRIAL & ENGINEERING CHEMISTRY and the Division of Industrial and Engineering Chemistry of the American Chemical Society

Here is the table of contents:

- Molecular Theories of Liquids and Mixtures
- Molecular Thermodynamics of Chemical Reactions
- Irreversible Thermodynamics in Engineering
- Applications of Statistical Mechanics: Equilibrium Configurational Properties of Fluids and Fluid Mixtures
- Equations of State
- Corresponding States Principle: A Review of Current Theory and Practice
- Correlating and Predicting Thermodynamic Data—Reference Substance Equations and Plots
- Enthalpies of Fluids at Elevated Pressures and Low Temperatures
- PVT Measurements on Petroleum Reservoir Fluids and Their Uses
- Thermodynamic Excess Properties of Binary Liquid Measures—The Role of Empiricism
- Group Contributions in Mixtures
- Calculation of High-Pressure Vapor-Liquid Equilibria
- The Adsorption of Gas Mixtures—A Thermodynamic Approach
- Physico-Chemical Measurements by Gas Chromatography
- Thermodynamic Aspects of Capilarity
- The Thermodynamic Properties of Cryogenic Fluids: Survey of Data
- Calculation of Complex Chemical Equilibria
- A General Purpose Physical Data System for Computer Process Calculations

350 pages with index **Clothbound** **$11.00**

Order from:

SPECIAL ISSUES SALES
AMERICAN CHEMICAL SOCIETY
1155 SIXTEENTH STREET N.W.
WASHINGTON, D.C. 20036

NOTES

COMMUNICATIONS TO THE EDITOR

AUTHOR INDEX

THE JOURNAL OF
PHYSICAL CHEMISTRY

VOLUME 74, NUMBER 13 JUNE 25, 1970

Analysis of Ion–Molecule Reactions in Allene and Propyne by Ion Cyclotron Resonance[1]

by Michael T. Bowers,

Department of Chemistry, University of California, Santa Barbara, Santa Barbara, California 93106

Daniel D. Elleman,

Jet Propulsion Laboratory, California Institute of Technology, Pasadena, California 91103

Rebecca M. O'Malley, and Keith R. Jennings,

Department of Chemistry, The University, Sheffield, S3 7 HF, England *(Received November 3, 1969)*

Thermal energy product distributions and their energy dependencies for the $C_3H_4^+$ ions in allene and propyne are determined using ion cyclotron resonance (ICR). Reaction sequences for the $C_3H_3^+$, $C_3H_2^+$, and C_3H^+ primary ions are also determined from double resonance results. These data are compared with the medium pressure mass spectral data of Myher and Harrison taken at 3.4-eV ion exit energy. Significant differences between the ICR and medium pressure product distributions are observed. Double resonance results indicate the discrepancies arise mainly from the difference in energy of the reactant ions in the two techniques. In addition, at thermal energies, secondary $C_3H_5^+$ ions undergo the condensation reaction

$$C_3H_5^+ + C_3H_4 \longrightarrow C_6H_7^+ + H_2$$

and *do not* undergo the hydride ion abstraction reaction

$$C_3H_5^+ + C_3H_4 \longrightarrow C_3H_3^+ + C_3H_6$$

This latter reaction was observed by Myher and Harrison in their higher energy experiments. Isotopic mixing experiments indicate that a *four-centered* intermediate is important in many of the condensation reactions of allene and propyne.

Introduction

Investigations have recently been carried out of the kinetics and mechanisms of ion–molecule reactions which occur in a number of unsaturated systems. The initial studies were on ethylene,[2] and the technique used was ion cyclotron resonance.[2-4] Although considerable information was obtained on the reaction scheme, relative rates of formation, lifetimes of intermediate complexes and on the dependence of the disintegration of the complex on internal energy, the main emphasis of the initial study was an exposition of the experimental techniques necessary for a detailed investigation of ion–molecule reactions in unsaturated molecules. Parallel investigations have been made of the acetylene[5] and vinyl fluoride[4] systems, and in each case, there is considerable agreement with results obtained by medium

(1) This research was supported in part by Contract No. NAS 7-100 extended to the Jet Propulsion Laboratory by the National Aeronautics and Space Administration, and in part by the Science Research Council (Great Britain).

(2) M. T. Bowers, D. D. Elleman, and J. L. Beauchamp. *J. Phys. Chem.*, **72**, 3599 (1968).

(3) (a) J. D. Baldeschwieler, *Science*, **159**, 263 (1968); (b) J. L. Beauchamp, L. R. Anders, and J. D. Baldeschwieler, *J. Amer. Chem. Soc.*, **89**, 4569 (1967).

(4) R. M. O'Malley and K. R. Jennings, *J. Mass Spectrom. Ion Phys.*, **2**, 441 (1969).

(5) R. M. O'Malley and K. R. Jennings, *ibid.*, **2**, 257 (1969).

Table I: Double Resonance Results for the Principal Reactions in Propyne-d_4 and Allene-d_4

	Reaction[a]	Propyne-d_4 Per cent change[b]	Propyne-d_4 ΔH, kcal/mol[c]	Allene-d_4 Per cent change[b]	Allene-d_4 ΔH, kcal/mol[c]
(1)	$C_3D_4^+ \cdot \rightarrow C_3D_5^+ + C_3D_3\cdot$	+43	−37	+28	−38
(2)	$C_3D^+ \rightarrow C_4D_3^+ + C_2D_2$	−12	−29	−13	−31
(3)	$C_3D_2^+ \cdot \rightarrow C_4D_4^+ \cdot + C_2D_2$	−21	−60	−16	−62
(4)	$C_3D_3^+ \rightarrow C_4D_4^+ \cdot + C_2D_3\cdot$	+2	+47	+1	+45
(5)	$C_3D_4^+ \cdot \rightarrow C_4D_4^+ \cdot + C_2D_4$	+37	−19	−3	−20
(6)	$C_3D_3^+ \rightarrow C_4D_5^+ + C_2D_2$	−7	−7	−8	−9
(7)	$C_3D_4^+ \rightarrow C_4D_5^+ + C_2D_3\cdot$	+7	−38	+5	−39
(8)	$C_3D_5^+ \rightarrow C_4D_5^+ + C_2D_4$	−7	−11	−4	−13
(9)	$C_3D_2^+ \cdot \rightarrow C_5D_3^+ + CD_3\cdot$	+8	−6	+8	−8
(10)	$C_3D_3^+ \rightarrow C_5D_3^+ + CD_4$	+3	+50	+3	+48
(11)	$C_3D_3^+ \rightarrow C_5D_5^+ + CD_2\cdot$	+43	+48	+2	+46
(12)	$C_3D_4^+ \cdot \rightarrow C_5D_5^+ + CD_3\cdot$	−1	−38	−5	−40
(13)	$C_3D_3^+ \rightarrow C_6D_5^+ + D_2$	−14	−14	−14	−16
(14)	$C_3D_4^+ \cdot \rightarrow C_6D_5^+ + D_2 + D\cdot$	+10	+10	+1	+8
(15)	$C_3D_4^+ \cdot \rightarrow C_6D_7^+ + D\cdot$	−25	−29	−30	−30
(16)	$C_3D_5^+ \rightarrow C_6D_7^+ + D_2$	−6	−16	−1	−18
(17)	$C_4D_4^+ \cdot \rightarrow C_7D_7^+ + D\cdot$	−11	−77	−7	−79
(18)	$C_6D_5^+ \rightarrow C_9D_7^+ + D_2$	−30	−60	~0	−62
(19)	$C_3D_4^+ \cdot \rightarrow C_3D_3^+ + C_3D_5\cdot$	+2	−43	+2	−44
(20)	$C_3D_5^+ \rightarrow C_3D_3^+ + C_3D_6$	0	+1	0	−1

[a] In each case the neutral reactant is C_3D_4. [b] The numbers in this column give the percentage change in the product ion intensity for a 0.03 V/cm rf field applied to the reactant ion in the source region. The single resonance intensities are given in Table II. [c] Heats of formation were taken from J. L. Franklin, J. G. Dillard, H. M. Rosenstock, J. T. Herron, K. Draxl, and F. H. Field, "Ionization Potentials, Appearance Potentials, and Heats of Formation of Gaseous Positive Ions," NSRDS-NBS 26, U. S. Department of Commerce, 1969. In all cases the most stable ionic form was used.

pressure mass spectrometry[6] and tandem mass spectrometry.[7] However, the published data do not, in general, lend themselves to detailed mechanistic interpretations, partly because of the high degree of symmetry in the acetylene and ethylene systems and partly because of the role played by charge-transfer reactions in the vinyl halide systems.[6,8,9]

Using a medium pressure mass spectrometer, Myher and Harrison[10] have investigated the ion–molecule reactions in the slightly more complex allene and propyne systems. They characterized most of the reactions in both systems and through use of selective isotopic substitution obtained some information regarding mechanistic details. Their most significant finding is the proton transfer reaction from the parent $C_3H_4^+$ ion to neutral propyne proceeds *via* a direct mechanism while the condensation reactions (*i.e.*, carbon transfer reactions) go through some kind of complex intermediate.

In this work, the allene and propyne systems have been studied by ion cyclotron resonance mass spectrometry in an effort to define more clearly the role of the multiple carbon–carbon bond in ionic condensation reactions in unsaturated systems. In addition to mechanistic information, relative reaction rate constants for thermal energy ions are obtained and are compared with those obtained by Myher and Harrison for higher energy ions. Double resonance studies are used to confirm the general reaction scheme and to assign correctly the important thermal energy ion condensation reactions.

In order to elucidate further the importance of the unsaturated carbon–carbon bond in ion–molecule condensation reactions in these systems, mixtures of allene and propyne with ethylene and propene are investigated. As in the pure allene and propyne systems, extensive isotopic labeling is used in an effort to trace the history of the hydrogen atoms in the product ions. In addition, intermediate complexes of the same ionic formula are formed from a variety of ionic and neutral reactants to study the effects of internal energy and ionic structure on the product distribution.

Experimental Section

The experiments in this paper were performed on two spectrometers, one at the Jet Propulsion Laboratory and the second in the Department of Chemistry, The University, Sheffield, England. Both instruments are of the same general design. The latter is a commercial unit of Varian Instruments (No. 5900) and has been described previously.[4] The instrumental details

(6) J. A. Herman and A. G. Harrison, *Can. J. Chem.*, **47**, 957 (1969).
(7) J. H. Futrell and T. O. Tiernan, *J. Phys. Chem.*, **72**, 158 (1968).
(8) J. A. Herman, J. J. Myher, and A. G. Harrison, *Can. J. Chem.*, **47**, 647 (1969).
(9) B. M. Hughes, T. O. Tiernan, and J. H. Futrell, *J. Phys. Chem.*, **73**, 829 (1969).
(10) J. J. Myher and A. G. Harrison, *ibid.*, **72**, 1905 (1968).

of the spectrometer at JPL has been thoroughly discussed elsewhere.[11-13] In all experiments the electron beam currents were regulated between 1×10^{-9} and 2×10^{-8} A with resulting ion currents less than 1×10^{-12} A. The double resonance results in Table I were taken on the JPL instrument at 186-KHz observing frequency, 47-eV ionizing electron energy, 0.35-V/cm source drift field, 0.16-V/cm resonance drift field, and 0.03-V/cm irradiating field. The distance from the electron beam to the end of the source region is 2.54 cm. The resonance region is 5.1 cm long. The cell cross section is 2.54 cm (trapping) × 2.1 cm (drift). For comparison purposes, the single resonance data in Table II were taken under the same conditions as the double resonance data in Table I. The relative rate data (Table III) and isotopic distribution data (Table IV and Table VI) were taken at conversions of less than 25% in all cases. Due to the field sweep nature of the spectra, the heights of the peaks of the secondary ions were normalized by dividing by their respective masses. The relative rates reported here thus reflect this normalization.

Table II: Normalized Uncorrected Single Resonance Intensities for Propyne-d_4 and Allene-d_4 at Same Conditions As Double Resonance Data of Table I[a]

Ion	m/e	Propyne-d_4	Allene-d_4
C_3D^-	38	0.009	0.012
$C_3D_2^+$	40	0.018	0.024
$C_3D_3^+$	42	0.213	0.185
$C_3D_4^+$	44	0.089	0.161
$C_3D_5^+$	46	0.063	0.024
$C_4D_3^+$	54	0.029	0.033
$C_4D_4^+$	56	0.022	0.039
$C_4D_5^+$	58	0.038	0.030
$C_5D_3^+$	66	0.012	0.007
$C_5D_5^+$	70	0.029	0.026
$C_6D_5^+$	82	0.057	0.047
$C_6D_7^+$	86	0.327	0.331
$C_7D_7^+$	98	0.055	0.051
$C_9D_7^+$	122	0.027	0.019

[a] The propyne-d_4 data were taken at 7×10^{-6} Torr and the allene-d_4 data at 8×10^{-6} Torr.

Table III: Relative Rates of Reaction for $C_3H_4^+$ Ions in Propyne and Allene

	Propyne		Allene	
Secondary ion	ICR	Medium pressure mass spec[a]	ICR	Medium pressure mass spec[a]
$C_3H_3^+$	...	0.03	...	0.01
$C_3H_5^+$	0.17	0.34	0.04	0.06
$C_4H_4^+$	0.04	0.06	0.06	0.10
$C_4H_6^+\cdot$	0.04	0.04	...	0.01
$C_5H_5^+$	0.04	0.06	0.03	0.02
$C_6H_5^+$	0.06	0.02	0.04	0.02
$C_6H_6^+\cdot$	0.01	...	0.01	...
$C_6H_7^+$	0.66	0.45	0.81	0.76

[a] Reference 10. Data for 1.7-eV ion exit energy.

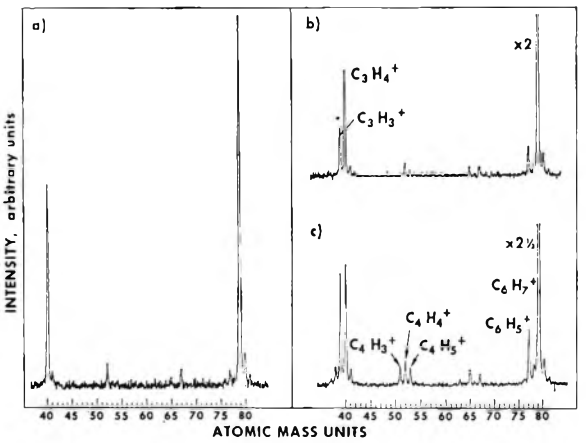

Figure 1. Single resonance spectra of allene at 2×10^{-5} Torr: (a) 11 eV; (b) 15.5 eV; (c) 32 eV.

The gases used were of research quality and were obtained from Matheson, Phillips Petroleum, and Merck Sharpe and Dohme. All gases were used as received. Purities were checked by low-pressure ICR measurements, and no measurable impurities were observed.

Results and Discussion

A. Allene and Propyne. The ion chemistry of both allene and propyne have been previously discussed by Myher and Harrison[10] and is quite rich, as indicated by the spectra in Figure 1. Most of the reactions can be sorted out by merely varying the electron energy, although at higher energies the number of reactant ions becomes large and this procedure becomes less enlightening. Conclusive evidence for a reaction can be obtained using the ion cyclotron double resonance technique, however.[2,3b,14] Alternatively, the ratio-plot technique of Myher and Harrison[10] may be used with generally reliable results although the evidence for reaction is somewhat less direct than in the double resonance experiment. The results of our double resonance studies are given in Table I and essentially agree with the reactions proposed by Myher and Harrison.[10] There are several differences, but these are primarily in reactions of minor ions where identification is difficult. For instance, we observe a small amount of $C_6H_6^+\cdot$ product at thermal energies while Myher and Harrison do not mention the ion at all. There is one somewhat important difference, however, that serves to distinguish ICR from the medium pressure technique in which ions have

(11) M. T. Bowers, D. D. Elleman, and J. King, *J. Chem. Phys.*, **50**, 1840 (1969).

(12) M. T. Bowers, D. D. Elleman, and J. King, Jr., *ibid.*, **50**, 4787 (1969).

(13) M. T. Bowers and D. D. Elleman, *ibid.*, **51**, 4606 (1969).

(14) J. L. Beauchamp and S. E. Buttrill, Jr., *ibid.*, **48**, 1783 (1968).

Table IV: Isotopic Distribution in C_3H_4–C_3D_4 Mixtures

Reaction		Propyne		Allene		
		ICR	Ref 10	ICR	Ref 10	Random
$C_3D_4^{+\cdot} + C_3H_4$	$\rightarrow C_6H_4D^+ + CD_3\cdot$	0.77	0.98	0.47	0.43	0.167
	$\rightarrow C_5H_3D_2^+ + CD_2H\cdot$	0.90	1.00	1.00	1.21	1.00
$C_3H_4^+ + C_3D_4$	$\rightarrow C_5H_2D_3^+ + CDH_2\cdot$	1.00	0.70	1.00	1.00	1.00
	$\rightarrow C_5HD_4^+ + CH_3\cdot$	0.93	1.07	0.37	0.34	0.167
$C_3D_4^{+\cdot} + C_3H_4$	$\rightarrow C_4H_4^{+\cdot} + C_2D_4$	NO[a]	...	NO[a]	...	0.03
	$\rightarrow C_4H_3D^{+\cdot} + C_2D_3H$	1.12	...	0.18	...	0.44
$C_3H_4^{+\cdot} + C_3D_4$	$\rightarrow C_4H_2D_2^{+\cdot} + C_2D_2H_2$	1.00	...	1.00	...	1.00
	$\rightarrow C_4HD_3^{+\cdot} + C_2DH_3$	1.20	...	0.15	...	0.44
	$\rightarrow C_4D_4^{+\cdot} + C_2H_4$	NO[a]	...	NO[a]	...	0.03

[a] Not observable due to interference from $C_4H_4^{+\cdot}$ and $C_4D_4^{+\cdot}$ ions formed from $C_3H_4^{+\cdot}$ with C_3H_4 and $C_3D_4^{+\cdot}$ with C_3D_4.

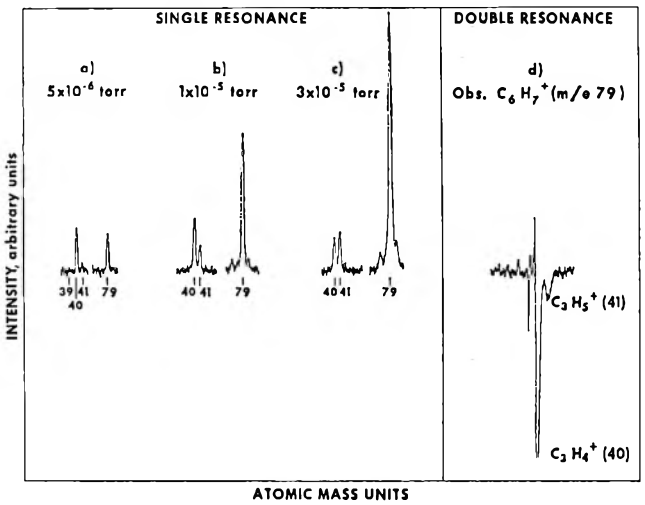

Figure 2. Single resonance spectra in propyne at 11 eV showing parent ion and major product ions. (a) 5×10^{-6} Torr; (b) 1.5×10^{-5} Torr; (c) 3×10^{-5} Torr. Note the absence of any signal at m/e of 39. In (d), the double resonance of the $C_6H_7^+$ ion (m/e 79) at 1×10^{-5} Torr and 30 eV shows major contributions from both $C_3H_4^+$ (m/e 40) and $C_3H_5^+$ (m/e 41). The sharp signals in the region of the mass 39 ion are due to the interaction of the first harmonic of the irradiating oscillator with the observing oscillator.

translational energies in excess of thermal. Myher and Harrison state that the dominant reaction of secondary $C_3H_5^+$ ions is the hydride ion abstraction

$$C_3H_5^+ + C_3H_4 \longrightarrow C_3H_3^+ + C_3H_6 \qquad (R1)$$

with a $\Delta H \cong 0$. We find that at thermal energies this reaction does not proceed to a measurable extent but rather that the condensation reaction is the only important reaction of $C_3H_5^+$. Support for the predominance of (R2) at thermal energies is given in Figure 2. The negative double resonance result, $C_6H_7^+ - [C_3H_5^+]$, conclusively confirms R2. The absence of a $C_3H_3^+$ (m/e 39) peak at 80% conversion of $C_3H_4^{+\cdot}$ strongly implies that (R1) does not proceed to a measurable extent at thermal energies. Myher and Harrison's data (3.4-eV ion exit energy) indicate $C_3H_3^+$ accounts for approximately 10% of the ionization at 80% $C_3H_4^{+\cdot}$ conversion. (R2) is also predominant at thermal energies when $C_3H_5^+$ is generated from ethylene. Again no evidence for (R1) is found. The existence of (R2) may explain the third-order contribution to the $C_6H_7^+$ ion obvious in the propyne pressure plots of Myher and Harrison.[10] Most of their medium pressure data were reported at ion exit energies of 3.4 eV. Hence, (R1) is probably slightly endothermic and needs translationally hot $C_3H_5^+$ ions to proceed.[15] Reaction R1 was, in fact, observed to give a small positive double resonance signal at 0.15-V/cm irradiation field. The maximum $C_3H_5^+$ energy corresponding to this field is[2,12] about 5 eV. Since $C_3H_5^+$ is a secondary ion and the irradiation performed in the source region of the spectrometer, it is likely the actual average energy of the $C_3H_5^+$ ion is much less than 5 eV, however. Interestingly the analogous hydride ion abstraction reaction to form $C_3H_3^+$ from parent $C_3H_4^{+\cdot}$ ions is also not observed at thermal translational energy even though this latter reaction is exothermic by as much as 44 kcal/mol. A significant positive double resonance signal for this reaction is observed, however (reaction 19, Table I). It is very possible these hydride ion abstraction reactions proceed *via* a direct mechanism rather than through a long-lived complex. If such is the case, it is probable that $C_3H_3^+$ is originally formed in the linear form I rather than the triangular form II. CNDO and extended

$^+CH_2—C\equiv CH$ (I)

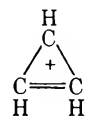

II

(15) Using heats of formation from J. L. Franklin, J. G. Dillard, H. M. Rosenstock, J. T. Herron, K. Draxl, and F. H. Field, "Ionization Potentials, Appearance Potentials, and Heats of Formation of Gaseous Positive Ions," NSRDS-NBS 26, 1969, we calculate the ΔH of (R1) to be -2 kcal/mol for allene and 0 kcal/mol for propyne in agreement with Myher and Harrison (ref 10). However, the competing reaction R2 is calculated to be exothermic by 4–38 kcal/mol and apparently completely dominates the reaction dynamics at low energies.

Hückel molecular orbital calculations indicate the triangular form II is much more stable than the linear isomer I. The formation of linear $C_3H_3^+$ from thermal $C_3H_4^{+\cdot}$ and $C_3H_5^+$ may not be thermochemically favored, and the reactions need translational energy to proceed.

The difference in reactant ion energy between the thermal ICR experiments and the medium pressure mass spectrometer experiments is further underscored in the product distributions from propyne and allene parent ions. These data are summarized in Table III. The most significant difference is in the relative rate of formation of $C_3H_5^+$ and $C_6H_7^+$ ions in propyne.

$$C_3H_4^{+\cdot} + C_3H_4 \xrightarrow{k_3} C_3H_5^+ + C_3H_3 \qquad \text{(R3)}$$

$$C_3H_4^{+\cdot} + C_3H_4 \xrightarrow{k_4} C_6H_7^+ + H \qquad \text{(R4)}$$

From the double resonance results of Table I (reactions 1 and 15), it is apparent that k_3 significantly increases with $C_3H_4^{+\cdot}$ energy and k_4 significantly decreases. Under the conditions of the double resonance in Table I, the maximum $C_3D_4^{+\cdot}$ translational energy is 0.4 eV ($C_3D_5^+$ formation) and 1.2 eV ($C_6D_7^+$ formation). These energies are of the order of those used in the medium pressure mass spectral data of Myher and Harrison.[10] The energy discrepancy between the thermal ICR experiments and the mass spectral measurements accounts for the difference in relative rates of (R3) and (R4) in Table III and emphasizes the importance of reactant ion energy on product distributions.

Often it is possible to deduce mechanistic information by analysis of product distributions of isotopically substituted molecules. Such an analysis was the basis for Myher and Harrison's conclusion that the proton transfer reaction R3 proceeded by a direct mechanism and the condensation reaction R4 *via* an intermediate complex. Additional detailed information is available in the isotopic mixing studies on several of the condensation reactions in allene and propyne. The product distribution of the $C_5(H,D)_5^+$ ions for mixtures of allene plus allene-d_4 and propyne plus propyne-d_4 are given in Table IV along with Myher and Harrison's data. It is apparent that $CD_3\cdot$ and $CH_3\cdot$ are preferentially eliminated in the propyne system and that more nearly random scrambling appears to occur in the allene system. The data indicate that a specific mechanism is operative (at least in part) that transmits hydrogen atom information from the reactants to the products without complete randomization in the intermediate complex.

The isotopic mixing data for loss of ethylene from the $(C_6H_4D_4^{+\cdot})^*$ complex are even more enlightening. The allene system preferentially loses $C_2H_2D_2$ at approximately three times the random prediction while in propyne $C_2H_2D_2$ is eliminated at approximately one-half the random prediction. For allene, this result is strongly suggestive of the following "four-center" mechanism.

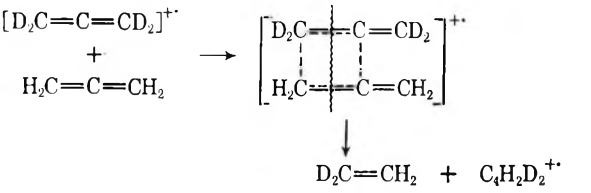

It is not nearly as easy to write an analogous mechanism for loss of ethylene from $(C_6H_8^{+\cdot})^*$ in propyne. A plausible $(C_6H_8^{+\cdot})^*$ fragmentation scheme, however, that is consistent with the isotopic mixing data of Table III, is shown below. The difficulty in deducing a facile

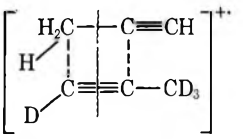

mechanism consistent with the isotopic distribution data probably is reflected in the smaller amount of elimination of ethylene in the propyne system relative to the allene system. Interestingly, the double resonance data (Table I, reaction 5) show a large difference in energy dependence for the loss of ethylene from the $[C_6H_8^{+\cdot}]^*$ complex in propyne and allene. Loss of ethylene is greatly enhanced by $C_3H_4^{+\cdot}$ translational energy in propyne and slightly depressed in allene. This result is consistent with the difficulty in writing a facile ethylene loss mechanism in propyne relative to allene and in fact may indicate a different mechanism is at play in the propyne system at higher $C_3H_4^{+\cdot}$ translational energies.

Further evidence for the four-center intermediate comes from the elimination of acetylene from the $(C_6H_8^{+\cdot})^*$ complex. The allene system does not eliminate acetylene to a measurable extent while it is a significant product in the propyne system (Table II). A sister mechanism to that given above can be written.

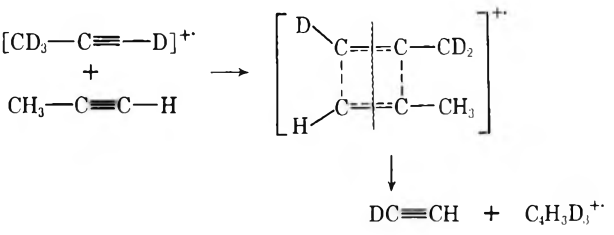

Due to interference from $C_4(H,D)_4^{+\cdot}$ ions it was difficult to obtain an accurate isotopic distribution of the $C_4(H,D)_6^{+\cdot}$ products. Myher and Harrison[10] reported the distribution for the reaction

$$\begin{aligned} [CD_3{-}C{\equiv}CH]^{+\cdot} &\longrightarrow C_2H_2 + C_4H_6^{+\cdot} \\ + \qquad\quad &\longrightarrow C_2HD + C_4D_5H^{+\cdot} \\ CD_3{-}C{\equiv}C{-}H &\longrightarrow C_2D_2 + C_4D_4H_2^{+\cdot} \end{aligned}$$

however, yielding acetylene elimination $C_2H_2/C_2HD/C_2D_2$ of 1.00/0.40/0.45 with random being 1.00/12.00/15.00. This evidence strongly supports the formation of the four-centered intermediate.

The $C_4H_4^{+}\cdot$, $C_4H_6^{+}\cdot$, and $C_5H_5^{+}$ ions are such minor products in allene and propyne, however, that it is not possible to say conclusively that the other reactions in these systems proceed *via* the above mechanisms. An investigation of systems in which analogous condensation reactions are more important was therefore made.

B. Ethylene–Allene and Ethylene–Propyne Mixtures. Since the ion–molecule reactions in ethylene[2,4] and allene and propyne have been well characterized, it is straightforward to identify the cross reactions in ethylene–allene and ethylene–propyne mixtures. Spectra for a 1:1.25 mixture of $CH_3—C\equiv H$ and $CH_2=CH_2$ at 1.9×10^{-5} Torr and 11.8 eV are given in Figure 3. It is evident that the primary cross reactions of $C_2H_4^{+}\cdot$ and $C_3H_4^{+}\cdot$ are

$$\left.\begin{matrix} C_2H_4^{+}\cdot(m/e\ 28) \\ + \\ CH_3—C\equiv CH \end{matrix}\right\} \xrightarrow{k_{5a}} C_4H_5^{+}(m/e\ 53) + \cdot CH_3 \quad \text{(R5a)}$$

$$\left.\begin{matrix} C_2H_4^{+}\cdot(m/e\ 28) \\ + \\ CH_3—C\equiv CH \end{matrix}\right\} \xrightarrow{k_{5b}} C_5H_7^{+}(m/e\ 67) + \cdot H \quad \text{(R5b)}$$

$$\left.\begin{matrix} C_3H_4^{+}\cdot(m/e\ 40) \\ + \\ CH_2=CH_2 \end{matrix}\right\} \xrightarrow{k_{6a}} C_4H_5^{+}(m/e\ 53) + \cdot CH_3 \quad \text{(R6a)}$$

$$\left.\begin{matrix} C_3H_4^{+}\cdot(m/e\ 40) \\ + \\ CH_2=CH_2 \end{matrix}\right\} \xrightarrow{k_{6b}} C_5H_7^{+}(m/e\ 67) + \cdot H \quad \text{(R6b)}$$

The relative contributions of (R5) and (R6) to $C_4H_5^{+}$ and $C_5H_7^{+}$ can be determined using ion-ejection techniques.[16] The results of pulse ejecting $C_2H_4^{+}\cdot$ and $C_3H_4^{+}\cdot$ are presented in Figures 3b and 3c, respectively. Owing to the limited resolution of the ejection process, both $C_3H_4^{+}\cdot$ and $C_3H_5^{+}$ are simultaneously pulse ejected in the data of Figure 3c. Double resonance experiments indicate the $C_3H_5^{+}$ fragment does not significantly contribute to either the $C_4H_5^{+}$ or $C_5H_7^{+}$ responses under the condition of these experiments, however.[17] The relative rates k_{5a}/k_{5b} and k_{6a}/k_{6b} as well as the analogous reactions in ethylene–allene mixtures are collected in Table V. There is a considerably larger loss of methyl group in the propyne–$C_2H_4\cdot^{+}$ reactions than in allene–$C_2H_4^{+}\cdot$ in spite of the fact that the estimated excess internal energy of the $(C_5H_8^{+}\cdot)^*$ intermediate complex is identical for both systems. When $C_3H_4^{+}\cdot$ is the reactant ion and C_2H_4 the neutral the same trend holds true indicating that either the structure or internal energy of the $C_3H_4^{+}\cdot$ reactant ion is different for $[CH_3C\equiv CH]^{+}\cdot$ than for $[CH_2=C=CH_2]^{+}\cdot$. Also, the $[C_4H_5^{+}]/[C_5H_7^{+}]$ ratio varies considerably from system to system. There is no clear correlation with the internal energy in the $(C_5H_8^{+})^*$ intermediate. These data are being analyzed further utilizing the quasi-equilibrium theory of unimolecular decomposition.[18]

The results of isotopic mixing studies are given in Table VI. The $C_5(H,D)_7^{+}$ ions exhibit an H–D isotope effect typical of these systems. The $C_4(H,D)_5^{+}$

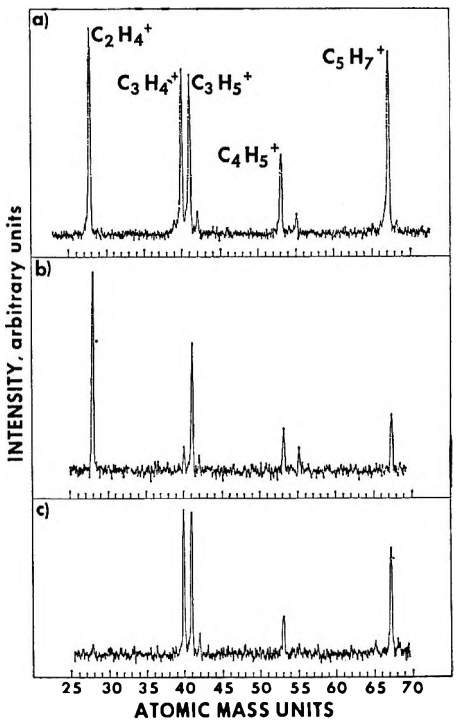

Figure 3. Spectra of a 2.5:1 mixture of ethylene–propyne at 1.9×10^{-5} Torr and 11.8-eV electron energy: (a) Single resonance; (b) $C_2H_4^{+}$ pulse ejection spectrum; (c) $C_3H_4^{+}$–$C_3H_5^{+}$ pulse ejection spectrum.

Table V: Ratio of Decomposition Products from the $[C_5H_8^{+}\cdot]^*$ Complex for Various Reactant Systems

Reactants	Internal energy of $[C_5H_8^{+}\cdot]^*$ in kcal/mol[a]	$[C_4H_5^{+}]/[C_5H_7^{+}]$
$C_2H_4^{+}\cdot + CH_2=C=CH_2$	80	0.58 ± 0.10
$C_2H_4^{+}\cdot + CH_3—C\equiv CH$	78	0.98 ± 0.10
$(CH_2=C=CH_2)^{+}\cdot + CH_2=CH_2$	73	0.21 ± 0.05
$(CH_3—C\equiv CH)^{+}\cdot + CH_2=CH_2$	76	0.46 ± 0.10
$C_3H_6^{+}\cdot + H—C\equiv C—H$	65	0.12 ± 0.05[b]
$c\text{-}C_3H_6^{+}\cdot + H—C\equiv C—H$	81	0.30 ± 0.10[b]
$C_2H_2^{+}\cdot + CH_3—CH=CH_2$	103	0.0 ± 0.10[b,c]
$C_2H_2^{+}\cdot + c\text{-}C_3H_6$	111	*b, d*

[a] Heats of formation were taken from J. L. Franklin, J. G. Dillard, H. M. Rosenstock, J. T. Herron, K. Draxl, and F. H. Field. In all cases the heat of formation of $C_5H_8^{+}\cdot$ was taken as 219 kcal/mol (1,3-pentadiene). The above internal energies could be reduced by as much as 50 kcal/mol depending on the $C_5H_8^{+}\cdot$ structure. [b] Data from ref 19. [c] $C_5H_7^{+}$ observed but $C_4H_5^{+}$ not observed. [d] Neither $C_5H_7^{+}$ nor $C_4H_5^{+}$ observed.

(16) J. L. Beauchamp and J. T. Armstrong, *Rev. Sci. Instrum.*, **40**, 123 (1969). Applications of ion ejection techniques can be found in ref 7 and 8.

(17) $C_3H_5^{+}$ does react with C_2H_4 to form $C_5H_7^{+}$, but at the low pressures of these experiments this reaction is not observed as evidenced by the absence of a $C_5H_9^{+}$ peak (see ref 2).

(18) For a review see M. Vestal, "Fundamental Processes in Radiation Chemistry," Interscience Publishers, New York, N. Y., 1968, p 59.

Table VI: Isotopic Distribution in C_2D_4–C_3H_4 Mixtures[a]

Reaction		Propyne	Allene	Random
$C_2D_4^+ \cdot + C_3H_4$	$\rightarrow C_4H_4D^+ + CD_3\cdot$	0.27	0.32	0.167
	$\rightarrow C_4H_3D_2^+ + CD_2H\cdot$	1.00	0.90	1.00
$C_3H_4^+ \cdot + C_2D_4$	$\rightarrow C_4H_2D_3^+ + CDH_2\cdot$	0.99	1.00	1.00
	$\rightarrow C_4HD_4^+ + CH_3\cdot$	0.33	0.35	0.167
$C_2D_4^+ \cdot + C_3H_4$	$\rightarrow C_5H_3D_4^+ + H\cdot$	1.00	1.00	1.00
$C_3H_4^+ \cdot + C_2D_4$	$\rightarrow C_5H_4D_3^+ + D\cdot$	0.67	0.65	1.00
$C_3H_6^+ + C_3H_4$	$\rightarrow C_6H_4D_3^+ + D_2$	0.40	0.42	0.50
	$\rightarrow C_6H_3D_4^+ + HD$	1.00	1.00	1.00
	$\rightarrow C_6H_2D_5^+ + H_2$	0.47	0.39	0.30

[a] Similar results were obtained with C_3D_4–C_2H_4 mixtures. Due to the weakness of many of the signals it was not possible to do ion ejection experiments to determine individual contribution of $C_2H_4^+$ and $C_3H_4^+$ ions.

data indicate that while there is approximately twice the random amount of $\cdot CH_3$ and $\cdot CD_3$ eliminated, there is not a significant difference between the allene and propyne mixtures. Thus, while ethylene–propyne mixtures would prefer to eliminate $\cdot C(H,D)_3$ nearly twice as readily as allene–ethylene mixtures on an absolute basis, there is apparently the same degree of scrambling of the hydrogens in the methyl group in both systems. This result contrasts with the pure propyne and allene systems where propyne preferentially loses $\cdot CD_3$ or $\cdot CH_3$ rather than the mixed $\cdot CH_2D$ or $\cdot CD_2H$ radicals (relative to random prediction). The somewhat statistical distribution in C_3H_4–C_2D_4 mixtures points up an effect also evident in the data of other similar systems. Even though there is relatively conclusive evidence for certain specific mechanisms (*e.g.*, selective loss of $\cdot CH_3$ in propyne mixtures) there is in no case evidence that any one mechanism occurs to the exclusion of all others.

As mentioned earlier, $C_3H_5^+$ reacts with C_3H_4 to form $C_5H_7^+$ quite efficiently but does not yield significant amounts of $C_3H_3^+$ (at least at thermal energies). The isotopic mixing data of this reaction are included in Table VI and indicate essentially random scrambling in the $[C_6(H,D)_9^+ \cdot]^*$ complex. The deviations between the allene and propyne systems are not large enough to be significant.

Isotope mixing experiments on the $CD_3C{\equiv}CD$/$CH_3CH{=}CH_2$ system indicate preferential loss of $\cdot CH_3$ and $\cdot CD_3$ groups from the collision complex. In the $CD_2{=}C{=}CD_2$/$CH_3CH{=}CH_2$ system only the $\cdot CH_3$ radical is preferentially lost. It appears that the methyl groups play little part in the reaction dynamics and a four-center complex may be important in reactions in C_3H_4–propene mixtures. A more complete account of this work will be published elsewhere.[19]

In summary, analysis of the ion–molecule reactions in propyne and allene and mixtures of propyne and allene with propene suggests a mechanism for the condensation reactions of the "four-centered" type where the attached R groups ($\cdot CH_3$ in this study) generally play a reduced role in isotopic scrambling. Mixtures of the 3-carbon unsaturates with acetylene and ethylene give results that are consistent with the above mechanism but they are not in themselves conclusive (due, apparently, to the high degree of symmetry of C_2H_2 and C_2H_4). Additional experiments are being carried out on more complicated systems in the hope of obtaining more definitive results. It is hoped from this systematic study that the nature and scope of ion–molecule reaction mechanisms in unsaturated systems can be characterized.

Acknowledgments. The support of the Directors Discretionary Fund of the Jet Propulsion Laboratory, California Institute of Technology, is gratefully acknowledged.

(19) M. T. Bowers and D. D. Elleman, to be published.

The Kinetics and Mechanism of Carbon Monoxide Oxidation over Silver Catalysts

by George W. Keulks and Charles C. Chang

Department of Chemistry and Laboratory for Surface Studies, University of Wisconsin at Milwaukee, Milwaukee, Wisconsin 53201 *(Received February 19, 1970)*

The oxidation of carbon monoxide with gaseous oxygen on a powdered silver catalyst was studied at 100° in a recirculation reactor. The kinetics were determined to be first order in carbon monoxide, zero order in oxygen, and a negative first order in carbon dioxide. Over the temperature range 80–130°, the activation energy was 13.6 kcal/mol. When isotopic $^{18}O_2$ was used and the CO_2 trapped, the isotopic distribution of the CO_2 was 95% $C^{16}O^{18}O$, 2.5% $C^{16}O_2$, and 2.5% $C^{18}O_2$. However, if the CO_2 was not trapped, the isotopic distribution in the CO_2 tended to approach equilibrium. This change in the isotopic distribution was shown to be a result of the subsequent equilibration of the CO_2 over the silver catalyst. Neither the oxidation reaction nor the CO_2 equilibration reaction proceed through CO_3 intermediates involving chemisorbed oxygen. A detailed reaction scheme is proposed.

Introduction

The silver-catalyzed oxidation of carbon monoxide has been studied in a flow reactor by Benton and Bell.[1] At low conversions, and when carbon monoxide was in excess, they found that the reaction rate was proportional to the carbon monoxide pressure and independent of the oxygen pressure. This rate dependence suggested a two-step mechanism. According to Benton and Bell, the first step was the chemisorption of oxygen on silver. The carbon monoxide then reacted with the chemisorbed oxygen either by impinging on it from the gas phase or from an adsorbed state next to adsorbed oxygen or on top of adsorbed oxygen.

Titani, *et al.*,[2] on the other hand, found that under similar reaction conditions the reaction rate was proportional to the oxygen pressure and independent of the carbon monoxide pressure. Yamada[3] explained this contradiction in the kinetics by showing that the rate of the oxidation depended on the history of the catalyst. When silver had not been thoroughly reduced, the rate of the oxidation became proportional to the oxygen pressure. He concluded that Benton and Bell conducted their studies on thoroughly reduced silver, whereas Titani, *et al.*, had used silver poisoned with oxygen.

We felt that the use of a recirculation reactor would allow us to examine in greater detail the kinetics of the oxidation reaction. In addition, we felt that the use of oxygen-18 would enable us to gain a clearer understanding of the mechanism of the reaction.

Experimental Section

Recirculation Reactor. Because of the relatively high exothermic heat of reaction for the oxidation of carbon monoxide, all of the experiments were conducted in a Pyrex recirculation reactor having a volume of 350 cm^3. Gases were introduced into the circulation loop *via* a gas-handling manifold, and the pressure was measured by oil and mercury U-tube manometers. Gas circulation through the loop was accomplished by a magnetically operated pump. The pump was capable of pumping speeds of 150 cm^3 (STP)/min when the pressure in the circulation loop was 100 Torr to greater than 1000 cm^3 (STP)/min when the pressure in the loop was 500 Torr. Most of the experiments described in this work were conducted at a total pressure of 200 Torr. At this pressure the pump delivered a flow rate of approximately 500 cm^3 (STP)/min.

The circulation loop was connected to a conventional vacuum system incorporating a two-stage mercury diffusion pump. The ultimate vacuum produced with this system was 2×10^{-7} Torr. The circulation loop, as well as the catalyst tube, was protected against mercury vapor by a cold trap maintained at −78° and by the use of gold leaf traps.

The catalyst tube itself was constructed out of 2-mm Pyrex capillary tubing. On the inlet to the catalyst section was a spiral of 3 ft of 4-mm Pyrex tubing. The spiral was added in order to guarantee that the incoming gas would be preheated to the temperature of the heating medium. Most of the oxidations were carried out at 100 ± 1°. This temperature was achieved by means of a boiling water bath. For temperatures other than 100°, a constant temperature oil bath was used.

Analysis. Analysis of the gas mixture was accomplished by a Varian Quadrupole Residual Gas Analyzer (QRGA) directly coupled to the circulation loop. The QRGA was capable of unit mass resolution at mass 50.

(1) A. F. Benton and R. T. Bell, *J. Amer. Chem. Soc.*, **56**, 501 (1934).

(2) (a) T. Titani and I. Shiwatari, *J. Chem. Soc. Jap.*, **65**, 13 (1944); (b) T. Titani and N. Yamada, *ibid.*, **65**, 244 (1944); (c) T. Titani and S. Nakata, *ibid.*, **65**, 305 (1944).

(3) N. Yamada, *Bull. Chem. Soc. Jap.*, **27**, 36 (1954).

In order to reduce the production of CO at the hot filament of the ionizer during the admission of oxygen, a rhenium filament was used. The mass 30 peak due to the production of $C^{18}O$ when $^{18}O_2$ was introduced was negligible. The Bayard-Alpert gauge used to measure the pressure in the QRGA was not operated during the analysis.

The partial pressures of CO, O_2, and CO_2 were determined by comparing their respective peak heights to the peak height for argon, which was used as an internal standard (usually CO and CO_2 were not determined simultaneously). The relative sensitivities of the various gases were checked after each experiment, but they were found to remain constant from month to month. When mixtures of known composition were introduced into the circulation loop and then analyzed with the QRGA, the analysis agreed to within $\pm 0.5\%$ with the known composition.

The rate of the oxidation was determined by following either the rate of formation of CO_2 or, when the CO_2 was trapped, the rate of disappearance of CO. When the reaction rate was followed by the rate of formation of CO_2, 5–6 Torr of argon was used for the internal standard. When the reaction rate was followed by the rate of disappearance of CO, 19–20 Torr of argon was used for the internal standard. The more sensitive oil U-tube manometer was always used to measure the argon pressure.

Procedure. Normally, 1 to 2 g of silver powder was used as the catalyst. The standard procedure was to pretreat the silver at 310° with hydrogen (300 Torr) for 2 hr. After evacuation of the loop to a pressure of less than 10^{-6} Torr, the silver catalyst was cooled to 100° and then isolated from the loop. The desired pressures of argon, carbon monoxide, and oxygen were then introduced into the loop, and the total pressure brought up to 200 Torr with helium. In order to achieve a homogeneous mixture, these gases were circulated through the loop for 30 min. At the end of this period, analysis by the QRGA indicated that the gas composition was homogeneous. The gas flow was then diverted over the heated silver catalyst and the rate of the reaction was determined by analyzing the gas composition with the QRGA. Depletion of the gas mixture from the loop for all of the QRGA analyses amounted to only 4–5% of the total pressure.

Catalysts. The catalysts used in this study were of two types: Ag(I)–Mallinckrodt reagent grade silver powder of 99.93% purity. The impurities included 0.005% chloride, 0.001% copper, 0.002% lead, 0.002% iron, and 0.06% sulfate.

Ag(II)–silver powder prepared from the thermal decomposition *in vacuo* of silver carbonate which had been prepared by the method described by Barnes and Stone.[4] A silver nitrate solution (0.1 *N*) was prepared from reagent grade silver nitrate (Baker Analyzed reagent) in a dark room. To the silver nitrate solution, a 0.1 *N* solution of sodium bicarbonate was added. The mixture was then allowed to stand for 3 days in the dark. The precipitated silver carbonate was filtered and washed numerous times with distilled water. After drying at 100°, the silver carbonate was decomposed *in vacuo* at 310° for 24 hr. The decomposition procedure was then followed by reduction with 300 Torr of hydrogen at 310° for 12 hr.

Gases. The carbon monoxide and oxygen were Baker Analyzed research grade supplied in 1-l. Pyrex bulbs. The oxygen-18 (99.3% ^{18}O, 0.3% ^{17}O) was obtained from Yeda Research and Development Co., Rehovoth, Israel. The argon used for the internal standard was Baker High Purity (99.996%); the hydrogen used for reduction of the silver after each experiment was Baker Ultra-pure (99.999%).

Results

Kinetics. The activity of the commercial silver powder, Ag(I), was very erratic,[5] which made it impossible to determine the kinetic rate law by a differential method. The kinetics were therefore assumed to be those determined by Benton and Bell, *i.e.*, first order in carbon monoxide and zero order in oxygen. The differential rate expression conforming to these kinetics was integrated, and the experimental data were tested against the integrated rate expression.

With oxygen as the limiting reactant and under the conditions of constant temperature and volume, the fractional conversion[6] is given by

$$f = \frac{P_{CO_2} - P_{CO_2}^0}{2P_{O_2}^0}$$

where $P_{CO_2}^0$, P_{CO_2} = pressures of CO_2 at $t = 0$ and $t = t$ respectively, and $P_{O_2}^0$ = pressure of O_2 at $t = 0$. The resulting integrated rate expression in terms of the fractional conversion, f, is

$$\ln\left(1 - \frac{2P_{O_2}^0}{P_{CO}^0} f\right) = -kt \qquad (1)$$

The experimental data from the experiments conducted on various samples of Ag(I) were tested against eq 1 on a Univac 1108 computer. All of the computer plots indicated a marked deviation from linearity. A typical plot is shown in Figure 1.

Because the experimental data did not fit the assumed kinetics, the kinetic rate law was modified to include inhibition by the product, carbon dioxide. Integration

(4) P. A. Barnes and F. S. Stone, "Reactivity of Solids," J. W. Mitchell, Ed., Wiley-Interscience, New York, N. Y., 1969, p 261.

(5) The erratic behavior in activity is believed to be due to the slow removal of impurities in the silver powder and not due to a continual change in surface area. An independent study of the surface area of Ag(I) as a function of pretreatments similar to reaction conditions showed that the surface area was relatively constant at 1800 cm^2/g.

(6) M. Boudart, "Kinetics of Chemical Processes," Prentice-Hall, Inc., Englewood Cliffs, N. J., 1968, Chapter 1.

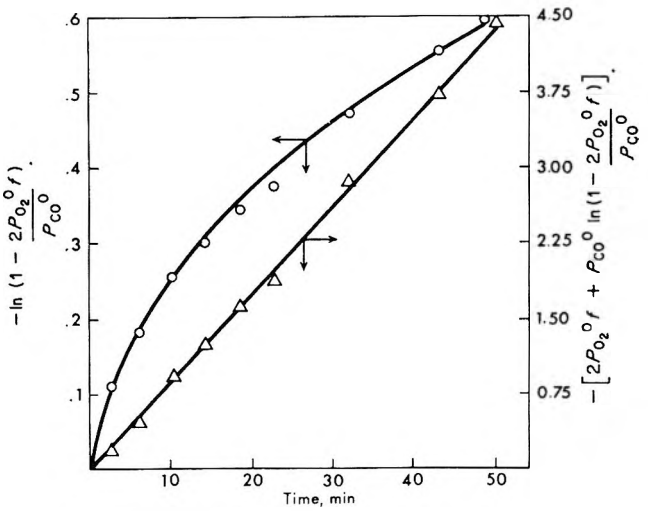

Figure 1. Integrated rate expression plots for the oxidation of carbon monoxide at 100°: O, first order in CO, zero order in O_2; △, first order in CO, zero order in O_2, negative first order in CO_2; P_{CO}^0 = 30 Torr, $P_{O_2}^0$ = 10 Torr.

of the differential rate law under the condition of constant volume and in terms of the fractional conversion yields the following expression

$$2P_{O_2}^0 f + P_{CO}^0 \ln\left(1 - \frac{2P_{O_2}^0}{P_{CO}^0} f\right) = -kt \qquad (2)$$

Subsequent testing of the experimental data against eq 2 produced linear plots as indicated for a representative set of data in Figure 1. Because of the excellent fit to this integrated rate expression, we concluded that the kinetics of carbon monoxide oxidation over silver are first order in carbon monoxide, zero order in oxygen, and negative first order in carbon dioxide.

In order to test this kinetic rate law more thoroughly, we ran a number of experiments in which the carbon dioxide was frozen out of the gas mixture by liquid nitrogen. If the carbon dioxide inhibits the oxidation rate, then in these experiments the experimental data should conform to eq 1. In every case the data were found to give an excellent fit to this expression. A typical plot is shown in Figure 2.

Further evidence for the inhibition of the rate by carbon dioxide was gained by adding initially some carbon dioxide. In these experiments the initial reaction rate was much slower. The reaction rate was also found to be reduced sharply when carbon dioxide was introduced into the gas phase during the oxidation. This was accomplished by removing the liquid nitrogen trap during the reaction.

Similar results were found with the self-prepared silver powder, Ag(II). In the absence of carbon dioxide, the reaction was first order in carbon monoxide and zero order in oxygen. In the presence of carbon dioxide, the reaction also showed a negative first-order dependence on carbon dioxide partial pressure. A distinct advantage of Ag(II) over Ag(I), however, was

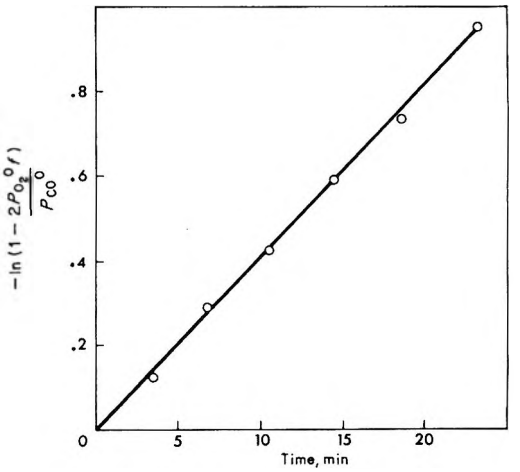

Figure 2. First-order rate plot for the oxidation of carbon monoxide at 100°. Carbon dioxide was removed by a liquid nitrogen trap; P_{CO}^0 = 31 Torr, $P_{O_2}^0$ = 10 Torr.

the relatively stable catalytic activity. This stable catalytic activity allowed us to test the kinetics by the differential method. When carbon monoxide was in excess, the kinetics were confirmed to be first order in carbon monoxide and zero order in oxygen. The results are summarized in Table I.

Table I: Effect of Partial Pressures on the Reaction Rate

P_{CO}^0, Torr	$P_{O_2}^0$, Torr	Initial rate of CO_2 formation,[a] Torr min^{-1}
30	10	0.55
60	10	1.08
60	20	1.15

[a] Determined by taking the slope of the P_{CO_2} *vs.* time curve at $t \approx 0$. One gram of catalyst having a surface area of 1580 cm^2/g was used for the experiments.

Activation Energy. In order to determine the activation energy for the oxidation, the reaction was also studied at 82 and 132° with the Ag(II) catalyst. With 30 Torr of CO and 10 Torr of O_2 and trapping the carbon dioxide, specific rate constants were determined from eq 1. An Arrhenius plot of ln k *vs.* $1/T$ yielded an activation energy of 13.6 kcal/mol. This is in excellent agreement with the value of 13.3 kcal/mol reported by Benton and Bell.

Tracer Studies. A number of experiments were conducted with pure $^{18}O_2$ or a mixture of $^{18}O_2$ and $^{16}O_2$. The homomolecular exchange of oxygen, *i.e.*

$$^{18}O_2 + {}^{16}O_2 \rightleftarrows 2{}^{16}O{}^{18}O$$

was not detected at 100° during the oxidation of carbon monoxide. In fact, even in the absence of carbon monoxide, the homomolecular exchange reaction did not occur at 100°.

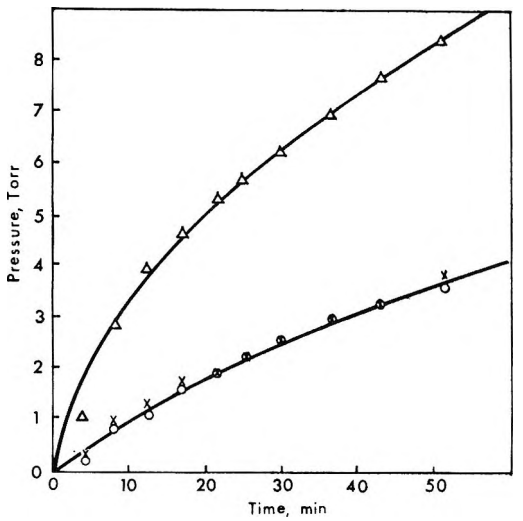

Figure 3. Isotopic distribution of the CO_2 when $C^{16}O$ was oxidized with $^{18}O_2$ at 100°: O, $C^{16}O_2$; △, $C^{16}O^{18}O$; X, $C^{18}O_2$. P_{CO}^0 = 129 Torr, $P_{^{18}O_2}^0$ = 14 Torr.

The CO molecule retained its integrity during the oxidation reaction. The small amount of mass 30 ($C^{18}O$) observed in the mass spectrum could be attributed to the fragmentation patterns of the isotopic forms of CO_2.

When carbon monoxide was oxidized with pure $^{18}O_2$, and the resultant CO_2 allowed to circulate over the silver, all three isotopic forms of CO_2 were observed as shown in Figure 3. It should be noted that even though pure $^{18}O_2$ was used, $C^{16}O_2$, and $C^{18}O_2$ were formed in equal amounts. The isotopic distribution in the CO_2 was not at equilibrium initially, but tended to approach equilibrium with time as indicated on Table II.

Table II: Isotopic Distribution of Carbon Dioxide[a]

Time, min	P_{44}[b]	P_{46}[b]	P_{48}[b]	K[c]
3.5	0.3	1.0	0.2	17
7.6	0.8	2.7	0.7	13
11.8	1.2	3.9	1.0	13
16.5	1.6	4.5	1.5	8
21.1	1.9	5.3	1.9	8
25.3	2.1	5.8	2.1	8
29.7	2.4	6.4	2.4	7
36.5	2.8	7.0	2.8	6
43.6	3.1	7.7	3.1	6
51.5	3.7	8.2	3.5	5

[a] Catalyst used was Ag(I), having a total surface area of 1800 cm^2. P_{CO}^0 = 129 Torr, $P_{^{18}O_2}^0$ = 14 Torr. [b] P_{44}, P_{46}, and P_{48} refer to the partial pressures of $C^{16}O_2$, $C^{16}O^{18}O$, and $C^{18}O_2$, respectively. [c] $K = ((P_{46})^2/(P_{44})(P_{48}))$, at equilibrium K = 4.

The equal amounts of $C^{16}O_2$ and $C^{18}O_2$ and the approach toward equilibrium isotopic distribution in CO_2 with time strongly indicated a subsequent equilibration reaction of the $C^{16}O^{18}O$ which was the predominant isotopic species. As expected, when a mixture of $^{16}O_2$ and $^{18}O_2$ was used, the $C^{16}O_2$ and $C^{18}O_2$ concentrations were no longer equal. However, if the CO_2 is assumed to undergo subsequent equilibration after it is formed, then the concentration of $C^{16}O_2$ should follow the statistical relationship

$$P_{C^{16}O_2} = P_{C^{16}O^{18}O} + 2P_{C^{18}O_2} \times \frac{P_{^{16}O_2}^0}{P_{^{18}O_2}^0} + P_{C^{18}O_2}$$

where $P_{C^{16}O_2}$ = calculated pressure of $C^{16}O_2$, $P_{C^{16}O^{18}O_2}$ = observed pressure of $C^{16}O^{18}O$ calculated from mass 46 peak, $P_{C^{18}O_2}$ = observed pressure of $C^{18}O_2$ calculated from mass 48 peak, $P_{^{16}O_2}^0$ = initial pressure of $^{16}O_2$, $P_{^{18}O_2}^0$ = initial pressure of $^{18}O_2$. All of the data for the experiments utilizing isotopic mixtures of oxygen followed this relationship.

In order to minimize the occurrence of a subsequent equilibration reaction of CO_2, several experiments were conducted in which the CO_2 was frozen out of the gas mixture in the cold trap. The oxidation was allowed to go to completion. Then, with the cold trap still immersed in liquid nitrogen, the residual gases were evacuated. After the cold trap was warmed to room temperature, analysis of the CO_2 showed that the isotopic distribution was 95% $C^{16}O^{18}O$, 2.5% $C^{16}O_2$, and 2.5% $C^{18}O_2$ when a small amount (0.1 g) of the Ag(I) catalyst was used. With 0.1 g of the Ag(II) catalyst the isotopic distribution was 90% $C^{16}O^{18}O$, 5% $C^{16}O_2$, and 5% $C^{18}O_2$. When larger quantities (up to 1.5 g) of the catalysts were used, the concentration of $C^{16}O^{18}O$ decreased with a corresponding increase in the $C^{16}O_2$ and $C^{18}O_2$ concentrations. Thus it appears that when CO is oxidized with pure $^{18}O_2$, the initial product is $C^{16}O^{18}O$. The small amounts of $C^{16}O_2$ and $C^{18}O_2$ observed are believed to be due to the subsequent equilibration reaction occurring on the silver catalyst as the gas mixture passes through the catalyst bed.

Equilibration of CO_2. Experiments were conducted in an attempt to obtain additional information on the unexpected equilibration of CO_2. The exchange reaction only occurred on silver which had been exposed to oxygen. This fact was confirmed by preparing $C^{16}O^{18}O$ (95%) by oxidizing carbon monoxide with $^{18}O_2$ and trapping the CO_2 formed as described above. This material was then used as the reactant in other experiments.

The possibility of the CO_2 equilibrating by a homogeneous mechanism was examined by circulating $C^{16}O^{18}O$ through an empty reactor maintained at 100°. No change in isotopic composition was detected for circulation periods up to 3 hr.

The equilibration reaction was also studied over silver which had been given the normal pretreatment with hydrogen (see Experimental Section). The isotopic composition of the CO_2 changed only slightly over a 2-hr period. However, when the silver was exposed

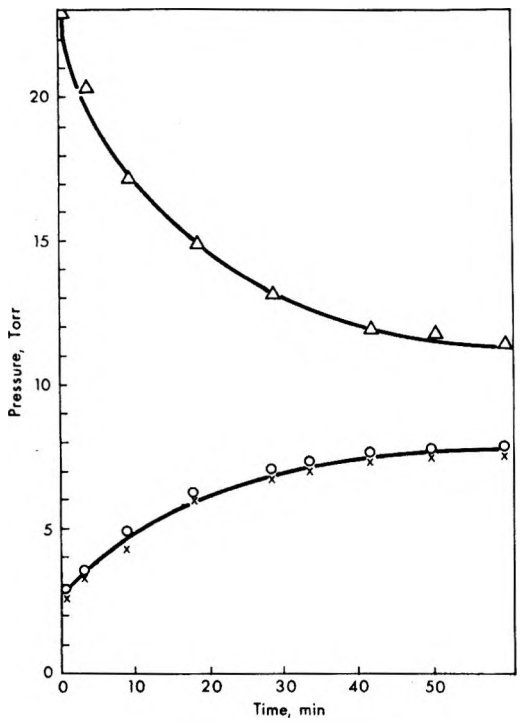

Figure 4. Equilibration of $C^{16}O^{18}O$ at 100° over a silver catalyst that had been exposed to oxygen: ○, $C^{16}O_2$; △, $C^{16}O^{18}O$; X, $C^{18}O_2$.

to oxygen either by adding a small amount to the CO_2 or by using a silver catalyst which had just been used for CO oxidation, the equilibration reaction occurred rapidly, as shown in Figure 4. The mixture reached approximately equilibrium composition in 60 min. The ratio of partial pressures for the CO_2 exchange expressed as

$$K = \frac{(P_{C^{16}O^{18}O})^2}{(P_{C^{16}O_2})(P_{C^{18}O_2})}$$

is given as a function of time in Table III.

Table III: Ratio of Partial Pressures *vs.* Time for CO_2 Exchange over Silver

	Time, min						
	0	4	9	18	29	42	60
K	113	60	25	12	8	6	5

As shown in Figure 5, the CO_2 exchange data fit the first-order kinetic rate expression

$$-\ln \frac{X_t - X_\infty}{X_0 - X_\infty} = kt$$

where X_0 and X_∞ are the mole fraction of oxygen-18 in $C^{16}O^{18}O$ at $t = 0$ and $t = \infty$, the X_t is the mole fraction at time t.

These experiments provided further evidence that the $C^{16}O_2$ and $C^{18}O_2$ isotopic forms were produced by a

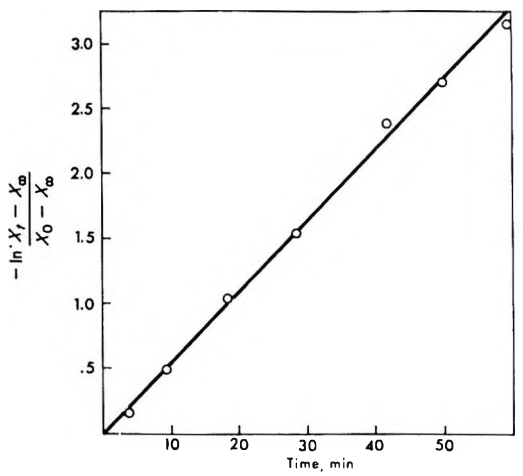

Figure 5. First-order rate plot for the isotopic equilibration of CO_2 over silver at 100°: $P_{C^{16}O_2}{}^0 = 2.2$ Torr, $P_{C^{16}O^{18}O}{}^0 = 22.3$ Torr, $P_{C^{18}O_2}{}^0 = 2.0$ Torr.

homomolecular equilibration reaction and, further, that the exchange reaction was occurring only on silver catalysts which had been exposed to oxygen. To test this hypothesis further, an experiment was conducted using 6.9 g of the silver catalyst having a total surface area of 1.9×10^4 cm^2. The catalyst was first pretreated with 10 Torr of $^{18}O_2$ at 100° for 2 hr. If it can be assumed that this treatment produces at least monolayer coverage with chemisorbed oxygen atoms, then the surface would provide an oxygen atom pool of approximately 10^{19} atoms. The reactor was then charged with 1.6 Torr of $C^{16}O_2$ which provided 3.6×10^{19} oxygen atoms in the gas phase. Because of the nearly equivalent concentration of oxygen atoms in the gas phase and on the surface, we felt that if the heterogeneous exchange reaction was taking place, it could be easily detected. After several hours of circulation, no incorporation of ^{18}O into the CO_2 was detected.

The silver also did not catalyze the exchange between CO_2 and O_2 at 100° nor between CO_2 and CO. When a mixture of $^{18}O_2$ (9 Torr) and $C^{16}O_2$ (6 Torr) was circulated over the silver catalyst, no change in the isotopic distribution of O_2 or CO_2 was observed. When a mixture of CO_2 (16 Torr; 25% $C^{16}O_2$, 58% $C^{16}O^{18}O$, 17% $C^{18}O_2$) and $C^{16}O$ (7.5 Torr) was circulated over the silver catalyst, the CO_2 was observed to undergo equilibration as described earlier. However, the $C^{16}O$ maintained its integrity as evidenced by the constancy of the mass 28 and 30 peaks after correcting for the fragmentation of the isotopic CO_2.

Discussion

The results reported herein indicate that the kinetics of the silver-catalyzed oxidation of carbon monoxide are first order in carbon monoxide, zero order in oxygen, and negative first order in carbon dioxide. These kinetics are in good agreement with those reported by Benton and Bell. Because their results were obtained

in a flow reactor operating at low conversion, their kinetics would be expected to approximate more closely the results we obtained when CO_2 was trapped from the gas phase. In these experiments the kinetics were indeed first order in carbon monoxide and zero order in oxygen. The close agreement in the activation energy indicates that the rate-determining step is the same in the two cases.

The kinetic results and the tracer experiments, however, have provided us with a clearer understanding of the mechanism. In agreement with Benton and Bell, we interpret the zero-order dependence in oxygen to indicate a strong oxygen chemisorption. The lack of equilibrium of $^{16}O_2$ with $^{18}O_2$, either independently or during reaction with carbon monoxide, indicates that the oxygen is irreversibly chemisorbed.

The actual form of chemisorbed oxygen is not entirely clear. Apparently the oxygen does dissociate under reaction conditions, but does not again desorb once it has dissociated (no $^{16}O^{18}O$ detected). The results of other workers[7-13] indicate that oxygen chemisorption at elevated temperatures may produce several forms of adsorbed oxygen. The two most likely forms seem to be O_2^- ions and O^- ions. Thus, if the oxygen chemisorption is at all reversible, then the reversibility would have to be due to the O_2^- ions and not O^- ions. It would seem likely, though, that both forms would be active for the oxidation of CO.

The first-order dependence in carbon monoxide can be interpreted as being due to a reaction from a weakly chemisorbed layer or to a direct reaction from the gas phase. A recent infrared study[14] of carbon monoxide adsorption on silver at room temperature indicated that CO only adsorbed on silver that had been exposed to oxygen. There was no evidence for the adsorption of carbon monoxide on clean silver metal. We, therefore, interpret the first-order dependence on CO as indicating the weak chemisorption of CO on chemisorbed oxygen ions. The lack of oxygen-18 incorporation into the CO molecule during reaction with $^{18}O_2$ or with isotopic CO_2 is in agreement with this weak chemisorption. These experiments also indicate that the CO does not participate in the formation of an adsorbed CO_2 or CO_3-type species which can dissociate again into CO and adsorbed oxygen.

When the CO_2 was frozen out of the reaction mixture, essentially only one isotopic form of CO_2 ($C^{16}O^{18}O$) was observed when $C^{16}O$ was oxidized with $^{18}O_2$. This indicates that the oxidation does not involve a CO_3 surface intermediate. This is substantiated by the lack of ^{18}O incorporation into the CO molecule during the reaction with $^{18}O_2$ and by the lack of exchange between CO and isotopic CO_2.

The negative first-order dependence on CO_2 pressure can be interpreted as the competition of CO_2 with CO for adsorption on the oxygen ion sites. This is in agreement with the results of other workers. Benton and Drake[7] determined that CO_2 did not adsorb on silver above 0°, but did adsorb on silver containing a surface oxide.[15] Czanderna[16] also reported that CO_2 did not adsorb on bare silver metal. However, he did observe that the CO_2 adsorbed on silver which had been treated with oxygen. In fact, he found that the number of CO_2 molecules adsorbed corresponded exactly to the number of oxygen atoms preadsorbed on the silver surface. The lack of CO_2 adsorption on polycrystalline silver films was also observed by Lawson.[17]

The mechanism of the CO_2 equilibration reaction is still somewhat unclear. We determined that it did not occur homogeneously, nor was it greatly catalyzed by reduced silver. In order to obtain efficient catalysis, the silver needed to be exposed to oxygen. The lack of ^{18}O incorporation into the CO_2 *via* the heterogeneous exchange reaction with surface oxygen indicates that it does not occur through a CO_3 surface species. Apparently, the equilibration is simply a homomolecular reaction between CO_2 molecules that are adsorbed on oxygen ions. The intermediate in this equilibration may be a "C_2O_4" complex similar to that postulated by Smith[18] for CO oxidation on copper.

In summary, we suggest that a plausible reaction sequence for the oxidation of carbon monoxide near 100° on silver can be expressed by the following equations [O(ads) = O_2^- and O^-]

$$O_2(g) \longrightarrow O(ads) \quad (3)$$

$$CO(g) + O(ads) \rightleftarrows CO \cdot O(ads) \quad (4)$$

$$CO \cdot O(ads) \longrightarrow CO_2(g) \quad (5)$$

$$CO_2(g) - O(ads) \rightleftarrows CO_2 \cdot O(ads) \quad (6)$$

$$2CO_2 \cdot O(ads) \rightleftarrows C_2O_4 \cdot 2O(ads) \quad (7)$$

The rate-determining step for the oxidation is the reaction of weakly chemisorbed CO with the surface oxygen on which it is adsorbed, as indicated by eq 5.

Acknowledgment. We acknowledge financial assistance for partial support of this work from the Petroleum Research Fund and the National Science Foundation-Departmental Science Development Program Grant.

(7) A. F. Benton and L. C. Drake, *J. Amer. Chem. Soc.*, **56**, 255 (1934).
(8) G. H. Twigg, *Trans. Faraday Soc.*, **42**, 284 (1946).
(9) W. W. Smeltzer, *Can. J. Chem.*, **34**, 1046 (1956).
(10) L. Ya. Margolis, *Advan. Catal.*, **14**, 451 (1963).
(11) A. W. Czanderna, *J. Phys. Chem.*, **68**, 2765 (1964).
(12) Y. L. Sandler and D. D. Durigon, *ibid.*, **69**, 4201 (1965).
(13) T. B. Gruenwald and G. Gordon, *J. Catal.*, **6**, 220 (1966).
(14) G. W. Keulks and A. Ravi, *J. Phys. Chem.*, **74**, 783 (1970).
(15) A. F. Benton and L. C. Drake, *J. Amer. Chem. Soc.*, **56**, 506 (1934).
(16) A. W. Czanderna, *J. Vac. Sci. Tech.*, 308 (1966).
(17) A. Lawson, *J. Catal.*, **11**, 295 (1966).
(18) A. W. Smith, *ibid.*, **4**, 172 (1965).

A Kinetic Study of the Addition of Trifluoromethyl Radicals to Ethylene in Hydrocarbon Solution[1]

by Richard A. Weir, Pierre P. Infelta, and Robert H. Schuler

Mellon Institute Radiation Research Laboratories and Department of Chemistry, Carnegie-Mellon University, Pittsburgh, Pennsylvania 15213 *(Received January 28, 1970)*

The addition of CF_3 radicals to ethylene in competition with their reaction with iodine has been studied in cyclohexane and heptane solutions. Measurements in both solvents at room temperature give the relative rate of the former to the latter reaction as ~0.0035. In heptane the temperature coefficient of the rate constant ratio over the range −80 to 25° corresponds to an activation energy difference of 1290 cal/mol. For the addition reaction itself the activation energy is estimated as 3500 cal/mol, the steric factor as 0.03, and the absolute reaction rate constant at room temperature as $3 \times 10^6\ M^{-1}\ \text{sec}^{-1}$. This latter value is essentially identical with that found in a recent study in the vapor phase.

It is known from previous studies that in both the vapor[2] and liquid phases[3] CF_3 radicals are considerably more reactive toward abstraction of hydrogen from hydrocarbons than are CH_3 radicals. During the course of studies of the radiolysis of CF_3Br–C_2H_4–I_2 solutions it was found that the CF_3 radicals produced from the CF_3Br add quite readily to the ethylene to form trifluoropropyl radicals. These latter radicals are then scavenged by the iodine to form $CF_3C_2H_4I$ which is the observed product. The results of a somewhat detailed study of the competition between the reaction of CF_3 radicals with iodine

$$CF_3\cdot + I_2 \xrightarrow{k_1} CF_3I + I\cdot \qquad (1)$$

and with ethylene

$$CF_3\cdot + C_2H_4 \xrightarrow{k_2} CF_3C_2H_4\cdot \qquad (2)$$

are reported here. While the present work was in progress a report[4] appeared on vapor phase experiments in which the rate of reaction 2 was examined in competition with scavenging by H_2S. The two studies taken together provide comparative data for the liquid and vapor phases on the rates of a reaction which has a low activation energy but which still proceeds somewhat more slowly in the liquid phase than does a process which is primarily controlled by diffusion.

Experimental Section

CF_3 radicals were produced by the γ-ray irradiation of a 0.1 *M* solution of CF_3Br or CF_3Cl in cyclohexane or heptane.[3] The hydrocarbons used were Phillips Research grade and were chromatographed through silica gel prior to sample preparation. Commercial samples of CF_3Br, CF_3Cl, and C_2H_4 were distilled on a vacuum line at low temperature, and the resultant cuts were shown to be free of any significant impurity by mass spectrometry. The desired amount of solute was measured volumetrically and added to the outgassed hydrocarbon sample. The irradiation cell had little vapor volume (<10%) so that essentially all of the solute was in solution.

Irradiations of 5- or 10-min duration were carried out inside a cylindrical ^{60}Co γ-ray source at an absorbed dose rate of 5.6×10^{18} eV g^{-1} hr^{-1}. Only a small fraction (~10%) of the iodine reacted during this period. Irradiations were at room temperature and at −22, −45.2, −63.5, and −78.5°. The latter four temperatures were conveniently maintained by slush baths of carbon tetrachloride, chlorobenzene, chloroform, and Dry Ice–trichloroethylene.

A sample of $CF_3C_2H_4I$ used for developing the chromatographic separation procedures described below was prepared by heating a CF_3I–C_2H_4 mixture.[5] The resultant sample was gas chromatographed, and the major product was trapped and examined mass spectrometrically. The most abundant ion observed in the mass spectrum of this component was at mass 224 which corresponds to the parent ion from $CF_3C_2H_4I$. All other ions of an abundance greater than 1% represent fragments of $CF_3C_2H_4I$ as do all ions observed in a spectrum run at an ionizing energy of 14 V. This gas chromatographic fraction is undoubtedly mostly $CF_3C_2H_4I$. However one extraneous ion with an abundance of 0.8% does occur in the 70-V spectrum at mass 102 (corresponding to CF_3CH_2F). Attempts at further purification did not change its relative abundance at all, and an examination of the pressure dependence seems to rule out its production by an ion–molecule reaction. The source of this ion is, at the moment,

(1) Supported in part by the U. S. Atomic Energy Commission.

(2) For a summary of typical vapor phase abstraction rate constants see A. F. Trotman-Dickenson, *Advan. Free Radical Chem.*, **1**, 1 (1965).

(3) P. P. Infelta and R. H. Schuler, *J. Phys. Chem.*, **73**, 2083 (1969).

(4) J. M. Sangster and J. C. J. Thynne, *ibid.*, **73**, 2746 (1969).

(5) R. N. Haszeldine, *J. Chem. Soc.*, 2856 (1949).

not obvious but may possibly be a fluorination reaction on the filament of the ion source.

Radioiodine ($^{131}I_2$) was used to scavenge the radicals, and the product alkyl iodides of interest (CF_3I and $CF_3C_2H_4I$) were separated chromatographically at room temperature. The overall radiochromatographic procedure used was much the same as that reported previously[3,6,7] although some modification was necessary because C_2H_5I is produced in addition to CF_3I and $CF_3C_2H_4I$. Because of its high volatility the retention time of CF_3I is extremely short. Under the conditions used its elution is complete within 10 min, and it is easily separated from the higher boiling alkyl iodides (methyl iodide has a retention time ~15 min and that for all other alkyl iodides is greater). Although ethyl and propyl iodide can be readily separated, $CF_3C_2H_4I$ is considerably more volatile than is C_3H_7I, and on the columns used (25% silicone grease on 30–60 mesh firebrick) its retention time is only ~25% greater than that of C_2H_5I. The difference is sufficient that separation of small samples is no special problem. However, because large samples (0.5 cc) were used in the analysis to get reasonable activity levels for the counting, the peaks of the C_2H_5I and $CF_3C_2H_4I$ were broadened considerably and overlapped to a significant extent when injected in the normal manner. Though the problem is more severe with the cyclohexane solutions than with the heptane solutions, some overlap occurs even in the latter case. The widths of these peaks were reduced to those of small samples when the sample was injected into a preheated section of column so that the more volatile components were rapidly separated from the bulk solvent. The analytical procedure adopted was, therefore, to take up into a syringe immediately after opening the cell 0.5 cc of the irradiated solution and inject it into a 100-cm long precolumn. The first half of this precolumn was packed with dry firebrick and heated sufficiently to vaporize the entire sample within 1 min. The second half of this precolumn was packed with coated firebrick and kept at room temperature. It served to trap the bulk of the radioiodine and prevent the main column from becoming contaminated. This precolumn was repacked between runs.

As in the other radiochromatographic studies with $^{131}I_2$ the main column was 250 cm long and at room temperature. The separated alkyl iodides were trapped in 3 cc of 2,2,4-trimethylpentane in cells maintained at Dry Ice temperature and counted in a well-type scintillation counter. By placing two traps in series it was shown that ~3% of the CF_3I passed the first trap. In the individual experiments this loss was either measured directly or an average correction applied. In general because of the very high volatility of CF_3I, considerable caution had to be used in sample transfer. Trapping of C_2H_5I and $CF_3C_2H_4I$ was shown to be quantitative. The activity in the first 10-min cut was taken to represent the CF_3I. Cuts from 43–55 and 60–80 min were taken for the C_2H_5I and $CF_3C_2H_4I$, respectively. From runs on ethylene solutions with no added source of CF_3 it was shown that ~2% of the C_2H_5I activity should be collected in the 5-min cut between the two main peaks. It was assumed that there was no encroachment on the $CF_3C_2H_4I$ peak, and the runs were deemed valid if the activity in the central 55–60-min cut did not significantly exceed this value. No significant activity was detected in the 60–80-min cut in experiments where C_2H_4 was not present.

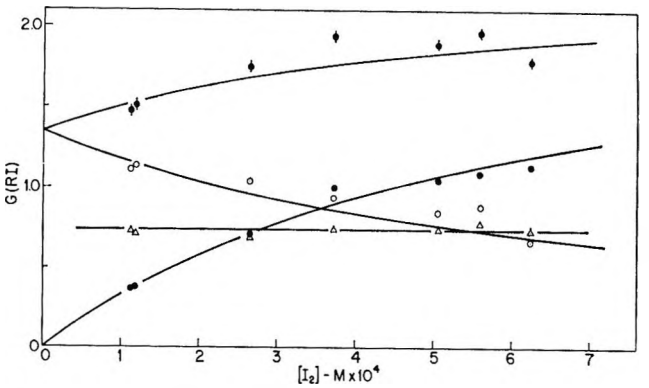

Figure 1. Dependence of the CF_3I (●), $CF_3C_2H_4I$ (○), CF_3I + $CF_3C_2H_4I$ (◐), and C_2H_5I (△) yields on iodine concentration for cyclohexane solutions containing 0.1 M ethylene. The curves for the CF_3I and $CF_3C_2H_4I$ yields (and the sum) are calculated from eq I and II with $G(CF_3) = 2.53$, $k_2/k_1 = 3.58 \times 10^{-3}$, and $k_3[RH]/k_1 = 2.88 \times 10^{-4}$.

Results and Discussion

The initial studies were carried out in cyclohexane solution at room temperature, and the results obtained as a function of iodine concentration at an ethylene concentration of 0.1 M are illustrated in Figure 1. First it should be noted that an ethyl iodide yield is observed which is independent of iodine concentration. Ethyl radicals are, of course, produced by the addition of hydrogen atoms to the ethylene and should be efficiently scavenged at iodine concentrations above 10^{-5} M.[6] As has recently been indicated,[8] they are also produced by ion transfer to the solute, but for solutions containing 0.1 M CF_3Br both of these processes should be independent of iodine concentration. At this concentration of CF_3Br the yield of C_2H_5 radicals is 0.7 and is almost identical with that found in solutions containing similar concentrations of CH_3Br and C_2H_4. The constancy of the yield indicates that addition of ethyl radicals to ethylene is not significantly competitive with the scavenging reactions. In contrast the CF_3 radicals both add to the ethylene (reaction 2) and also abstract hydrogen from the solvent (reaction 3)

(6) R. R. Kuntz and R. H. Schuler, *J. Phys. Chem.*, **67**, 1004 (1963).
(7) L. McCrumb and R. H. Schuler, *ibid.*, **71**, 1953 (1967).
(8) K.-D. Asmus, J. M. Warman, and R. H. Schuler, *ibid.*, **74**, 246 (1970).

$$CF_3\cdot + RH \xrightarrow{k_3} CF_3H + R\cdot \qquad (3)$$

so that the scavenging efficiency and thus the yield of CF_3I increase markedly with iodine concentration. This increase is partially at the expense of a decreased yield of $CF_3C_2H_4I$. The competition between reactions 1 and 3 has previously been investigated in cyclohexane, and the value of k_3/k_1 has been shown to be ~450 times the analogous ratio for methyl radicals[3] so that over the concentration region studied the total yield of the two products should increase. Reactions 1, 2, and 3 appear to be the only important ones involving the disappearance of CF_3 radicals. Assuming that the $CF_3C_2H_4$ radicals produced in reaction 2 are quantitatively scavenged, as are the C_2H_5 radicals, we can write for the CF_3I and $CF_3C_2H_4I$ yields

$$G(CF_3I) = G(CF_3)\frac{k_1[I_2]}{k_1[I_2] + k_2[C_2H_4] + k_3[RH]} \qquad (I)$$

and

$$G(CF_3C_2H_4I) = G(CF_3)\frac{k_2[C_2H_4]}{k_1[I_2] + k_2[C_2H_4] + k_3[RH]} \qquad (II)$$

where $G(CF_3)$ is the CF_3 radical yield appropriate to the particular solution. Measurement of the relative yields of CF_3I and $CF_3C_2H_4I$ (in fact only the relative activities in the two cuts need be measured) at a particular I_2 and C_2H_4 concentration gives all the information required to determine the relative rate constants for reactions 1 and 2. Thirteen determinations of this ratio in cyclohexane at room temperature (in addition to the seven sets of data reported in Figure 1, six determinations were made at C_2H_4 concentrations other than 0.1 M) gave a value of 0.00358 ± 0.00021 (root-mean-square deviation).

$$\frac{k_2}{k_1} = \frac{G(CF_3C_2H_4I)/[C_2H_4]}{G(CF_3I)/[I_2]} \qquad (III)$$

With k_2/k_1 known the sum of eq I and II can be cast into the form of a simple competitive expression, *i.e.*

$$G(CF_3I) + G(CF_3C_2H_4I) = G(CF_3)\frac{1}{1 + \dfrac{k_3[RH]}{k_1([I_2] + (k_2/k_1)[C_2H_4])}} \qquad (IV)$$

where $[I_2] + (k_2/k_1)[C_2H_4]$ is the iodine equivalent of the total scavenger in competition with reaction 3. The CF_3 yield can therefore be determined from the intercept of a plot of the reciprocal of the sum of the iodide yields against the reciprocal of $[I_2] + (k_2/k_1)\cdot[C_2H_4]$ and the quantity $k_3[RH]/k_1$ from the intercept and slope. For the solutions 0.1 M in CF_3Br and 0.1 M in C_2H_4 these values are $G(CF_3) = 2.53$ and $k_3[RH]/k_1 = 2.88 \times 10^{-4}$ M. The values previously reported for these quantities for solutions 0.1 M in CF_3Br alone were, respectively, 2.34 and 2.97×10^{-4} M.[3] The addition of ethylene to cyclohexane solutions appears to cause a slight increase in the yield of decomposition of CF_3Br, as it also does in the case of CH_3Br. The agreement between these two measurements of $k_3[RH]/k_1$ is, of course, independent of the $CF_3\cdot$ yield and is seen to be very good.

With a knowledge of $G(CF_3)$, k_2/k_1, and k_3/k_1 the dependence of the yields of CF_3I and $CF_3C_2H_4I$ are completely described by eq I and II, and the curves of Figure 1 are plotted accordingly. The CF_3I yields follow the calculated curve somewhat better than do the $CF_3C_2H_4I$ yields, probably reflecting the greater difficulty in the measurement of this latter quantity. Also it is noted that the presentation given in Figure 1 requires determination of absolute yields whereas measurement of k_2/k_1 involves only relative yields.

Similar measurements were made in heptane at room temperature and are reported in Table I. The ratio k_2/k_1 observed here is slightly less than that found in cyclohexane, but since the error limits overlap it is difficult to say whether or not there is a real difference or whether, in fact, the ratios are essentially identical. A competitive plot of total iodide product *vs.* effective solute concentration, as per eq IV, is given in Figure 2. It is seen that the results for the sum of the CF_3I and $CF_3C_2H_4I$ yields obtained from the solution containing ethylene fall on top of those for CF_3I observed from the ethylene-free solutions. The linear relationship of Figure 2 corresponds to $G(CF_3) = 2.66$ and $k_3[RH]/k_1 = 1.57 \times 10^{-4}$ (with $[C_7H_{16}] = 6.8$ M, $k_3/k_1 = 2.30 \times 10^{-5}$). The first quantity is only slightly higher than that found in cyclohexane. This agreement is reasonable in view of the similarity between the yields observed for electron scavenging by CH_3Br in various

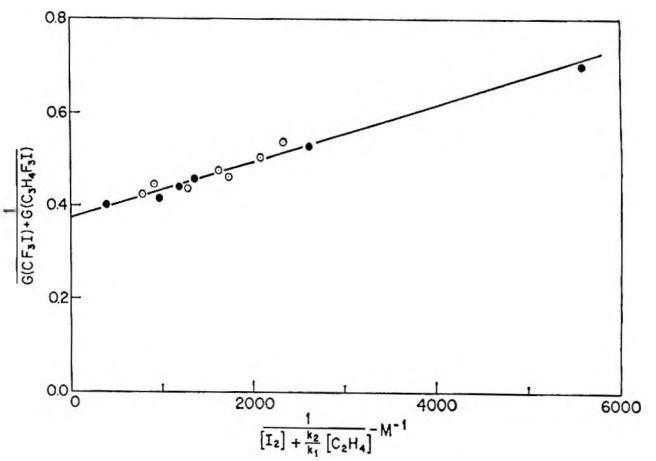

Figure 2. Competition plot of the data obtained at room temperature from ethylene-free (●) and ethylene-containing (○) solutions. See text and eq IV—k_2/k_1 is taken at 3.31×10^{-3}. The rate constant ratio k_3/k_1 determined from the slope and intercept is 2.3×10^{-5}.

Table I: Competitive Scavenging of $CF_3\cdot$ in Heptane

T, °C	$[C_2H_4]$, M	$[I_2]$, mM	$G(CF_3I)$	$G(C_2H_5I)$	$G(CF_3C_2H_4I)$	$\frac{k_2}{k_1} \times 10^3$
25	0.0204	0.510	1.89	0.40	0.27	3.54
	0.0511	0.311	1.25	0.59	0.73	3.53
	0.101	0.095	0.43	0.72	1.44	3.17
	0.101	0.281	0.99	0.74	1.11	3.09
	0.101	0.436	1.30	0.76	0.98	3.26
	0.101	0.948	1.76	0.67	0.60	3.21
	0.200	0.438	0.89	0.79	1.36	3.37
						Av 3.31 ± 0.17[a]
	(0.102	0.433	0.94	0.83	0.72	3.23)[b]
−45	0.0206	0.757	1.90	0.44	0.10	1.82
	0.0519	0.767	1.79	0.54	0.21	1.71
	0.101	0.087	0.59	0.70	1.17	1.69
	0.102	0.226	1.02	0.71	0.81	1.76
	0.102	0.434	1.36	0.70	0.51	1.60
	0.101	0.661	1.57	0.68	0.39	1.64
	0.203	0.683	1.24	0.75	0.60	1.63
						Av 1.69 ± 0.08

[a] Root-mean-square deviation. [b] 0.1 M CF_3Cl used as the $CF_3\cdot$ source in the experiment; 0.1 M CF_3Br in all others.

hydrocarbons.[9] The rate constant ratio is slightly less than that found in cyclohexane, although if one normalizes the ratios for the number of secondary hydrogen atoms in the two compounds, the relative rates become almost identical. One is concerned here with the rate of the reaction with the solvent relative to that for a diffusion-controlled process so that changes in the solvent are expected to have a fairly pronounced effect. It is noted that at room temperature the self-diffusion coefficient for heptane is approximately twice that for cyclohexane[10] so that the absolute rate for the scavenging reaction is undoubtedly somewhat slower in the latter solvent. In any event the rates for the abstraction of hydrogen from these two hydrocarbons must be quite comparable.

It is, of course, of interest to examine the temperature dependence of the relative reaction rates. In these experiments either the iodine or ethylene concentration can be varied, and as a result it is possible to measure the ratio k_2/k_1 over fairly diverse conditions. This is desirable because, in view of the 300-fold difference between the two rate constants, it might be expected that the temperature coefficient would be quite large. If the preexponential factors for the two competing reactions are identical, then the temperature coefficient should correspond to an activation energy difference of 3400 cal/mol and amount to a factor of 20 for a 100° decrease in the temperature. Measurements made at lower temperatures in heptane show that the temperature coefficient is, in fact, considerably less than this. The pertinent data are reported in Table I and Figure 3. Measurements at the lower temperatures were limited by solubility of iodine in the heptane (~2×10^{-4} M at −80°) so that the most extensive measurements were carried out at −45° with the experiments at the other temperatures being used only for corroboration. It is seen that lowering the temperature from 25 to −45° reduces k_2/k_1 by only a factor of 2. The line of Figure 3 is drawn through the mean values at these

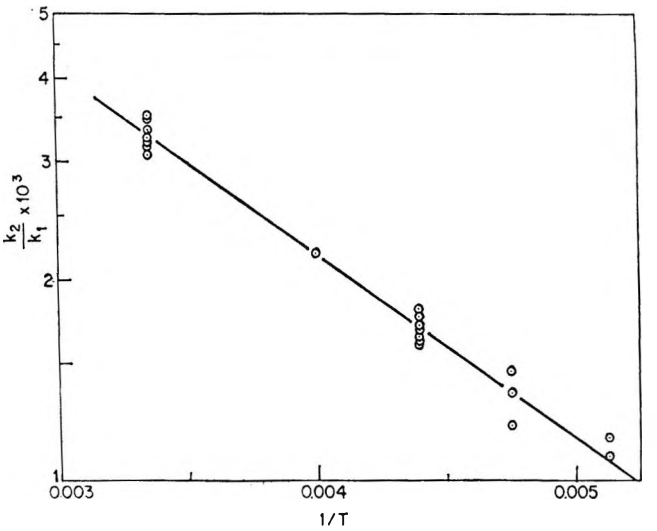

Figure 3. Arrhenius plot of the rate constant ratios k_2/k_1 obtained in heptane over the temperature interval 25 to −78.5°. The linear relationship is drawn through the mean values of the ratios measured at 25 and −45° and corresponds to an activation energy of 1290 cal/mol.

(9) S. J. Rzad and J. M. Warman, *J. Chem. Phys.*, 49, 2861 (1968); S. J. Rzad and J. M. Warman, *ibid.*, in press.

(10) D. W. McCall, D. E. Douglass, and E. W. Anderson, *ibid.*, 31, 1555 (1959).

temperatures and, assuming a simple Arrhenius relationship, corresponds to an activation energy difference of 1290 cal/mol. Treating the deviations indicated in Table I in terms of probable errors in the mean gives the probable error of the activation energy as ±30 cal. At room temperature this activation energy corresponds to a factor of 0.113 and leaves a ratio of 0.0293 in the preexponential factors to account for the relative rates, *i.e.*

$$k_2/k_1 = 0.0293e^{-1290/RT} \qquad \text{(V)}$$

For the results in heptane at −45° a plot of the total yield for CF_3I and $CF_3C_2H_4I$ according to eq IV shows considerable scatter and covers too short a concentration range to enable determination of significant values for the radical yield or rate constant ratio. At this temperature five additional measurements of the CF_3I yield from solutions containing only CF_3Br and iodine gave CF_3I yields which increased from 1.65 to 2.16 over the iodine concentration range of 0.34 to 1.02 mM. From these measurements the CF_3 radical yield is 2.4 (±0.1) and $k_3[RH]/k_1$ is 1.5 (±0.1) × 10^{-4} M. This latter value is essentially the same as that observed at room temperature. It is seen that there is very little temperature coefficient to the competition between reactions 1 and 3. It was previously pointed out[3] that in the case of cyclohexane little temperature coefficient is expected since the activation energy for the diffusion process (which presumably controls the scavenging reaction) is comparable to that for abstraction. It is, however, somewhat surprising that in the case of heptane, where the activation energy for self-diffusion is lower, the temperature coefficient is not somewhat larger.

It is also noted in Table I that at the various ethylene concentrations the ethyl radical yields are essentially the same at 25 and −45°. If these data are interpreted in terms of a simple competition between addition of hydrogen atoms to ethylene and abstraction of hydrogen from the solvent, then at both temperatures the yield of hydrogen atoms from the 0.1 M CF_3Br solutions is ~0.90 and the relative rate constants are ~300. These values are essentially the same as those observed in cyclohexane.[7] However, here, as in the case of cyclohexane, there is very likely an ionic contribution to the ethyl radical yield which would make both of the above values somewhat high. In spite of this latter complication the data of Table I indicate that there is little temperature coefficient to the competition between the addition and abstraction processes involving hydrogen atoms.

If we take the absolute rate constant for k_1 as ~10^9 M^{-1} sec^{-1},[3] then at room temperature k_2 is ~3 × 10^6 M^{-1} sec^{-1}. This latter value agrees well with the value of 3.5 × 10^6 M^{-1} sec^{-1} given by the work of Sangster and Thynne[4] in the gas phase at 296°K. This gas phase value was determined by scavenging the radicals with H_2S, determining the $CF_3C_2H_5$ and $CF_3C_4H_9$ produced, and comparing the measured relative rates with the known rate for the reaction of CF_3 radicals with H_2S. Ultimately its value is based on the absolute rate for recombination of CF_3 radicals determined by Ayscough[11] in rotating sector experiments and can be compared with the rate for the abstraction by CF_3 of hydrogen from cyclohexane which has also been determined[12] relative to the recombination of CF_3 radicals. A rate constant of 5 × 10^4 M^{-1} sec^{-1} was obtained or a factor of 70 lower than that for the addition reaction. For hydrocarbon solutions a similar comparison can be made *via* the competitions with iodine, *i.e.*

$$\frac{k_2}{k_3} = \frac{k_2/k_1}{k_3/k_1} \qquad \text{(VI)}$$

which for cyclohexane is 3.58 × 10^{-3}/3.16 × 10^{-5} = 113 and for heptane is 3.31 × 10^{-3}/2.30 × 10^{-5} = 144. The relative rates for addition of CF_3 radicals to ethylene *vs.* abstraction of hydrogen from the hydrocarbon are thus comparable in the liquid and vapor phases.

The above comparisons make it clear that the rate of the reaction between CF_3 radicals and iodine must be essentially controlled by diffusion and therefore should have a temperature coefficient of the magnitude of that for self-diffusion (~2.2 kcal[10]) and a steric factor close to unity. The steric factor for the reaction of CF_3 radicals with ethylene is estimated from the present study to be ~0.03 so that the overall efficiency per encounter must be relatively low. The diffusion barrier will no longer control the rate of the reaction, and the measured difference in activation energies will correspond to the difference between the actual activation energy for the addition reaction and that for the diffusion; *i.e.*, in these experiments one is essentially measuring the temperature coefficient of reaction 2 relative to that for diffusion of CF_3 radicals. The activation energy for reaction 2 is, therefore, estimated as the sum of 2.2 and 1.3 or ~3.5 kcal/mol. This estimate of the activation energy should be quite close to the gas phase value. If this activation energy is applied to the absolute rate of 3 × 10^6 M^{-1} sec^{-1} indicated above, then the preexponential term is 1.1 × 10^9 and the "collision frequency" in the liquid is the reasonable value of 1.1 × 10^9/0.03 or 4 × 10^{10} M^{-1} sec^{-1}. From their measurements in the gas phase over the temperature range 291–473°K Sangster and Thynne reported a temperature coefficient corresponding to a somewhat lower activation energy (2370 ± 491 cal/mol in their case) but also a fivefold smaller preexponential

(11) P. B. Ayscough, *J. Chem. Phys.*, 24, 944 (1956).

(12) S. W. Charles and E. Whittle, *Trans. Faraday Soc.*, 56, 794 (1960).

term (2.45×10^8). At room temperature these two differences cancel, and the actual rates are quite comparable as indicated above.

Although Sangster and Thynne find that in their studies trifluoropropyl radicals add to the ethylene to some extent, the scavenger used by them (H_2S) is considerably less efficient than iodine, and the overall chemistry appears to be somewhat more complex. In the present study such addition would be manifest as a decrease in the apparent value of k_2/k_1 with increased ethylene concentration or an increase with increased iodine concentration. It is seen in Table I that at both 25 and $-45°$ a tenfold increase in either ethylene or iodine has little, if any, effect on the value of k_2/k_1. There is therefore no evidence in the present study that any significant addition of these radicals to ethylene occurs in competition with the very rapid scavenging by iodine.

In addition to the factual results reported above, the present work demonstrates the ease with which kinetic investigations of this type can be carried out using γ-ray initiation as the source of radicals. In particular, studies at low temperatures are readily carried out. The high reproducibility and freedom from trivial experimental problems makes accurate determinations of activation energies possible.

Kinetic Studies on the Autoxidation of 3,5-Di-*t*-butylpyrocatechol[1,2]

by Charles A. Tyson and Arthur E. Martell[3]

Departments of Chemistry, Illinois Institute of Technology, Chicago, Illinois, and Texas A & M University, College Station, Texas *(Received September 10, 1969)*

The use of 3,5-di-*t*-butylpyrocatechol in 50% methanol as a model for the autoxidation of pyrocatechol to *o*-quinone is explored. Manometric studies indicate a first-order dependence on substrate under conditions where O_2 concentration is held constant by recycling. Rate constants for the disappearance of H_2L, HL^-, and L^{2-} forms of the substrate are calculated. The rate of oxygen uptake is found to follow combined first- and second-order kinetics, and possible mechanistic interpretations of these results are discussed. Equilibrium constants for the *o*-semiquinone anion radical dismutation are found by combined esr and potentiometric measurements, and the rate constants are estimated from rapid-flow esr experiments. A novel apparatus for simultaneous measurements by manometry, spectroscopy, and titrimetry and for manometric experiments in buffer-free systems is described. Kinetic studies by esr provide information on possible autoxidation mechanisms.

A kinetic investigation of the autoxidation of pyrocatechols to *o*-quinone is necessary to provide the basis for a similar study of the metal-catalyzed oxidation. Because of the complex nature of pyrocatechol autoxidation,[4-7] 3,5-di-*t*-butylpyrocatechol (35DTBP) was chosen as an alternate substrate. Autoxidation of this derivative yields the *o*-quinone (35DTBQ), which is stable and easily characterized.[5,8] Previous esr studies on 3,5-di-*t*-butyl-*o*-benzosemiquinone (35DTBSQ) indicate that this species is also relatively stable in solution.[9,10] Blocking the 3 and 5 positions appears to reduce the rate of solvolytic attack on the quinonoid nucleus, which complicates the autoxidation of pyrocatechol.[11,12] Peroxy adducts in the *para* positions, characteristic of 2,4,6-tri-*t*-butylpyrocatechol autoxidation,[13,14] were not observed in high resolution esr work.[15] Degradation products are colorless[5] and do not interfere with spectral product analysis or kinetic investigations.

In this work the 3,5-di-*t*-butylpyrocatechol–O_2 system is studied by manometric, esr, and spectrophotometric

(1) Abstracted in part from a thesis submitted to the Faculty of Illinois Institute of Technology in partial fulfillment of the requirements for the degree of Doctor of Philosophy.

(2) This work was supported by Research Grants WP-00744 and WP-01197 from the Water Pollution Administration of the Department of the Interior.

(3) Address inquiries to Arthur E. Martell at the Department of Chemistry, Texas A & M University, College Station, Tex. 77843.

(4) J. R. Gillette, D. Watland, and G. Kalnitsky, *Biochim. Biophys. Acta*, **15**, 526 (1954).

(5) R. R. Grinstead, *Biochemistry*, **3**, 1308 (1964).

(6) L. B. Wingard, Jr., *Dissertation Abstr.*, **26**, 5942 (1966).

(7) F. Rohrscheid, A. L. Balch, and R. H. Holm, *Inorg. Chem.*, **5**, 1542 (1966).

(8) L. Horner and W. Durckheimer, *Z. Naturforsch.*, **18b**, 1002 (1963).

(9) K. Ley and E. Muller. *Angew. Chem.*, **70**, 469 (1958).

(10) J. J. Conradi and G. A. MacLaren, *J. Amer. Chem. Soc.*, **82**, 4745 (1960).

(11) D. R. Eaton, *Inorg. Chem.*, **3**, 1628 (1964).

methods in 50% methanol containing 0.10 *M* KNO_3 with several objectives in mind. First, the rate law for autoxidation is to be determined and compared insofar as possible with that reported for pyrocatechol.[16] Second, reasons for the lower reported yields of 35DTBQ in the absence of metal ions are needed as an aid in understanding why Mn(II) and Co(II) catalysts are so efficient. Third, the kinetics in the absence of metal ions is needed for comparison with the metal-catalyzed oxidation. Fourth, an interpretation of the kinetics in terms of probable autoxidation mechanisms was considered possible and useful.

In regard to the last objective, the difficulty in quantitatively resolving whether one- or two-electron transfer to oxygen is involved in the rate-determining step has long puzzled organic chemists.[17] Since 60–65% of the electron density in *o*-benzosemiquinones is concentrated at the oxygen atoms a second electron could easily be transferred before the reactants escape into the bulk of the solution.[15,17] Rapid dismutation between pyrocatechols and their quinones (and the high reactivity of these quinones) has so far made this problem impossible to solve kinetically. Nonetheless, it is worthwhile to determine forward and back dismutation constants in the event that these might be low enough due to steric interference of the *t*-butyl groups to use rapid techniques to resolve the one-electron, two-electron problem.

Experimental Section

Reagents. 3,5-Di-*t*-butyl-*o*-benzoquinone was prepared from a concentrated solution of the pyrocatechol *via* Mn(II)-catalyzed oxidation in 50% methanol and recrystallized once from isooctane (mp 113.2–113.8°; lit.[8] mp 113°). The electronic and ir spectra corresponded to those published.[18,19] Oxygen gas mixtures were analyzed (to 1 part per 10,000) and supplied by Matheson Co. The oxygen atmosphere referred to as 100% oxygen was 99.4% oxygen by analysis. All other materials are as described earlier.[20]

Instruments. Standard analytical instruments used in the experimental work are an automatic di-functional recording titrator[21] (International Instrument Co., Canyon, Calif.), Beckman DK-2 recording spectrophotometer, and a Varian V-4502-12 electron paramagnetic resonance spectrometer. A Beckman Research pH meter was used to check pH meter readings of the titrator.

Description of Apparatus. The apparatus used in the kinetic studies was of the "bubble-type," constant volume variety, designed to made simultaneous measurements by the techniques of manometry, titrimetry, and spectroscopy and to operate in buffer-free solutions. The latter two techniques include automatic recording instruments and full automation is potentially possible.

Two flow systems are involved. The reaction solution is saturated with the desired atmosphere by using a small bellows pump which cycles the gas through a glass frit beneath the surface of the solution and through the manometric device. A second flow system involves peristaltic pumping of the reaction solution from the reaction cell through flexible tubing to a suitable detection unit (esr, ultraviolet, or visible spectroscopy) and back to the cell. Only one previous instance of a gas cycle system having been used in manometric studies was found.[22] In the apparatus employed, provision apparently was not made for either simultaneous kinetic measurements of more than one variable, or automatic pH control.

A sketch of the reaction cell and cover appears in Figure 1. A greased rubber O-ring sits in a groove inside the Teflon cover and provides an air-tight seal with the glass wall. Six holes in the cover (top insert, Figure 1) accommodate a glass and calomel electrode pair set in O-ring sockets, two hypodermic needles for separate addition of acid and base, a $^1/_4$-in. brass swage lock with Teflon pressure fitting to hold the glass frit, and a $^3/_8$-in. brass swage lock with similar fitting for the gas exit tube. The reaction solution return line is sealed into the elbow of the glass exit tube with epoxy resin.

At the bottom of the reaction cell is a solution outlet. A Teflon disk, high enough to minimize bubbles from entering the liquid line, rests on the bottom of the cell when spectral measurements are being made. A Teflon-coated magnetic stirrer rests on top of the disk and its rotating action pulls gas bubbles down and away from the glass frit, effectively saturating the solution with them. Oxygen depletion in the liquid lines can be minimized by maintaining a high pump rate and short flow lines. A three-way Teflon stopcock in the solution exit line just after the O-ring allows the removal of aliquot samples during the course of a reaction.

(12) D. C. Reitz, J. R. Hollahan, F. Dravnicks, and J. E. Wertz, *J. Chem. Phys.*, **34**, 1457 (1961).

(13) H. R. Gersmann and A. F. Bickel, *J. Chem. Soc.*, 2771 (1959).

(14) G. M. Coppinger, *J. Amer. Chem. Soc.*, **79**, 2758 (1957).

(15) C. Trapp, C. A. Tyson, and G. Giacometti, *ibid.*, **90**, 1394 (1968).

(16) M. A. Joslyn and G. E. K. Branch, *ibid.*, **57**, 1779 (1935). A complete kinetic treatment of the work in the paper by Joslyn and Branch is not possible because of the absence of product and stoichiometric data, limiting the extent of comparison. Recent experiments in acetonitrile indicate that the molar ratio of oxygen consumed to pyrocatechol initially present is appreciably greater than unity (see H. Musso and H. Doepp, *Chem. Ber.*, **100**, 3627 (1967)).

(17) H. Musso in "Oxidative Coupling of Phenols," W. I. Taylor and A. R. Battersby, Ed., Marcel Dekker Inc., New York, N. Y., 1967, pp 64, 75.

(18) W. Flaig, T. Ploetz, and A. Kullmer, *Z. Naturforsch.*, **10b**, 668 (1955).

(19) K. Ley and E. Muller, *Chem. Ber.*, **89**, 1402 (1956).

(20) C. A. Tyson and A. E. Martell, *J. Amer. Chem. Soc.*, **90**, 3379 (1968).

(21) J. B. Neilands and M. D. Cannon, *Anal. Chem.*, **27**, 29 (1955).

(22) Yu. V. Suzdalinitskaya and K. I. Matveev, *Kinet. Katal.*, **5**, 194 (1964).

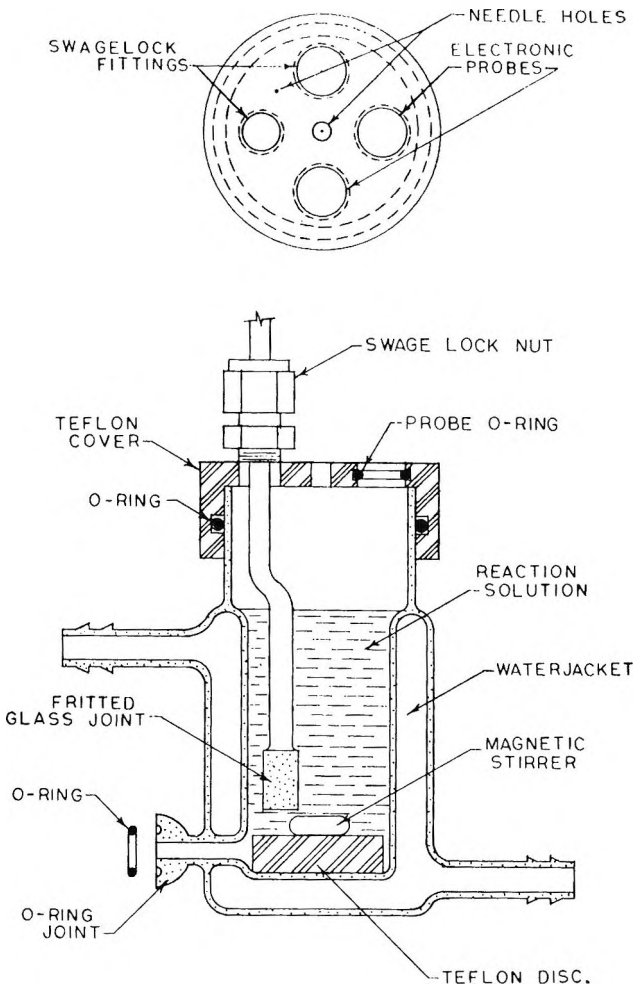

Figure 1. Reaction cell, top insert: top section of Teflon cover. Bottom insert: cross section of Pyrex reaction cell with cover in position.

An automatic titrator with syringe device for addition of acid or base for pH control was used to eliminate the need for buffer. Provision for other reagents was made possible by means of a hypodermic needle inserted through a narrow hole drilled in the Teflon cover. With this experimental arrangement pH control to ± 0.03 units or better was achieved in systems with 1.0×10^{-2} *M* substrate and to ± 0.05 units with less than 2.0×10^{-3} *M* substrate present. Automatic control could usually be established within 15 sec of the start of the reaction.

The gas pump is placed near the reaction vessel in a separate chamber constructed of a brass inner wall and masonite outer wall. Metal screws bolt a plexiglass cover tightly against a rectangular rubber washer which sets on top of the walls and houses swage locks for intake and outlet gas lines. The gas pump is of the aquarium variety with negligible temperature buildup from the electromagnet. Temperature control to $\pm 0.1°$ is maintained by circulating bath water through copper coils circling the brass inner wall.

In the manometric studies water-jacketed reference fuel type burets and Krebs solution were used. Fluid level displacement of the gas pump is of the order of 5 mm. Most reproducible results were obtained with the present design for reactions with half-lives between 0.5 and 30 min.

Experimental Techniques. For manometric reactions alone a Teflon plug was inserted in the solution outlet of the reaction cell, and the liquid return line was closed. Substrate was weighed in and 60 ml of slightly acidified stock solution (pH 3.50) was added. With cover and connections in place the reaction atmosphere was bubbled through for 0.5 to 1 hr. After closing off the system to the external atmosphere, the bubbler was started. When the fluid level in the open arm stabilized, a "shot" of NaOH, estimated in advance to be sufficient to bring the system to reaction pH, was added manually with the syringe. The syringe was then clamped on the autotitrator drive unit and the pH control switched on. Fluid level readings were taken at 15- or 30-sec intervals initially and converted into standard conditions using an external barometer.

Analytical Procedure for 3,5-Di-t-butyl-o-benzoquinone. 3,5-Di-*t*-butyl-*o*-benzoquinone absorbs strongly between 390 and 420 mμ and under the experimental conditions (pH <11.0) the hydroxy adduct[23] and the semiquinone do not interfere. The value of ϵ_M for the *o*-quinone at 404 mμ is $1.58 \times 10^3\ M^{-1}\ cm^{-1}$ in 0.10 *M* KNO_3, 50% methanol, and the Beer's law plot of absorbance *vs.* concentration is linear through 1.22×10^{-3} *M* *o*-quinone.

Analytical Procedure for Hydrogen Peroxide. Aliquots of 25 ml of the reaction mixture were taken after quenching the solution with acid to stop the autoxidation and were extracted twice with equal volumes of dichloromethane. The acidified methanol–water layer showed no appreciable visible or uv absorption to 220 mμ. The extracted aqueous layer was titrated with 0.974 *N* Ce(IV) with ferroin as an indicator.[24] A small correction (<1.5%) was applied for the peroxide lost to the organic layer by assuming the solubility of hydrogen peroxide and water were the same in the organic component.[25] Reproducibility with Ce(IV) was $\pm 1\%$.

Analytical Procedure for 3,5-Di-t-butyl-o-benzosemiquinone. Free-radical species were observed in kinetic runs on the autoxidation using esr spectroscopy. When the spectrum was magnified, it was identified positively to be that of 3,5-di-*t*-butyl-*o*-benzosemiquinone radical ion.[15] No other radicals were observed.

(23) C. A. Bishop and L. K. J. Tong, *Tetrahedron Lett.*, **41**, 3043 (1964).

(24) I. M. Kolthoff and R. Belcher, "Volumetric Titrations," Vol. III, Interscience Publishers, New York, N. Y., 1957, pp 456, 465.

(25) J. Hollo and A. Wieg, *Chem. Abstr.*, **49**, 13701*i* (1955); *Budapesti Musz. Egyet. Mizograzd. Kem. Technol. Tansz. Evk.*, **3–8**, 78 (1952–1954); *Chem. Ind.* (London), **20**, 120 (1942).

Table I: Dependence of k_{obsd} on $[H^+]$[a]

−Log $[H^+]$[b]	Mol of O_2 uptake × 10^3	Mol of 35DTBQ[c] × 10^3	Mol of H_2O_2[c] × 10^3	Reaction time, min	$10^2\alpha_1$[d]	$10^7\alpha_2$[d]	10^4k_{obsd},[e] min^{-1}
8.00	4.00	3.98	3.48	14	0.440	0.0088	0.717
8.10	5.26	5.03	4.08	14	0.566	0.0126	0.931
8.22	4.92	4.84	4.34	14	0.733	0.0243	1.002
8.35	6.22	5.94	5.16	14	0.990	0.0442	1.359
8.36	6.28	5.75	4.62	14	0.996	0.0456	1.410
8.38	7.25	7.15	5.46	14	1.05	0.0504	1.450
8.49	6.60	6.24	5.34	12	1.36	0.0839	1.555
8.64	6.02	5.81	5.02	9	1.79	0.1555	1.73
8.87	7.64	7.15	5.90	16	3.17	0.468	2.04
8.93	7.80	6.00	5.48	14	3.96	0.736	2.80
9.19	7.82	5.06	4.25	16	6.81	2.25	3.71
9.24	7.52	5.92	4.75	12	6.95	2.83	3.97
9.34	10.15	8.54	4.26	12	8.79	3.84	4.10
9.46	10.02	6.89	1.56	12	11.3	6.50	5.34
9.56	7.20	4.41	0.78	16	13.8	10.0	5.61
9.67	8.41	3.86	1.43	9	17.1	15.9	6.40
9.70	9.79	3.33	1.10	7	18.1	18.1	6.95
9.83	8.83	3.18	1.40	5	23.1	31.2	7.46
10.10	8.87	3.07	0.49	12	35.4	88.8	10.1
10.25	9.80	3.21	0.70	7.5	44.0	156.0	13.5
10.6	8.87	2.33	0.24	2.5	63.8	506.0	22.1

[a] Experimental conditions: 35DTBP concentration adjusted to 1.00×10^{-2} *M*; 0.10 *M* KNO_3 50 wt % methanol, 25°, 100% O_2 atmosphere. [b] Solvent ion product is 1.34×10^{-14} M^2. [c] Average of two determinations. [d] $\alpha_1 = [HL^-]/[S]$; $\alpha_2 = [L^{2-}]/[S]$. [e] Corrected for solvent partial pressure. Reference to 760 mm, 25°.

In the kinetic runs thin-bore (1.5 mm i.d.) Pyrex glass tubing passing completely through the esr spectrometer cavity was used as a sample cell. The 10-G range from 3386 to 3396 was swept every 0.5 min from the time the solution was brought to reaction pH with base. The free-radical concentration was determined by integrating the area under the absorption peak at moderate signal strength and low to moderate modulation amplitude and comparing it with an area *vs.* concentration plot for 4-carbamido-2,2,5,5-tetramethyl-Δ^3-pyrroline-1-oxyl, a stable free radical, under identical experimental conditions.

Results

Stoichiometry. The stoichiometry of the reaction was determined in two ways. The yield of *o*-quinone product was first studied as a function of experimental pH, where pH is $-\log [H^+]$ in 50% methanol, 0.10 *M* KNO_3.[20] It was observed that in reactions at high alkalinity, the absorbance at 404 mμ reached a maximum height rapidly, and thereafter decreased to a value intermittent between zero and the maximum. The per cent yield of *o*-quinone could then be estimated from 100 times the maximum absorbance divided by the theoretical absorbance which should have been observed for complete consumption of starting material. The results of several runs in the presence and in the absence of 1:100 Mn (II)–35DTBP are shown in Figure 2. Reaction times were >1 hr for low pH runs and this

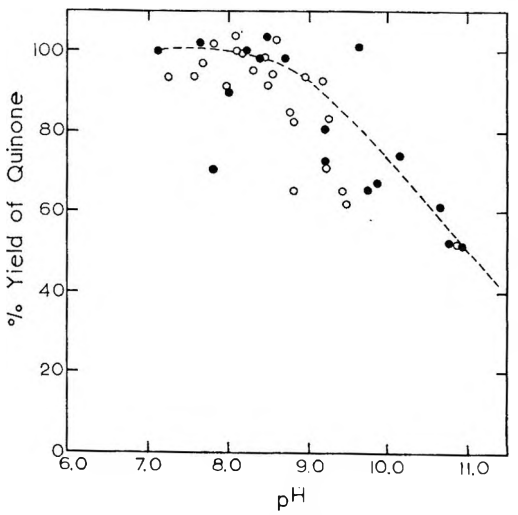

Figure 2. Per cent yield of 3,5-di-*t*-butyl-*o*-benzoquinone *vs.* reaction pH. Spectrophotometric measurements in which A_{max} compared with A_∞ expected, based on $[S]_0$. $[S]_0$ varied from 6.5×10^{-4} to 1.40×10^{-3} *M*. ○, 1:100 Mn(II)–35DTBP; ●, 35DTBP alone. 50% methanol, 0.10 *M* KNO_3, 25°.

ratio of Mn(II) to 35DTBP had no appreciable catalytic effect.

In a second series of experiments O_2 consumed, and *o*-quinone and H_2O_2 formed, were simultaneously determined at different times during reaction. At pH <8.7 and low reaction time the quantity of hydrogen peroxide titrated was within 10% of stoichiometric (Table I) and can be expressed by the equation

$$35DTBP + O_2 \xrightarrow{k_{obsd}} 35DTBQ + H_2O_2 \quad (1)$$

As reaction pH and time are increased the yield of hydrogen peroxide decreases to a greater extent than that of *o*-quinone.

Explanations for these lower yields were sought in terms of a reaction between hydrogen peroxide and the organic components in the system. *o*-Quinone autoxidation does not occur in neutral solution and oxygen uptake ceases coincident with attainment of A_{max} at 404 mμ. Hydrogen peroxide, however, does react with 35DTBQ in mildly alkaline solutions, confirming earlier observations in 75% methanol–water,[5] at rates increasing with alkalinity, but not in neutral solution. In the latter case 50 ml of 1.0×10^{-3} *M* 35DTBQ in 50% methanol, 0.10 *M* KNO_3, under air, to which 0.14 ml of 30% H_2O_2 was added, showed no change at 404 mμ after 1 hr but the yellow quinone color was completely discharged within 30 sec when the solution was made strongly alkaline. Control experiments in mildly alkaline solutions using chromotropic acid impregnated filter paper[26] showed negligible formaldehyde present from solvent oxidation. Highly reproducible results in the analytical determination of H_2O_2, which forms a nontitratable complex with formaldehyde,[27] is further evidence of minimal solvent oxidation.

Hydrogen peroxide may also decompose, either restoring oxygen to the atmosphere or reacting with substrate. In the absence of oxygen no reaction was observed spectrophotometrically between H_2O_2 (tenfold excess) and 35DTBP. Also, only an 8% loss titer over a 10-day period occurred for a peroxide solution in this 0.10 *M* KNO_3 medium with no pyrocatechol present. When 0.10 *M* $KHCO_3$ was added to this solution over half the titer was lost in 5 min. The reactivity of 35DTBP toward H_2O_2 is the same as that reported for 3,5-dimethyl-2-hydroxy-1,4-hydroquinone.[28]

On the basis of these experiments, the data in Table I was tested for the overall stoichiometry expressed by eq 1 together with 2–4, where P is equal to degradation

$$H_2O_2 + 35DTBQ \longrightarrow P \quad (2)$$

$$2H_2O_2 \longrightarrow 2H_2O + O_2 \quad (3)$$

$$H_2O_2 + 35DTBP \longrightarrow 35DTBQ + 2H_2O \quad (4)$$

products. In runs above pH 9.6 this overall stoichiometry satisfies the results exactly.

Dismutation Equilibria. The equilibrium constant (eq 5) for the dismutation reaction was determined

$$2SQ\cdot^- \underset{k_r}{\overset{k_f}{\rightleftharpoons}} Q + L^{2-} \qquad K_{SQ}^{QL} = \frac{[Q][L^{2-}]}{[SQ\cdot^-]^2} \quad (5)$$

from direct potentiometric and esr measurements in the first pK region for 35DTBP ($SQ\cdot^-$ is semiquinone anion, Q is quinone, and L^{2-} is pyrocatechol dianion). Spectrophotometric methods, used frequently in the past,[29-32] were precluded because of the high pK_2 for 3,5-di-*t*-butylpyrocatechol[20] and complications from hydroxide adduct formation[23,29] and/or degradation.[32] The method here also differs from that of Yamazaki and Ohnishi,[33] who determined the rate constant for forward and back dismutation reaction of *p*-benzosemiquinone by esr, and that of Smith and Carrington,[34] who studied dismutation of the pyrocatechol radical in a similar way.

The appropriate material balance equations were combined to give

$$K_{SQ}^{QHL} = \frac{\left(T_Q - \frac{[SQ\cdot^-]}{2}\right)\left(T_L - \frac{[SQ\cdot^-]}{2}\right)}{[SQ\cdot^-]^2[H^+](K_2^H[H^+] + 1)} \quad (6)$$

where K_{SQ}^{QHL} is a constant for the overall reaction

$$H^+ + 2SQ\cdot^- \rightleftharpoons HL^- + Q \quad (7)$$

A value of 3.75×10^{13} M^{-1} was determined for K_{SQ}^{QHL} from two runs of 3.42×10^{-3} *M* *o*-quinone and two different substrate concentrations. Using 14.7 for log K_1^H,[4] K_{SQ}^{QL} for eq 5 is 7.5×10^{-2}, of the same order of magnitude as for the more stable *p*-benzosemiquinones.[29] By combination with log K_2^H the equilibrium constant $K_{SQ}^{QH_2L}$ for the process

$$2H^+ + 2SQ\cdot^- \overset{K_{SQ}^{QH_2L}}{\rightleftharpoons} H_2L + Q \quad (8)$$

is found to be 8.48×10^{23} M^{-2}. These are the first reported dismutation constants involving an *o*-quinone radical anion.

Rapid-flow esr experiments at pH 7.6 and 8.6 in 0.1 *M* KHP buffers were used to obtain estimates of k_r and k_f, respectively. These were found to be

$$k_r = 4 \times 10^7\ M^{-1}\,sec^{-1} \text{ and } k_f = 1.0 \times 10^9\ M^{-1}\,sec^{-1}$$

Manometric Runs. Tabulations of initial rate constants, corrected for external atmospheric pressure and solvent partial pressure, as a function of pH and substrate concentration appear in Tables I and II. Reported rate constants have been corrected for solvent partial pressure, about 10 ± 1% of atmospheric for 50% methanol, by division by $(P_{atm} - p_{solv})/(P_{atm})$ where $p_{solv} = 0.485 \times p_{me} + 0.60 \times p_{H_2O}$ at reaction temperature. These factors are derived from known partial pressure data at two temperatures spanning

(26) "Spot Tests in Organic Analysis," 5th ed, Elsevier Publishing Co., Amsterdam, 1956, pp 334, 335.

(27) B. L. Dunicz, D. D. Perrin, and D. W. G. Style, *Trans. Faraday Soc.*, **47**, 1210 (1951).

(28) J. F. Corbett, *J. Chem. Soc., C*, 611 (1967).

(29) C. A. Bishop and L. K. J. Tong, *J. Amer. Chem. Soc.*, **87**, 501 (1965).

(30) H. Diebler, M. Eigen, and P. Matthies, *Z. Naturforsch.*, **16b**, 629 (1961).

(31) N. K. Bridge and G. Porter, *Proc. Roy. Soc.*, **A244**, 276 (1958).

(32) J. H. Baxendale and H. R. Hardy, *Trans. Faraday Soc.*, **49**, 1433 (1953).

(33) I. Yamazaki and T. Ohnishi, *Biochim. Biophys. Acta*, **112**, 469 (1966).

(34) I. C. P. Smith and A. Carrington, *Mol. Phys.*, **12**, 439 (1967).

Table II: Dependence of k_{obsd} on [35DTBP][a]

Mol of 35DTBP × 10^3	Mol of O_2 uptake × 10^3	Mol of 35DTBQ[b] × 10^3	Mol of H_2O_2[b] × 10^3	Reaction time, min	$10^1 k_{obsd}$,[c] min^{-1}
2.41	1.81	1.85	1.70	7	2.19
3.48	1.84	1.64	1.64	5	1.79
4.26	2.74	2.77	2.65	12	1.98
4.59	2.58	2.69	3.09	12	2.20
4.78	2.72	2.62	2.60	5	2.10
6.57	4.55	4.43	4.30	7	1.72
6.95	5.50	5.44	4.85	12	2.15
10.48	5.45	...	4.89	10	2.25
14.2	5.33	5.86	5.10	12	1.03
19.1	9.68	9.52	6.50	12	2.23
25.0	8.43	6.04[d]	7.61	12	1.30
39.8	15.6	5.25[d]	13.3	12	1.59
				Av	1.88

[a] Experimental conditions: pH 8.55, 0.10 *M* KNO_3, 50% methanol, 25°, 100% O_2 atm. [b] Average of two readings. [c] Corrected for solvent partial pressure by division of k_{obsd} by $(P_{atm} - p_{solv})/P_{atm}$. [d] Precipitate present.

25°.[35] Rate constants are reported for reactions at 25°, 760 mm.

Rate constants for disappearance of H_2L, HL^-, and L^{2-} forms may be calculated from the pH dependence of the reaction. If the concentrations of HL^- and L^{2-} are insignificant with respect to that of H_2L, we have

$$k_{obsd} = k_0 + (k_1 - k_0)\alpha_1 + (k_2 - k_0)\alpha_2 \qquad (9)$$

where k_0, k_1, and k_2 are the respective first-order rate constants and α_1 and α_2 are molar fractions of substrate present as monoanion and dianion. A plot of k_{obsd} (Table I) *vs.* α_1 is linear up to $\alpha_1 = 0.14$. The direct determination of k_2 is impossible with the present experimental arrangement even at lower [35DTBP], because this rate constant is too high. Consequently, k_0 and k_1 were determined graphically to be 5.6×10^{-2} and 4.2×10^0 min^{-1}, respectively, and k_2 was estimated to be 7×10^3 min^{-1} from a least-squares fit of the data in Table I to eq 9. This value for k_2 is only an estimate.

The results in Table II indicate that 35DTBP disappearance is first order over the concentration range 2.4×10^{-3} to 4.0×10^{-2} *M*. Above $[35DTBP]_0 = 2.0 \times 10^{-2}$ *M* and at pH 8.55 *o*-quinone is salted out of solution.

Reactions at different oxygen pressures were run at different alkalinities between pH 8.25 and 9.75. The initial rate constants k_0' were divided by those obtained from runs under 100% pressure (Table I) at the same pH and the average results at each oxygen pressure appears in Table III. The constant k_{obsd} can be seen to be a linear function of oxygen pressure from 1 atm to considerably below 0.60 atm.

Combined First- and Second-Order Kinetics. Manometric runs showed pronounced deviation from the expected first-order kinetics with time. The effect is shown clearly in typical runs in Figure 3. Here n_{O_2} represents the mole fraction of 35DTBP unreacted, based on the assumption that the ratio of 1 mol of O_2/mol 35DTBP reacting (eq 1) holds. For all runs at high alkalinities good linear plots were obtained for more than one half-life. At alkalinities below pH 9.5 the plots show curvature indicating a decrease in the net rate of oxygen uptake relative to first-order kinetics with time. 35DTBQ did not inhibit the reaction, based on spectrophotometric experiments. Going to 68% (wt/wt) CH_3OH, changing ionic strength and 35DTBP concentration, did not remove the curvature effect.

Table III: Dependence of k_{obsd} on Oxygen Pressure[a]

% Oxygen in atmosphere[b]	Ratio k_0'/k_{obsd}[c]
100.0	...
80.1	0.820
59.8	0.586
20.9	0.309

[a] Experimental conditions: manometric technique, 1.0×10^{-2} *M* 35DTBP, 0.10 *M* KNO_3, 50% methanol, 25°. [b] Corrected for solvent partial pressure. [c] k_0' is the initial first-order rate constant from runs in less than 100% oxygen atmosphere; k_{obsd} is the initial first-order rate constant from runs at same pH in 100% oxygen atmosphere (data in Table I), average of five runs each atmosphere.

Replots of the experimental points as dx/xdt *vs.* x, where x is the concentration of unreacted substrate, were linear (examples, inset in Figure 4) in all cases. This suggested the following rate law

$$-\frac{dx}{dt} = (k' - k''x)x \qquad (10)$$

Two general schemes could be used to explain these kinetics. For some reason preequilibrium conditions may not be maintained during the reaction and α_1 and α_2 decrease with time. For the region below pH 8.7 (eq 11) where $(k_2 - k_0)\alpha_2$ does not contribute significantly

$$-\frac{dx}{dt} = [k_1 + (k_1 - k_0)\alpha_1]x \qquad (11)$$

to the kinetics based on known K_n^H for 35DTBP[4] and values for the rate constants determined above. Assume $\alpha_1 = f(x)$, and since $\alpha_1 \to 0$ before $x \to 0$ (Figure 3), $\alpha_1 = \beta(x_0 - x_\infty)$ where $\beta = \alpha_{1,0}/(x_0 - x_\infty)$ and subscripts 0 and ∞ are for times $t = 0$ and t when $\alpha_1 = 0$, respectively. When $\alpha_1 = 0$, a limiting rate, $-dx/dt = k_0x$, should be observed, but experimental verification of this is complicated by a small amount of H_2O_2 decomposition which becomes relatively significant as the reaction progresses. Therefore the hypothesis must be tested in the region where k_{obsd} varies ($t = 0$ to 15 min)

(35) "International Critical Tables," Vol. III, McGraw-Hill Publications, New York, N. Y., 1928, p 290.

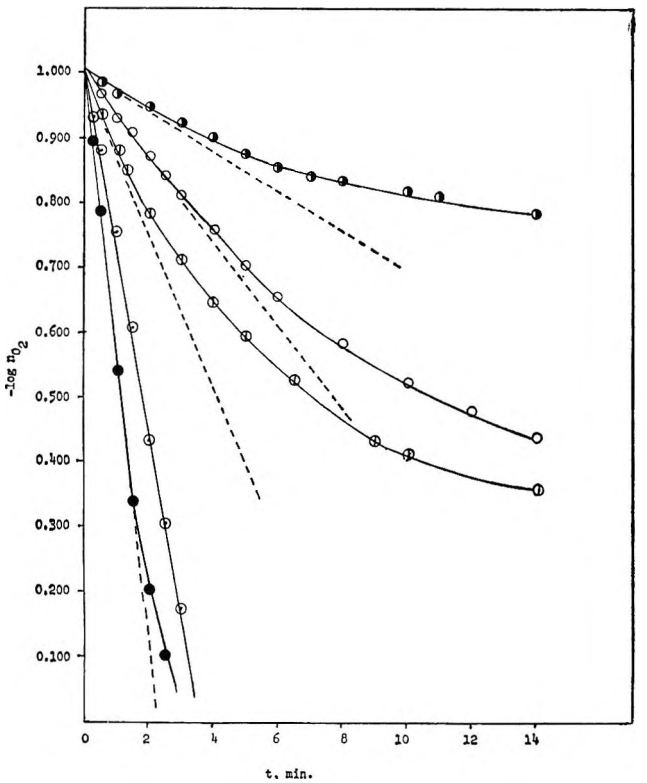

Figure 3. Manometric runs. $-\text{Log } n_{O_2}$ *vs.* reaction time, in min n_{O_2} based on theoretical consumption of O_2 assuming eq 1 holds exclusively. ◑, pH 8.00; ○, pH 8.38; ⊕, pH 8.87; ⊙, pH 9.67; ●, pH 10.1. 50% methanol, 0.10 *M* KNO_3, 25°. ---- Theoretical first-order plots.

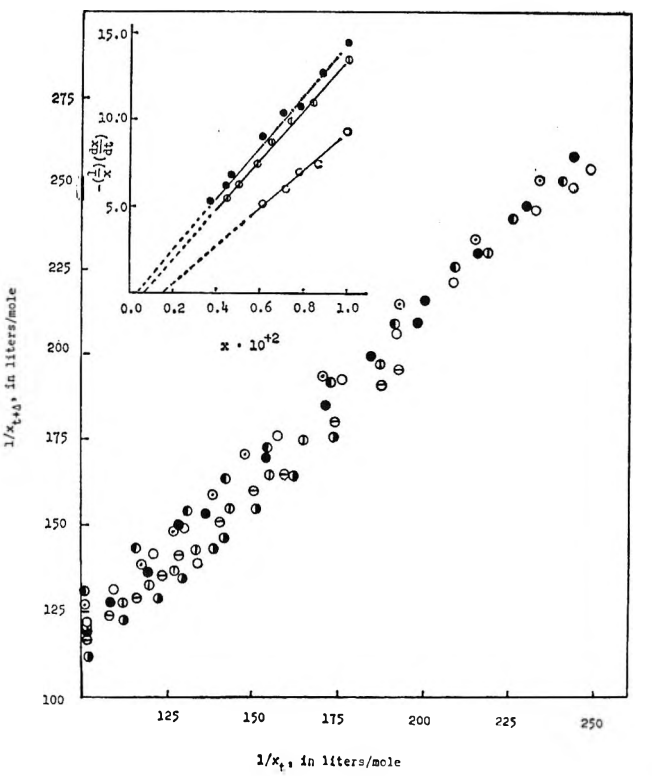

Figure 4. Manometric runs below pH 8.5 (Table I). $(1/x_{t+\Delta})$ *vs.* $(1/x_t)$, in M^{-1}. ◑, pH 8.00; ●, pH 8.10; ○, pH 8.22; ⊕, pH 8.35; ⊖, pH 8.36; ⊙, pH 8.38; ◐, pH 8.49. Δ = 1 min. Inset: $1/x(dx/dt)$ *vs.* x, x = unreacted [35DTBP]. Data from Table I. ○, pH 8.10; ⊕, pH 8.35, ●, pH 8.38.

as follows. Substituting α_1 in (10), letting $(k_1 - k_0) = \gamma k_0$, integrating, and rearranging, one obtains

$$\frac{1}{x} = \frac{Be^{k_0(1-\gamma\beta x_\infty)t} - \gamma\beta}{1 - \gamma\beta} \qquad (12)$$

where B is the constant of integration. If now $(1/x)$ is differentiated at t and constant intervals, Δ, and the partials are obtained by division, then

$$\frac{\partial(1/x_{t+\Delta})}{\partial(1/x_t)} = e^{k_0(1-\gamma\beta x_\infty)\Delta} \qquad (13)$$

Plotting $1/x_{t+\Delta}$ against $1/x_t$ at different Δ should yield a family of straight lines with slopes given by (14). In Figure 4 all runs below pH 8.5 are so treated for Δ = 1 min, and the plots are linear with slopes between 0.92 and 1.03. No trends are observed and the average of the slopes is 0.96. The observed linearity is taken as a further test of the correctness of eq 10 in describing the kinetics. (Table IV lists the results expected from $1/x_{t+\Delta}$ *vs.* $1/x_t$ plots. Only combined first- and second-order kinetics satisfy the observed reaction rates.) The narrow range of slopes (within experimental error) reflects the relative insensitivity of $\beta_{x\infty}$ over the narrow pH range studied.

For systems which exhibit good kinetic reproducibility with time, suitable for computer analysis, the above approach has an advantage over logarithmic treatments.[36] because the iterative step, based on preliminary estimates of x_∞, is eliminated. Here, x_∞ can be determined directly from the relationship

Table IV: $1/x_{t+\Delta}$ *vs.* $1/x_t$ Plots for Various Rate Laws[a]

Order	Rate expression	$\partial(1/x_{t+\Delta})/\partial(1/x_t)$
0	$-\frac{dx}{dt} = k$	$\left\{\frac{x_0 - k(t+\Delta)}{x_0 - kt}\right\}^{2}$ [b]
1	$-\frac{dx}{dt} = kx$	$e^{+k\Delta}$ [c]
2	$-\frac{dx}{dt} = kx^2$	1.0
Combined 0 and 1	$-\frac{dx}{dt} = k_0 + k_1x$	$\frac{(Be^{-k_1t} - k_0)^2}{(Be^{-k_1(t+\Delta)} - k_0)^2}$ [b]
Combined 1 and 2	$-\frac{dx}{dt} = (k_0 + k_1x)x$	$e^{k_0(1-\gamma\beta x_\infty)\Delta}$

[a] x is the mole fraction of the reactant. [b] Not constant; B is the constant of integration. [c] k may also equal $k_{obsd} - k_{inh}$, where k_{inh} is a first-order inhibition rate constant. [d] $\gamma = (k_1 - k_0)/k_0$; $\beta = \alpha_{1,0}/(x_0 - x_\infty)$ for the case where α_1 changes with time; or $k_1 - k_s x_0$, where k_i = initial autoxidation rate constant and k_s = rate constant for side reaction, may also describe results.

(36) K. J. Pedersen, *Acta Chem. Scand.*, 6, 285 (1952).

$$x_\infty = \{k_0 - 2.303 \log (\text{slope})\}x_0/\{k_{obsd} - 2.303 \log (\text{slope})\} \quad (14)$$

(slope from eq 13) and plots of k_{obsd} *vs.* $(x - x_\infty)$ should be linear with y intercept k_0. These plots were made for runs at low pH and, while there was some scatter in the results, the average intercept was 5.3×10^{-2} min^{-1}. Considering the lack of sensitivity under the experimental conditions, this agreement must be considered fortuitous.

One may equally well assume that a side reaction involving one of the products is occurring. Thus

$$-\frac{dx}{dt} = \{k_i - k_s(x_0 - x)\}x \quad (15)$$

where k_i = initial first-order rate constant for oxygen uptake, k_s = rate constant for the unknown reaction, and $(x_0 - x)$ is the product concentration. If k_s is pH independent, the ratio k_i/k_s increases with increasing alkalinity, and rate behavior approaches first-order kinetics throughout the entire run. This is qualitatively consistent with the results in Figure 3. Such a side reaction apparently does not come about by second-order decomposition of H_2O_2, restoring O_2 to the atmosphere, since this is inconsistent with linear k_{obsd} *vs.* x plots. Also, the rate of H_2O_2 decomposition was found to be too low to account for the observed curvature in Figure 3 under identical conditions. Similarly, 35-DTBP dimerization would show $-dx/xdt$ *vs.* x plots which intersect the origin, but this is clearly not the case (Figure 4, inset).

Table V: Semiquinone Yields in Kinetic Runs Compared with Predicted[a]

10^2[35DTBP]	pH	10^6[35DTBSQ] (max obsd)	10^6[35DTBSQ] (calcd)	% of calcd value
2.216[b]	9.10	2.48	1.462	170
2.487[b]	9.44	4.98	3.38	140
2.727[b]	10.00	13.73	12.40	110
2.988[b]	10.06	12.28	15.15	80
1.196	11.06	40.6	30.3	130
0.972	11.15	(36.1)[c]	28.2	130

[a] Experimental conditions: 0.10 *M* KNO_3, 50% methanol, 25°, 100% O_2 atmosphere. [b] Precipitate present. [c] Estimated value.

Electron Spin Resonance Runs. Semilogarithmic plots of [35DTBSQ] in the kinetic runs with those calculated from eq 16 is made in Table V on the assumption that dismutation is established faster than autoxidation proceeds. Maximum [35DTBSQ] should be observed at the halfway point of the autoxidation ($t_{1/2}$), *i.e.*

$$[35DTBSQ] = \left(\frac{(T_L/2)^2}{(1 + K_1^H[H^+] + K_1^H K_2^H[H^+]^2)7.5 \times 10^{-2}}\right)^{1/2} \quad (16)$$

when [35DTBP] = [35DTBQ]. There is fair agreement between calculated and observed values for $[35DTBSQ]_{max}$ at most alkalinities, but there is noticeable trend toward higher observed values as reaction pH decreases.

Spectrophotometric Runs. A limited number of kinetic runs were also made by following the increase in absorbance at 404 mμ as a measure of *o*-quinone formation. Slopes of tangents to the curves in the initial reaction stages gave first-order rate constants in good agreement with those derived from manometric runs, but the scatter was greater. No induction periods were observed in any runs. A least-squares curve-fitting program for consecutive first-order reactions was applied to data from spectrophotometric runs at high alkalinities without success because of failure to obtain convergence.

Discussion

Pyrocatechol and 35DTBP behave similarly in that all three forms are autoxidizable in solution and monoanion is the principal species undergoing autoxidation under mildly alkaline conditions (pK_1 region). A 125-ml aqueous solution of 0.1 *M* pyrocatechol monoanion has an initial absorption rate of 221 cm^3 of O_2 *M*/min compared with 2760 cm^3 *M*/min for 35DTBP monoanion in 0.10 *M* KNO_3, 50% methanol. No induction periods nor wall effects have been noticed in either study. The two media are sufficiently similar to suggest, in line with electrochemical studies,[37] that 35-DTBP is more readily autoxidizable, but that apart from the difference in rate coefficients, 35DTBP may in fact serve as a satisfactory model for the pyrocatechol to *o*-benzoquinone reaction.

The oxygen uptake kinetics of pyrocatechol and 35-DTBP do differ, however, in that with the latter the rate of oxygen uptake is found to exhibit a second-order decrease with time in moderately alkaline solutions. The effect is associated with the autoxidation system under study, because there was no appreciable difference in rates or time course plots with pyrocatechol using bubble-type and Warburg instruments and because the Mn(II)-catalyzed autoxidation does give the expected first-order oxygen uptake with time.[38]

Side reactions then appear to be responsible for the second-order effect. There is the possibility that at low alkalinities more autoxidizable species (the mono- and dianion) are not replenished fast enough to sustain the initial rate (eq 11–13). The overall autoxidation rate would than fall to that of the least reactive species. This explanation is unlikely because constant alkalinity is maintained, and the rate constant for neutral-

(37) L. Horner and E. Geyer, *Chem. Ber.*, **98**, 2016 (1965); O. Ryba, J. Petranek, and J. Pospisil, *Collect. Czech. Chem. Commun.*, **30**, 2157 (1965); W. Flaig, H. Beutelspacher, H. Reimer, and E. Kalke, *Justus Liebigs Ann. Chem.*, **719**, 96 (1969).

(38) C. A. Tyson and A. E. Martell, manuscript in preparation.

ization and [OH^-] are both high (instant attainment of equilibrium in potentiometric studies).[20] It would appear also that 35DTBP dimerization and H_2O_2 decomposition are ruled out by the rate expression (eq 15). The second-order effect then apparently involves stoichiometric ratios of one of the products with 35DTBP, but the nature of this reaction remains obscure.

A side reaction involving product, particularly if reversible, could lead to low 35DTBQ yields and/or reduced rates at high [35DTBP] in the absence of metal ion catalysts. Positive factors contributing to low *o*-quinone yields are an H_2O_2 reaction with 35DTBQ at high alkalinities (Table I) and shifts in the acid–base buffer equilibrium, resulting in a decrease in [OH^-] with time (over one pH unit with $KHCO_3$). Under some conditions induced H_2O_2 decomposition can increase the rate of product formation and the yield, but reactions reported here (Figure 2) still require more than 1 hr for completion, which is not efficient compared with metal catalysis.[5]

Kinetic and other data were analyzed for the possibility of resolving the 35DTBP → 35DTBQ mechanism. Several reaction pathways are possible after initial electron transfer to oxygen and most of these have been summarized by LuValle and Weissberger.[39] Mechanisms involving semiquinone or *o*-quinone pyrocatechol dimers or reversible adducts cannot be ruled out entirely until the reason for the fall off in uptake rate is determined. Evidence from potentiometric, spectrophotometric, esr (both equilibrium and kinetic experiments), and inhibition (no effect with 35DTBQ added initially) studies is all negative with respect to detection of dimers. In any respect, if they exist, these are side reactions having little bearing on the one-electron, two-electron transfer problem.[17]

Autoxidation of 35DTBSQ does not compete with that of 35DTBP for several reasons. There was no induction period observed in any manometric or spectrophotometric run, a criterion for this reaction pathway to be dominant (*e.g.*, durosemiquinone).[40] The semiquinone concentration would not be greater than that determined by dismutation equilibria (Table V). The disappearance of semiquinone would be first order and pH independent in contrast to what is observed (Figure 5). If autoxidation of semiquinone is fast relative to that of substrate, a condition which must subtend from the availability of other reaction pathways with potentially high rate constants, it is hard to explain why the 35DTBSQ signal in kinetic and product identification studies lasts as long as it does.

The reaction mechanisms applicable are (1) semiquinone is first formed, followed by disproportionation to give 35DTBQ (eq 5, 7, and 8) and (2) the *o*-quinone is first formed in a two-electron transfer reaction, and semiquinone results from the reaction of 35DTBQ with starting material.

A central problem is the disposition of superoxide

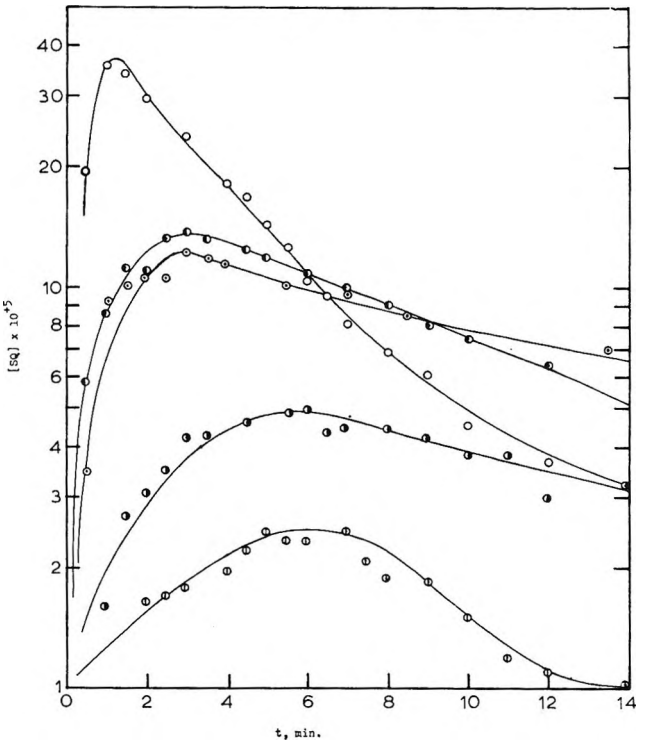

Figure 5. Esr runs. Molar concentration of 35DTBSQ ($\times 10^6$) *vs.* reaction time, in min: ◑, pH 9.10; ◑, pH 9.44; ◐, pH 10.00; ⊙, pH 10.05; ○, pH 11.15. 50% methanol, 0.10 *M* KNO_3, 24–25°.

radicals, likely to be present in mildly alkaline solutions.[41-44] It is most probable that $O_2\cdot^-$ does not have a sufficiently long lifetime in the bulk of the solution to react with semiquinone radicals in subsequent steps, because secondary radical species were not detected in esr work and because $O_2\cdot^-$ disproportionation should be fast in 50% methanol, as it is in aqueous solution ($k = 10^7$–$10^9/M^{-1}$ min.[41,42] That is, for a reaction between 35DTBSQ and $O_2\cdot^-$ to be competitive it must have a rate constant comparable to or greater than that of $O_2\cdot^-$ disproportionation, which means that the former reaction would be indistinguishable kinetically from a two-electron transfer. It should also be noted from Table I that the maximum amount of $O_2\cdot^-$ disproportionation possible, as estimated from the difference in 35DTBQ and H_2O_2 yields for reactions in Table II, quenched at shorter times, is markedly lower. In the absence of quantitative data on the extent of H_2O_2 decomposition

(39) J. E. LuValle and A. Weissberger, *J. Amer. Chem. Soc.*, **69**, 1567 (1947).

(40) T. H. James and A. Weissberger, *ibid.*, **60**, 98 (1938).

(41) J. Rabani, W. A. Mulac, and M. S. Matheson, *J. Phys. Chem.*, **69**, 53 (1965); J. Rabani and S. O. Nielson, *ibid.*, **73**, 3736 (1969).

(42) G. Czapski and L. M. Dorfman, *ibid.*, **68**, 1169 (1964).

(43) G. Czapski and B. H. J. Bielski, *ibid.*, **67**, 2180 (1963).

(44) J. H. Baxendale, W. G. Barb, P. George, and K. R. Hargrave, *Trans. Faraday Soc.*, **47**, 462, 591 (1951).

with substrate not present, which should significantly lower the 15% maximum observed, we must conclude that disproportionation is a minor pathway for disposition of $O_2 \cdot^-$ radicals.

Superoxide radicals then disappear either through a reaction with 35DTBP (termed hereafter, a free-radical mechanism)[45] or with 35DTBSQ (termed an ionic mechanism)[45] or both. It may be demonstrated, using steady-state approximations, that all three possibilities lead to essentially identical rate expressions and are consequently indistinguishable. Also, the high reactivity of 35DTBP toward free radicals was demonstrated by adding a stoichiometric amount of DPPH radicals to an acidified solution and observing the instantaneous bleaching of the purple hydrazyl color.

The esr data were analyzed for the possibility of resolving the mechanism. Several researchers[46] succeeded in doing this with enzyme reactions by showing that k_r' is too small relative to k_{obsd} in eq 17 to account for the observed semiquinone concentrations.

$$\frac{d[SQ \cdot^-]}{dt} = k_{obsd}[35DTBP] + k_r'[35DTBQ][35DTBP] - k_f[SQ \cdot^-]^2 \quad (17)$$

where

$$k_r' = k_r/(1 + [H^+]K_1^H + [H^+]^2K_1^HK_2^H)$$

Comparison of k_r and k_f with k_{obsd} at neutral pH's for autoxidation of 10^{-3} to 10^{-2} M 35DTBP indicates that the mechanism could not be resolved (k_r = 8.5 M^{-1} min^{-1} at pH 7.6, [35DTBP] = 4.0 × 10^{-3} M, whereas k_{obsd} = 6 × 10^{-2} min^{-1} at the same pH). The atmospheric pressure would have to be increased several orders of magnitude to overcome the limited solubility of oxygen and to attain a high enough autoxidation rate to distinguish directly between pathways.

From time to time investigators have alluded to semiquinone as an intermediate in the autoxidation of pyrocatechol, implying that a free-radical mechanism occurs. No evidence for or against this point of view insofar as the *o*-quinone reaction is concerned has been found in the present work, and none has been found in the literature. The work here does not rule out the possibility that sensitive rapid-flow esr measurements in near neutral solutions may provide such evidence for the H_2L species. What is important to recognize in advance is that such kinetic evidence need not hold for the more autoxidizable HL^- or L^{2-} species.

Acknowledgment. The authors gratefully acknowledge the assistance of Dr. Helen Brooks in running the rapid-flow experiments.

(45) J. K. Kochi, *Science*, 155, 415 (1967).

(46) T. Nakamura, "Free Radicals in Biological Systems," M. S. Blois, Jr., H. W. Brown, R. M. Lemmon, R. O. Lindblom, and M. Weissbluth, Ed., Academic Press, Inc., New York, N. Y., 1961, p 169 (laccase); I. Yamazaki and L. H. Piette, *Biochem. Biophys. Acta*, 50, 62 (1961) (ascorbic acid oxidase); I. Yamazaki, H. S. Mason, and L. H. Piette, *Biochem. Biophys. Res. Commun.*, 1, 336 (1959) (peroxidase).

Kinetics of the Gas-Phase Pyrolysis of Poly(difluoramino)fluoromethanes[1]

by J. M. Sullivan, A. E. Axworthy, and T. J. Houser[2]

Rocketdyne, Division of North American Rockwell Corporation, Canoga Park, California *(Received November 14, 1969)*

The gas-phase thermal decompositions of tetrakis(difluoramino)methane, $C(NF_2)_4$, tris(difluoramino)fluoromethane, $FC(NF_2)_3$, and bis(difluoramino)difluoromethane, $F_2C(NF_2)_2$, were investigated over the temperature range 190–460° in stirred flow, tubular, and static reactors. The reactions are first-order, nonchain processes with C–N bond rupture as the rate-determining step in each case. The rate constants are given by the Arrhenius expressions: $C(NF_2)_4$, $k = 10^{16.14} \exp(-40{,}400/RT)$ sec^{-1}; $FC(NF_2)_3$, $k = 10^{16.45} \exp(-48{,}300/RT)$ sec^{-1}; $F_2C(NF_2)_2$, $k = 10^{15.75} \exp(-53{,}600/RT)$ sec^{-1}. The activation energies give a measurement of the bond dissociation energies for the first C–N bond in each molecule. All three compounds appear to decompose directly to NF_2, F, and the corresponding C=NF compound [*i.e.*, $(NF_2)_2C{=}NF$, $F(NF_2)C{=}NF$, and $F_2C{=}NF$, respectively]. Some of the $N_2F_4(NF_2)$ is converted into NF_3 *via* reaction with F atoms. The stable products (N_2, CF_4, NF_3, and CF_3NF_2) are formed from reactions of the C=NF intermediates. Fluorine atom abstraction reactions are shown not to occur. This explains the nonchain character of these decompositions.

Introduction

Recently, considerable kinetic data have become available on the thermal decomposition of perhalogenated polynitroalkanes both in the liquid and gas phases.[3–8] The decompositions of these polynitro compounds are first order with activation energies from 35 to 48 kcal/mol and unusually high Arrhenius *A* factors of $10^{15.5}$ to $10^{18.5}$ sec^{-1}. In general, the initial and rate-determining step is considered to be the rupture of a C–NO_2 bond[5] as postulated by Sullivan and Axworthy.[4]

$$RNO_2 \longrightarrow R\cdot + NO_2$$

The high *A* factors result from the reduced frequencies of the four rocking modes of R and NO_2 relative to the R–NO_2 axis in the transition state.[9]

We have investigated the gas-phase thermal decompositions of the series of poly(difluoramino)methanes—$C(NF_2)_4$, $FC(NF_2)_3$, and $F_2C(NF_2)_2$—using stirred flow, tubular, and static reactors. The rate parameters obtained are quite analogous to the polynitro compounds, again suggesting that the rate-determining step involves the simple cleavage of a C–N bond. By following the product distribution as a function of residence time, we were able to definitely establish that the initial step is C–N bond rupture and gain considerable insight into the processes occurring after the rate-determining step.

Apparatus and Experimental Techniques

Stirred Flow Reactor. A major portion of the data was obtained using a gas-phase, stirred flow reactor.[10,11] In this system the gas to be investigated is passed through a reactor that promotes complete mixing. Under conditions of steady flow, the system reaches a steady state in which the concentrations of the reactant gases and products are uniform throughout the reactor.

The compound to be investigated was contained in a 1.5-ft^3 stainless steel tank as an approximately 1% mixture with helium. The total pressure of the gases within the tank ranged from 30 to 100 psig. The flow rate was controlled using a Nupro fine metering valve. Additives were mixed with helium and introduced from an auxiliary tank.

The construction of the reactor is shown in Figure 1. The body of the reactor was a high-pressure, 90-ml monel bomb. The gases flowed into the center of the reactor through five 0.016-in. diameter orifices (four to the sides and one to the bottom). The reactor was heated electrically, and the temperature was measured with a chromel–alumel thermocouple mounted within the thermocouple well. The flow rate of the exit stream was measured with a soap bubble flow meter from which the gas was vented at atmospheric pressure.

The gases leaving the reactor were analyzed by gas chromatography. The chromatograph was a custom-

(1) This work was supported by the U. S. Air Force and the Advanced Research Projects Agency under Contracts No. AF04(611)-9380, AF04(611)-10544, and ARPA Order No. 24.

(2) Chemistry Department, Western Michigan University, Kalamazoo, Mich.

(3) H. P. Marshall, F. G. Borgardt, and P. Noble, Jr., *J. Phys. Chem.*, **69**, 25 (1965).

(4) J. M. Sullivan and A. E. Axworthy, *ibid.*, **70**, 3366 (1966).

(5) G. M. Nazin, G. B. Manelis, G. N. Nechiporenko, and F. I. Dubovitsky, *Combust. Flame*, **12**, 102 (1968).

(6) H. P. Marshall, F. B. Borgardt, and P. Noble, Jr., *J. Phys. Chem.*, **72**, 1513 (1968).

(7) G. M. Nazin, G. B. Manelis, and F. I. Dubovitsky, *Izv. Akad. Nauk SSSR Ser. Khim.* No. 11, 2631 (1968).

(8) G. M. Nazin, G. B. Manelis, and F. I. Dubovitsky, *ibid.*, No. 12, 2801 (1968).

(9) S. W. Benson, "Thermochemical Kinetics," John Wiley & Sons, Inc., New York, N. Y., 1968.

(10) K. G. Denbigh, *Trans. Faraday Soc.*, **40**, 352 (1944); **44**, 479 (1948); and B. Stead, F. M. Page, and K. G. Denbigh, *Discussions Faraday Soc.*, **2**, 263 (1947).

(11) W. C. Herndon, *J. Chem. Educ.*, **41**, 425 (1964).

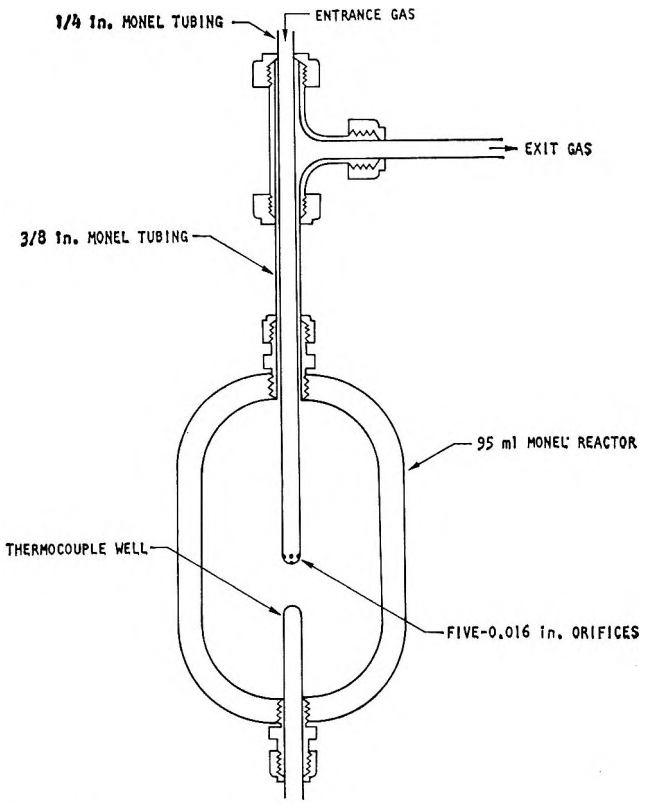

Figure 1. Stirred flow reactor.

built instrument, specifically designed to handle corrosive gases and employed a nickel thermal conductivity detector. Periodic sampling of the exit gas from the reactor, to determine reactant consumption and product formation, was accomplished with a Beckman 104176 gas-sampling valve connected directly between the reactor and the flow meter in the reactor exit stream. The reactor was equipped with a bypass to permit initial concentrations to be measured.

For a single-reactant, n-order reaction in a stirred flow reactor, the concentration of reactant at steady state is given by

$$dN/dt = C_0U - CU - k_nC^nV = 0 \qquad (1)$$

where N is the moles of reactant in the reactor, C_0 and C are the concentrations of reactant in the inlet stream and at the exit, respectively, U is the volume flow rate, V is the volume of the reactor, and k_n the specific rate constant. C_0, C, and U are corrected to reactor temperature. From eq 1

$$(C_0 - C)/C^n = k_n\tau \qquad (2)$$

where $\tau \equiv V/U$ is the average residence time in the reactor.

The utility of the stirred flow reactor is based on the assumption that there is complete mixing within the reactor. A series of experiments was conducted to test the validity of this assumption. If a few Torr of a stable tracer gas in 1 atm of helium is allowed to flow

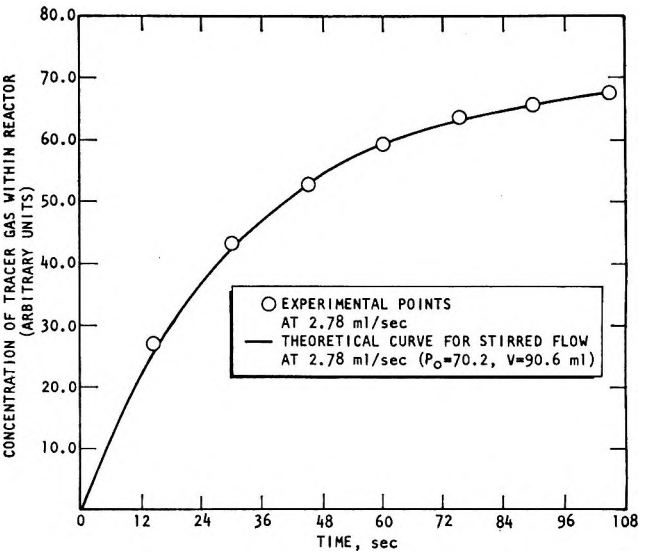

Figure 2. Approach to steady state in stirred flow reactor.

into a stirred flow reactor, which initially contains only helium, the partial pressure of the tracer gas should approach a steady state exponentially according to the equation

$$C = C_0(1 - e^{-t/\tau}) \qquad (3)$$

where the time, t, is measured from the initial response of the recorder. Equation 3 is obtained by integrating eq 1 for $dN/dt \neq 0$ and $k_n = 0$.

Mixing experiments were conducted at room temperature and 1 atm using $FC(NF_2)_3$ at 9 Torr as the tracer gas. The concentration of tracer gas leaving the reactor was monitored continuously by connecting the exit stream from the reactor directly to a thermal conductivity cell. Runs were made at flow rates of 0.29–9.9 ml/sec. In each case, the experimental values fit the theoretical concentrations given by eq 3. The results of a typical room temperature run at 2.78 ml/sec are shown in Figure 2. Experiments at 300° using nitrogen as the tracer gas at flowrates of 0.81–30.1 ml/sec are reported elsewhere[12] for this reactor. The results are again in agreement with eq 3.

Tubular Reactors. Two tubular reactors were employed to extend the range of experimental conditions investigated. The system was the same except that the stirred flow reactor was replaced by one of the tubular reactors.

The first tubular reactor consisted of 366 cm of $^1/_4$-in. monel tubing coiled to fit into a furnace. The internal diameter of the tubing was 0.180 in., and the volume of the heated reactor was 59.2 ml. The interior of the furnace was packed with aluminum foil to ensure even heating of the reactor. The temperature of the reactor was measured with three chromel–alumel

(12) J. M. Sullivan and T. J. Houser, *Chem. Ind.* (London), 1057 (1965).

thermocouples located at the top, center, and bottom of the coil, respectively. The three temperatures were found to agree within 0.7° at 300°. This reactor offered a convenient way of altering the surface-to-volume ratio to investigate the possible heterogeneity of the decomposition reactions. The surface-to-volume ratio of the 60-ml tubular reactor was approximately eight times that of the 90-ml stirred flow reactor.

The second tubular reactor was constructed from $^1/_8$-in. copper tubing. The length of the heated tube was 112 cm and the internal diameter was 0.165 cm; hence, the volume was 2.4 ml. This small reactor was used primarily to investigate the product distributions at much higher temperatures and shorter residence times (10–190 msec) than were obtainable in the larger reactors.

For tubular flow reactors under conditions of plug flow, the integrated rate expression for a first-order reaction is given by

$$k_1\tau = \ln (C_0/C) \qquad (4)$$

Static Reactor. The static reactor consisted of a 160-ml monel bomb connected directly to a Beckman gas chromatographic sampling valve. Samples were taken by evacuating the 1.5-ml sample loop, expanding gases from the reactor into the loop, and rotating the loop into the carrier gas stream of the gas chromatograph. The stirred, constant-temperature bath contained Dow Corning 200 silicone fluid. The Teflon-coated reactor was similar except that it was coated internally with Teflon 851-204 (from aqueous solution) and baked at 250°.

Chemicals. Gaseous samples of $C(NF_2)_4$, $FC(NF_2)_3$, and $F_2C(NF_2)_2$ at purities of 96, 91, and 96%, respectively, were supplied by Minnesota Mining and Manufacturing Co. The impurities consisted primarily of air along with small quantities of decomposition products. Owing to the extreme tendency of these compounds to explode violently, no attempt at further purification was undertaken. However, as will be shown, the impurity contents of these samples are not critical since the decompositions proceed *via* nonchain processes, the rates of which are unaffected by decomposition products and a wide variety of additives.

Samples of $(NF_2)_2C{=}NF$, $F(NF_2)C{=}NF$, $F_2C{=}NF$, and CF_3NF_2 were generously supplied by the Minnesota Mining and Manufacturing Co. and were generally of 90–95% purity. Samples of CF_4, N_2, N_2F_4, NF_3, and the additives F_2, O_2, N_2O_4, and NO were obtained at the highest purities available and used without further purification.

Product Analysis. The products and intermediates of decomposition were identified by trapping them (using slush baths at various temperatures) and comparing their gas chromatographic, mass spectrometric, and infrared characteristics with those of known compounds.

Gas chromatography was the principal technique used to measure the concentrations of reactants, products, and intermediates. The chromatographic columns and conditions used for these analyses are shown in Table I.

Table I: Gas Chromatography Columns and Conditions

	Retention time, min					
Species	Column A[a] 45 ml/min[f]	85 ml/min	Column B[b] 45 ml/min	Column C[c] 60 ml/min	Column D[d] 60 ml/min	Column E[e] 60 ml/min
$C(NF_2)_4$	20	9				
$FC(NF_2)_3$	9					
$F_2C(NF_2)_2$			20	35.5		
$(NF_2)_2C{=}NF$	9					
$F(NF_2)C{=}NF$				31.8		
$F_2C{=}NF$				21.2		
CF_3NF_2				18.4		
N_2F_4				19.9		
N_2				↑	5.2	3.3
CF_4				15.0	0.8	9.8
NF_3				↓	16.3	11.2

[a] 7.5 ft of 30 wt % halocarbon oil on Chromasorb W (acid washed), 25°; products and intermediates gave composite peaks at 3 and 5 min, respectively, at carrier gas flow of 45 ml/min. [b] Column A plus 20 ft of 30 wt % perfluorotributylamine on Celite 345, 25°; products and intermediates gave composite peaks at 15 and 16 min, respectively. [c] 17 ft of 30 wt % halocarbon oil on Chromasorb W (acid washed) plus 40 ft of 30 wt % perfluorotributylamine on Celite 345, −22°; a peak for $FC(NF_2)_3$ was eluted after 1.5 hr but was too broad to be usable. [d] Linde 5A molecular sieve, 25°; CF_4 and NF_3 gave poorly shaped peaks that were not usable. [e] Activated Alumina, −22°. [f] Carrier gas flow rate.

Kinetics of Pyrolysis

Rates and Kinetic Parameters. The thermal decomposition rates of $C(NF_2)_4$, $FC(NF_2)_3$, and $F_2C(NF_2)_2$ were investigated over the temperature range 190–460° using the three types of reactors described, with most of the data being obtained with the stirred flow reactor. Each of these compounds was found to decompose by a first-order process.

The first-order rate constants were calculated from eq 2 and 4 for the stirred flow and tubular reactors, respectively. C_0 and C for each reactant are related to the integrated chromatographic peak areas, A_0 and A, by $C = F_iA$, where F_i is the calibration factor for that species.[13] Since F_i cancels from eq 2 and 4, no calibration is necessary to obtain first-order rate constants.

The first-order nature of the decompositions in the stirred flow reactor is demonstrated in Figure 3, which gives a plot of $(A_0 - A)/A$ *vs.* τ for $C(NF_2)_4$, $FC(NF_2)_3$, and $F_2C(NF_2)_2$ at 232, 338, and 398°, respectively. In

(13) Experiments were conducted to establish that F_i is constant for these compounds over the concentration ranges employed.

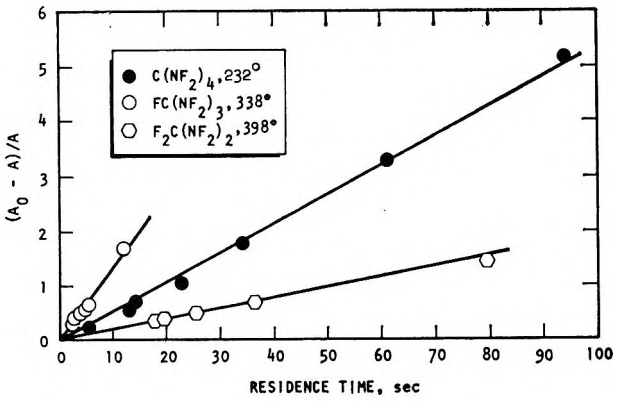

Figure 3. First-order plots.

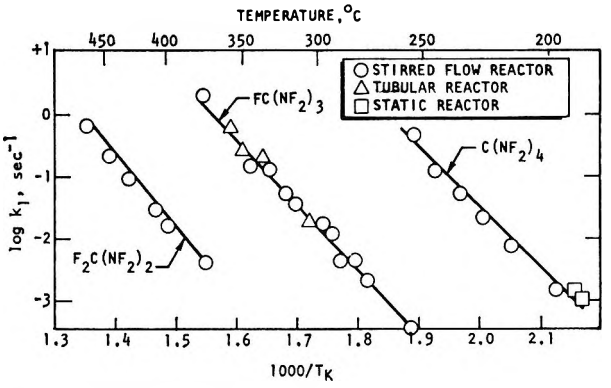

Figure 4. Arrhenius plots.

each case a straight line through the origin was obtained as predicted by eq 2. Significantly poorer fits were obtained for $n = {}^1/_2$ and $n = {}^3/_2$ in eq 2.

The experimental data and calculated first-order rate constants are available elsewhere.[14] The average rate constants obtained at each temperature are shown in the Arrhenius plots of Figure 4. $C(NF_2)_4$ was investigated over the temperature range 189.5–254.3°. The rate constants at 189.5 and 191.5° were obtained using the uncoated and Teflon-coated static reactors, respectively. The remainder of the rate constants for $C(NF_2)_4$ in Figure 4 were obtained with the stirred flow reactor. The rate constants for $FC(NF_2)_3$ over the temperature range 253–377°, obtained with the 90-ml stirred flow reactor and the 60-ml tubular reactor, are also plotted in Figure 4. The rates are in quite good agreement despite the fact the tubular reactor had a surface-to-volume ratio, S/V, approximately eight times that of the stirred flow reactor. The first-order rate constants for the decomposition of $F_2C(NF_2)_2$ in the stirred flow reactor (Figure 4) were obtained over the temperature range 372–457°.

The Arrhenius parameters for the decomposition of $C(NF_2)_4$, $FC(NF_2)_3$, and $F_2C(NF_2)_2$ are presented in Table II. These were obtained by least-squares fits of the flow reactor data to the Arrhenius expression.

Table II: Arrhenius Parameters

Compound	Log A	E, cal/mol
$C(NF_2)_4$	16.14 ± 0.17	40,400 ± 400
$FC(NF_2)_3$	16.45 ± 0.20	48,300 ± 600
$F_2C(NF_2)_2$	15.75 ± 0.17	53,600 ± 400

Influence of Additives upon the Pyrolysis Rates. The first-order rate constants for the thermal decomposition of $FC(NF_2)_3$ were found to be unaffected by the addition of relatively high concentrations of N_2F_4, F_2, O_2, N_2O_4, or NO.[14] In these experiments, the ratios of additive concentration to $FC(NF_2)_3$ concentration were, respectively, 1.2, 0.6, 0.1, 0.8, and 0.4. The lack of effect of N_2F_4, which is completely dissociated to NF_2 radicals at reaction temperature,[15] indicates that NF_2 does not abstract F atoms from $FC(NF_2)_3$. It was also found that the addition of the less stable $FC(NF_2)_3$ to $F_2C(NF_2)_2$ does not affect the decomposition rate of $F_2C(NF_2)_2$.

Homogeneity of Decomposition. Four factors indicate that a heterogeneous component was not contributing to the rate-determining process in the thermal decompositions of these species. (1) The rates were unaffected by continued passivation of the reactors over a period of several months. (2) The observed Arrhenius parameters are higher than normally expected for a heterogeneous reaction.[16] (3) The rates of $C(NF_2)_4$ decomposition were the same in Teflon-coated and uncoated static reactors and were in agreement with the rates obtained in the stirred flow reactor. (4) The rate of $FC(NF_2)_3$ pyrolysis was the same in tubular and stirred flow reactors even though the S/V ratio of the former was eight times that of the latter.

Bond Dissociation Energies. All available data suggest that the initial and rate-determining step in each of these decompositions involves the rupture of a C–N bond

$$F_xC(NF_2)_{4-x} \longrightarrow F_x\dot{C}(NF_2)_{3-x} + \cdot NF_2 \qquad (5)$$

Because the reverse of eq 5 would be expected to have close to zero activation energy, the measured activation energies (Table II) for the decomposition of $C(NF_2)_4$, $FC(NF_2)_3$, and $F_2C(NF_2)_2$ yield a direct measure of the bond dissociation energy for the first C–N bond in each of these molecules. These activation energies are plotted in Figure 5. It may be seen that linear extrapolation to the next member of the series, CF_3NF_2,

(14) The experimental data have been deposited as Document No. NAPS-00898 with the ASIS National Auxiliary Publication Service, c/o CCM Information Corp., 909 3rd Ave., New York, N.Y. 10022. Remit $1.00 for microfiche or $3.00 for photocopies payable to CCMIC-NAPS.

(15) "JANAF Thermochemistry Tables," Dow Chemical Co., Midland, Mich.

(16) J. M. Thomas and W. J. Thomas, "Introduction to the Principles of Heterogeneous Catalysis," Academic Press, New York, 1967, p 55.

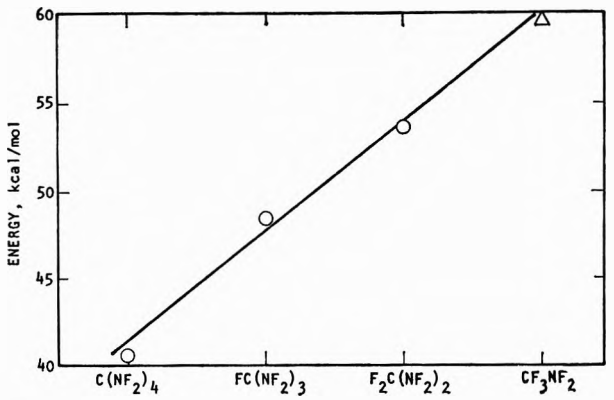

Figure 5. Comparison of activation energies for $C(NF_2)_4$, $FC(NF_2)_3$, and $F_2C(NF_2)_2$ with the bond dissociation energy of CF_3NF_2.

would predict a C–N bond of about 60 kcal/mol. The C–N bond in CF_3NF_2 measured by the electron impact technique[17] is 59.7 as shown in Figure 5. It appears, therefore, that the replacement of an NF_2 group by an F atom increases the bond dissociation energy for the first C–N bond by about 6.3 kcal/mol.[18] This explains the marked differences in the thermal stabilities of these compounds.

Products of Pyrolysis

Product Distribution as a Function of Residence Time. The product distributions from the species $C(NF_2)_4$, $FC(NF_2)_3$, and $F_2C(NF_2)_2$ at 224, 339, and 424°, respectively, are presented in Figures 6, 7, and 8 as a function of residence time. In these initial experiments, gas chromatographic calibration factors were not measured, and column *C* was employed which did not separate N_2, CF_4, and NF_3 (Table I). Therefore, the concentration of each entity is indicated by its gas chromatographic peak area. Hence, although Figures 6, 7, and 8 show the effect of residence time on product distribution, they give only approximate indications of the relative concentrations of the various species. In subsequent experiments, calibration factors were determined and columns were developed to separate N_2, CF_4, and NF_3. It was found that all three are major products from each of these reactions. The analytical techniques employed in this investigation were not capable of detecting F_2; it is possible that F_2 also is a product.

Products from $C(NF_2)_4$. It may be seen from Figure 6 that the concentrations of the species N_2, NF_3, CF_4, and CF_3NF_2 rise continuously with residence time in a manner indicating that they are stable products. The compounds $(NF_2)_2C{=}NF$, $F(NF_2)C{=}NF$, $F_2C{=}NF$, and N_2F_4 rise to a maximum and then decrease in a manner indicating that they are either thermally unstable products or are reaction intermediates (*i.e.*, react with radicals or other molecules formed in the pyrolysis). Throughout this paper, these species will be referred to as "intermediates."

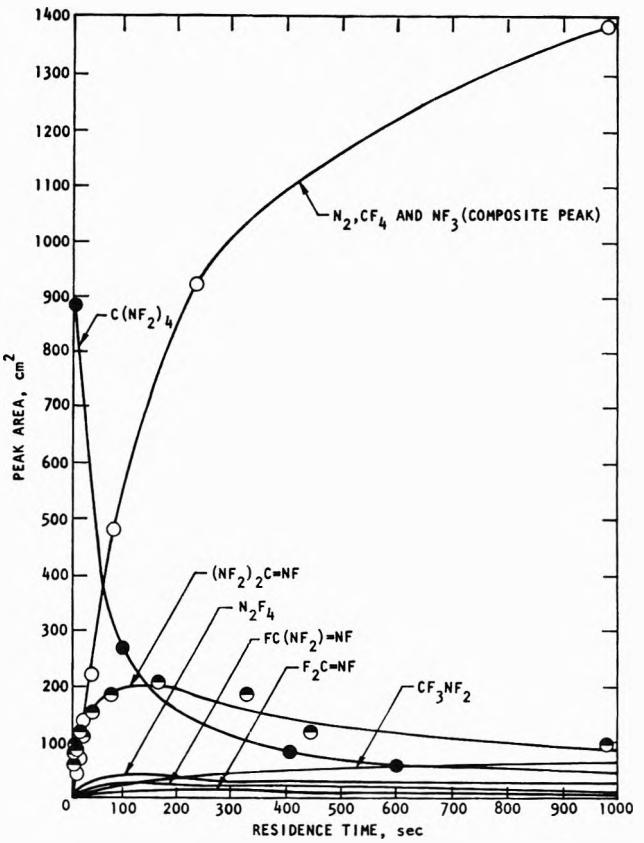

Figure 6. Product distribution from $C(NF_2)_4$ as a function of residence time at 224°.

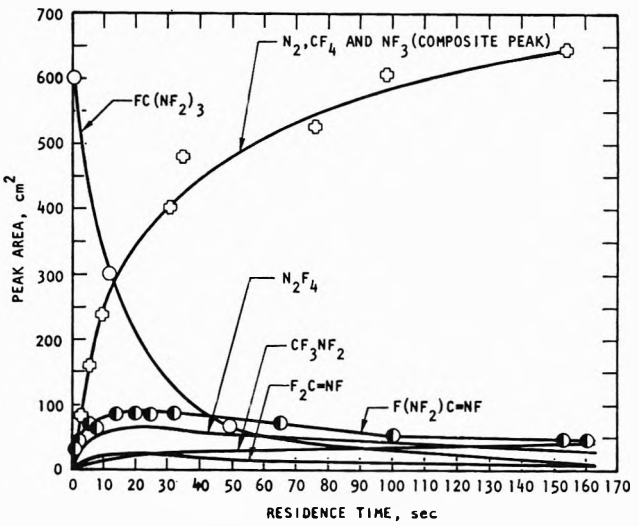

Figure 7. Product distribution from $FC(NF_2)_3$ as a function of residence time at 339°.

Neither $FC(NF_2)_3$ nor $F_2C(NF_2)_2$ was detected as a product of this reaction, even though both of these species are thermally more stable (Figure 4) than $C(NF_2)_4$. This has important implications in the mechanism that we propose.

(17) Unpublished results from Rohm and Haas Co.

(18) Nazin, *et al.*,[7] found that the replacement of NO_2 by F increased D(C–N) by 4–6 kcal/mol in the polynitrofluoroalkanes.

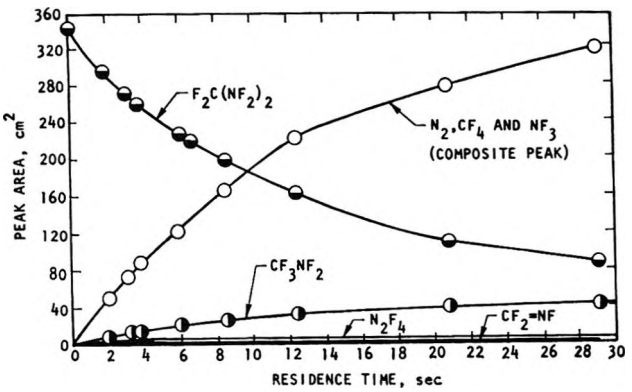

Figure 8. Product distribution from $F_2C(NF_2)_2$ as a function of residence time at 424°.

Products from $FC(NF_2)_3$. The products from $FC(NF_2)_3$ at 339°, presented in Figure 7, are identical with those from $C(NF_2)_4$ except for the absence of $(NF_2)_2C{=}NF$. The stable products are N_2, NF_3, CF_4, and CF_3NF_2 (minor product), while the intermediates are $F(NF_2)C{=}NF$, $F_2C{=}NF$, and N_2F_4. The behavior of the intermediates with residence time is quite analogous to the $C(NF_2)_4$ case. It was definitely established that $F_2C(NF_2)_2$ is not present either as an intermediate or product. $F_2C(NF_2)_2$ is more stable than $FC(NF_2)_3$, and it was shown that the addition of $FC(NF_2)_3$ did not influence the rate of $F_2C(NF_2)_2$ decomposition. Thus, if $F_2C(NF_2)_2$ were formed, it would have been detected.

Products from $F_2C(NF_2)_2$. As seen from Figure 8, the products from $F_2C(NF_2)_2$ at 424° are identical with those from $FC(NF_2)_3$ except for the absence of $F(NF_2)$-$C{=}NF$. The products are N_2, CF_4, NF_3, and CF_3NF_2 (minor product), while the intermediates are $F_2C{=}NF$ and N_2F_4. N_2 is a major product from $F_2C(NF_2)_2$ even though the radicals formed during the initial C–N bond rupture contain only one N atom.

Product Distribution at Short Residence Times. In the case of $C(NF_2)_4$ and $FC(NF_2)_3$, considerable information is obtained by examining the product distribution at the shortest residence times employed.

For $C(NF_2)_4$ at 224° the shortest residence time was 4.0 sec. The integrated peak areas (in arbitrary units) for the products and intermediates were $(NF_2)_2C{=}NF$, 50; N_2, CF_4, NF_3 composite, 36; N_2F_4, 6.0; $F(NF_2)C{=}NF$, 3.3; CF_3NF_2, 3.3; and $F_2C{=}NF$, 0. Hence the most abundant species is the double-bonded intermediate $(NF_2)_2C{=}NF$.[19] At this short residence time, the amount of $(NF_2)_2C{=}NF$ in the products is approximately 70% of the $C(NF_2)_4$ which has decomposed.

For $FC(NF_2)_3$ at 339°, the shortest residence time was 0.51 sec. The peak areas were $F(NF_2)C{=}NF$, 20.5; N_2, CF_4, NF_3 composite, 18.4; N_2F_4, 8.3; $F_2C{=}NF$, 2.0; and CF_3NF_2, 0.8. Again, the major species is the corresponding double-bonded intermediate $F(NF_2)C{=}NF$. Approximately 50% of the $FC(NF_2)_3$ which decomposes is recovered as $F(NF_2)C{=}NF$.

At longer residence times the moles of $(NF_2)_2C{=}NF$ and $F(NF_2)C{=}NF$, respectively, recovered per mole of $C(NF_2)_4$ and $FC(NF_2)_3$ decomposed become progressively less (see Figures 6 and 7). The results at short residence times indicate that the formation of the double-bonded intermediates, $(NF_2)_2C{=}NF$ and $F(NF_2)C{=}NF$, is a major initial process in thermal decomposition of $C(NF_2)_4$ and $FC(NF_2)_3$, respectively.

Thermal Stability of N_2F_4. In Figures 6, 7, and 8 the concentration of N_2F_4 is seen to rise to a maximum and then decrease at longer residence times.

The thermal stability of N_2F_4 was measured in the stirred flow reactor to determine whether this behavior might be attributed to thermal instability of N_2F_4. It is recognized, of course, that at these temperatures N_2F_4 is almost completely dissociated to NF_2 radicals, but these radicals recombine to N_2F_4 before reaching the chromatographic column. When an N_2F_4–Hel mixture was passed through the heated reactor, decomposition occurred at temperatures above 550°, but the results were very erratic and nonreproducible indicating a heterogeneous reaction. However, these experiments did demonstrate that N_2F_4 does not decompose at a measurable rate below 550°. Hence, the behavior of N_2F_4 in Figures 6, 7, and 8 cannot be attributed to thermal instability.

Variation of Products and Intermediates with Temperature. The temperature dependence of the yield of the principal intermediates, $(NF_2)_2C{=}NF$ from $C(NF_2)_4$ and $F(NF_2)C{=}NF$ from $FC(NF_2)_3$, was investigated to establish the role of these species in the decomposition mechanism.

Figure 9 shows plots of $(NF_2)_2C{=}NF$ concentration *vs.* per cent $C(NF_2)_4$ decomposed at 198 and 250° for the same initial concentration of $C(NF_2)_4$. These results clearly demonstrate that the observed $(NF_2)_2C{=}NF$ concentrations are strongly temperature dependent, with much more $(NF_2)_2C{=}NF$ being formed at 250 than at 198°. Also, the residence time at which the maximum concentration occurs is shifted to lower per cent decomposition at the lower temperature. At 198°, the maximum occurs at about 17% reaction, while at 250° the maximum occurs at about 59% reaction.

Very similar behavior was observed in the case of $FC(NF_2)_3$ decomposition. Figure 10 gives similar plots for $F(NF_2)C{=}NF$ from $FC(NF_2)_3$ at 303 and 355°. Again, the observed concentration of the principal intermediate is seen to be very strongly temperature dependent. Similary to $C(NF_2)_4$, the maximum concentration occurs at about 18% decomposition at 303°, while at 355° the maximum is shifted to about 70% reaction.

(19) Although the gas chromatographic peak area for $(NF_2)_2C{=}NF$ is larger than for the composite N_2, CF_4, NF_3 peak, the total concentration of N_2, CF_4, and NF_3 is actually higher than $(NF_2)_2C{=}NF$ because the calibration factors, F_i, are higher for the lower molecular weight species.

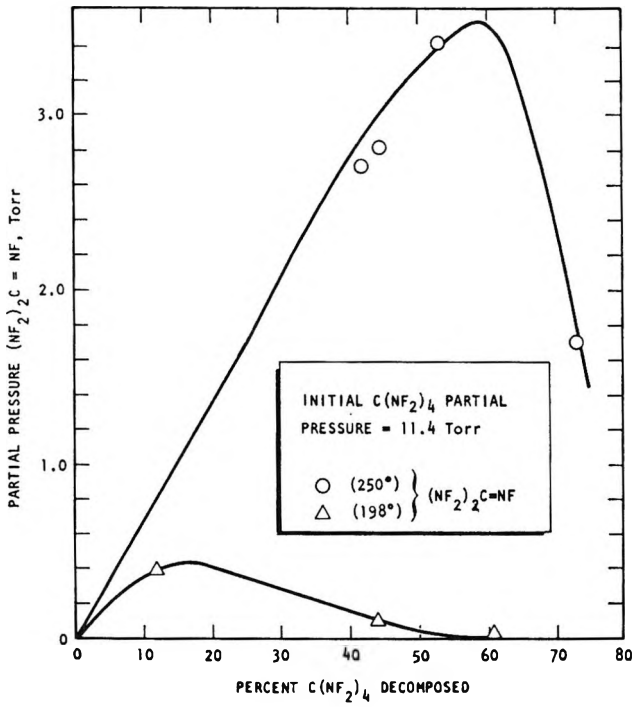

Figure 9. Influence of temperature on formation of $(NF_2)_2C=NF$ from $C(NF_2)_4$.

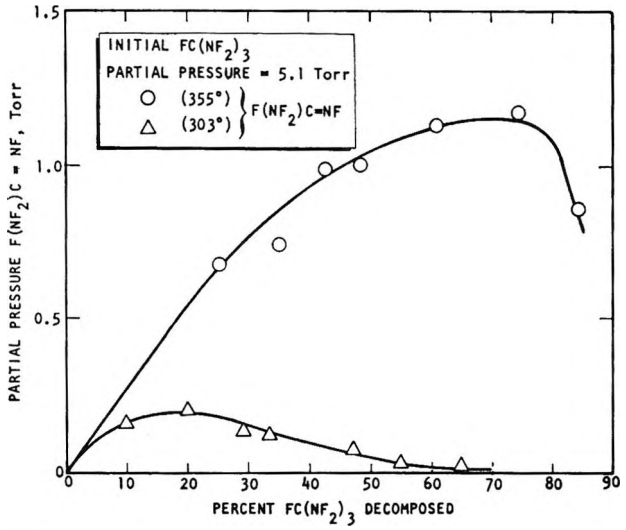

Figure 10. Influence of temperature on formation of $F(NF_2)C=NF$ from $FC(NF_2)_3$.

These results suggest that stable product formation from $FC(NF_2)_3$ should be retarded initially at higher temperatures, because of the increased formation of the principal intermediate, $F(NF_2)C=NF$. That this is indeed the case may be seen by comparing Figures 11 and 12 in which the concentrations of N_2, NF_3, and CF_4 as a function of residence time at 322 and 354°, respectively, are plotted. As seen, higher concentrations of N_2, NF_3, and CF_4 are formed initially per mole of $FC(NF_2)_3$ decomposed at the lower temperature. For example, at 50% decomposition, one-half as much N_2 is ed at 354 as at 322°.

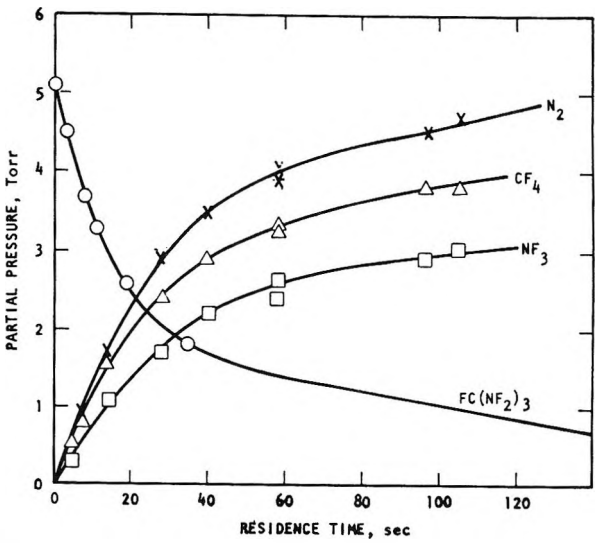

Figure 11. Formation of N_2, NF_3, and CF_4 from $FC(NF_2)_3$ at 322°.

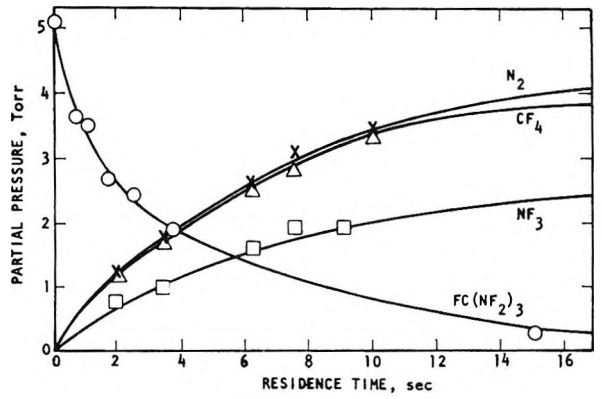

Figure 12. Formation of N_2, NF_3, and CF_4 from $FC(NF_2)_3$ at 354°.

In view of the above results, it appeared of interest to investigate the decomposition of $C(NF_2)_4$ at much higher temperatures and consequently much shorter residence times than were obtainable in the 90-ml stirred flow reactor. For this purpose, the small 2.4-ml tubular reactor was employed.

The results of a series of experiments conducted at 344° and residence times from 7 to 190 msec are presented in Figure 13. $C(NF_2)_4$ is more than 99% decomposed at residence times above approximately 60 msec. The principal products under these conditions are $(NF_2)_2C=NF$, NF_3, and N_2F_4. In agreement with the trend in Figure 9, the concentration of $(NF_2)_2C=NF$ reaches approximately 85% of the initial $C(NF_2)_4$ concentration at this higher temperature and then begins to decompose slowly at longer residence times.

It would appear from Figure 13 that the species present at the second highest concentration is NF_3. It should be noted, however, that N_2F_4 is completely dissociated into NF_2 at this temperature and partial pressure. Thus, the concentration of NF_2 radicals in

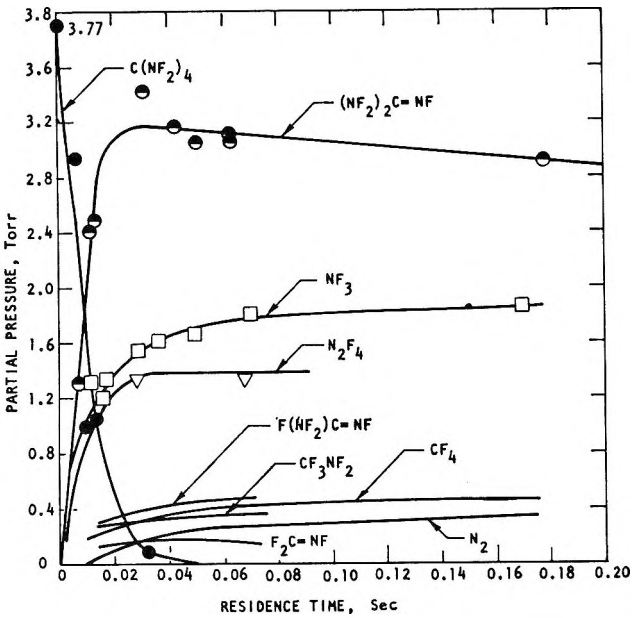

Figure 13. Product distribution from $C(NF_2)_4$ as a function of residence time at 344°.

the reactor is actually greater than that of NF_3. Smaller amounts of $F(NF_2)C{=}NF$, $F_2C{=}NF$, CF_3NF_2, CF_4, and N_2 are also formed under these conditions.

Kinetic Model

Because of the complexity of the products and intermediates which form after the initial C–N bond rupture, additional experiments were required to establish the exact nature of the secondary processes that occur. These results and the overall kinetic processes will be discussed before discussing the mechanism of the individual reactions.

The high concentrations of NF_2 at short residence times is very strong evidence that the initial and rate-determining step in the thermal decompositions of $C(NF_2)_4$, $FC(NF_2)_3$, and $F_2C(NF_2)_2$ is the simple rupture of the C–N bond. The influence of temperature upon the principal intermediates $(NF_2)_2C{=}NF$ and $F(NF_2)$-$C{=}NF$ (Figures 9 and 10) and the results presented in Figure 13 are in agreement with a kinetic model in which it is assumed that $C(NF_2)_4$ and $FC(NF_2)_3$ decompose by the following overall processes

$$C(NF_2)_4 \xrightarrow{\text{I}} (NF_2)_2C{=}NF + xNF_2 + (1 - x)NF_3 + xF \xrightarrow{\text{II}} \text{products} \quad (6a)$$

$$FC(NF_2)_3 \xrightarrow{\text{I}} F(NF_2)C{=}NF + xNF_2 + (1 - x)NF_3 + xF \xrightarrow{\text{II}} \text{products} \quad (6b)$$

where the processes leading to products, step II, have lower activation energies than the rate-determining process in step I (C–N bond rupture). Thus, higher maximum yields of $(NF_2)_2C{=}NF$ and $F(NF_2)C{=}NF$ are obtained at higher temperatures.

The processes by which $(NF_2)_2C{=}NF$ or $F(NF_2)C{=}NF$ react to form stable products and other intermediates in the above model for the decomposition of $C(NF_2)_4$ and $FC(NF_2)_3$, respectively (step II of eq 6), were investigated by first assuming that $(NF_2)_2C{=}NF$ and $F(NF_2)C{=}NF$ disappear solely by thermal decomposition. To determine if this were a valid assumption, the thermal decompositions of $(NF_2)_2C{=}NF$ and $F(NF_2)C{=}NF$ were investigated in the stirred flow reactor.[20] The following calculations were made to test this assumption.

Assuming the kinetic model shown in eq 6, the observed maximum concentrations of the principal intermediate (Figures 9, 10, and 13) can be put on a more quantitative basis. Equation 6 can be written

$$A \xrightarrow{k_a} B \xrightarrow{k_b} \text{products} \quad (7)$$

where A and B are the concentrations of the reactant and principal double-bonded intermediate, respectively. If it is assumed that B decomposes by a first-order process, then for a stirred flow reactor

$$dB/dt = k_aA - k_bB - B/\tau = 0 \quad (8)$$

The residence time at which B reaches a maximum, τ_{max}, can be obtained by differentiating eq 8 after substituting for A from eq 2. This gives

$$\tau_{max} = (k_ak_b)^{-1/2} \quad (9)$$

From eq 2, the percentage of A decomposed is given by $P = 100k_a(1 + k_a\tau)^{-1}$. Therefore, P_{max}, which is the percentage of A reacted at maximum B, is given by

$$P_{max} = 100[1 + (k_b/k_a)^{1/2}]^{-1} \quad (10)$$

The form of eq 10 is in agreement with the experimentally observed shifting of the maximum concentrations of the principal intermediates to higher per cent reaction at higher temperatures (Figure 9).

On the basis of eq 8, it is possible to predict the maximum yield of $(NF_2)_2C{=}NF$, B_{max}/A_0, as a function of temperature, assuming still that $(NF_2)_2C{=}NF$ is

Table III: Formation of $(NF_2)_2C{=}NF$ from $C(NF_2)_4$ as a Function of Temperature

Temp, °C	τ_{max}, sec		P_{max}, %		B_{max}/A_0	
	Obsd	Calcd	Obsd	Calcd	Obsd	Calcd
198	180	260	19	39	0.04	0.15
250	7	17	58	73	0.26	0.54

(20) A. E. Axworthy and J. M. Sullivan, *J. Phys. Chem.*, in preparation. The kinetics and mechanism of the decomposition of $(NF_2)_2C{=}NF$ and $F(NF_2)C{=}NF$ will be reported. $(NF_2)_2C{=}NF$ decomposition is apparently heterogeneous over the temperature range 210 to 323° with $k_1 = 10^{3.5}\exp(-12{,}360/RT)$ sec^{-1}. The decomposition products from $(NF_2)_2C{=}NF$ are $F(NF_2)C{=}NF$, $F_2C{=}NF$, CF_3NF_2, N_2, CF_4 and small amounts of N_2F_4 and NF_3. The products from $F(NF_2)C{=}NF$ are $F_2C{=}NF$, CF_3NF_2, N_2, and CF_4.

Table IV: Influence of Additives on the Intermediate and Products Formed during the Thermal Decomposition of $FC(NF_2)_3$

Temp, °C	τ, sec	Partial pressure of $FC(NF_2)_3$, Torr	Additive	Additive partial pressure, Torr	Peak area				
					CF_3NF_2	$F_2C{=}NF$	N_2F_4	$F(NF_2)C{=}NF$	N_2, NF_3, CF_4 composite
339.5	57.1	4	None	0	17.5	6.1	22.9	29.1	238
340.3	53.9	4	None	0	16.9	6.1	24.0	32.8	254
340.1	54.1	4	N_2F_4	6	19.8	19.8	...	62.1	280
340.1	54.8	4	N_2F_4	6	18.0	17.6	...	57.2	286
339.9	55.9	4	None	0	17.0	7.3	24.0	37.7	258
339.3	11.8	1.5	None	0	9.1	8.3	11.5	44.6	151
339.5	11.9	1.5	None	0	9.4	9.0	11.7	42.7	152
339.5	12.0	1.5	F_2	1.3	12.1	2.4	2.2	25.0	240
339.1	11.9	1.5	F_2	1.3	17.3	3.5	2.6	17.1	270

consumed only by pyrolysis. From eq 8, the ratio of $(NF_2)_2C{=}NF$ to $C(NF_2)_4$ is given by

$$B/A = k_a(k_b + 1/\tau)^{-1} \quad (11)$$

Thus, the ratio of $(NF_2)_2C{=}NF$ concentration to initial $C(NF_2)_4$ concentration is given by

$$B/A_0 = k_a A[(k_b + 1/\tau)A_0]^{-1} \quad (12)$$

The calculated and observed values (Figure 9) of τ_{max}, P_{max}, and B_{max}/A_0 for the formation of $(NF_2)_2C{=}NF$ from $C(NF_2)_4$ are presented in Table III as a function of temperature. It may seen that the trend with temperature is that which would be predicted by a kinetic model, eq 6, in which each molecule of $C(NF_2)_4$ forms one molecule of $(NF_2)_2C{=}NF$ which then decomposes (heterogeneously). However, the observed values of τ_{max}, P_{max}, and B_{max}/A_0 in Table III are all smaller than the predicted values indicating that $(NF_2)_2C{=}NF$ also reacts by processes other than simple thermal decomposition.[21]

Application of the above model to the decomposition of $FC(NF_2)_3$ results in even greater discrepancies between the observed and calculated quantities. $F(NF_2)C{=}NF$ is sufficiently stable[20] that very high yields of this intermediate should be obtained from $FC(NF_2)_3$. That this is not the case (Figure 10) again indicates the predominance of processes other than thermal decomposition.

The most likely processes for the consumption of $(NF_2)_2C{=}NF$ and $F(NF_2)C{=}NF$ are reactions with NF_2 or F atoms. For this reason, experiments were conducted to determine the influence of added NF_2 and F_2 on the concentrations of $(NF_2)_2C{=}NF$ and $F(NF_2)C{=}NF$ formed from $C(NF_2)_4$ and $FC(NF_2)_3$, respectively. It was reported above that these additives do not alter the decomposition rate of $FC(NF_2)_3$. It was found[14] that the addition of N_2F_4 at a concentration of 4.5 Torr increased by about 25% the concentration of $(NF_2)_2C{=}NF$ formed from $C(NF_2)_4$ (at 240°, τ = 9 sec, and $C(NF_2)_4$ = 6 Torr). The influence of added N_2F_4 and F_2 on the product distribution from $FC(NF_2)_3$ at 340° is shown in Table IV. Addition of N_2F_4 (τ = 55 sec) causes a twofold increase in $F(NF_2)C{=}NF$ concentration, while the addition of F_2 (τ = 12 sec) decreases the concentrations of $F(NF_2)C{=}NF$ and N_2F_4 by factors of about 2 and 4, respectively.

The results of these experiments suggest that F atoms formed in the initial decomposition process attack the principal intermediates $(NF_2)_2C{=}NF$ and $F(NF_2)C{=}NF$, while NF_2 promotes their longevity by itself reacting with fluorine to form NF_3. That this is apparently the case is demonstrated by the data in Table V, which shows the influence of N_2F_4 on the peak areas for N_2, CF_4, and NF_3 formed from $FC(NF_2)_3$ at 323° and residence times of about 4 sec. The addition of N_2F_4 is seen to increase the concentration of NF_3 by more than a factor of 2.

Table V: Influence of N_2F_4 on Formation of N_2, NF_3, and CF_4 from $FC(NF_2)_3$ at 323°

U, ml/sec	τ, sec	Partial pressure $FC(NF_2)_3$, Torr	Partial pressure N_2F_4, Torr	Peak area		
				N_2	CF_4	NF_3
2.20	4.19	3.5	0	107	158	75
2.24	4.11	3.6	0	106	156	77
2.30	4.01	3.5	3.8	116	136	163
2.28	4.04	3.7	3.5	114	148	166

The products[20] from the pyrolyses of $(NF_2)_2C{=}NF$ and $F(NF_2)C{=}NF$ are the same as those from $C(NF_2)_4$ and $FC(NF_2)_3$, respectively, except that higher yields of N_2F_4 and NF_3 are obtained from $C(NF_2)_4$ and $FC(NF_2)_3$. It appears, therefore, that $(NF_2)_2C{=}NF$ and $F(NF_2)C{=}NF$ each yield essentially the same products whether

(21) A similar calculation can be made for the tubular reactor data at 344° in Figure 13 [S. W. Benson, "The Foundations of Chemical Kinetics," McGraw-Hill, New York, N. Y., 1960, p 34]. The decomposition rate of $(NF_2)_2C{=}NF$ was not measured in this reactor, but an approximate k_b value of 0.6 sec^{-1} can be obtained from the final slope of the $(NF_2)_2C{=}NF$ curve in Figure 13. This gives a calculated value of B_{max}/A_0 of 0.96 *vs.* an observed value (Figure 13) of 0.84, indicating that more than one reaction path occurs for $(NF_2)_2C{=}NF$ even at this higher temperature (*i.e.*, approximately 10% reacts by processes other than pyrolysis).

decomposed thermally or by F atom attack. When $C(NF_2)_4$ and $(NF_2)_2C{=}NF$ were each pyrolyzed at 528° in the 2.4-ml tubular reactor, the same product distribution was obtained as a function of residence time, except for higher concentrations N_2F_4 and NF_3 from $C(NF_2)_4$; at this high temperature, nearly all of the $(NF_2)_2C{=}NF$ formed from $C(NF_2)_4$ should decompose thermally.

Mechanism

The formation of N_2F_4 and $(NF_2)_2C{=}NF$ as initial decomposition products is strong evidence that the initial step in $C(NF_2)_4$ pyrolysis is the cleavage of a C–N bond

$$C(NF_2)_4 \longrightarrow \cdot C(NF_2)_3 + NF_2 \quad (13)$$

followed by the first or both of the following processes

$$\cdot C(NF_2)_3 \longrightarrow (NF_2)_2C{=}NF + F \quad (14)$$

$$\cdot C(NF_2)_3 + NF_2 \longrightarrow (NF_2)_2C{=}NF + NF_3 \quad (15)$$

The fact that the concentration of NF_3 is less than that of $(NF_2)_2C{=}NF$ (Figure 13) indicates that reaction 15 is not the predominant process. Reaction 14 is apparently so rapid that no other process can compete, including the reverse of reaction 13 which would lead to inhibition by added N_2F_4. Much or all of the NF_3 probably results from reaction of NF_2 radicals with fluorine atoms generated in reaction 14.

$$NF_2 + F + M \longrightarrow NF_3 + M \quad (16)$$

According to the proposed kinetic model, the remainder of the products—N_2, CF_4, CF_3NF_2, $F(NF_2)C{=}NF$, and $F_2C{=}NF$—are formed from reactions of the primary intermediate $(NF_2)_2C{=}NF$. Reactions analogous to eq 13, 14, and 15 are proposed for $FC(NF_2)_3$ decomposition. Although the data are sparse in the case of $F_2C(NF_2)_2$, the similarity of its product distribution (Figure 8) with those for $C(NF_2)_4$ and $FC(NF_2)_3$ (Figures 6 and 7) suggests that the mechanism is similar.

The absence of chain processes in this system of compounds is of particular interest. The experimental observation that NF_2 does not influence the rate of decomposition and that $FC(NF_2)_3$ is not a product of $C(NF_2)_4$ pyrolysis indicates that reactions such as eq

$$\cdot NF_2 + C(NF_2)_4 \longrightarrow (\cdot NF)C(NF_2)_3 + NF_3 \quad (17)$$

$$\cdot C(NF_2)_3 + C(NF_2)_4 \longrightarrow FC(NF_2)_3 + (\cdot NF)C(NF_2)_3 \quad (18)$$

17 and 18 do not occur. Benson[22] has pointed out that reactions such as eq 17 involving fluorine abstraction are likely to have prohibitively high activation energies; this accounts for the nonchain character of these reactions.

(22) Reference 9, p 122.

Pressure Dependence of Carbon Trioxide Formation in the Gas-Phase Reaction of $O(^1D)$ with Carbon Dioxide[1a]

by W. B. DeMore and C. Dede[1b]

Jet Propulsion Laboratory, California Institute of Technology, Pasadena, California 91103 *(Received February 11, 1970)*

The reaction $O(^1D) + CO_2 + M \rightarrow CO_3 + M$ has been studied at $-30°$ over the pressure range of 100–2500 psi. The method involved photolysis (2537 Å) of O_3–CO_2 mixtures pressurized with He or Ar. Detection of CO_3 was based on the fact that its formation is accompanied by removal of atomic oxygen, which in turn is reflected by a decrease in the O_3 concentration. Blank experiments using N_2 instead of CO_2 showed that other paths for loss of atomic oxygen were relatively negligible. Although CO_3 formation was detected by this method, the dominant process at all pressures was quenching of $O(^1D)$ to $O(^3P)$, which evidently proceeds *via* a CO_3^* intermediate: $O(^1D) + CO_2 \rightarrow CO_3^* \rightarrow CO_2 + O(^3P)$. The observed pressure dependence of CO_3 formation indicates that the lifetime of CO_3^* before predissociation to $CO_2 + O(^3P)$ is about 10^{-11} to 10^{-12} sec.

Introduction

There is little doubt that CO_3 is formed in Dry Ice[2,3] or liquid CO_2[4] by the reaction

$$O(^1D) + CO_2 (+ M) \longrightarrow CO_3 (+ M) \qquad (1)$$

In the gas phase the situation is less clear, particularly in regard to the pressure dependence of (1) and the relative importance of the quenching reaction

$$O(^1D) + CO_2 \longrightarrow O(^3P) + CO_2 \qquad (2)$$

There are reports of CO_3 formation in the gas phase at relatively low pressures, such as the work of Clerc and Reiffsteck at 1 atm[5] and Arvis at 1 Torr.[6] On the other hand, there is evidence from the work of Young, Black, and Slanger,[7a] at 15 Torr, and of Paraskevopoulos and Cvetanovic,[7b,c] at 1 atm, that $O(^3P)$ is produced upon removal of $O(^1D)$ by CO_2.

The question of CO_3 formation is important in a number of connections involving CO_2 photolysis, but is especially pertinent to the photochemistry of planetary atmospheres which are rich in CO_2.

The present report describes experiments designed to measure the rate and pressure dependence of (1) in the gas phase. The results show that the CO_3-forming reaction is negligibly slow compared to the quenching process (2) at all pressures which are ordinarily relevant to laboratory or atmospheric studies.

Method

Mechanism. It is convenient to write down a detailed mechanism for the $O(^1D)$–CO_2 interaction, as follows

$$O(^1D) + CO_2 \underset{k_r}{\overset{k_f}{\rightleftarrows}} CO_3^* \xrightarrow{k_d[M]} CO_3 + M \qquad (3)$$

$$CO_3^* \xrightarrow{k_p} CO_2 + O(^3P)$$

$$CO_3^* \xrightarrow{k_{pq}} CO_2 + O(^3P)$$

The rate constants k_f, k_r, k_p, k_d, and k_{pq} refer to the forward, reverse, predissociation, third-body deactivation, and physical quenching reactions, respectively. A full kinetic description of this process requires a knowledge of the rate of $O(^1D)$ disappearance, the rate of CO_3^* formation, and the rate of formation of either $O(^3P)$ or CO_3 as a function of pressure.

Some information is available from previous work. There is evidence that $O(^1D)$ is removed by CO_2 with a rate constant perhaps as high as 10^{-10} cm^3 sec^{-1}.[7] Further, there are indications that all $O(^1D)$ removal proceeds *via* the CO_3^* intermediate, as shown by the following discussion. The $O(^1D)$–CO_2 reaction in liquid CO_2[4] gave no detectable $O(^3P)$, but at the same time the rate of CO_3 formation was fast enough (measured relative to the $O(^1D)$–C_3H_8 reaction) to account for all the observed rate of $O(^1D)$ removal by CO_2 in the gas phase (again measured relative to C_3H_8).[8] These comparisons imply strongly that $k_f \gg k_{pq}$.

We may also deduce that $k_r \leq (k_p + k_d [M])$, to account for the fact that, as seen above, $O(^1D)$ is removed by CO_2 at nearly the collisional rate.

(1) (a) This paper presents the results of one phase of research carried out at the Jet Propulsion Laboratory, California Institute of Technology, under Contract No. NAS7-100, sponsored by the National Aeronautics and Space Administration. (b) Summer employee at the Jet Propulsion Laboratory, 1969.

(2) N. G. Moll, D. R. Clutter, and W. E. Thompson, *J. Chem. Phys.*, **45**, 4469 (1966).

(3) E. Weissberger, W. H. Breckinridge, and H. Taube, *ibid.*, **47**, 1764 (1967).

(4) W. B. DeMore and C. W. Jacobsen, *J. Phys. Chem.*, **73**, 2935 (1969).

(5) M. Clerc and A. Reiffsteck, *J. Chem. Phys.*, **48**, 2799 (1968).

(6) M. Arvis, *J. Chim. Phys.*, **66**, 517 (1969).

(7) (a) R. A. Young, C. Black, and T. G. Slanger, *J. Chem. Phys.*, **49**, 4758 (1968); (b) G. Paraskevopoulos and R. J. Cvetanovic, *J. Amer. Chem. Soc.*, **91**, 7572 (1969); (c) G. Paraskevopoulos and R. J. Cvetanovic, *J. Chem. Phys.*, **50**, 590 (1969).

(8) K. F. Preston and R. J. Cvetanovic, *ibid.*, **45**, 2888 (1966).

The additional quantity needed is the ratio k_p/k_d. This ratio can be determined by measurements of the pressure dependence of CO_3 formation, as shown below.

We consider the photolysis of O_3 at 2537 Å in a mixture containing CO_2, O_2, O_3, and a pressurizing gas, M. The initial step is

$$O_3 + 2537\ \text{Å} \xrightarrow{\phi} O_2 + O(^1D) \qquad (4)$$

The quantity ϕ is the quantum yield of $O(^1D)$ production. By suitable choice of reaction conditions (CO_2 in great excess over O_2 and O_3, and using He or Ar as the pressurizing gas), we need consider only the reaction of $O(^1D)$ with CO_2. The following mechanism then applies

$$O(^1D) + CO_2 \underset{k_r}{\overset{k_f}{\rightleftarrows}} CO_3^* \text{ (singlet)} \qquad (5)$$

$$CO_3^* \text{ (singlet)} \xrightarrow{k_p} CO_2 + O(^3P) \qquad (6)$$

$$CO_3^* + M \xrightarrow{k_d} CO_3 + M \qquad (7)$$

$$O(^3P) + O_2 + M \xrightarrow{k_a} O_3 + M \qquad (8)$$

$$O(^3P) + O_3 \xrightarrow{k_o} 2O_2 \qquad (9)$$

$$CO_3 + CO_3 \longrightarrow 2CO_2 + O_2 \qquad (10)$$

Inclusion of reaction 10 is based on the earlier work in liquid CO_2,[4] which suggested disproportionation as the major CO_3 loss path. The quantum yield of O_3 disappearance, Φ_{O_3}, is given by

$$\frac{\Phi_{O_3}}{\phi} = \frac{k_d[M]}{k_d[M] + k_p} + \frac{2k_p}{k_d[M] + k_p(1 + k_a[O_2][M]/k_0[O_3])} \qquad (11)$$

Under the conditions of these experiments, it can be shown that $k_a[O_2][M] \gg k_0[O_3]$, based on measured values of the ratio k_a/k_0.[9] Thus

$$\frac{\phi}{\Phi_{O_3}} = 1 + \frac{k_p}{k_d[M]} \qquad (12)$$

There is no reason to doubt that $\phi \sim 1$,[10] so a plot of $\Phi_{O_3}^{-1}$ *vs.* $[M]^{-1}$ will yield the ratio k_p/k_d from the slope.

This experimental approach is the same as that previously used to demonstrate the formation of CO_3 in liquid CO_2.[4] It is based on the premise that atomic oxygen, and therefore O_3, can only disappear through irreversible CO_3 formation. As in the previous work, it was necessary to demonstrate experimentally that other possible paths of $O(^3P)$ loss were negligible. This was done in the present work by blank experiments in which N_2 was substituted for CO_2. (See Results section.)

Apparatus. The photolyses were carried out in a cylindrical stainless steel cell fitted with quartz windows at each end. The optical path length was 5 cm.

Table I: Effect of Pressure on the Quantum Yields of Ozone Photolysis in the Presence of CO_2 or N_2

P_{total}, psi	Pressurizing gas	P_{O_2}, mm	$P_{substrate}$ (CO_2 or N_2, psi)	Φ_{O_3} in CO_2	Φ_{O_3} in N_2
100	He	50	35	0.007	0.004
100	He	50	65	0.013	0.002
250	He	50	35	0.022	0.004
250	He	50	65	0.023	0.002
500	He	50	35	0.037[a,h]	0.003
500	He	50	65	0.033[b]	0.001
500	He	25	65	0.048	...
500	Ar	50	65	0.040	...
1000	He	50	35	0.064[c]	0.002
1000	He	50	65	0.062[d]	0.005
1000	N_2	50	35	0.013	...
1000	N_2	50	65	0.025	...
1000	He	150	65	0.049	...
1000	He	400	65	0.038	0.007
1000	Ar	0	65	0.059	0.009
1000	Ar	50	65	0.059	...
1000	Ar	80	65	0.065	...
1000	Ar	350	65	0.070	...
1250	He	50	35	0.063	...
1250	He	50	65	0.067[e]	0.006
1250	Ar	50	65	0.077	...
1250	Ar	80	65	0.076	...
2000	He	50	65	0.119[f]	0.008
2000	He	150	65	0.067	...
2500	He	50	35	0.127	...
2500	He	50	65	0.165[g]	...

[a] Average of 2 experiments.[h] Average deviation 0.006. [b] Average of 6 experiments. Average deviation 0.008. [c] Average of 3 experiments. Average deviation 0.010. [d] Average of 13 experiments. Average deviation 0.009. [e] Average of 3 experiments. Average deviation 0.008. [f] Average of 5 experiments. Average deviation 0.024. [g] Average of 3 experiments. Average deviation 0.025. [h] Each experiment consisted of about 5 photolysis rate measurements taken on a given mixture. Thus, Φ_{O_3} from each experiment was an average of about 5 values. The average deviation within a given experiment was similar to that between different experiments.

The cell was designed to operate at pressures up to 3000 psi. The temperature of the cell was controlled by a flow of chilled N_2 gas which passed through a copper tube wrapped around the cell. The cell was suspended in an evacuated chamber.

Most of the experiments were at −30°, with reaction mixtures of 35 or 65 psi of CO_2, 50 mm of O_2, 1–2 mm of O_3, and sufficient He or Ar to bring the total pressure within the experimental range of 100–2500 psi.

The source of 2537 Å light was a low-pressure Hg lamp, and the light intensity was measured with a calibrated Eppley thermopile. The O_3 concentration was monitored spectrophotometrically, using an extinction coefficient of 3030 M^{-1} cm^{-1} at 2537 Å.

(9) F. Kaufman, *Prog. React. Kinet.*, **1**, 1 (1961).

(10) W. B. DeMore and O. F. Raper, *J. Chem. Phys.*, **44**, 1780 (1966).

The initial O_3 optical densities were usually about 3.5, and a series of photolysis rate measurements was taken until the OD was reduced to about 1.0.

The helium used as pressurizing gas was of 99.995% minimum purity (Gardner Cryogenics), and in some experiments was passed through a U-tube immersed in liquid N_2. The Ar and N_2 were of 99.996% minimum purity. Three grades of CO_2 were used, including Matheson Research Grade (99.995% minimum), Coleman Instrument Grade (99.99% minimum), and CO_2 of the latter grade which was further purified by passing over CuO at a red heat followed by freezing and pumping.

Results

Quantum Yield Measurements. Table I shows the observed values of Φ_{O_3} with either CO_2 or N_2 as the substrate. Φ_{O_3} was always higher with CO_2 than with N_2, and the difference increased with increasing total pressure. No appreciable difference was noted in experiments with 65 psi of CO_2 and 35 psi of CO_2. This latter result is expected, because no competing path for $O(^1D)$ loss should be significant at either CO_2 pressure. The only possible dependency on CO_2 pressure would arise through a difference in the efficiencies of CO_2 and He as third bodies.

Use of Ar as the pressurizing gas gave O_3 quantum yields about the same, or perhaps slightly higher, than those obtained with He. Since CO_2 removes $O(^1D)$ at least 2000 times faster than does Ar,[11] this failure of Ar to reduce Φ_{O_3} is consistent with the proposed mechanism. With N_2 as pressurizing gas, Φ_{O_3} was sharply reduced. Here, a competing path for $O(^1D)$ removal (quenching by N_2) is significant. As expected, Φ_{O_3} was then higher at 65 psi of CO_2 than at 35 psi of CO_2. Based on the relative $O(^1D)$ quenching efficiencies of N_2 and CO_2[7,8,11] the Φ_{O_3} values for 35 psi of CO_2 and 65 psi of CO_2 should have declined by factors of about 7 and 4, respectively. The observed reductions (Table I) were somewhat less than this, but nevertheless within the experimental error.

With N_2 as the substrate rather than CO_2, the quantum yields were low, but not zero as predicted by eq 11. Evidently a slow photochemical loss of O_3 by some path other than $O(^3P) + O_3$ was operative.

The dark rate of O_3 loss was negligible compared to the photochemical rate in the CO_2 experiments, and accounted for not more than 30% of the photochemical rate with N_2 as substrate.

Φ_{O_3} showed no dependence on the O_3 concentration over the experimental range of a factor of 3. Also, as shown in Table I, no significant dependence on the O_2 was found, even when no O_2 was added. This is not inconsistent with eq 11, because at the temperature and pressures of these experiments, trace amounts of O_2, resulting from partial O_3 decomposition, are sufficient to scavenge all $O(^3P)$.

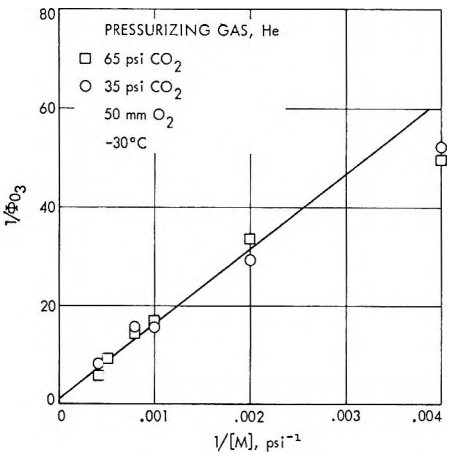

Figure 1. Plot of data in Table I according to eq 12.

Several experiments were carried out to test the possibility that the difference in Φ_{O_3} for CO_2 and N_2 might be due to some unknown feature of the CO_2 mixture, such as an impurity in the CO_2. For example, several grades of CO_2 (see Experimental Section) were used, but no appreciable difference in photolysis rates was noted. Addition of 0.13 mm of H_2 to a mixture at 1000 psi produced no significant change in Φ_{O_3}. Also, addition of 0.18 mm of H_2O (most of which froze out on the walls upon cooling to $-30°$) had no effect. These latter two experiments argue against any role of an OH-catalyzed chain decomposition of O_3 in this work. Coating the cell walls with Kel-F grease or with Teflon produced no change, nor did addition of a magnetically driven stirrer. All these observations tend to support the hypothesis that the observed O_3 disappearance was due to a homogeneous, gas-phase reaction involving CO_2 itself.

Evaluation of the Ratio k_p/k_d. Figure 1 shows a plot of $\Phi_{O_3}^{-1}$ *vs.* $[M]^{-1}$ for those experiments in Table I in which the pressurizing gas was He. Before plotting, the Φ_{O_3} values for 250 and 500 psi were reduced by 0.003 as a first-order correction for the nonzero rate of photolysis obtained when the CO_2 was replaced by N_2. No correction was made at the higher pressures. The data for 100 psi were not included because of the high-percentage uncertainty in Φ_{O_3} at that low pressure.

The intercept, while not accurately defined by the data, is consistent with a value near unity, as would be expected if $\phi = 1$. From the slope, we find

$$k_p/k_d = 1.6 \times 10^4 \text{ psi} = 2.6 \times 10^{22} \text{ cm}^{-3} \quad (13)$$

We take $k_d/f = 4.8 \times 10^{-10}$ cm^3 sec^{-1}. The quantity f is the collisional deactivation efficiency, and the

(11) W. B. DeMore, *J. Chem. Phys.*, 52, 4309 (1970). Preston and Cvetanovic (ref 8) have reported a value of about 100 for the relative CO_2–Ar quenching efficiencies. That value would lead to the prediction of about a 15% decrease in Φ_{O_3} in the experiment with 65 psi CO_2 and Ar added to 1250 psi total pressure, which is contrary to observation. However, the present results are not sufficiently precise to permit any decision on which quenching ratio is more nearly correct.

collision rate constant was calculated for collisions of He and CO_3* using $\sigma_{He} = 2.2$ Å and $\sigma_{CO_3*} = 5.0$ Å. This calculation ignores the fact that M consisted partly of CO_2, because there was little difference in Φ_{O_3} for 35 and 65 psi of CO_2. It then follows that

$$k_p/f = 1.2 \times 10^{13}\ \text{sec}^{-1} \quad (14)$$

Assuming that $f \sim 10^{-1}$ or 10^{-2}, the predissociation rate k_p is then about 10^{11}–10^{12} sec^{-1}.

This estimate of k_p confirms the earlier conclusion (see Method section) that k_r is negligible in the CO_3 scheme represented by eq 3, because the expected value of k_r is only about 10^8 sec^{-1}.[12]

The overall rate constant for CO_3 formation in the low-pressure limit is $k = k_f k_d/k_p$. The rate constant for quenching of $O(^1D)$ to $O(^3P)$ is

$$k_q = k_f k_p/(k_r + k_p + k_d[M]) \quad (15)$$

At low pressures, this reduces to $k_q = k_f$, so that at 1 atm, for example, the quenching reaction is 10^3 faster than CO_3 formation.

Related Experiments. Supplementary experiments of a somewhat different nature have also been carried out in connection with our study of CO_3 formation. In one case, mixtures of O_3, CO_2, and He at 22° (O_3 pressure about 50 μ, CO_2 in the mm range, and sufficient He to bring the total pressure to 1 atm) were photolyzed at 2537 Å in a 40-m White cell. The light intensity was not measured, but is believed to have been at least 10^{16} quanta/cm^2 sec. No infrared absorption attributable to CO_3 was detected, which would indicate that the steady-state CO_3 pressure was less than about 1 μ. This result is consistent with our conclusion from the high-pressure experiments that CO_3 formation at 1 atm is extremely inefficient.

In another experiment, mixtures of O_3 in liquid CO_2 at −45° were irradiated at 2537 Å and simultaneously scanned from 2 to 5 μ in the infrared. The apparatus was similar to that previously used,[4] except that a crossed beam cell with sapphire windows was incorporated. Although the rapid O_3 photolysis indicating CO_3 formation was observed as before,[4] no infrared absorption at or near the reported CO_3 bands[2] was detected. This observation supports the suggestion that CO_3 rapidly disappears by reaction 10.

Discussion

To detect CO_3, we have utilized the fact that its formation is accompanied by removal of atomic oxygen from the photolysis mixture, which results in a decrease in the O_3 concentration. The observed pressure dependence of Φ_{O_3} in the photolysis of O_3–CO_2 mixtures, when contrasted with the blank experiments involving O_3–N_2 mixtures, makes it reasonably certain that CO_3 formation has in fact been observed.

However, the most significant point of this work is not that CO_3 can be formed in the gas phase, but rather that reaction 1 is inefficient at low pressures. In this connection, it is necessary to show that the present experiment does not in some way mask CO_3 formation, and thereby give a falsely low efficiency for reaction 1. This is particularly true in view of the fact that the present results indicate a much stronger pressure dependence than would be implied by the results of previous workers.[5,6]

There is no doubt that O_3 photolysis gives $O(^1D)$, and therefore our method could only fail if O_3 were somehow regenerated from CO_3. This could occur by either of the following reactions.

$$CO_3 \longrightarrow CO_2 + O \quad (16)$$

$$CO_3 + O_2 \longrightarrow CO_2 + O_3 \quad (17)$$

It is not clear, however, why these processes would occur in the present work but not in that of ref 5 and 6, especially since the present experiments were at a lower temperature. Also, these processes would not be expected to show the type of pressure dependence which was observed, and reaction 17 would not be consistent with the lack of dependence of Φ_{O_3} on the O_2 concentration.

Reaction 16 could in principle be effected by photolysis of CO_3. However, O_3 strongly absorbs the 2537-Å light, and there was no evidence of any dependence of Φ_{O_3} on the O_3 concentration. Also, the liquid-phase experiments showed that the steady-state CO_3 concentration is low compared to O_3 and failed to show any indication of CO_3 absorption in the uv. A final point is that the photolysis reaction probably would not show the observed pressure dependence, although this is not certain.

It might be thought that our derived value of 10^{11} to 10^{12} sec^{-1} for k_p is too high, considering that the predissociation process (reaction 6) is spin-forbidden. However, this process should be regarded as the unimolecular fission of vibrationally excited CO_3*. Processes of this type involving the splitting off of an atom may have preexponential factors as high as 10^{15} sec^{-1}. The excess vibrational energy of CO_3*, coupled with the relatively few degrees of freedom of CO_3, permits the dissociation rate to approach to perhaps $^1/_{10}$ the preexponential factor. Thus the observed rate still allows for a "forbiddenness factor" of 10^{-2} to 10^{-3}. This is approximately the expected range for this type of process.[13]

In connection with the preceding paragraph, it is appropriate to compare the CO_3 results with those previously obtained for N_2O[14] and CO_2.[15] In the latter cases the analogous reactions are

(12) M. Shimizu, *Icarus*, **9**, 593 (1968).
(13) E. K. Gill and K. J. Laidler, *Can. J. Chem.*, **36**, 1570 (1958).
(14) W. DeMore and O. F. Raper, *J. Chem. Phys.*, **37**, 2048 (1962).
(15) O. F. Raper and W. B. DeMore, *ibid.*, **40**, 1053 (1964).

$$O(^1D) + N_2 + M \longrightarrow N_2O + M \quad (18)$$

and

$$O(^1D) + CO + M \longrightarrow CO_2 + M \quad (19)$$

However, even in liquid N_2 (or liquid CO) the dominant processes were predissociation

$$O(^1D) + N_2 \longrightarrow N_2O^* \longrightarrow O(^3P) + N_2 \quad (20)$$

$$O(^1D) + CO \longrightarrow CO_2^* \longrightarrow O(^3P) + CO \quad (21)$$

This indicates either that the rates of collisional deactivation of N_2O^* and CO_2^* are smaller than that of CO_3^*, or else that k_p is lower for CO_3^*, perhaps because of the increased complexity of the molecule.

The present experiments with N_2 at high pressures of He confirm that reaction 18 is insignificant in the gas phase, relative to reaction 1. This is consistent with the liquid-phase results.

Formation of CO_3 by the $O(^1D)$–CO_2 reaction has occasionally been invoked[16,17] to explain apparent anomalies in the photochemical balances of the Mars and Venus atmospheres. The results of the present work show, however, that CO_3 formation by this reaction is negligible at the low-pressure regions of the atmospheres where the photochemical processes occur.

(16) M. B. McElroy, *J. Geophys. Res.*, **73**, 1513 (1968).
(17) M. B. McElroy and D. H. Hunten, *ibid.*, **75**, 1188 (1970).

Standard Potentials of the Silver–Silver Bromide Electrode in Propylene Glycol and the Silver–Silver Iodide Electrode in Ethylene and Propylene Glycols at Different Temperatures and Related Thermodynamic Quantities

by K. K. Kundu, Debabrata Jana, and M. N. Das

Physical Chemistry Laboratories, Jadavpur University, Calcutta-32, India *(Received October 13, 1969)*

Standard potentials of Ag–AgBr electrodes in propylene glycol and of Ag–AgI electrodes in both ethylene and propylene glycols have been determined from the emf measurements of the cells of the type H_2(g, 1 atm)|HOAc(m_1), NaOAc(m_2), NaX(m_3) glycols|AgX–Ag, where X = Br or I, at nine different temperatures in the range 5–45°. The necessary thermodynamic dissociation constants of acetic acid (HOAc) in the respective solvents at the same temperature range were first determined from the emf measurements of the cells of the type H_2(g, 1 atm)|HOAc(m_1), NaOAc(m_2), NaCl(m_3), glycol|AgCl–Ag, the standard potentials of Ag–AgCl electrode being known from an earlier study. These potentials, along with other relevant potentials determined earlier, were utilized to compute the standard free energies, entropies, and enthalpies of the solvated hydrogen halides: HCl, HBr, and HI for both ethylene and propylene glycols as well as for water. The corresponding quantities accompanying the transfer of hydrogen halides from water to glycols have also been computed. The chemical effect of solvents on the transfer process obtained by subtracting the electrostatic contribution computed from Born as well as Hepler's model (free energy only) from the total transfer quantities have been examined in the light of relative solvation of three halide ions in glycols with respect to that in water.

In continuation of our previous studies on the standard potentials of the silver–silver halide electrodes in both ethylene and propylene glycols at different temperatures,[1,2] we have undertaken studies on the standard potentials of the Ag–AgBr electrode in propylene glycol and the Ag–AgI electrode in ethylene and propylene glycols at nine temperatures ranging from 5 to 45°.

(1) K. K. Kundu, P. K. Chatterjee, D. Jana, and M. N. Das, *J. Chem. Eng. Data*, in press.
(2) U. Sen, K. K. Kundu, and M. N. Das, *J. Phys. Chem.*, **71**, 3665 (1967).

Preliminary experiments with HBr and HI solutions in glycols, particularly propylene glycol, indicated a gradual drift in the observed emf values which were perceptible beyond a concentration of 0.03 m or so, especially at higher temperatures. This is perhaps due to the slow reactions of the acids with the solvent forming halohydrins, and in the case of HI solution perhaps this is also partly due to the oxidation of HI. Hence, the method of using the cell of the type

$$H_2|HX(m), \text{solvent}|AgX\text{–}Ag \qquad (I)$$

was not considered suitable. A method essentially similar to Owen's buffer method[3] for Ag–AgBr was, therefore, adopted in the present study, with suitable modifications necessitated by the fact that a proper adjustment of the concentrations in the solvents is difficult owing to a high viscosity of the solvents. The modified method thus essentially consists of two parts: (1) the determination of the dissociation constant (K_a) of any suitable acid, *viz.* acetic acid, and (2) emf measurements on the hydrogen–silver–silver halide cell with solutions comprising the buffer mixture of the same acid and the respective halides. The dissociation constants of acetic acid (HOAc) in both the glycols were first determined at different temperatures by using a cell of the type

$$H_2(g, 1\text{ atm})|(HOAc(m_1), NaOAc(m_2), NaX(m_3), \text{glycol}|AgX\text{–}Ag \qquad (II)$$

where X = Cl. The evaluated K_a values of the acid were utilized to evaluate standard potentials of both Ag–AgBr and Ag–AgI electrodes in propylene glycol and of the Ag–AgI electrode in ethylene glycol from the measured emf values of cell II, where X = Br or I.

Experimental Section

Ethylene glycol (E. Merck) and propylene glycol (L.R., B.D.H.) were purified in the same manner as described earlier.[4] The physical properties such as boiling point, refractive index, and density were similar to those reported earlier.[1]

Acetic acid (G.R., Merck) was further purified by partially freezing the sample, decanting off the liquid portion, and then distilling the recrystallized sample before use. Potassium iodide (G.R., Merck) was dried in an oven kept at 200°.

Solutions of sodium glycoxide required for the preparation of NaX (X = Cl or Br) from HX solutions and sodium acetate solutions from acetic acid solution in the respective solvents were prepared in the same way as described earlier.[5]

The buffer mixtures consisting of acetic acid, sodium acetate, and sodium halide (X = Cl or Br) were prepared in the following way. A weighed amount of standard sodium glycoxide solution was added to a weighed amount of standard HX solution (preparation described earlier[4]) whereby NaX was produced, sodium glycoxide being in excess. To the same solution was then added a weighed amount of standard acetic acid solution in the same solvent. Cell solutions of required ionic strengths were made by diluting the buffer mixtures with the solvent. The buffer mixtures containing iodide were prepared by adding a weighed quantity of standard sodium glycoxide solution to a weighed quantity of acetic acid solution, to which a proper amount of standard KI solution was then added. The concentrations of KI solutions were usually calculated from the weights taken but were also checked in some cases by the usual gravimetric estimation of the halide ion.

The method of preparation of the hydrogen gas electrode and Ag–AgCl and Ag–AgBr electrodes has been described earlier.[4] The Ag–AgI electrode was of the thermal type as described by Bates.[6]

The electrodes were kept for aging in the solvents for a few days in the dark. The electrodes having bias potentials of the order of 0.1 mV were used. The electrodes were preserved in glycols and kept in the dark when not in use.

The general experimental procedure was exactly the same as that described earlier.[1] The behavior of the electrodes in the buffer mixtures was excellent and consistent within ±0.0001 V.

Results and Discussion

Dissociation Constants of Acetic Acid in Glycols. The observed emf (E_x) of cell II and the dissociation constant (K_a) of acetic acid for both the solvents are related by

$$\frac{E_X - (E_m^\circ)_{Ag-AgX}}{k} + \log \frac{m_{HOAc} m_{X^-}}{m_{OAc^-}} = pK_a - \log \frac{\gamma_{HOAc}\gamma_{X^-}}{\gamma_{OAc^-}} \qquad (1)$$

where $(E_m^\circ)_{Ag-AgX}$ is the standard potential of Ag–AgX electrodes (in molal scale) in the corresponding solvent, $k = 2.3026\,RT/F$, and γ_i the activity coefficient of the species concerned. Since the activity coefficient factor, $\log \gamma_{HOAc}\gamma_{X^-}/\gamma_{OAc^-}$, consists of the log of the ratio of the activity coefficients of two singly charged ions and that of a nonionic species in the numerator, the effective contribution would be negligibly small even at appreciable ionic strengths and would be zero at zero ionic strength. As a result, the left-hand side of eq 1, denoted by pK_a', could be related as

$$pK_a' = pK_a - \log \frac{\gamma_{HOAc}\gamma_{X^-}}{\gamma_{OAc^-}} = pK_a + f(\mu) \qquad (2)$$

where μ is the ionic strength of the solution. Thus,

(3) B. B. Owen, *J. Amer. Chem. Soc.*, **57**, 1526 (1935).
(4) K. K. Kundu and M. N. Das, *J. Chem. Eng. Data*, **9**, 87 (1964).
(5) K. K. Kundu and M. N. Das, *ibid.*, **9**, 82 (1964).
(6) R. G. Bates, *J. Amer. Chem. Soc.*, **60**, 2983 (1938).

Table I: Emf in Volts of Cell II in Propylene Glycol at Different Temperatures

			Temp, °C								
m_1	m_2	m_3	5	10	15	20	25	30	35	40	45
0.00517	0.00557	0.00488	0.6472	0.6498	0.6525	0.6553	0.6580	0.6607	0.6635	0.6662	0.6690
0.0138	0.0130	0.0127	0.6212	0.6235	0.6260	0.6282	0.6304	0.6325	0.6350	0.6376	0.6397
0.0201	0.0140	0.0182	0.6055	0.6077	0.6093	0.6110	0.6135	0.6156	0.6172	0.6193	0.6223
0.0210	0.0180	0.0199	0.6080	0.6099	0.6124	0.6138	0.6157	0.6171	0.6192	0.6216	0.6231
0.0265	0.0228	0.0251	0.6025	0.6046	0.6073	0.6089	0.6104	0.6120	0.6136	0.6152	0.6173
0.0110	0.0370	0.0176	0.6440	0.6470	0.6495	0.6522	0.6547	0.6572	0.6601	0.6627	0.6652
0.0188	0.0180	0.0440	0.5912	0.5930	0.5948	0.5966	0.5984	0.6001	0.6018	0.6036	0.6054
0.0421	0.0410	0.0401	0.5936	0.5958	0.5979	0.5993	0.6012	0.6031	0.6050	0.6069	0.6088
0.0498	0.0503	0.0487	0.5904	0.5923	0.5941	0.5959	0.5970	0.5985	0.6003	0.6022	0.6040
pK_a of acetic acid			9.41	9.38	9.36	9.34	9.32	9.31	9.30	9.28	9.27

Table II: Emf in Volts of Cell II in Ethylene Glycol at Different Temperatures

			Temp, °C								
m_1	m_2	m_3	5	10	15	20	25	30	35	40	45
0.00489	0.00507	0.00494	0.6536	0.6559	0.6582	0.6605	0.6628	0.6652	0.6675	0.6698	0.6721
0.00978	0.01017	0.00987	0.6376	0.6394	0.6413	0.6431	0.6448	0.6468	0.6486	0.6505	0.6523
0.0156	0.0155	0.0153	0.6262	0.6279	0.6295	0.6311	0.6327	0.6343	0.6359	0.6375	0.6392
0.0196	0.0204	0.0199	0.6208	0.6226	0.6244	0.6261	0.6279	0.6297	0.6314	0.6332	0.6349
0.0253	0.0251	0.0252	0.6149	0.6164	0.6179	0.6194	0.6208	0.6223	0.6238	0.6253	0.6268
0.0288	0.0321	0.0295	0.6145	0.6160	0.6175	0.6190	0.6205	0.6220	0.6234	0.6250	0.6266
0.0327	0.0375	0.0348	0.6115	0.6130	0.6145	0.6159	0.6174	0.6188	0.6204	0.6218	0.6232
0.0356	0.0432	0.0400	0.6088	0.6101	0.6115	0.6128	0.6142	0.6155	0.6168	0.6182	0.6196
0.0399	0.0465	0.0441	0.6065	0.6077	0.6090	0.6104	0.6116	0.6129	0.6142	0.6154	0.6167
pK_a of acetic acid			8.70	8.63	8.58	8.53	8.48	8.44	8.40	8.35	8.31

plotting pK_a' against μ and the extrapolation of the resulting plot to $\mu = 0$ would give the value of pK_a of the acid in the respective solvents.

Assuming complete dissociation of the salt NaX, the values of m_{X^-} could be taken as m_3, the stoichiometric concentration of NaX. As the dissociation constants of the acid are of the order of 10^{-8} to 10^{-9} in the two glycols,[5] no correction for the dissociation of HOAc should be necessary. Similarly, the change of effective concentration of OAc^- as well as of HOAc due to solvolytic reaction, such as $OAc^- + SH = S^- + HOAc$, would be of remote possibility, as can be seen from simple calculations based on the procedure described in an earlier paper.[7] The emf data (E_X) against the corresponding molalities of the acid (m_1), acetate ion (m_2) and the halide ion (m_3) for each buffer solution in the two solvents at different temperatures are presented in Tables I and II. The ionic strength (μ) was taken to be equal to $(m_2 + m_3)d_0$, where d_0 is the density of the solvent at the respective temperature. The pK_a values were calculated from the observed emf values (E_X) of the cell II, containing the buffer solutions of definite compositions, and taking the standard potentials $(E_m^\circ)_{Ag-AgX}$ for the corresponding solvent at different temperatures as reported earlier.[1,2] The pK_a values for each solvent, obtained from extrapolation of pK_a' to $\mu = 0$ at different temperatures, are presented in Tables I and II. These values can be represented in the form of equations of the Harned–Robinson type, obtained by the method of least squares, as shown below for propylene glycol

$$pK_a = \frac{827.82}{T} + 4.817 + 0.00581T \qquad (3)$$

and ethylene glycol

$$pK_a = \frac{1360.24}{T} + 2.176 + 0.00585T \qquad (4)$$

Standard Potentials of Ag–AgBr in Propylene Glycol and of Ag–AgI Electrode in Ethylene and Propylene Glycols. The values of dissociation constants of acetic acid in the solvents at different temperatures as evaluated above have been utilized for the determination of standard potentials $(E_m^\circ)_{Ag-AgX}$ in the respective solvents, where X denotes Br or I. Equation 1, on rearrangement, takes the form

$$E_X^{\circ\prime} = E_X - k(pK_a) + k \log \frac{m_1 m_3}{m_2}$$

$$= (E_m^\circ)_{Ag-AgX} - k \log \frac{\gamma_{HOAc}\,\gamma_{X^-}}{\gamma_{OAc^-}}$$

$$= (E_m^\circ)_{Ag-AgX} + f(\mu) \qquad (5)$$

(7) S. K. Banerjee, K. K. Kundu, and M. N. Das, *J. Chem. Soc.*, *A*, 166 (1967).

Table III: Emf in Volts of Cell II in Propylene Glycol at Different Temperatures (X = Br)

			Temp, °C								
m_1	m_2	m_3	5	10	15	20	25	30	35	40	45
0.00496	0.00512	0.00518	0.5114	0.5144	0.5174	0.5205	0.5235	0.5266	0.5296	0.5327	0.5358
0.00985	0.01022	0.01031	0.4957	0.4985	0.5014	0.5042	0.5071	0.5100	0.5128	0.5157	0.5172
0.0166	0.0146	0.0160	0.4814	0.4838	0.4862	0.4885	0.4909	0.4933	0.4956	0.4980	0.5005
0.0218	0.0191	0.0209	0.4750	0.4770	0.4791	0.4811	0.4832	0.4862	0.4883	0.4904	0.4925
0.0272	0.0238	0.0260	0.4680	0.4704	0.4728	0.4751	0.4774	0.4798	0.4821	0.4844	0.4868
0.0293	0.0304	0.0307	0.4690	0.4713	0.4737	0.4760	0.4783	0.4806	0.4828	0.4851	0.4874
0.0376	0.0334	0.0342	0.4631	0.4652	0.4672	0.4693	0.4713	0.4734	0.4754	0.4774	0.4794
0.0483	0.0388	0.0412	0.4557	0.4576	0.4596	0.4615	0.4634	0.4654	0.4673	0.4692	0.4711
0.0424	0.0474	0.0438	0.4620	0.4640	0.4660	0.4680	0.4700	0.4720	0.4740	0.4760	0.4780
0.0505	0.0497	0.0502	0.4550	0.4570	0.4589	0.4608	0.4628	0.4647	0.4666	0.4685	0.4705

Table IV: Emf in Volts of Cell II in Propylene Glycol at Different Temperatures (X = I)

			Temp, °C								
m_1	m_2	m_3	5	10	15	20	25	30	35	40	45
0.00539	0.00450	0.00436	0.3267	0.3298	0.3332	0.3365	0.3397	0.3432	0.3466	0.3499	0.3533
0.0104	0.00971	0.00895	0.3103	0.3136	0.3170	0.3201	0.3234	0.3266	0.3298	0.3330	0.3362
0.0166	0.0157	0.0153	0.2975	0.3006	0.3040	0.3069	0.3100	0.3134	0.3157	0.3187	0.3217
0.0204	0.0199	0.0203	0.2915	0.2943	0.2970	0.2998	0.3027	0.3053	0.3079	0.3107	0.3132
0.0263	0.0243	0.0249	0.2873	0.2898	0.2923	0.2948	0.2972	0.2997	0.3020	0.3046	0.3070
0.0312	0.0289	0.0303	0.2824	0.2846	0.2870	0.2894	0.2917	0.2941	0.2965	0.2990	0.3014
0.0336	0.0356	0.0342	0.2827	0.2850	0.2873	0.2895	0.2918	0.2941	0.2962	0.2986	0.3009
0.0404	0.0395	0.0393	0.2775	0.2797	0.2818	0.2839	0.2860	0.2881	0.2902	0.2924	0.2944
0.0454	0.0442	0.0436	0.2758	0.2777	0.2795	0.2813	0.2830	0.2849	0.2867	0.2885	0.2903
0.0484	0.0492	0.0492	0.2726	0.2745	0.2765	0.2785	0.2804	0.2824	0.2842	0.2863	0.2882

Table V: Emf in Volts of Cell II in Ethylene Glycol at Different Temperatures (X = I)

			Temp, °C								
m_1	m_2	m_3	5	10	15	20	25	30	35	40	45
0.00463	0.00465	0.00493	0.3345	0.3373	0.3400	0.3428	0.3455	0.3484	0.3512	0.3540	0.3558
0.0111	0.00982	0.0101	0.3140	0.3165	0.3190	0.3214	0.3244	0.3264	0.3290	0.3327	0.3345
0.0152	0.0153	0.0153	0.3073	0.3098	0.3122	0.3146	0.3170	0.3194	0.3218	0.3242	0.3267
0.0203	0.0198	0.0201	0.2997	0.3019	0.3042	0.3064	0.3080	0.3109	0.3131	0.3154	0.3180
0.0267	0.0238	0.0248	0.2919	0.2941	0.2964	0.2986	0.3014	0.3032	0.3055	0.3078	0.3100
0.0303	0.0296	0.0302	0.2892	0.2914	0.2935	0.2957	0.2984	0.3001	0.3023	0.3045	0.3067
0.0334	0.0348	0.0352	0.2882	0.2901	0.2921	0.2941	0.2962	0.2981	0.3009	0.3022	0.3043
0.0381	0.0397	0.0393	0.2846	0.2867	0.2887	0.2908	0.2931	0.2948	0.2967	0.2977	0.3009
0.0406	0.0448	0.0438	0.2838	0.2857	0.2876	0.2895	0.2920	0.2934	0.2953	0.2973	0.2998
0.0472	0.0504	0.0502	0.2793	0.2812	0.2831	0.2850	0.2874	0.2888	0.2907	0.2926	0.2953

The plotting of the functions $E_X^{\circ\prime}$ against ionic strengths of the corresponding systems resulted in straight lines, which on extrapolation to $\mu = 0$ gave the intercepts equal to $(E_m^\circ)_{Ag-AgBr}$ in propylene glycol and $(E_m^\circ)_{Ag-AgI}$ in both the glycols.

$E_X^{\circ\prime}$ functions were computed from the observed E_X values at the corresponding compositions of the solutions in each system, which are presented in Tables III, IV, and V at different temperatures. In Table VI are collected the E° values on the molal scale for the Ag–AgBr electrode in propylene glycol and Ag–AgI electrode in ethylene and propylene glycols at nine temperatures. The same table also shows the standard potentials on the molar and mole fraction scales as computed from the usual relations.

The E_m° values can be fitted in the form of equations of the Harned–Robinson type using the least-squares method, as given below for propylene glycol

$$(E_m^\circ)_{Ag-AgBr} = -0.1633 - 1.48 \times 10^{-3}(t - 25) - 1.39 \times 10^{-6}(t - 25)^2 \quad (6)$$

$$(E_m^\circ)_{Ag-AgI} = -0.3468 - 1.38 \times 10^{-3}(t - 25) - 1.13 \times 10^{-6}(t - 25)^2 \quad (7)$$

and ethylene glycol

Table VI: Standard Potentials in Volts of Ag–AgX Electrodes in Glycols on Different Scales at Different Temperatures

	Temp, °C								
	5	10	15	20	25	30	35	40	45
					Ag–AgBr in Propylene Glycol				
$E_m°$	−0.1342	−0.1411	−0.1489	−0.1560	−0.1633	−0.1706	−0.1784	−0.1857	−0.1937
$E_c°$	−0.1320	−0.1390	−0.1470	−0.1542	−0.1616	−0.1691	−0.1771	−0.1845	−0.1927
$E_N°$	−0.2576	−0.2668	−0.2767	−0.2861	−0.2956	−0.3052	−0.3152	−0.3247	−0.3349
					Ag–AgI in Propylene Glycol				
$E_m°$	−0.3197	−0.3258	−0.3332	−0.3399	−0.3468	−0.3535	−0.3609	−0.3676	−0.3749
$E_c°$	−0.3175	−0.3237	−0.3313	−0.3381	−0.3451	−0.3520	−0.3596	−0.3664	−0.3739
$E_N°$	−0.4431	−0.4515	−0.4610	−0.4700	−0.4791	−0.4881	−0.4977	−0.5066	−0.5161
					Ag–AgI in Ethylene Glycol				
$E_m°$	−0.2728	−0.2774	−0.2928	−0.2877	−0.2928	−0.2979	−0.3032	−0.3079	−0.3146
$E_c°$	−0.2672	−0.2719	−0.2774	−0.2823	−0.2874	−0.2926	−0.2980	−0.3028	−0.3096
$E_N°$	−0.4060	−0.4139	−0.4209	−0.4281	−0.4357	−0.4431	−0.4508	−0.4579	−0.4670

$$(E_m°)_{Ag-AgI} = -0.2928 - 1.03 \times 10^{-3}(t - 25) - 1.90 \times 10^{-6}(t - 25)^2 \quad (8)$$

Standard Free Energies, Entropies and Enthalpies of the Solvated Electrolytes. The standard electrode potentials of cell II and their temperature coefficients are essentially related to the standard free energy ($\Delta G°$) and entropy ($\Delta S°$) changes involved in the reaction

$$^1/_2H_2(g, 1 \text{ atm}) + AgX(s) = Ag(s) + HX(soln) \quad (9)$$

and hence, the latter quantities could be calculated from the relations

$$\Delta G° = \Delta G°_{HX(soln)} + G°_{Ag(s)} - {}^1/_2G°_{H_2}(g, 1 \text{ atm}) - \Delta G°_{AgX(s)} = -nFE° \quad (10)$$

and

$$\Delta S° = \bar{S}°_{HX(soln)} + S°_{AgX(s)} - S°_{AgX(s)} - {}^1/_2S°_{H_2}(g, 1 \text{ atm}) = nF\left(\frac{dE°}{dT}\right)_P \quad (11)$$

The standard molal free energy of formation $\Delta G°_{HX(soln)}$ of solvated HX (X = Cl, Br, or I) assumed to be completely ionized is then given by

$$\Delta G°_{HX(soln)} = \Delta G°_{AgX(s)} - nFE° \quad (12)$$

The values for the standard free energies of formation have been calculated for the corresponding solvated hydrogen halides in ethylene and propylene glycols and are listed in Table VII. The standard free energies of formation of AgX were obtained from Latimer.[8]

The standard molal entropies of formation of the solvated hydrogen halides were likewise calculated from relation 13 and these are tabulated in Table VII. The relevant entropy data were also obtained from Latimer.[8] These values of standard free energy of formation, when combined with the respective molal entropies, give the heats of formation of the solvated hydrogen halides. These enthalpies of formation are also listed in Table VII. The thermodynamic quantities presented in Table VII all refer to the molal scale. For the sake of comparison, all the corresponding data in the glycols as well as in water are also collected in Table VII. It can be observed from these data that in propylene glycol the resulting free energies, entropies, as well as enthalpies of solvated hydrogen halides tend to be less negative as the halides are in the order of Cl^-, Br^-, and I^-. A similar trend is also observed in the case of free energy and enthalpy data for ethylene

Table VII: Standard Free Energies, $\Delta G°_{HX(soln)}$, Heats of Formation $\Delta H°_{HX(soln)}$, and Partial Molal Entropies, $\bar{S}°_{HX(soln)}$, of Hydrogen Halides in Glycols and Water

$\Delta G°_{HX(soln)}$, kcal/mol	$\Delta H°_{HX(soln)}$, kcal/mol		$\bar{S}°_{HX(soln)}$, cal/mol, deg
	Ethylene Glycol		
HCl[a]	−26.77	−26.28	1.6
HBr[b]	−20.61	−19.32	4.3
HI	−9.08	−6.55	8.5
	Propylene Glycol		
HCl[b]	−25.48	−27.89	−8.1
HBr	−19.17	−20.12	−3.2
HI	−7.86	−7.62	+0.8
	Water		
HCl[c]	−31.34	−27.32	13.5
HBr[d]	−24.57	−18.67	19.8
HI[e]	−12.34	−4.78	25.4

[a] U. Sen, K. K. Kundu, and M. N. Das, *J. Phys. Chem.*, **71**, 3665 (1967). [b] K. K. Kundu, P. K. Chatterjee, D. Jana, and M. N. Das, *J. Chem. Eng. Data*, in press. [c] H. S. Harned and B. B. Owen, "The Physical Chemistry of Electrolyte Solutions," 3rd ed, Reinhold Publishing Corp., New York, N. Y., 1958, p 462. [d] H. B. Hetzer, R. A. Robinson, and R. G. Bates, *J. Phys. Chem.*, **66**, 1423 (1962). [e] H. B. Hetzer, R. A. Robinson, and R. G. Bates, *ibid.*, **68**, 1929 (1964).

(8) W. M. Latimer, "Oxidation Potentials," 2nd ed, Prentice Hall, Inc., Englewood Cliffs, N. J., 1952.

Table VIII: Thermodynamic Quantities (P) Accompanying the Transfer of Hydrogen Halides from Water to Glycols at 25°[a]

HX	$\Delta P_t°$			$\Delta P_t°(Cl^- - X^-)$			$\Delta P_{t,el}°(Cl^- - X^-)$			$\Delta P_{t,ch}°(Cl^- - X^-)$		
	$P = G$	S	H	G	S	H	G	S	H	G	S	H
						Ethylene Glycol						
HCl[b]	3.12	−7.1	1.02	0	0	0	0	0	0	0	0	0
HBr[c]	2.50	−10.6	−0.66	0.62	3.5	1.68	0.09[B] 0.20[H]	−0.5	−0.06	0.53[B] 0.42[H]	4.0	1.74
HI	1.78	−14.3	−1.65	1.34	7.2	2.67	0.21[B] 0.47[H]	−1.2	−0.14	1.13[B] 0.87[H]		
						Propylene Glycol						
HCl[b]	4.16	−16.0	−0.61	0	0	0	0	0	0	0	0	0
HBr	3.69	−17.3	−1.46	0.47	1.3	0.85	0.13[B] 0.27[H]	−1.0	−0.16	0.34[B] 0.20[H]	2.3	1.01
HI	2.77	−18.8	−2.84	1.39	2.8	2.23	0.29[B] 0.63[H]	−2.2	−0.35	1.10[B] 0.76[H]	5.0	2.58

[a] Values of $P = G$ and H are expressed in kcal/mol and that of $P = S$ are expressed in cal/mol, deg^{-1}. B and H indicate that calculations are based on Born and Hepler's model, respectively. [b, c] See footnotes *a* and *b* of Table VII.

glycol and water, while the respective entropy data become more and more positive for ethylene glycol as well as for water. Since a major part of these data comprises the characteristic property of Ag(s), AgX(s), and of the gaseous H_2, the real effect of solvent is greatly masked. Thus a convenient way to examine the solvent effect on these thermodynamic properties accompanying the reaction is to calculate the energetics involved in the transfer of 1 mole of hydrogen halides from water to the solvent concerned.

Free Energy, Entropy, and Enthalpy of Transfer of Hydrogen Halides from Water to Glycols. For the process HX (in water) → HX (in solvent) the free energy of transfer could be defined by

$$\Delta G°_{t(HX)} = {}_s\bar{G}°_{HX} - {}_w\bar{G}°_{HX} = {}_s\Delta G°_{HX(soln)} - {}_w\Delta G°_{HX(soln)} \quad (13)$$

where $\bar{G}°_{HX}$ denotes molar free energy of HX in solution and the subscripts s and w denote solvent and water, respectively. The effect of solvent on the free energy of transfer should, however, be more clearly reflected in the mole fraction scale, because that will eliminate free energy changes due to concentration changes. Thus the free energy of transfer is directly given by

$$\Delta G°_{t(HX)} = -F[{}_sE_N° - {}_wE_N°] \quad (14)$$

The values of $\Delta G_t°$(HX) in kilocalories for propylene and ethylene glycols, calculated from the standard potentials in the solvents at 25°, are listed in Table VIII. The values are probably accurate within ±0.012 kcal.

Similarly, the standard entropy changes, $\Delta S_t°$(HX), accompanying the transfer of HX from water to either solvent at 25° have been evaluated from the temperature coefficients of the standard potentials of the Ag–AgX electrodes in the two solvents and water. The corresponding enthalpy changes, $\Delta H_t°$(HX), have also been computed from the respective values of $\Delta G_t°$(HX) and $\Delta S_t°$(HX). The thermodynamic quantities so obtained for both the glycols are presented in Table VIII.

Since the process involves the transfer of charged particles, the hydrogen ion and the halide ion, from water to another solvent having a different dielectric constant, the related thermodynamic quantities comprise two parts: electrostatic (el) and nonelectrostatic or chemical (ch). Thus for free energy change

$$\Delta G_t° = \Delta G_{t,el}° + \Delta G_{t,ch}° \quad (15)$$

and so for the other thermodynamic quantities, $\Delta S_t°$ and $\Delta H_t°$. The nonelectrostatic contribution reflects the chemical nature of the solvent with respect to water which includes the basicity as well as the solvating capacity of the solvent.

The electrostatic contribution to the free energy of transfer may be computed, although approximately, from the much-used Born relation. This is, however, based on an oversimplified model and involves uncertainties with regard to the dielectric constant and radii of the solvated ions. The modified equation due to Hepler,[9] which takes into account the dielectric saturation in the ionic force field, may be better, but even then the uncertainty factor in the ionic radii would remain. Of all the ions, the effective radius of the solvated proton is the most difficult to assess, and to avoid the uncertainty from this source, we shall consider only the differences in the free energies of transfer of HCl and HBr as well as of HCl and HI, *i.e.*, the quantities $\Delta G_t°$(HCl) − $\Delta G_t°$(HBr) and $\Delta G_t°$(HCl) − $\Delta G_t°$(HI), respectively. These differences actually repre-

(9) L. G. Hepler, *Aust. J. Chem.*, 17, 587 (1964).

sent $\Delta G_t^\circ(Cl^-) - \Delta G_t^\circ(X^-)$, where X^- is Br^- or I^-, since the free energy term corresponding to the hydrogen ion cancels out. Henceforth, these differences will be denoted by $\Delta G_t^\circ(Cl^- - X^-)$ and the corresponding values for the entropy and enthalpy by $\Delta S_t^\circ(Cl^- - X^-)$ and $\Delta H_t^\circ(Cl^- - X^-)$, respectively.

The electrostatic contribution, $\Delta G_{t,el}^\circ(Cl^- - X^-)$, to the total quantity $\Delta G_t^\circ(Cl^- - X^-)$ has been computed for 25°, on the basis of Born as well as Hepler equation, taking the radii of Cl^-, Br^-, and I^- as 1.81, 1.95, and 2.16 Å (crystallographic radii),[10] respectively. Similarly, the electrostatic contribution $\Delta S_{t,el}^\circ(Cl^- - X^-)$ to the total entropy change $\Delta S_t^\circ(Cl^- - X^-)$ has also been computed for 25° from the differential form of Born eq 2, using the reported values of the temperature coefficients of the dielectric constants of the media.[11,12] From a knowledge of $\Delta G_{t,el}^\circ(Cl - X)$ and $\Delta S_{t,el}^\circ(Cl^- - X^-)$, the electrostatic part of the enthalpy change, $\Delta H_{t,el}^\circ(Cl^- - X^-)$ has also been evaluated. Hence, the nonelectrostatic or chemical parts of the quantities, $\Delta G_{t,ch}^\circ(Cl^- - X^-)$, $\Delta S_{t,ch}^\circ(Cl^- - X^-)$ and $\Delta H_{t,ch}^\circ(Cl^- - X^-)$, have been obtained by subtracting the electrostatic contributions from the total values. It should be noted, however, that although free energy calculations from Born or Hepler equations may be good enough, the uncertainties in the calculated entropy and enthalpy values are much greater. Even then, it may be worthwhile to attempt some general conclusions of a qualitative nature from these derived quantities, shown in Table VIII.

It may be seen from Table VIII that the total free energies of transfer, $\Delta G_t^\circ(HX)$, for all the three hydrogen halides, from water to either of the glycols are positive, and that the magnitude decreases in the order: HCl, HBr, HI, the values for propylene glycol being larger than those for ethylene glycol. This indicates that the overall effect of permittivity as well as of chemical nature (which mainly reflects the relative basicity and solvating capacity) of the solvent makes the transfer of HI, HBr, and HCl, at the respective standard states from water to either glycol increasingly unfavorable.

If we now tentatively accept the views of Izmailov, *et al.*,[13,14] and Feakins, *et al.*,[15] that, to a first approximation, the free energy of transfer $\Delta G_t^\circ(HX)$ is a linear function of $(r_{X^-})^{-1}$, the reciprocal of the radius of the ion X^-, the limiting value of $\Delta G_t^\circ(HX)$, as $(r_{X^-})^{-1}$ tends to zero, would furnish a measure of the free energy of transfer of the hydrogen ion, since $\Delta G_t^\circ(X^-)$ for an ion of infinite radius, when $(r_{X^-})^{-1} = 0$, should approach a value of negligible magnitude. The relative values of $\Delta G_t^\circ(HX)$ for either glycol suggest that the plots of $\Delta G_t^\circ(HX)$ against $(r_{X^-})^{-1}$ will result in a negative value for $\Delta G_t^\circ(H^+)$.

Similarly, the plots of $\Delta G_t^\circ(Cl^- - X^-)$ against $(r_{X^-})^{-1}$ would lead to a value of $\Delta G_t^\circ(Cl^-)$ at $(r_{X^-})^{-1} = 0$. The data for $\Delta G_t^\circ(Cl^- - X^-)$ for the three halide ions suggest that the resulting value of $\Delta G_t^\circ(Cl^-)$ will be a positive quantity. It may be noted that simultaneous extrapolations of the plots of $\Delta G_t^\circ(HX)$ and $\Delta G_t^\circ(Cl^- - X^-)$ against $(r_{X^-})^{-1}$, if suitably aimed at having the least discrepancies in the extrapolated values of $\Delta G_t^\circ(H^+)$ and $\Delta G_t^\circ(Cl^-)$ with respect to the experimental value of $\Delta G_t^\circ(HCl)$, should lend an extra confidence to the extrapolations. The positive values of $\Delta G_t^\circ(HX)$ as well as of $\Delta G_t^\circ(Cl^- - X^-)$ obviously lead to the conclusion that the positive magnitude of $\Delta G_t^\circ(X^-)$ for any halide ion must be larger than the negative magnitude of $\Delta G_t^\circ(H^+)$. Moreover, the value of $\Delta G_t^\circ(X^-)$, which remains always positive, gradually decreases from Cl^-, through Br^-, to I^-.

A part of the positive value of $\Delta G_t^\circ(X^-)$ for any halide ion must naturally arise from electrostatic effect. But the values of $\Delta G_{t,ch}^\circ(Cl^- - X^-)$, as evaluated on the basis of Born equation and given in Table VIII, suggest that even if the calculated values of $\Delta G_{t,ch}^\circ(Cl^- - X^-)$ be plotted against $(r_{X^-})^{-1}$, or better $(r_{X^-})^{-2}$ because of the ion–dipole interaction involved in the "chemical" effect, would also result in large positive values of $\Delta G_{t,ch}^\circ(X^-)$ for all the three halide ions. Since the "chemical" effect on the free energy of an ion of nonprotogenic nature in solution arises mainly from the solvation of the ion, $\Delta G_{t,ch}^\circ(X^-)$ should reflect the solvating capacities of the solvent concerned and water toward this ion. The resulting positive magnitudes of $\Delta G_{t,ch}^\circ(X^-)$ for all the halide ions presumably indicate that water possesses a larger solvating capacity toward halide ions than either of the glycols. Besides, the relative magnitudes of $\Delta G_{t,ch}^\circ(X^-)$ for the three halide ions indicate that the relative degree of solvation in either of the solvents decreases from Cl^-, through Br^-, to I^-. This sequence is in agreement with that of the decreasing force field around the ion because of its increasing size and consequent decreasing charge density which should largely influence the solvation of the ion.

The results computed from Hepler's model also indicate a similar type of behavior for the halide ions in both the glycols, although the absolute magnitudes of the respective quantities get altered to some extent for obvious reasons.

Since the solvation of anions is expected to occur through positively charged hydrogen centers of the

(10) L. Pauling, "The Nature of the Chemical Bond," Cornell University Press, Ithaca, N. Y., 1940.

(11) G. Akerlof, *J. Amer. Chem. Soc.*, **54**, 4125 (1932).

(12) G. O. Curme and F. Johnston, "Glycols," Reinhold Publishing Corp., New York, N. Y., 1952.

(13) V. V. Aleksandrov and N. A. Izmailov, *Zh. Fiz. Khim.*, **23**, 404 (1958).

(14) N. A. Izmailov, *Dokl. Akad. Nauk*, **127**, 104 (1959); *Zh. Fiz. Khim.*, **34**, 2414 (1960).

(15) D. Feakins and P. Watson, *Chem. Ind.*, 2008 (1965); *J. Chem. Soc.*, 4686, 4734 (1963).

isolated hydroxylated solvent dipoles oriented toward the anions,[16] it is not unreasonable to infer from the expected positive magnitudes of $\Delta G_{t,ch}^{\circ}(X^-)$ that the relative charge density on hydrogen atoms on water dipoles should exceed that on glycolic dipoles. This suggests that water dipoles are more acidic compared to glycolic dipoles. Similarly, it can be inferred from the expected negative magnitudes of $\Delta G_t^{\circ}(H^+)$ and hence $\Delta G_{t,ch}^{\circ}(H^+)$ (in view of positive contribution of $\Delta G_{t,el}^{\circ}(H^+)$ arising from lower dielectric constants of glycols) that water dipoles are less basic compared to glycolic dipoles. This is also in conformity with what is expected from the relative charge densities on negatively charged oxygen centers on the isolated dipoles of the respective solvents.

As in the case of free energy values, the thermodynamic quantities $\Delta S_t^{\circ}(HX)$ and $\Delta H_t^{\circ}(HX)$, if plotted against $(r_{X^-})^{-1}$, should yield the values of $\Delta S_t^{\circ}(H^+)$ and $\Delta H_t^{\circ}(H^+)$ at $(r_{X^-})^{-1} = 0$. The trends of the values of $\Delta S_t^{\circ}(HX)$ and $\Delta H_t^{\circ}(HX)$ for the three halides indicate that $\Delta S_t^{\circ}(H^+)$ and $\Delta H_t^{\circ}(H^+)$ should be highly negative. Again, from the trends of the total quantities $\Delta H_t^{\circ}(HX)$ and $\Delta S_t^{\circ}(HX)$, it follows that $\Delta S_t^{\circ}(X^-)$ and $\Delta H_t^{\circ}(X^-)$ should have relatively high positive magnitudes, decreasing from Cl^-, through Br^-, to I^-. The same conclusion may also be drawn from the trends of the values of $\Delta S_t^{\circ} \cdot (Cl^- - X^-)$ and $\Delta H_t^{\circ}(Cl^- - X^-)$. Considering the nonelectrostatic quantities $\Delta S_{t,ch}^{\circ}(Cl^- - X^-)$ and $\Delta H_{t,ch}^{\circ}(Cl^- - X^-)$ given in Table VIII, it may also be concluded, as for the corresponding free energy values, that $\Delta S_{t,ch}^{\circ}(X^-)$ and $\Delta H_{t,ch}^{\circ}(X^-)$ are all positive, decreasing in the order Cl^-, Br^-, I^-.

Free energy ($\Delta G_{t,ch}^{\circ}$) values discussed earlier have indicated that glycols have smaller solvating capacities toward halide ions than water. We may now check whether the corresponding $\Delta S_{t,ch}^{\circ}$ and $\Delta H_{t,ch}^{\circ}$ values substantiate this conclusion. Now, all structure forming processes including solvation of ions are exothermic and accompanied by loss of entropy, whereas structure-breaking processes including desolvation of ions are endothermic, entailing increases in entropy. The transfer of an ion from water to a glycol will involve dehydration of the hydrated ion in aqueous solution and solvation of the free ion in the glycolic solvent. The algebraic sum of ΔS° or ΔH° for these two processes will largely determine the overall entropy or enthalpy change, if we ignore the relatively smaller changes in these quantities accompanying changes in the liquid structure consequent on dehydration in water or solvation in glycol.

Hence, if glycols possess smaller solvating capacities toward halide ions than water, the chemical entropy of transfer, $\Delta S_{t,ch}^{\circ}(X^-)$ for any of these ions from water to glycol will be positive, as would be obtained on the basis of arguments set forth earlier. Again, from Cl^- through Br^-, to I^-, the halides show a decreasing degree of solvation in any solvent and hence there occurs a decreasingly ordered structure. The iodide ion is little solvated in either water or glycol, so that the entropy of transfer, although positive, should be the smallest for this ion. For the most solvated chloride ion, $\Delta S_{t,ch}^{\circ}(X^-)$ should be the highest. Similar reasonings apply equally well to $\Delta H_{t,ch}^{\circ}(X^-)$ values. Thus, the chemical contributions toward all three thermodynamic quantities accompanying the transfer process indicate that so far as the halide ions are concerned, water is a stronger solvating agent than the glycols.

Acknowledgment. The work was done under a project financed by the National Bureau of Standards, Washington, D. C.

(16) D. Feakins in "Physico-Chemical Processes in Mixed Aqueous Solvents," F. Franks, Ed., Heinemann Educational Books Ltd., London, 1967.

Thermodynamics of Self-Ionization of Ethylene and Propylene Glycols

by K. K. Kundu, P. K. Chattopadhyay, Debabrata Jana, and M. N. Das

Physical Chemistry Laboratories, Jadavpur University, Calcutta-32, India *(Received October 13, 1969)*

Autoprotolysis constants (K_s) of ethylene and propylene glycols have been determined at nine temperatures (5–45°), from emf measurements of cells of the type

Pt, H_2(g, 1 atm)|MS, MBr, glycol|AgBr–Ag

where S denotes the lyate ion and M stands for Na or K. The experimental data can be expressed in the form of Harned–Robinson type equations, using least-squares calculations, as given below for ethylene glycol and propylene glycol.

$$pK_s = \frac{3487.25}{T} + 0.927 + 0.01079T$$

$$pK_s = \frac{3372.00}{T} + 2.571 + 0.01120T$$

Thermodynamic quantities, $\Delta H°$, $\Delta G°$, $\Delta S°$, and $\Delta C_p°$, for the processes have been evaluated at nine temperatures by using the well-known relations comprising the constants of the above equations. The evaluated thermodynamic quantities associated with the self-ionization of these solvents and of water have been utilized to throw some light on the structural aspects as well as on the relative acid–base strengths of the three solvents, using Born's model to compute the electrostatic parts of the thermodynamic functions.

The autoprotolysis or self-ionization constant of an amphiprotic solvent is quite a significant quantity in respect to its importance in giving a quantitative measure of the extreme limits of acidity and basicity in the solvent. Hence, the autoprotolysis constants of many amphiprotic solvents and their aqueous mixtures have been worked out. As expected, it has been found that since this self-ionization process accompanies charge separation, it is highly dependent on the dielectric constant as well as the intrinsic acidity and basicity of the solvent. This contention has also been amply demonstrated, especially in the cases of mixed solvents like dioxane–water,[1] methanol–water,[2] ethanol–water[3] and glycol–water.[4]

Besides the free energy changes, heats and entropies of self-ionization of amphiprotic solvents should be no less important in offering a clearer insight with regard to the changes in structural aspects of the solvents and thus in forming a clearer understanding of the energetics involved in the overall process. The present paper describes our findings on these aspects for two amphiprotic solvents namely, ethylene glycol and propylene glycol.

Methods

Since the thermodynamic parameters such as $\Delta G°$, $\Delta H°$, $\Delta S°$, and $\Delta C_p°$ for self-ionization of an amphiprotic solvent can be easily calculated from the constants of the equation of Harned–Robinson[5] type

$$pK_s = \frac{A^*}{T} - D^* + C^*T \qquad (1)$$

to be obtained by the method of least squares from the data of pK_s at different temperatures, it is necessary to find experimentally the autoprotolysis constants (K_s) of the solvent at different temperatures. The autoprotolysis of an amphiprotic solvent is generally represented by the equation

$$SH + SH \rightleftharpoons SH_2^+ + S^- \qquad (2)$$

where SH denotes the solvent molecule, SH_2^+ the lyonium ion, and S^- the lyate ion. The autoprotolysis constant K_s of the solvent is then given by the equilibrium constant of the process 2, *i.e.*

$$K_s = \frac{a_{SH_2^+}a_{S^-}}{a_{SH}^2} = \frac{a_{SH_2^+}m_{S^-}\gamma_{S^-}}{a_{SH}^2} \qquad (3)$$

where a denotes the activity, m the molality, and γ the activity coefficient.

The values of K_s for the two glycols have been determined at nine temperatures in the range 5–45° at 5° intervals, using a cell of the type

Pt, H_2(g, 1 atm)|MS, MBr (solvent)|AgBr–Ag (A)

where M denotes Na or K.

(1) H. S. Harned and L. D. Fallon, *J. Amer. Chem. Soc.*, **61**, 2374 (1939).

(2) J. Koskikallio, *O. Soumen Kem.*, **30B**, 38, 43, 111 (1957).

(3) B. Gutbezahl and E. Grunwald, *J. Amer. Chem. Soc.*, **75**, 559, 665 (1953).

(4) S. K. Banerjee, K. K. Kundu, and M. N. Das, *J. Chem. Soc., A*, 166 (1967).

(5) H. S. Harned and R. A. Robinson, *Trans. Faraday Soc.*, **36**, 973 (1940).

Table I: Emf in Volts of Cell A for the Evaluation of pK_s Values of Ethylene Glycol at Different Temperatures

		Temp, °C								
m_{S^-}	m_{Br^-}	5	10	15	20	25	30	35	40	45
0.00396	0.00516	0.8242	0.8253	0.8265	0.8279	0.8292	0.8305	0.8322	0.8330	0.8347
0.00666	0.00901	0.8232	0.8243	0.8255	0.8269	0.8285	0.8298	0.8310	0.8322	0.8340
0.00860	0.00116	0.8236	0.8248	0.8260	0.8276	0.8286	0.8300	0.8314	0.8326	0.8340
0.0137	0.0185	0.8239	0.8253	0.8265	0.8279	0.8293	0.8308	0.8321	0.8336	0.8350
0.0193	0.0252	0.8248	0.8260	0.8272	0.8288	0.8299	0.8315	0.8330	0.8343	0.8359
0.0244	0.0318	0.8245	0.8257	0.8269	0.8283	0.8297	0.8311	0.8323	0.8348	0.8355
0.0248	0.0323	0.8251	0.8263	0.8275	0.8289	0.8302	0.8318	0.8333	0.8346	0.8360
0.0277	0.0374	0.8245	0.8260	0.8270	0.8285	0.8297	0.8313	0.8324	0.8338	0.8350
0.0328	0.0428	0.8255	0.8268	0.8279	0.8292	0.8306	0.8317	0.8328	0.8344	0.8355
0.0367	0.0479	0.8255	0.8267	0.8279	0.8292	0.8306	0.8317	0.8328	0.8344	0.8356
0.0489	0.0670	0.8250	0.8262	0.8274	0.8290	0.8301	0.8317	0.8330	0.8345	0.8360

Table II: Emf in Volts of Cell A for the Evaluation of the pK_s Values of Propylene Glycol at Different Temperatures

		Temp, °C								
m_{S^-}	m_{Br^-}	5	10	15	20	25	30	35	40	45
0.00086	0.00378	0.8130	0.8140	0.8151	0.8162	0.8173	0.8184	0.8195	0.8206	0.8217
0.00538	0.00627	0.8450	0.8467	0.8484	0.8501	0.8518	0.8536	0.8554	0.8570	0.8587
0.00470	0.01050	0.8290	0.8306	0.8322	0.8337	0.8353	0.8368	0.8383	0.8399	0.8414
0.00913	0.01090	0.8447	0.8472	0.8486	0.8500	0.8514	0.8528	0.8542	0.8556	0.8570
0.00990	0.0202	0.8323	0.8330	0.8344	0.8357	0.8370	0.8383	0.8396	0.8409	0.8423
0.0210	0.0292	0.8424	0.8440	0.8455	0.8470	0.8485	0.8501	0.8516	0.8532	0.8547
0.0227	0.0438	0.8354	0.8368	0.8381	0.8396	0.8409	0.8423	0.8437	0.8451	0.8465
0.0153	0.0677	0.8152	0.8162	0.8173	0.8183	0.8193	0.8204	0.8215	0.8225	0.8236
0.0117	0.0842	0.8046	0.8054	0.8063	0.8071	0.8080	0.8088	0.8096	0.8104	0.8112

The general experimental procedure has been described earlier.[4,6-8]

Results and Discussion

The emf of cell A is given by

$$E = E^\circ_{Ag-AgBr} - \frac{2.303RT}{F} \log a_{SH_2^+} a_{Br^-}/a_{SH} \quad (4)$$

Substituting the values of $a_{SH_2^+}$ by $K_s a_{SH}^2/m_{S^-}\gamma_{S^-}$ from eq 3 and writing $m_{Br^-}\gamma_{Br^-}$ for a_{Br^-}, we have by rearranging the terms in eq 4

$$\frac{F(E - E^\circ_{Ag-AgBr})}{2.303RT} + \log \frac{m_{Br^-}}{m_{S^-}} = -\log K_s - \log \frac{\gamma_{Br^-} a_{SH}}{\gamma_{S^-}} \quad (5)$$

The term $\log (\gamma_{Br^-} a_{SH})/\gamma_{S^-}$ becomes zero at zero ionic strength ($\mu = 0$), since by convention the terms become unity and a_{SH} also becomes unity for the pure solvent when $\mu = 0$. A plot of the quantity on the left-hand side, which may be denoted by pK_s', against μ should, therefore, yield pK_s on extrapolation to $\mu = 0$. In eq 4 the term a_{SH} is very often assumed to be unity and dropped out for all concentrations, since the solutions used are generally dilute enough. The a_{SH} term should, however, occur in eq 4, since the reaction taking place in cell A involves the solvent as shown below

$$^1/_2H_2(g) + AgX(s) + SH \longrightarrow SH_2^+(solution) + X^-(solution) + Ag(s)$$

Similarly, in eq 3, the term a_{SH}^2 is usually dropped out, being assumed unity, but that should be correct only for sufficiently dilute solutions.

The E_m° values used for the Ag–AgBr electrode at different temperatures were determined by the authors recently in this laboratory.[8,9] The emf data and the corresponding molalities of the lyate ion m_{S^-} and the halide ion m_{Br^-} are presented in Tables I and II. The pK_s values obtained from the extrapolations are given in Table III. The values given in Table III can be expressed in the form of equations of Harned–Robinson[5] type, obtained by the method of least squares, as follows: for ethylene glycol

$$pK_s = \frac{3487.25}{T} + 0.927 + 0.01079T \quad (6)$$

and for propylene glycol

$$pK_s = \frac{3372.00}{T} + 2.571 + 0.01120T \quad (7)$$

(6) K. K. Kundu and M. N. Das, *J. Chem. Eng. Data*, **9**, 87 (1964).

(7) K. K. Kundu and M. N. Das, *ibid.*, **9**, 82 (1964).

(8) K. K. Kundu, P. K. Chattopadhyay, D. Jana, and M. N. Das, *J. Chem. Eng. Data*, in press.

(9) K. K. Kundu, D. Jana, and M. N. Das, *J. Phys. Chem.*, **74**, 2625 (1970).

Table III: pK_s Values of Ethylene and Propylene Glycols at Different Temperatures

	Temp, °C								
	5	10	15	20	25	30	35	40	45
Ethylene glycol	16.47	16.30	16 14	15.99	15.84	15.71	15.57	15.44	15.32
Propylene glycol	17.81	17.64	17.50	17.35	17.21	17.08	16.96	16.83	16.73

Table IV: Free Energy, Enthalpy, Entropy, and Heat Capacity Changes[a] (in Molal Scale) Accompanying the Autoprotolysis of the Glycols and Water at Different Temperatures

	Temp, °C								
	5	10	15	20	25	30	35	40	45
					Ethylene Glycol				
$\Delta G°$	20.96	21.12	21.28	21.44	21.61	21.78	21.95	22.13	22.30
$\Delta H°$	12.14	12.00	11.86	11.71	11.57	11.42	11.27	11.11	10.96
$\Delta S°$	−31.7	−32.2	−32.7	−33.2	−33.7	−34.2	−34.7	−35.2	−35.7
$\Delta C_p°$	−27.5	−28.0	−28.5	−29.0	−29.4	−29.9	−30.4	−30.9	−31.4
					Propylene Glycol				
$\Delta G°$	22.67	22.87	23.08	23.28	23.49	23.70	23.92	24.13	24.35
$\Delta H°$	11.47	11.32	11.18	11.03	10.88	10.73	10.56	10.41	10.24
$\Delta S°$	−40.3	−40.8	−41.3	−41.8	−42.3	−42.8	−43.3	−43.8	−44.4
$\Delta C_p°$	−28.5	−29.0	−29.5	−30.0	−30.5	−31.0	−31.6	−32.1	−32.6
					Water				
$\Delta G°$	18.75	18.83	18.91	19.00	19.09	19.19	19.29	19.39	19.50
$\Delta H°$	14.42	14.20	13.98	13.75	13.52	13.28	13.04	12.80	12.56
$\Delta S°$	−15.6	−16.4	−17.1	−17.9	−18.7	−19.5	−20.2	−21.0	−21.8
$\Delta C_p°$	−43.4	−44.2	−45.0	−45.8	−46.6	−47.3	−48.1	−48.9	−49.7

[a] $\Delta G°$ and $\Delta H°$ values are in kcal/mol and $\Delta S°$ and $\Delta C_p°$ values are in cal/mol, °C.

The corresponding equation for water[5] is

$$pK_s = \frac{4471.33}{T} - 6.085 + 0.01705T \qquad (8)$$

The maximum deviations in pK_s values obtained from the eq 6 and 7 and those found experimentally lie within ±0.01 unit.

The thermodynamic quantities $\Delta G°$, $\Delta H°$, $\Delta S°$, and $\Delta C_p°$ for the self-ionization of the solvents were evaluated from the usual equations[10] comprising the constants of eq 1.

These values of $\Delta G°$, $\Delta H°$, $\Delta S°$, and $\Delta C_p°$ for the glycols and water at nine temperatures are given in Table IV. In Table V are collected the values $\Delta G°$, $\Delta H°$, and $T\Delta S°$ at 25° for the different solvents so far studied. The values of standard free energy and entropy changes on the mole fraction scale, $\Delta G_N°$ and $\Delta S_N°$ were calculated by the equations

$$\Delta G_N° = \Delta G° + 2.303RT \log \frac{1000}{M_{SH}} \qquad (9)$$

$$\Delta S_N° = \Delta S° - 2.303R \log \frac{1000}{M_{SH}} \qquad (10)$$

The values of $\Delta G_N°$ and $T\Delta S_N°$ for different solvents are also included in Table V. It may be noted that $\Delta H°$ has the same values on either scale for the solute. The $\Delta G_N°$ values are expected to reflect in a general way the composite effects of the dielectric constant and the intrinsic acidity as well as the basicity of the solvents. Thus, $\Delta G_N°$ values gradually increase as the dielectric constants of the solvents decrease, at least for the solvents of similar acidity and basicity. Since acetic acid as well as sulfuric acid is highly protogenic in nature, $\Delta G_N°$ values are expectedly lower than those of the other solvents, while NH_3 in spite of being a highly protophilic solvent has higher $\Delta G_N°$ values.

It is well known that in many systems the free energy function is less discriminating than either the enthalpy or entropy function. This is chiefly because many of the effects associated with enthalpy functions get compensated with the corresponding effects associated with entropy functions. Presumably in view of this, Feakins[11] is of the opinion that while free energy function is dominated by a contribution which does not reflect struc-

(10) H. S. Harned and B. B. Owen, "Physical Chemistry of Electrolytic Solutions," 3rd ed, Reinhold Publishing Corp., New York, 1957, p 762.

(11) F. Franks, Ed., "Physico-Chemical Processes in Mixed Aqueous Solvents," Heinemann Educational Books Ltd., London, 1967, p 148.

Table V: Thermodynamic Quantities[a] Accompanying Self-Ionization of Different Solvents, at 25°

	$\Delta G°$	$\Delta G_N°$	$\Delta H° = \Delta H_N°$	$T\Delta S°$	$T\Delta S_N°$	D_s
Water[5]	19.09	23.85	13.52	−5.57	−10.33	78.30
Ethylene glycol[b]	21.61	24.91	11.57	−10.04	−13.34	36.76
Methanol[14]	22.71	26.79	11.20	−11.51	−15.59	32.63
Propylene glycol[b]	23.49	26.54	10.88	−12.61	−15.66	31.00
Ethanol[14]	25.63	29.28	11.50	−14.13	−17.78	24.30
Acetic acid[14]	17.21	20.54	5.70	−11.51	−14.84	6.30
Sulfuric acid[15]	4.73	7.48	0.23	−4.50	−7.25	101
Ammonia[14]	41.31	46.16	26.70	−14.61	−19.46	22 (−34°)

[a] In kcal/mol. [b] From the present study.

tural features of the system, the corresponding enthalpy and entropy functions contain important structural contributions. For this reason also Hills,[11] Franks and Ives,[12] Bates[13] and many others stressed the importance of examining these two functions also besides the less discriminating free energy function. Thus it is expected that the heats $\Delta H_N°$ and entropies $\Delta S_N°$ of the self-ionization process should also involve the structural aspects of the solvents. The considerably less negative value of $T\Delta S_N°$ for water, as compared to those for other hydroxylic solvents, has been explained by Jolly[14] in terms of considerable structure breaking of water caused by an ion when it enters the strongly hydrogen-bonded structure of water. Gillespie, *et al.*,[15] however, in explaining the still smaller $T\Delta S_N°$ value for the autoprotolysis of H_2SO_4, held the view that the autoprotolysis of a protonic solvent like H_2SO_4, acetic acid, or water, forming SH_2^+ and S^- ions, does not have the same effect on the structure of the solvent as other ions do, since they differ from the SH molecule only by possessing one more or one less proton, and it is likely that they will cause little, if any, disruption of the structure. They further believe that the SH_2^+ and S^- ions will rather cause a strengthening of the hydrogen bonds around the ion and an increase in the "characteristic structure" of the solvent in bulk, involving a three-dimensional framework, resulting in a decrease in entropy. The larger negative $T\Delta S_N°$ values for weakly hydrogen-bonded solvents such as methanol and ethanol probably arise because the characteristic ions resulting from autoprotolysis presumably cause a considerable increase in the strength and the amount of hydrogen bonding. On the other hand, in the strongly hydrogen-bonded solvents such as water and H_2SO_4 the effect of the characteristic ions on the structure will be relatively much smaller, and hence the entropy changes accompanying the autoprotolysis are correspondingly small. In the light of this concept, the entropy changes accompanying the autoprotolysis of ethylene and propylene glycols indicate that these dihydroxy alcohols are no doubt relatively more associated than the monohydroxy alcohols due to increased hydrogen bonding, but the existence of any such "characteristic structure" in the bulk is at least less predominant in the glycolic solvents.

As is well known, the unique distribution of charge centers in isolated water dipoles tends to impart a so-called hydrogen-bonded tetrahedral structure to water. The absence of suitable charge distribution in isolated dipoles of glycols perhaps cannot lead to any such characteristic structure in the solvents, though some polymeric chain-like two-dimensional structure due to hydrogen bonding might very well be present in the glycolic solvents. The fairly less negative values of $T\Delta S_N°$ in water are presumably related to the breakdown of such characteristic structure and not of the hydrogen-bonded polymeric chains.

Since autoprotolysis involves charge separation, any conclusion regarding the chemical nature of solvents and their structural aspects that could be derived from the thermodynamic parameters accompanying the self-ionization of the solvents should be largely masked, due to the electrostatic effect arising from the difference in dielectric constants of the solvents. Hence, the foremost task is to make an assessment of this electrostatic effect.

In spite of the well-known limitations in regard to dielectric saturation as well as the assumed independence of radii of solvated ions in different solvents, Born eq 11 is often used in computing the electrostatic part of the thermodynamic quantities, resulting from the difference in permittivity of the solvents, but because of limited knowledge regarding the proton solvation in solvents other than water, it would be difficult to use Born equation as such. If, however, one is allowed to assume the solvated ions to be at least effectively spherical, it is possible to avoid the arbitrariness in choosing the radii of the ions in solvents by using the linear relation 12 predicted from simple Born equation at different temperatures, as was first demonstrated by

(12) F. Franks and D. J. G. Ives, *Quart. Rev. Chem. Soc.*, **20**, 1 (1966).

(13) R. G. Bates in "Hydrogen-Bonded Solvent Systems," A. K. Covington, and P. Jones, Ed., Taylor and Francis, London, 1968.

(14) W. L. Jolly, *J. Amer. Chem. Soc.*, **74**, 6199 (1952).

(15) R. J. Gillespie, E. A. Robinson, and C. Solomons, *J. Chem. Soc.*, 4321 (1960).

Baughan[16] and later confirmed by La Mer and Brescia.[17] According to the Born equation, electrostatic contribution to the standard free-energy change of the self-ionization process (eq 2) is

$$\Delta G_B^\circ = \frac{Ne^2}{2}\left(\frac{1}{r_+}+\frac{1}{r_-}\right)\frac{1}{D_s} \qquad (11)$$

where r_+ and r_- are the effective radii of the cation and the anion and D_s is the macroscopic dielectric constant.

Utilizing this simple Born equation, the standard heat change in self-ionization of the solvents can be represented by

$$\Delta H^\circ = (\Delta H^\circ)_{D_s=\infty} + \frac{Ne^2}{2}\left(\frac{1}{r_+}+\frac{1}{r_-}\right)\frac{1}{D_s}\left[1+\frac{T}{D_s}\left(\frac{dD_s}{dT}\right)\right] = (\Delta H^\circ)_{D_s=\infty} + \frac{C_B}{D_s}\left[1+\frac{T}{D_s}\left(\frac{dD_s}{dT}\right)\right] \ldots \qquad (12)$$

where C_B is a constant, containing the radius factor, and $(\Delta H^\circ)_{D_s=\infty}$ represents the nonelectrostatic, *i.e.*, chemical part of the enthalpy change, $(\Delta H^\circ)_{chem}$ accompanying the self-ionization process. This $(\Delta H^\circ)_{chem}$ would presumably incorporate the interaction energies due to ion–dipole, dipole–dipole, and other energy changes accompanying the self-ionization process except the electrostatic contribution arising from permittivity of the solvents. Equation 12 indicates that ΔH° should be a linear function of the quantity within the square brackets, provided that $(\Delta H^\circ)_{chem}$ is independent of temperature. Similarly, the entropy change is given by

$$\Delta S^\circ = (\Delta S^\circ)_{chem} + C_B\left[\frac{1}{D_s}\times\frac{d\ln D_s}{dT}\right] \ldots \qquad (13)$$

Hence, the plot of ΔS° against the quantity in square brackets in eq 13 should also be linear. Thus, the chemical part of ΔH° as well as of ΔS° can be evaluated without any prior computation of the numerical value of the radius factor C_B which is directly obtained from the slope of the linear plot.

The data for water, ethylene glycol, and propylene glycol are available for the self-ionization process and the necessary parameters (in molal scale for the solute) for the two types of plots (ΔH° and ΔS°) are given in Table VI. In Figure 1 are shown the plots which are found to be good straight lines for all the three solvents. For each solvent, the slopes obtained from the two plots, given in Table VII, are in reasonable agreement, as required by eq 12 and 13, which adds to the confidence in the computed quantities. The values of $(\Delta H^\circ)_{chem}$ and $(\Delta S^\circ)_{chem}$ being graphically obtained in this manner, it is easy to evaluate $(\Delta G^\circ)_{chem}$ accompanying the self-ionization process. The thermodynamic quantities thus derived for each solvent, on a molal scale, are shown

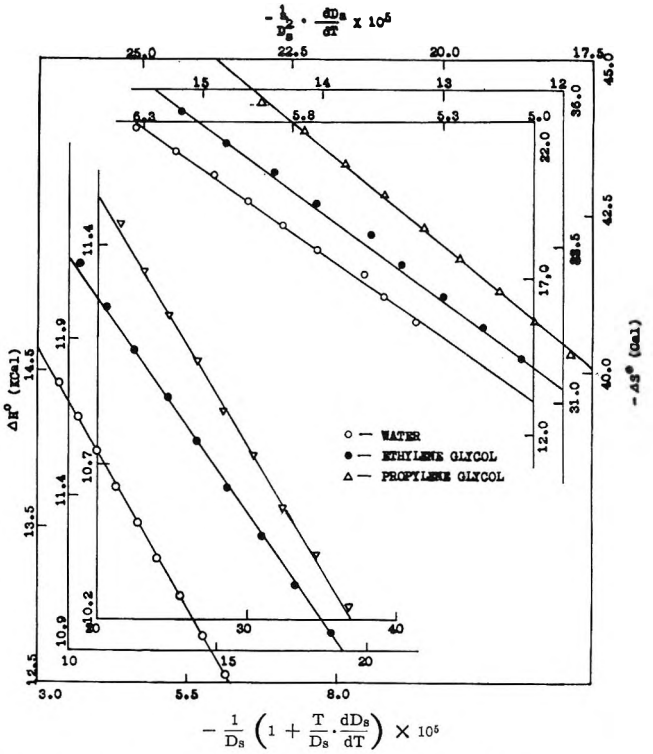

Figure 1. Variation of ΔH° *vs.* $\frac{1}{D_s}\left(1+\frac{T}{D_s}\frac{dD_s}{dT}\right)$ and ΔS° *vs.* $\frac{1}{D_s^2}\frac{dD_s}{dT}$ in water, ethylene glycol, and propylene glycol.

in Table VIII, where the corresponding data on a mole fraction scale are also included.

Though these data (on mole fraction scale) are now free from the effect of dielectric constant of the solvents, they still incorporate the composite effect of intrinsic acidity and basicity of the solvents in the case of $(\Delta G^\circ)_{chem}$ values and also that of the relative structural aspects of the solvents in the cases of $(\Delta H^\circ)_{chem}$ and $(\Delta S^\circ)_{chem}$ values. From the computed results which are now free from the effect of dielectric constant, it can be seen that the relative ease of self-ionization of the solvents is as follows: water > ethylene glycol > propylene glycol. Now it has been indicated earlier[9] that the order of acidity of water and glycols is as follows: water > glycols, and that of basicity: water < glycols. Again, it can be argued that due to the inductivity effect of methyl group in propylene glycol, the negative charge density on oxygen center should be larger than the corresponding quantity in ethylene glycol. As a result, the protonic character of H atom of the OH group in propylene glycol is less than that in ethylene glycol. Thus it is not unreasonable to infer that the order of acidity of the solvents is as follows: water > ethylene glycol > propylene glycol, and that of

(16) E. C. Baughan, *J. Chem. Phys.*, **7**, 951 (1939).

(17) V. K. La Mer and F. Brescia, *J. Amer. Chem. Soc.*, **62**, 617 (1940).

Table VI: Necessary Parameters for the Plots of ΔH° *vs.* $1/D_s[1 + T/D_s(dD_s/dT)]$ and ΔS° *vs.* $1/D_s^2(dD_s/dT)$ in the Glycols and Water

	Temp, °C								
	5	10	15	20	25	30	35	40	45
					Ethylene Glycol				
$\frac{1}{D_s}\left[1 + \frac{T}{D_s}\left(\frac{dD_s}{dT}\right)\right] \times 10^3$	−10.40	−11.31	−12.26	−13.25	−14.25	−15.35	−16.47	−17.65	−18.86
$\frac{1}{D_s^2}\left(\frac{dD_s}{dT}\right) \times 10^5$	−12.35	−12.67	−13.00	−13.34	−13.69	−14.05	−14.42	−14.80	−15.18
					Propylene Glycol				
$\frac{1}{D_s}\left[1 + \frac{T}{D_s}\left(\frac{dD_s}{dT}\right)\right] \times 10^3$	−21.38	−23.00	−24.68	−26.47	−28.32	−30.28	−32.33	−34.47	−36.72
$\frac{1}{D_s^2}\left(\frac{dD_s}{dT}\right) \times 10^5$	−17.92	−18.49	−19.07	−19.69	−20.32	−20.98	−21.64	−22.33	−23.04
					Water				
$\frac{1}{D_s}\left[1 + \frac{T}{D_s}\left(\frac{dD_s}{dT}\right)\right] \times 10^3$	−3.38	−3.68	−3.99	−4.31	−4.65	−5.00	−5.37	−5.75	−6.16
$\frac{1}{D_s^2}\left(\frac{dD_s}{dT}\right) \times 10^5$	−5.39	−5.50	−5.61	−5.72	−5.83	−5.95	−6.07	−6.19	−6.32

Table VII: Slopes[a] of the Plots of ΔH° *vs.* $1/D_s[1 + T/D_s(dD_s/dT)]$ and ΔS° *vs.* $1/D_s^2(dD_s/dT)$ in the Glycols and Water

	ΔH° / $\frac{1}{D_s}\left[1 + \frac{T}{D_s}\left(\frac{dD_s}{dT}\right)\right]$	ΔS° / $\frac{1}{D_s^2}\left(\frac{dD_s}{dT}\right)$
Ethylene glycol	139	139
Propylene glycol	80	80
Water	682	675

[a] Values are in kcal/mol.

$$\text{solvent aggregates} \xrightarrow{\Delta H_1^\circ} n\text{SH} \quad \text{(depolymerization)} \quad (1)$$

$$\text{SH} \xrightarrow{\Delta H_2^\circ} \text{S}^- + \text{H}^+ \quad \text{(acidic ionization)} \quad (2)$$

$$\text{H}^+ + \text{SH} \xrightarrow{-\Delta H_3^\circ} \text{SH}_2^+ \quad \text{(basic ionization)} \quad (3)$$

$$(\text{S}^- + \text{SH}_2^+) + (n-2)\text{SH} \xrightarrow{-\Delta H_4^\circ} (\text{SH}_2^+)_{\text{solv}} + (\text{S}^-)_{\text{solv}} \quad \text{(solvation)} \quad (4)$$

Thus, $(\Delta H)^\circ_{\text{chem}} = \Delta H_1^\circ + \Delta H_2^\circ - \Delta H_3^\circ - \Delta H_4^\circ = (\Delta H_1^\circ - \Delta H_4^\circ) + (\Delta H_2^\circ - \Delta H_3^\circ)$, negative sign before ΔH° values indicating exothermicity of the process.

Table VIII: Thermodynamic Quantities[a] Representing the Chemical Effects of Solvents Accompanying the Self-Ionization of Glycols and Water

	$(\Delta G^\circ)_{\text{chem}}$	$(\Delta G_N^\circ)_{\text{chem}}$	$(\Delta H^\circ)_{\text{chem}} = (\Delta H_N^\circ)_{\text{chem}}$	$(T\Delta S^\circ)_{\text{chem}}$	$(T\Delta S_N^\circ)_{\text{chem}}$
Water	10.45	15.21	16.68	6.23	1.47
Ethylene glycol	17.92	21.21	13.56	−4.36	−7.65
Propylene glycol	20.91	23.96	13.14	−7.77	−10.82

[a] All values are in kcal/mol.

basicity: water < ethylene glycol < propylene glycol. These inferences are, however, contrary to what has been suggested from our studies on proton-transfer equilibria,[7] but after all, the earlier conclusion was indeed too naive[18] in view of too many complexities involved in the proton-transfer equilibria.

Again $(\Delta H^\circ)_{\text{chem}}$ can be thought to be equal to the sum of the heat changes involved in the following steps (being free from dielectric constant effects on ionization)

Since steps 2 and 3 involve isolated molecules it can be assumed that the order of heat changes involved in those steps for different solvents would be parallel to that of free energy changes. Thus in view of the above contentions regarding the relative acidity and basicity of the solvents, the order of magnitudes of (ΔH_2°) and

(18) F. Franks, Ed., in "Physico-Chemical Processes in Mixed Aqueous Solvents," Heinemann Educational Books Ltd., London, 1967.

($-\Delta H_3°$) in the solvents should be as follows: $(\Delta H_2°)^{w} < (\Delta H_2°)^{Eg} < (\Delta H_2°)^{Pg}$ and $(-\Delta H_3°)^{w} < (-\Delta H_3°)^{Eg} < (-\Delta H_3°)^{Pg}$, where the superscripts denote water, ethylene glycol and propylene glycol, respectively. It follows immediately from the above inequalities that

$$(\Delta H_2° - \Delta H_3°)^{w} < (\Delta H_2° - \Delta H_3°)^{Eg} < (\Delta H_2° - \Delta H_3°)^{Pg}$$

Again, it can be seen from the Table VIII that the resulting $(\Delta H°)_{chem}$ values are in the order: $(\Delta H°)^{w}_{chem} > (\Delta H°)^{Eg}_{chem} > (\Delta H°)^{Pg}_{chem}$. Thus it is expected that the magnitudes of $(\Delta H_1° - \Delta H_4°)$ values should have the following order

$$(\Delta H_1° - \Delta H_4°)^{w} \gg (\Delta H_1° - \Delta H_4°)^{Eg} \gg (\Delta H_1° - \Delta H_4°)^{Pg}$$

and in these values of $(\Delta H_1° - \Delta H_4°)$ will be reflected the overall energetics due to structural changes accompanying self-ionization. This suggests that larger heat changes are involved in bringing a proper configurational change of water molecules to facilitate self-ionization which is perhaps due to the characteristic tetrahedral structure of water in the bulk, while the smaller values of $(\Delta H°)_{chem}$ and also $(\Delta H_1° - \Delta H_4°)$ for ethylene and propylene glycols indicate the absence of a similar type of characteristic structure in the bulk, in spite of larger association due to hydrogen bonding in glycols.

The positive $(T\Delta S_N°)_{chem}$ values for water further substantiate the view that the heat changes for structure disruption in water are so large that even the presence of order-producing characteristic ions like H_3O^+ and OH^- is unable to bring about an overall order, and causes an overall disorder instead. The larger negative values of $(T\Delta S_N°)_{chem}$ for ethylene and propylene glycols, on the other hand, indicate that perhaps owing to the absence of a similar characteristic structure in glycols, smaller amounts of heat changes are actually involved in affecting the proper configurational changes to facilitate the self-ionization, and hence the order-producing characteristic ions are able to bring about an overall order in glycols. Further analysis of the results should, however, await similar studies in other amphiprotic solvents.

Acknowledgment. The work was done under a project financed by the National Bureau of Standards, Washington, D. C.

The Photolysis and Radiolysis of 3-Methyl-2-butanone[1]

by Alfred A. Scala

Department of Chemistry, Worcester Polytechnic Institute, Worcester, Massachusetts 01609 *(Received December 29, 1969)*

In the photolysis of 3-methyl-2-butanone at 253.7 nm the major modes of fragmentation of the excited ketone molecules are $CH_3COCH(CH_3)_2^* \rightarrow CH_3CO + i\text{-}C_3H_7$ and $CH_3COCH(CH_3)_2^* \rightarrow CH_3 + COCH(CH_3)_2$. On the basis of experiments carried out with 3-methyl-2-butanone-α-d_4 it can be concluded that the loss of a methyl from the isopropyl group of the ketone occurs with the quantum yield of 0.020 ± 0.005: $CD_3COCD(CH_3)_2^* \rightarrow CD_3COCDCH_3 + CH_3$. No evidence was found for the occurrence of the Type III molecular elimination of propylene. In the vacuum ultraviolet photolysis in addition to the processes observed at 253.7 nm the loss of an H atom is observed. The following overall net reaction is the major process occurring: $CH_3COCH(CH_3)_2^* \rightarrow CH_3 + CO + C_3H_6 + H$. The molecular elimination of CH_3D from 3-methyl-2-butanone-α-d_4 occurs with a quantum yield of 0.020 ± 0.005 at both 147.0 and 123.6 nm: $CD_3COCD(CH_3)_2^* \rightarrow CD_3COCCH_3 + CH_3D$. In the radiolysis the major ion molecule reaction which occurs is the transfer of a proton from fragment ions to the ketone.

Introduction

Although the photolysis of ketones has been extensively investigated in the near-ultraviolet region,[2] few studies of the vacuum ultraviolet photolysis or radiolysis of ketones have been reported. As part of our continuing interest in the photolysis and radiolysis of ketones,[3] we have investigated the photolysis of 3-methyl-2-butanone and 3-methyl-2-butanone-α-d_4 at 253.7, 147, and 123.6 nm. The radiolysis of these ketones has also been briefly examined.

(1) This research was supported by the U. S. Atomic Energy Commission.

(2) For a review: J. G. Calvert and J. N. Pitts, Jr., Photochemistry, Wiley, New York, N. Y., 1966, Chapter 5.

The main purpose of the present study was to re-examine any evidence which might exist for the occurrence of a photoelimination process involving the intramolecular transfer of a β-hydrogen atom to the carbonyl carbon atom.

$$RCOC_nH_{2n+1} \longrightarrow RCOH + C_nH_{2n} \quad (1)$$

It is not irrelevant to note that this photoelimination reaction, which is sometimes called a "Norrish Type III" process, was originally proposed by Norrish and Appleyard[4] in order to account for the formation of ethylene in the vapor phase photolysis of 2-butanone. In a subsequent liquid phase study Bamford and Norrish[5] interpreted the formation of ethylene in the photolysis of 2-butanone and 3-pentanone by the same type of process. In more recent near-ultraviolet vapor and liquid phase photolysis studies of these ketones,[6] it became clear, however, that at least at 313 nm the formation of ethylene could be satisfactorily explained by the occurrence of free radical disproportionation reactions of the type

$$R + C_2H_5 \longrightarrow RH + C_2H_4 \quad (2)$$

R represents a free radical in the system. The minor importance of process 1 in the photolysis of 3-pentanone at 313 nm was also indicated[6,7] by the fact that free radical scavengers such as O_2 and I_2 reduced the quantum yield of ethylene to values less than 10^{-2}.

At wavelengths below 313 nm the situation is, however, not as clear. In the short wavelength photolysis of aldehydes and ketones the yields of olefinic products are definitely higher than anticipated by disproportionation reactions such as 2. Furthermore, the formation of these unsaturates is not eliminated upon the addition of free radical scavengers.[8] In a recent paper[3] we suggested that in the vacuum ultraviolet (147 and 123.6 nm) photolysis of 2-pentanone and 3-pentanone, decomposition of internally excited radicals rather than process 1 could account for the unscavengable olefins. On the other hand, Zahra and Noyes[9] reported evidence for the occurrence of the photoelimination process at 253.7 nm.

$$CH_3COCH(CH_3)_2^* \longrightarrow CH_3COH + C_3H_6 \quad (3)$$

Because at this wavelength energetic considerations make a hot radical mechanism unlikely, we felt that it would be worthwhile to investigate the photolysis of this ketone at 253.7 nm as well as at lower wavelengths. If a photoelimination reaction such as process 1 was observed to occur at 253.7 nm but not at 313 nm it might be expected that this process would be of greater importance at 147 and 123.6 nm or in the radiolysis where highly excited molecules are produced. It should be noted that thus far no unequivocal evidence has been obtained for the occurrence of process 1 in gas phase radiolysis.[3] However, in the liquid phase radiolysis of 2-pentanone, the formation of propylene was proposed[10] to occur by an elimination process such as process 1.

Experimental Section

All experimental procedures were similar to those reported earlier.[3] In addition, photolyses at 253.7 nm were conducted in a 185-cm^3 cylindrical quartz cell contained in an aluminum heating block. The temperature of the cell could be maintained constant to within $\pm 1°$. The light source was a Hanovia S-100 high-pressure mercury lamp which was used in combination with a Baird-Atomic third-order interference filter with peak transmission located at 253.7 nm. The absorbed intensity was 1.6×10^{13} quanta sec^{-1}. Actinometry was based upon the photolysis of 3-pentanone under identical conditions at 92°. At this temperature $\Phi_{CO} = 1.0$[2]. Extinction coefficients at 253.7 nm were measured using a 250-mm focal length Bausch and Lomb monochromator with entrance and exit slits of 1.0 and 0.5 mm, respectively. The extinction coefficients determined for 3-pentanone and 3-methyl-2-butanone were 14.7 and 11.5 l. mol^{-1} cm^{-1}, respectively. Actinometry in the vacuum ultraviolet at 123.6 nm was based upon the measurement of the ionization efficiency of 3-methyl-2-butanone as described elsewhere.[11] The ionization efficiency of 3-methyl-2-butanone at 123.6 nm is 0.20.

In the radiolysis, dosimetry was based upon saturation current measurements using a reaction vessel

Table I: Quantum Yields (Φ) of Products from the Photolysis of 3-Methyl-2-butanone at 253.7 nm[a]

	Temp, °C				
Product	27	90	145	171	27, 7% O_2 additive
CO	0.32	0.97	1.03	1.02	nd[b]
CH_4	0.084	0.60	0.78	0.77	nd
C_2H_6	0.021	0.041	0.010	0.007	0.0001
C_3H_8	0.18	0.29	0.48	0.47	0.0001
C_3H_6	0.16	0.11	0.082	0.063	0.001
i-C_4H_{10}	0.085	0.095	0.044	0.027	0.0003
2,3-Dimethylbutane	0.090	0.048	0.014	0.016	<0.001

[a] Total pressure, 20 Torr; intensity, 8.7×10^{10} quanta cm^{-3} sec^{-1}. [b] nd = not determined.

(3) A. A. Scala and P. Ausloos, *J. Phys. Chem.*, **70**, 260 (1966).
(4) R. G. W. Norrish and M. E. S. Appleyard, *J. Chem. Soc.*, 874 (1934).
(5) C. H. Bramford and R. G. W. Norrish, *ibid.*, 1531 (1938).
(6) P. Ausloos, *Can. J. Chem.*, **36**, 400 (1958).
(7) J. E. Jolley, *J. Amer. Chem. Soc.*, **79**, 1537 (1957).
(8) P. Ausloos and E. Murad, *ibid.*, **80**, 5929 (1958).
(9) Z. Zahra and W. A. Noyes, Jr., *J. Phys. Chem.*, **69**, 943 (1965).
(10) J. N. Pitts, Jr., and A. D. Osborne, *J. Amer. Chem. Soc.*, **83**, 3011 (1961).
(11) P. Ausloos and S. G. Lias, *Radiation Res. Rev.*, **1**, 75 (1968).

Table II: Vacuum Ultraviolet Photolysis and Radiolysis of 3-Methyl-2-butanone[a]

	147 nm			123.6 nm			Radiolysis			
	Additive			Additive						
Product	...	5% NO	10% O_2 Φ	...	5% NO	10% O_2 Φ	...	*M/N*	5% NO	*M/N*
H_2	22.9	15.0		87.0	53.4		121		61.4	
CO	100	100	0.90	100	100	0.48	100	0.68	100	0.62
CH_4	18.9	3.4		30.1	13.7		23.6		8.7	
C_2H_6	47.4	<0.01		53.4	<0.2		30.9		1.0	
C_2H_4	8.7	6.8	0.065	13.5	14.9	0.068	17.7		14.5	
C_2H_2	<0.1	nd		nd	nd		2.9		3.2	
C_3H_8	14.1	1.2		18.0	2.3		26.5		2.3	
C_3H_6	48.5	39.5	0.35	80.9	77.8	0.39	91.2	0.62	87.1	0.54
C_3H_4	<0.1	nd[b]		0.16	nd		1.7		1.6	
i-C_4H_{10}	25.7	<0.3		24.2	<0.7		27.9		<0.2	
2,3-Dimethyl butane	4.5	<0.1		3.4	<0.8		4.0		<0.2	

[a] Total pressure, 20 Torr. [b] nd = not determined.

Table III: Photolysis and Radiolysis of $CD_3COCD(CH_3)_2$. Isotopic Composition of Hydrogen, Methane, and Ethane

Wavelength, nm	Additive	Per cent distribution									
		H_2	HD	D_2	CD_4	CD_3H	CH_3D	CH_4	C_2D_6	CH_3CD_3	C_2H_6
313									100		
253.7					12.0	84.0		4.0	88.1	10.9	1.0
147.0		46.6	43.2	10.2	11.1	59.0	14.2	15.7	56.2	37.9	6.0
147.0	5% NO				5.6	21.5	58.9	14.0			
123.6		39.0	49.6	11.4	18.1	41.9	20.4	19.7	45.4	44.7	9.9
123.6	5% NO				10.6	34.1	39.4	15.9			
Radiolysis		34.0	52.1	13.9	21.7	32.3	22.7	23.3	48.2	40.9	10.9

described elsewhere.[12] The ion-pair yields (*M/N*) of the products given in this paper were calculated from the measured current in the saturation region. Taking a *W* value for 3-methyl-2-butanone of 24.7 eV/ion pair,[13] the dose rate in the radiolysis of 3-methyl-2-butanone was 2.5×10^{19} eV mol^{-1} sec^{-1}.

3-Methyl-2-butanone was obtained from Eastman Kodak Co. and carefully distilled on a spinning band column. Only those fractions were used which contained less than 0.02% impurity as determined by means of a gas chromatograph provided with a diisodecyl phthalate column. 3-Methyl-2-butanone-α-d_4 was prepared by Merck Sharp and Dohme, Ltd. of Canada. It was thoroughly degassed at −80° during several trap-to-trap distillations. Hydrocarbons up to C_6 were entirely absent and other chemical impurities were present to the extent of about 0.03%. According to the mass spectral cracking pattern, the 3-methyl-2-butanone-α-d_4 contained approximately 1% 3-methyl-2-butanone-d_5 and 6% 3-methyl-2-butanone-d_3, and at least 95% of the material was deuterated in the α-position.

The analytical procedure was identical with that described in a previous publication.[3] Analysis for acetaldehyde was carried out by expanding an aliquot of the material, immediately after irradiation, into a gas sampling valve of a gas chromatograph which was provided with a diisodecyl phthalate column. Introduction of prepared mixtures containing traces of acetaldehyde in 3-methyl-2-butanone indicated that the above technique should provide a reliable quantitative analysis of the acetaldehyde yield.

Results

The quantum yields observed for the products in the photolysis of 3-methyl-2-butanone at 253.7 nm at various temperatures along with the quantum yields at 27° in the presence of 7% oxygen are presented in Table I. No attempt was made to determine higher carbonyl-containing compounds in these experiments. However, several experiments were carried out at higher conversions (0.05–1.0%) in order to determine if acetaldehyde was produced in the photolysis at 27 and 60°. The results of these experiments indicate that in no case was acetaldehyde present in amounts in excess of 3% of the propylene.

(12) P. Ausloos and R. Gorden, Jr., *J. Chem. Phys.*, **41**, 1278 (1964).
(13) P. Adler and H. K. Bothe, *Z. Naturforsch.*, **20a**, 1700 (1965).

The product distributions observed in the photolysis of 3-methyl-2-butanone at 147 and 123.6 nm as well as the ion-pair yields (M/N) observed in the radiolysis of this ketone are presented in Table II. Here again acetaldehyde was never present in excess of 3% of the propylene.

The isotopic compositions of the hydrogen, methane, and ethane formed when 3-methyl-2-butanone-α-d_4 was photolyzed at the various wavelengths are presented in Table III. In addition to these results, it should be noted that no hydrogen was observed in the products of the photolysis at 253.7 nm. At all energies better than 95% of the propane consisted of C_3H_7D and $C_3H_6D_2$ and essentially all of the ethylene and propylene contained only one D atom.

Discussion

A. Photolysis at 253.7 nm. It will first be demonstrated that the majority of the products given in Table I can be accounted for by the occurrence of the primary dissociative processes

$$CH_3COCH(CH_3)_2^* \longrightarrow CH_3CO + i\text{-}C_3H_7 \quad (4)$$

$$\longrightarrow CH_3 + COCH(CH_3)_2 \quad (5)$$

As in the photolysis of acetone, it may be expected that, at 253.7 nm, a fraction of the acyl radicals formed in processes 4 and 5 will decompose as a result of the excess energy carried over from the primary process. Also, at the relatively low intensities used in this study the majority of the remaining acyl radicals will decompose thermally at temperatures above 90° before they can undergo radical combination reactions. This is corroborated by the fact that the Φ_{CO} is within experimental error unity at temperatures ranging from 90 to 171°. Because of the large increase in the carbon monoxide yield at 90° compared to 27° it is reasonable to relate differences in product yields at these temperatures primarily to the decomposition of the acyl radicals. The data in Table I indicate first that process 4 occurs to a greater extent than process 5 and that the $COCH(CH_3)_2$ radical is less stable than the acetyl radical (*i.e.*, a larger fraction of the $COCH(CH_3)_2$ decomposes at 27° compared to the CH_3CO). This is corroborated by the observation of Whiteway and Masson[14] that in the photolysis of diisopropyl ketone Φ_{CO} is unity at temperatures as low as 50°. Abstraction, combination, and disproportionation of the CH_3, and i-C_3H_7 radicals account for the hydrocarbon products. The increase in $\Phi_{C_2H_6}$ and $\Phi_{i\text{-}C_4H_{10}}$ when the temperature is raised from 27 to 90° can be ascribed to the thermal decomposition of the acetyl radicals formed in process 4. Methane and propane increase with an increase in temperature because they are mainly formed by H-atom abstraction reactions. This in turn accounts for the fact that the quantum yields of the combination products ethane, isobutane, and 2,3-dimethylbutane diminish when the temperature is raised from 90 to 171°. It is of incidental interest to note that the values of 3.8 and 4.5 obtained for $(i\text{-}C_4H_{10})^2/(C_2H_6)(C_6H_{12})$ at 27 and 90°, respectively, are in reasonable agreement with the statistically expected[15] value of 4. The much lower values for this relationship reported by Zahra and Noyes[9] remain unexplained. Also contrary to the latter study is the observation that $\Phi_{C_3H_6}$ decreases with increasing temperature. This can be ascribed to the diminishing importance of disproportionations of the type

$$R + i\text{-}C_3H_7 \longrightarrow RH + C_3H_6 \quad (6)$$

relative to abstraction reactions. R represents radical in the system. That free radicals are indeed the precursors of the hydrocarbon products is further demonstrated by the fact that addition of 7% oxygen reduces the quantum yield of these products to values well below 10^{-2}. Oxygen is known to interact with ketone molecules excited to the triplet state, but only at 313 nm have such effects been noticed.[2] Even at the latter wavelength the quenching of the excited state of higher ketones is only observed at pressures of oxygen which are considerably higher than those used in the present study.[16] The observation that propylene is formed with a quantum yield of only 10^{-3} in the oxygen scavenged system is no doubt a good indication that the photoelimination process 1 does not occur at 253.7 nm. This is further supported by the facts that the quantum yield of carbon monoxide is, within experimental error, unity from 90 to 171° and that acetaldehyde was not observed as a significant product (see Results). The small yield of propylene observed in the oxygen scavenged photolysis may arise from the decomposition of hot isopropyl peroxy radicals formed by the reaction of isopropyl radicals with oxygen. This is suggested by the recent observation of Kallend and Pitts[17] that hot ethyl peroxy radicals are the precursors of the ethylene formed when 3-pentanone is photolyzed at 313 nm in the presence of oxygen.

The above observations should be contrasted with those reported in a previous study[9] in which it was suggested that process 1 may occur with a quantum yield of 0.3 at 253.7 nm. It should, however, be noted that more recently, Dr. Roscher in Professor Noyes' laboratory[18] was unable to confirm the formation of acetaldehyde in the photolysis of 3-methyl-2-butanone.[19] As noted[18] by Dr. Roscher and Professor

(14) S. G. Whiteway and C. R. Masson, *J. Amer. Chem. Soc.*, **77**, 1508 (1955).

(15) A. F. Trotman-Dickenson, *Ann. Rept. Prog. Chem. (Chem. Soc. London)*, **55**, 36 (1958).

(16) (a) P. Ausloos and R. E. Rebbert, *J. Amer. Chem. Soc.*, **83**, 4897 (1961); (b) P. Borkowski and P. Ausloos, *J. Phys. Chem.*, **65**, 2257 (1961).

(17) A. S. Kallend and J. N. Pitts, Jr., *J. Amer. Chem. Soc.*, **91**, 1269 (1969).

(18) Private communication by Dr. David Roscher and Professor W. A. Noyes, Jr.

Noyes, this result, which casts doubt on the major evidence presented[9] for the occurrence of process 1, indicates that the Norrish Type III process does not occur in the photolysis of 3-methyl-2-butanone at 253.7 nm. The minor importance of process 1 is actually also demonstrated by the product distribution reported[9] at 27°. At this temperature, $\Phi_{C_3H_6}$ was reported to be as low as 0.11. Disproportionation reactions involving the i-C_3H_7 radical can account for nearly all of the propylene observed. It would be most unlikely that process 1 would occur at 60 or 127° but not at 27°.

It should finally be pointed out that the results given in Table I do not provide for the occurrence of chain reaction 7 which has been suggested to occur at tempera-

$$R + CH_3COCH(CH_3)_2 \longrightarrow RH + CH_3CO + C_3H_6 \quad (7)$$

tures as low as 60°. In the present study (Table I) the quantum yield of C_3H_6 actually diminishes with an increase in temperature while the Φ_{CO} remains within experimental error constant. We are at a loss to explain the discrepancies between this study and the previous one,[9] especially because there is no appreciable difference in intensity or pressure between the two investigations.

In addition to the dissociative processes 4 and 5 there is evidence that at 253.7 nm a small fraction of the excited ketone molecules decompose as follows.

$$CH_3COCH(CH_3)_2^* \longrightarrow CH_3COCHCH_3 + CH_3 \quad (8)$$

Such a process could readily account for the formation of CH_3CD_3 and CH_4 (Table III) in the photolysis of $CD_3COCD(CH_3)_2$.

$$CD_3COCD(CH_3)_2^* \longrightarrow CD_3COCDCH_3 + CH_3 \quad (9)$$

The quantum yield for process 9 at 253.7 nm can be estimated[20] to be 0.020 ± 0.005. Although C–C cleavage in alkyl groups has not previously been reported for ketones at 253.7 nm, such processes have been noted to occur in straight chain as well as branched aldehydes at wavelengths as high as 313 nm.[2]

B. Photolysis at 147 and 123.6 nm. A major difference between the product distribution at these energies (Table II) when compared with the product distribution at 253.7 nm (Table I) is the presence of hydrogen as an important product. Both the isotopic composition of the hydrogen and the reduction in the hydrogen yield relative to CO observed when nitric oxide is added to the system indicate that a large fraction of the hydrogen is formed by reactions of H atoms. The H atoms may be produced in a primary dissociative process and/or by the decomposition of internally excited propyl radicals formed in process 4. Since more than 100 kcal has to be partitioned between the two fragments formed in the primary process, secondary fragmentation will definitiely be of importance at the relatively low pressure at which these experiments were carried out. Since one cannot determine from these data whether the H atoms are formed by primary or secondary fragmentations, one can only say that the following overall decomposition (listed as reaction 10) may reasonably account for the

$$CH_3COCH(CH_3)_2^* \longrightarrow CH_3CO(\text{or } CH_3 + CO) + C_3H_6 + H \quad (10)$$

majority of the H atoms. The fact that acetone could not be observed as a product indicates that the majority of the acetyl radicals formed in process 10 decompose. Justification for the above mechanism follows from the fact that propylene is an important product whose yield in contrast to those of the alkanes is only slightly reduced upon the addition of NO. The propylene which is not scavenged by NO is apparently not formed by a photoelimination mechanism (process 3), because acetaldehyde is only a very minor product both at 147 and 123.6 nm (see Results). It could be argued that all of the CH_3COH and CH_3CHO which would be formed by the photoelimination process 3, decompose further and therefore acetaldehyde would not be observed as a product. Although this possibility cannot *a priori* be excluded, it seems a rather unlikely one in view of the fact that we are dealing with a relatively stable species. The very small yield of C_3H_4 and the large yield of C_3H_6 indicate that at least propylene does not decompose further.

The product distributions given in Table II clearly indicate that process 8 and/or the secondary fragmentation of a fraction of the isopropyl radicals occurs to a greater extent at 147 and 123.6 nm than at 253.7 nm. This is demonstrated by the fact that CH_3/CO is 0.66, 1.36, and 1.47 at 253.7, 147, and 123.6 nm, respectively, while i-C_3H_7/CO is 1.9, 0.56, and 0.50 at these respective wavelengths. The observed greater importance of process 8 and/or the secondary fragmentation of i-C_3H_7 at higher energies is consistent with expectation. Further corroboration of this interpretation of the data may be found in the isotopic composition of the ethane formed in the photolysis of $CD_3COCD(CH_3)_2$. It can be estimated that while CH_3/CD_3 is only 0.06 at 253.7 nm it is 0.34 and 0.49 at 147 and 123.6 nm, respectively. It can further be noted that $(CH_3CD_3)^2/C_2H_6 \times C_2D_6$ is equal to 4.3 and 4.4 at 147 and 123.6

(19) Dr. Roscher used a sensitive analytical color test method, while Dr. Zahra attempted to determine the acetaldehyde yield by gas chromatography. Because the same column was employed as the one used in the present study, and because other discrepancies exist between the two studies, it seems that extraneous experimental factors may have contributed to the formation of acetaldehyde in the previous study.

(20) At 27° the CH_3 radicals account for approximately 6% of the methyl radicals. $(CH_3/CD_3 = CH_3CD_3/2C_2D_6 = 0.06)$. Because under our experimental conditions approximately 30% of the acetyl radicals decompose (see Table I), the quantum yield of primary process 8 relative to that of 4 and 5 can be estimated to be 0.020.

nm, respectively, in reasonable agreement with the statistical expected value of 4.0.[15] This latter observation confirms that ethane is mainly formed by combination of methyl radicals. Similarly, the values of 3.1 and 3.2 obtained for $(i\text{-}C_4H_{10})^2/C_2H_6 \times C_6H_{14}$ at 147 and 123.6 nm, respectively, indicate that $i\text{-}C_4H_{10}$ and 2,3-dimethylbutane are mainly formed by combination of $i\text{-}C_3H_7$ with CH_3 and $i\text{-}C_3H_7$, respectively.

The methane distributions in Table III indicate that molecular elimination of methane as shown in reaction 11 occurs at 147 and 123.6 nm. It can be seen from these distributions that there is a larger amount of

$$CD_3COCD(CH_3)_2^* \longrightarrow CD_3COCCH_3 + CH_3D \quad (11)$$

CH_3D formed than would be predicted based upon an entirely free radical mechanism for the formation of methane. The occurrence of reaction 11 is further corroborated by the isotopic distributions of the methane formed in the presence of nitric oxide. At both 147 and 123.6 nm CH_3D is the major methane formed. An alternative to reaction 11 which involves the CD_3 as the source of the D atom in the molecular elimination of CH_3D, while not specifically excluded by the data, seems less likely than reaction 11 since 1,1 eliminations are far more common than 1,3 eliminations. When the data in Tables II and III are combined it may be estimated that the quantum yield for process 11 is 0.020 ± 0.005 at both wavelengths.[21]

Ethylene which is a relatively more important product in the vacuum ultraviolet photolysis than at 253.7 nm is probably produced by the decomposition of the internally excited carbonyl containing radical formed in process 8

$$CH_3COCHCH_3^* \longrightarrow CH_3CO + CHCH_3 \quad (12)$$

followed by the rearrangement reaction

$$CHCH_3 \longrightarrow CH_2CH_2 \quad (13)$$

The $CHCH_3$ radical could also arise from the decomposition of vibrationally excited $i\text{-}C_3H_7$ radicals as noted before. This interpretation is corroborated by the fact that the ethylene formed in the photolysis of $CD_3COCD(CH_3)_2$ is entirely $CHDCH_2$ (see Results). It should also be noted that the formation of ethylene is not inhibited by nitric oxide.

That the quantum yield of CO is not unity at these wavelengths is related to the observation that C–H cleavage is occurring and apparently a fraction of the ketone radicals produced in reactions 14 and 15 do not decompose to give CO as a product. The alternative

$$CH_3COCH(CH_3)^* \longrightarrow H + CH_2COCH(CH_3)_2 \quad (14)$$

$$\longrightarrow H + CH_3COC_3H_6 \quad (15)$$

to the production of CO probably involves the formation of a ketene. The observation that the yield of hydrogen parallels the deviation of the quantum yield

$$CH_2COCH(CH_3)_2 \longrightarrow CH_2CO + i\text{-}C_3H_7 \quad (16)$$

$$CH_3COC_3H_6 \longrightarrow C_3H_6CO + CH_3 \quad (17)$$

of CO from unity is consistent with this interpretation. The coupling of a ketone radical with another radical would also lead to a reduction in CO yield and these coupling products would not be detected in our analytical scheme.

The fate of the ions produced with an ionization efficiency of 0.20, when 3-methyl-2-butanone (I.P. = 9.3 eV) is irradiated at 123.6 nm (10 eV) will be discussed in the next section.

C. Radiolysis. Since ions as well as neutral excited molecules will be formed by electron impact in the radiolysis, it is difficult to determine the radiolytic mechanism in detail. However, some insight into the mechanism can be gained by a careful comparison of the product yields in the photolysis and radiolysis. The mass spectrum of the ketone also provides useful information, since it gives an indication of the ions that may be present, although their relative abundance may be somewhat different at the higher pressures at which the radiolysis experiments are carried out. The experimental data along with our study of the radiolysis of 2- and 3-pentanone[3] and previous studies of the reactions of ions with ketones[22] lead to the conclusion that the major ion–molecule reaction in this system is a proton transfer reaction from the various fragment ions (AH^+) to the ketone.

$$AH^+ + CH_3COCH(CH_3)_2 \longrightarrow A + C_5H_{11}O^+ \quad (18)$$

The 11.3-eV photoionization mass spectral cracking pattern of 3-methyl-2-butanone indicates that in addition to the parent ion the other major ions present are CH_3CO^+, $(CH_3)_2CHCO^+$, and $CH_3COCHCH_3^+$.[23] If we accept reaction 18 as the major ion–molecule reaction in this system then if any of these ions underwent the proton transfer they would lead to products which would either be ketenes or α,β-unsaturated ketones which would go undetected in our analytical scheme. Consequently, most of the ion–molecule reactions lead to products which are not determined in Table II. The 70-eV mass spectral cracking patterns of 3-methyl-2-butanone[24] and 3-methyl-2-butanone-α-d_4 indicate that the $C_2H_3^+$ and $C_3H_5^+$ ions each accounts for 7.8% of the total ionization while $C_3H_7^+$ accounts for 12%. It would be expected that acetylene and C_3H_4 (allene and methylacetylene) would be significant products in the radiolysis, although present in only trace amounts in the photolysis, since reaction 18

(21) This estimate is made by multiplying the quantum yield of methane by the CH_3D in excess of the "theoretical" CH_3D calculated by assuming $CD_4/CD_3H = CH_3D/CH_4$.

(22) I. B. Sandoval and P. J. Ausloos, *J. Chem. Phys.*, **38**, 2454 (1963).

(23) E. Murad and M. G. Inghram, *ibid.*, **40**, 3263 (1964).

(24) American Petroleum Institute, Research Project 44, No. 652.

occurring with $C_2H_3^+$ and $C_3H_5^+$ would result in the formation of C_2H_2 and C_3H_4. It can be seen from the data in Table II that this expectation is realized. Gas chromatographic analysis shows that about 90% of the C_3H_4 is methylacetylene and only 10% is allene. The observation that propylene is a relatively more important product in the radiolysis can be attributed both to the participation of the $C_3H_7^+$ ion in reaction 18 and to the increased importance of reaction 10 at higher energies. It should also be noted that these products attributed to the ion molecule reaction 18 are relatively insensitive to the presence of NO.

Table II indicates that ethylene is a relatively more important product in the radiolysis than in the photolysis. Since the $C_2H_5^+$ ion accounts for only 0.7% of the total ionization in the 70-eV mass spectral cracking pattern of 3-methyl-2-butanone the increased importance of ethylene is probably not due to the participation of the ethyl ion in process 18. The increased yield of ethylene observed in the radiolysis can be attributed to the increased importance of process 8 followed by processes 12 and 13. This is confirmed by the increase in the ratio CH_3/CD_3 (Table III) observed in the radiolysis, as predicted by this sequence.

The fate of the protonated ketone ($C_5H_{11}O^+$) formed in reaction 18 is uncertain. However, it seems probable that neutralization by an electron or negative ion would be accompanied by the simultaneous loss of an H atom.[6] These in turn would lead to the production of hydrogen by abstraction. Examination of the hydrogen yields in Table II indicates that hydrogen is a more important product in the radiolysis than in the photolysis. The isotopic composition of the hydrogen formed in the radiolysis clearly indicates that it is formed by reactions involving H atoms.

The results of this study clearly indicate that the Norrish Type III photoelimination reaction is of little or no significance in the vapor phase photolysis and radiolysis of 3-methyl-2-butanone.

Acknowledgment. I would like to thank Professor Noyes and Dr. Roscher for the communication of their results cited in reference 18 to me. I would also like to express my sincere appreciation to Dr. Ausloos for many helpful discussions.

Radiation-Induced Isomerization of the 1,2-Diphenylpropenes in Benzene and Cyclohexane

by Robert R. Hentz and H. G. Altmiller

Department of Chemistry and the Radiation Laboratory,[1] University of Notre Dame, Notre Dame, Indiana 46556
(Received December 11, 1969)

Photoexcited and photosensitized isomerizations of the 1,2-diphenylpropenes and their radiation-induced isomerizations in benzene and cyclohexane have been studied. For the concentration range studied, 2–50 mM, the photochemical results can be summarized as follows (multiplicity of the solute state excited is denoted by a superscript): ${}^1\phi_{t\to c} = {}^3\phi_{t\to c} = 0.545$ and ${}^1\phi_{c\to t} = {}^3\phi_{c\to t} = 0.455$, corresponding to $\phi_{t\to c}/\phi_{c\to t} = 1.20$. The 1,2-diphenylpropenes were found to be efficient quenchers of benzene fluorescence. For the lowest excited singlet of benzene, the products of lifetime and specific rate of excitation transfer were 1200 M^{-1} and 700 M^{-1} for the *trans* and *cis* isomers, respectively, as quenchers. Radiation-induced isomerizations of the 1,2-diphenylpropenes provide a measure of the yield of *solute* excited states, G^*, up to at least 0.1 M in cyclohexane and 1 M in benzene. Isomerization yields in cyclohexane are somewhat larger than those obtained earlier with *trans*-stilbene but can be accommodated by the same model. For solute concentrations greater than ~0.1 M in benzene, mechanistic complexity precludes a correlation between G^* and yields of solvent precursors. However, with a value from other work of ${}^1G_0 = 1.5$ for the lowest excited singlet of benzene, results for solute concentrations less than 0.1 M give ${}^3G_0 = 4.1$ for the yield of benzene triplets which do not have the lowest excited singlet as a precursor. Much of the published work on radiation-induced isomerizations in benzene can be interpreted in terms of ${}^1G_0 = 1.5$, ${}^3G_0 = 4.1$, and $\chi = 0.60$ for the intersystem crossing probability from the lowest excited singlet of benzene. Reconciliation with pulse-radiolysis results remains a major problem.

Introduction

A comprehensive study of radiation-induced isomerization of the stilbenes in benzene and cyclohexane has been reported.[2] At low stilbene concentrations, the G-value[3] ratio $G_{c\to t}/G_{t\to c}$ was found to approximate the corresponding quantum-yield ratio obtained in photochemical studies.[4,5] However, with increase in stilbene concentration beyond 0.01 M in cyclohexane and 0.1 M in benzene, the G-value ratio increases and becomes considerably larger than the quantum-yield ratio. Moreover, while $G_{t\to c}$ appears to reach an upper limit at a stilbene concentration near 0.1 M, particularly in benzene, $G_{c\to t}$ continues to increase. For interpretation of such results, it was postulated that $G_{c\to t}$ includes a catalytic contribution (apparently involving ionic processes) which increases in importance with increase in stilbene concentration and becomes significant at concentrations above ~0.01 M in cyclohexane and ~0.1 M in benzene. Consequently, for *cis*-stilbene concentrations in excess of the foregoing limits, $G_{c\to t}$ was considered *not* to provide a reliable measure of the yield of stilbene excited states. Recent results support such an interpretation.[6]

In the initial study,[2] radiation-induced isomerization of *trans*-stilbene was assumed to be free of complications and, therefore, $G_{t\to c}$ was used for calculation of the yield of stilbene excited states. It was suggested (and has been substantiated in recent work[6]) that the isomerization in cyclohexane is initiated by capture of an electron by *trans*-stilbene, with subsequent isomerization *via* stilbene excited states produced in charge-neutralization reactions. Thus, $G_{t\to c}$ is related, though in a complicated manner,[6] to the yield of scavengeable electrons in cyclohexane. However, it was argued that electron capture by stilbene in benzene does not become appreciable until a concentration is reached (~0.05 M) at which energy transfer from excited states of benzene to stilbene approaches completion.[2] Recent work has provided support for such an argument.[7] At low stilbene concentrations in benzene, then, $G_{t\to c}$ provides a measure of the yield of benzene excited states. The initial results[2] for $G_{t\to c}$ in benzene conformed satisfactorily to a Stern–Volmer plot from which $G_0^* = 5.4$ was obtained for the yield of benzene excited states. From characteristics of the Stern–Volmer plot and certain other arguments,[2] it was concluded that the contribution of excited singlet states of benzene corresponds to

(1) The Radiation Laboratory of the University of Notre Dame is operated under contract with the U. S. Atomic Energy Commission. This is AEC Document No. COO-38-694.

(2) R. R. Hentz, D. B. Peterson, S. B. Srivastava, H. F. Barzynski, and M. Burton, *J. Phys. Chem.*, **70**, 2362 (1966).

(3) The symbol G denotes a yield in molecules per 100 eV absorbed by the system.

(4) G. S. Hammond, J. Saltiel, A. A. Lamola, N. J. Turro, J. S. Bradshaw, D. O. Cowan, R. C. Counsell, V. Vogt, and C. Dalton, *J. Amer. Chem. Soc.*, **86**, 3197 (1964).

(5) S. Malkin and E. Fischer, *J. Phys. Chem.*, **68**, 1153 (1964).

(6) R. R. Hentz and H. P. Lehmann, *ibid.*, **73**, 4283 (1969).

(7) R. R. Hentz and W. V. Sherman, *ibid.*, **73**, 2676 (1969).

$^1G_0 \leq 0.5$; therefore, $G_0^* = 5.4$ was assumed to approximate the yield of benzene triplet states.

Hammond and coworkers[8] have reported results somewhat similar to ours for radiation-induced isomerization of the stilbenes in benzene; however, these authors have presented a quite different interpretation. They argue that, owing to self-quenching of the triplet and excited singlet states of *trans*-stilbene, $G_{t\rightarrow c}$ does *not* provide a measure of the yield of stilbene excited states at the higher concentrations whereas $G_{c\rightarrow t}$ does. Such a conclusion was supported by results for radiation-induced isomerization of the 1,2-diphenylpropenes in benzene. It was found that $G_{c\rightarrow t}/G_{t\rightarrow c}$ equals the corresponding quantum-yield ratio[4,8] at all concentrations of 1,2-diphenylpropenes up to 1 *M*, the largest concentration used, and that both of the 1,2-diphenylpropenes behave in the same way as *cis*-stilbene, *i.e.*, isomerization yields increase continuously with increase in solute concentration. The failure of isomerization yields, other than that of *trans*-stilbene, to reach a plateau at high solute concentrations was attributed to competition of the solute with bimolecular annihilation of benzene triplets in spurs. Solute triplet yields of $^3G = 12.3$ and $^3G = 9.9$ were obtained for 1 *M* solutions of *cis*-stilbene and the 1,2-diphenylpropenes, respectively, in benzene.

As noted in our initial paper,[2] a number of complications and inconsistencies are evident in studies of the photoexcited and photosensitized isomerizations of the stilbenes.[4,5] Recent work may have resolved certain of these problems.[9-12] It now appears that self-quenching of the *trans*-stilbene triplet does not occur;[11,12] however, self-quenching of the excited singlet of *trans*-stilbene does occur[9] and could, as suggested by Hammond,[8] be responsible for the observed plateau in $G_{t\rightarrow c}$ at concentrations of *trans*-stilbene above 0.1 *M*. Because Hammond, *et al.*,[4] report photochemical behavior of the 1,2-diphenylpropenes to be free of complications, the radiation study with 1,2-diphenylpropenes[8] assumes a special significance. Consequently, we have reexamined the photoexcited and photosensitized isomerizations of the 1,2-diphenylpropenes and their radiation-induced isomerization in benzene. In addition, we report results for radiation-induced isomerization of the 1,2-diphenylpropenes in cyclohexane.

Experimental Section

Materials. Purification procedures for benzene (Fisher Certified) and cyclohexane (Phillips Petroleum Co.) have been described.[2] Acetophenone (Aldrich Chemical Co.) was purified by vacuum distillation. All distillations were performed with a Nester-Faust spinning-band column. Solvents were stored over anhydrous calcium sulfate which was removed by a final bulb-to-bulb distillation on the vacuum line.

The *trans*-1,2-diphenylpropene (K and K Laboratories) was purified by slow crystallization from cyclohexane. The *cis* isomer was prepared by exposure of a benzene solution of 0.05 *M* *trans*-1,2-diphenylpropene and 0.05 *M* fluorenone to a water-cooled General Electric A-H6 high-pressure mercury lamp for about 3 hr. After photolysis the diphenylpropene was ~70% *cis*. Fluorenone was removed on a 4-ft × 26-mm column of Alcoa alumina by elution with benzene. The mixture of *cis* and *trans* isomers was separated by elution with a solution of 2% benzene in petroleum ether from a 13-mm diameter column which contained 200 g of Woelm neutral alumina per gram of mixture. Under these conditions, the *cis* isomer passed through the column in about 72 hr. The *trans* isomer was eluted with benzene. Solvent was evaporated from fractions containing only the *cis* isomer, and the isomer was recrystallized from pentane before use. The only impurity detectable in the *cis* isomer by gas chromatography was 0.01% of the *trans* isomer.

Procedures. The procedures for preparation of deaerated samples were essentially the same as described previously.[6,13] Solutions were prepared in Pyrex Low Actinic volumetric flasks which were opaque to wavelengths less than 5000 Å. Cells for γ irradiation were made from 13-mm o.d. Pyrex tubes. Photolysis cells were constructed from 13-mm o.d. Vycor 790 sealed to Pyrex with a graded-glass seal. Luminescence measurements were made in 1-cm square Suprasil cells joined to Pyrex. All cells were baked for 12 hr at the annealing temperature of Pyrex before use. Care was taken at all times to minimize exposure of solutions to light by wrapping cells in tin foil and working in dim light.

Solutions were γ irradiated at room temperature in a 4-kCi ^{60}Co source at dose rates to the Fricke dosimeter solution, based on $G(Fe^{3+}) = 15.6$, near 1.6×10^{18} eV ml^{-1} min^{-1}. Dose to a particular solution was calculated by correction for the electron density relative to that of the dosimeter.

Most photochemical experiments were performed with a "merry-go-round" device. Light intensities were determined by potassium ferrioxalate actinometry.[14] The 3130-Å and 3660-Å mercury lines were isolated from the emission of a Hanovia 673 A medium-pressure lamp. Use of a Corning C.S. 7-54 glass filter in combination with a solution of 0.30 g of K_2CrO_4 in 1 l.

(8) R. A. Caldwell, D. G. Whitten, and G. S. Hammond, *J. Amer. Chem. Soc.*, **88**, 2659 (1966).

(9) J. Saltiel, E. D. Megarity, and K. G. Kneipp, *ibid.*, **88**, 2336 (1966); a referee has pointed out that $k_q\tau = 2.6\ M^{-1}$ can be inferred from data of H. Stegemeyer. *Chimia*, **19**, 535 (1965).

(10) J. Saltiel, *J. Amer. Chem. Soc.*, **89**, 1036 (1967).

(11) J. Saltiel, *ibid.*, **90**, 6394 (1968).

(12) H. A. Hammond, D. E. DeMeyer, and J. L. R. Williams, *ibid.*, **91**, 5180 (1969).

(13) R. R. Hentz and W. V. Sherman, *J. Phys. Chem.*, **72**, 2635 (1968).

(14) C. G. Hatchard and C. A. Parker, *Proc. Roy. Soc., Ser A*, **235**, 518 (1956).

of 0.05 N NaOH gave relative intensities of 1.0, 0.17, and 0.03 at 3130, 3026, and 3340 Å, respectively. Only the 3660-Å line was passed by a Corning C.S. 7-37 filter in combination with a solution of 100 g of $CuSO_4 \cdot 5H_2O$ and 0.2 g of 2,7-dimethyl-3,6-diazacyclohepta-1,6-diene perchlorate in 1 l. of distilled water.

Luminescence measurements were made with a Cary Model 14 spectrofluorometer.[15] A Cary Model 14-R was used for absorption spectrophotometry.

Two gas-chromatographic instruments were used for determination of the 1,2-diphenylpropenes. An F and M Model 810 with a flame-ionization detector was used with a $^1/_4$-in. × 6-ft column of 20 wt % silicone grease on 60–80 mesh Chromosorb P; temperatures of oven, injection port, and detector were 200, 210, and 220°, respectively. A Beckman GC-5 with dual flame-ionization detectors was used with a $^1/_8$-in. × 12-ft column of 3 wt % silicone gum rubber on 60–80 mesh Chromosorb G; temperatures of oven, injection port, and detector were 160, 190, and 220°, respectively. With both instruments, retention time of the *cis* isomer was 4 min and that of the *trans* isomer was 7 min. Peak areas were measured with a disk chart integrator (Disk Instruments, Inc.) whenever possible or, when not, with a planimeter.

Results

Photochemistry. Figure 1 shows absorption spectra of the 1,2-diphenylpropenes measured in cyclohexane; the spectra in Figure 1 are in good agreement with published spectra measured in ethanol.[16] A molar extinction coefficient of 5.85 M^{-1} cm^{-1} at 3660 Å was obtained for acetophenone in cyclohexane.

Photostationary concentrations of the 1,2-diphenylpropene isomers were determined at four concentrations of 1,2-diphenylpropene (DPP) in cyclohexane with 0.05 M acetophenone excited at 3660 Å as triplet sensitizer.[4] Results are given in Table I. Each concentration ratio in Table I is an average of eight experiments; at each concentration of DPP, four experiments were begun with *cis*-DPP and four with *trans*-DPP. With 0.05 M acetophenone and 0.01 M of either *cis*-DPP or *trans*-DPP in cyclohexane, measurement of initial rates of the photosensitized (at 3660 Å) isomerizations gave $r_{t\to c}/r_{c\to t} = 1.16$.

Table I: The Ratio of Photostationary Isomer Concentrations in Acetophenone-Sensitized Isomerization of the 1,2-Diphenylpropenes in Cyclohexane

[DPP], mM	$[c]_s/[t]_s$	[DPP], mM	$[c]_s/[t]_s$
2.0	1.23	10.0	1.24
5.0	1.22	50.0	1.16

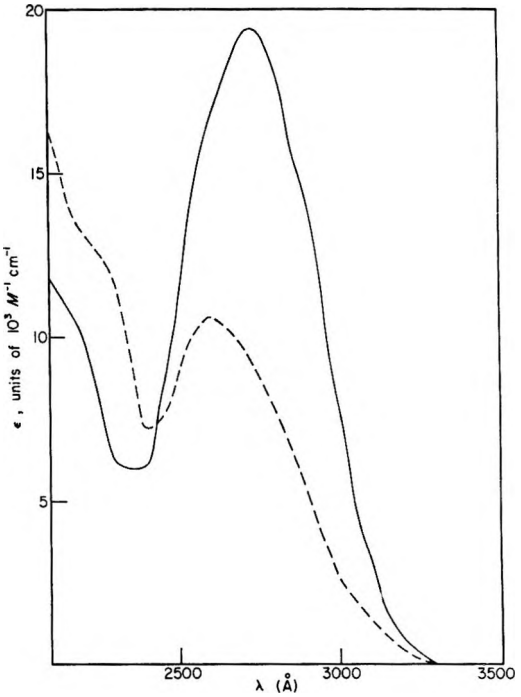

Figure 1. Absorption spectra of the 1,2-diphenylpropenes in cyclohexane: broken curve, *cis*; solid curve, *trans*.

Initial quantum yields of the photoexcited isomerizations were determined by excitation of the 1,2-diphenylpropenes at 3130 Å in cyclohexane solutions. Quantum yields were determined for three photolysis times at each of the concentrations 8, 20, and 50 mM. Maximum conversions were 5% at 8 mM, 2% at 20 mM, and 0.8% at 50 mM. The measured quantum yields were independent of photolysis time at each concentration and of concentration. Averages of all measurements with average deviations are $^1\phi_{t\to c} = 0.51 \pm 0.03$ and $^1\phi_{c\to t} = 0.43 \pm 0.01$.

Luminescence. The 1,2-diphenylpropenes are efficient quenchers of benzene fluorescence. Benzene solutions were excited at 2537 Å and fluorescence was measured at 2800 Å from the cell face used for excitation. At all solute concentrations used, except possibly for 4.86×10^{-3} M of the *trans* isomer, absorption by the solute of either the incident light or measured fluorescent light was negligible. Stern–Volmer plots for fluorescence quenching by each isomer are shown in Figures 2 and 3. Slopes of the plots give the product of specific rate of excitation transfer, ^1k, and lifetime, $^1\tau$, for the lowest excited singlet state of benzene. From Figures 2 and 3, values of $^1k^1\tau = 1200\ M^{-1}$ and $^1k^1\tau = 700\ M^{-1}$ are obtained for the *trans* and *cis* isomers, respectively.

Radiation Chemistry. All values of G for isomeriza-

(15) M. A. Dillon and M. Burton, "Pulse Radiolysis," M. Ebert, J. P. Keene, A. J. Swallow, and J. H. Baxendale, Ed., Academic Press, London, 1965, p 260.

(16) D. J. Cram and F. A. Abd Elhafez, *J. Amer. Chem. Soc.*, **74**, 5828 (1952).

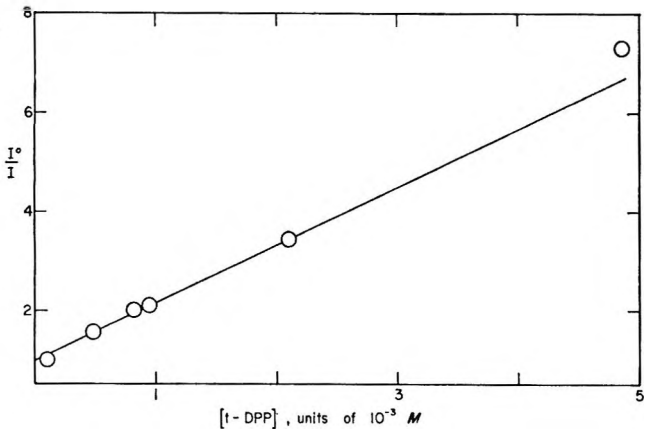

Figure 2. Stern–Volmer plot for quenching of benzene fluorescence, I, by *trans*-1,2-diphenylpropene.

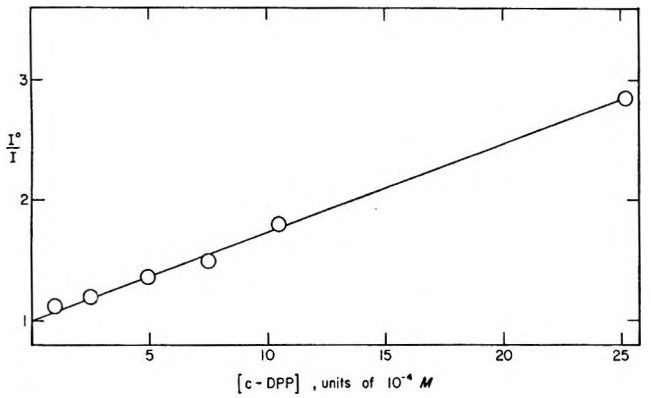

Figure 3. Stern–Volmer plot for quenching of benzene fluorescence, I, by *cis*-1,2-diphenylpropene.

tion of the 1,2-diphenylpropenes were calculated from the slopes of plots of yield *vs.* dose. Conversion of the initial isomer was less than 10% at the maximum dose in each plot. All such plots were linear. At low concentrations of the *cis* isomer a small positive intercept was observed. In all other cases, the yield–dose plot passed through the origin. No change in total concentration of the isomers was detectable in irradiated benzene solutions. Very little destruction of diphenylpropene was observed in cyclohexane solutions; $G(-\text{DPP})$ was less than 0.1 at concentrations less than 0.01 M. Figures 4 and 5 show the concentration dependence of G for isomerization of the 1,2-diphenylpropenes in benzene and cyclohexane.

Discussion

Photochemistry. The average of photostationary concentration ratios in Table I is $[c]_s/[t]_s = 1.21$, which is identical with the average value reported by Hammond and coworkers[4,8] for "high-energy" sensitizers. With the assumption that "high-energy" sensitizers transfer triplet excitation at the same specific rate to both isomers,[4] the photostationary concentration ratio corresponds to the ratio of isomerization quantum yields for excitation of each isomer into the triplet state.

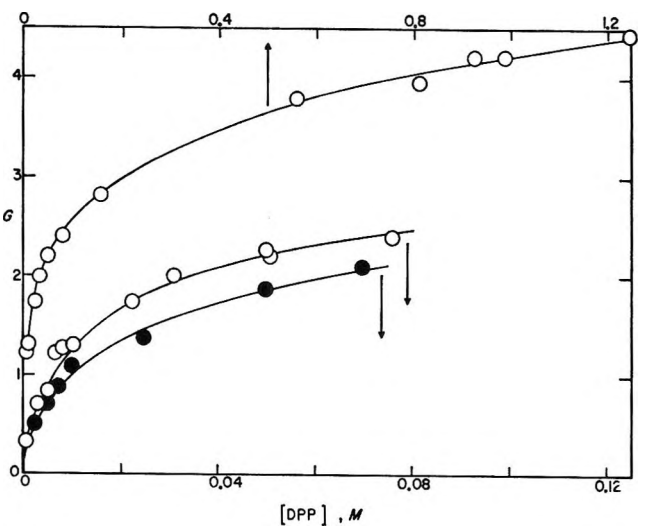

Figure 4. Radiation-induced isomerization of the 1,2-diphenylpropenes in benzene: ○, $G_{t\to c}$; ●, $G_{c\to t}$.

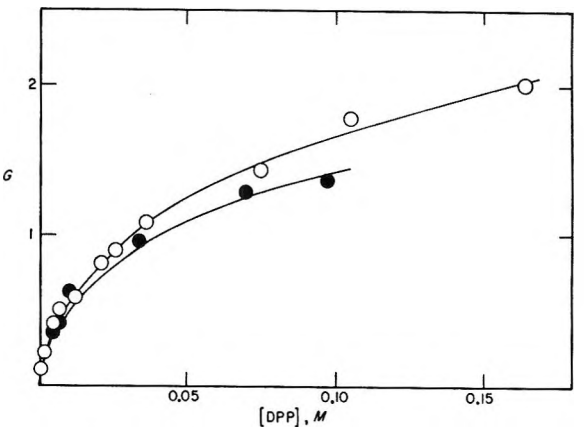

Figure 5. Radiation-induced isomerization of the 1,2-diphenylpropenes in cyclohexane: ○, $G_{t\to c}$; ●, $G_{c\to t}$.

Thus, from the photostationary-state results, ${}^3\phi_{t\to c}/{}^3\phi_{c\to t} = 1.21$. Such a value agrees satisfactorily with the ratio of initial rates, $r_{t\to c}/r_{c\to t} = 1.16$, of the acetophenone-sensitized isomerizations. For the benzophenone-sensitized isomerizations, Hammond, *et al.*,[4] have determined quantum yields from which values of ${}^3\phi_{t\to c} = 0.55$ and ${}^3\phi_{c\to t} = 0.45$ are obtained.

The measured values of ${}^1\phi_{t\to c} = 0.51$ and ${}^1\phi_{c\to t} = 0.43$ give ${}^1\phi_{t\to c}/{}^1\phi_{c\to t} = 1.19$ as compared to a value of 1.16 calculated from a reported[4] photostationary concentration ratio obtained by excitation of the 1,2-diphenylpropenes at 3130 Å. Failure of the excited-singlet quantum yields to sum to unity is probably attributable to a small (6%) actinometry error; neither of the 1,2-diphenylpropenes fluoresces. Adjustment to a sum of unity gives ${}^1\phi_{t\to c} = 0.54$ and ${}^1\phi_{c\to t} = 0.46$.

Photochemical behavior of the 1,2-diphenylpropenes does appear to be free of complications. The photochemical results are best summarized by ${}^1\phi_{t\to c} = {}^3\phi_{t\to c} =$

0.545 and ${}^1\phi_{c\to t} = {}^3\phi_{c\to t} = 0.455$, corresponding to $\phi_{t\to c}/\phi_{c\to t} = 1.20$.

Radiation-Induced Isomerizations. In contrast with studies of the radiation-induced isomerization of *cis*-stilbene,[6] no difficulties were encountered in determinations of G for isomerization of either of the 1,2-diphenylpropenes in benzene or cyclohexane. Also, in sharp contrast with the stilbene isomerizations,[2,6] $G_{t\to c}/G_{c\to t}$ remains within experimental error of the corresponding quantum-yield ratio (1.20) at all concentrations up to 0.1 M in cyclohexane (*cf.* Figure 5). Thus, there is no indication of a catalytic contribution in radiation-induced isomerization of the 1,2-diphenylpropenes.

As found in radiation-induced isomerization of the stilbenes at concentrations less than ~0.1 M in benzene,[2] values of $G_{t\to c}/G_{c\to t}$ calculated from results in Figure 4 are equal, within experimental error, to the corresponding quantum-yield ratio. However, in contrast with the stilbene results, Hammond and coworkers[8] report persistence of such equality up to 1 M of the 1,2-diphenylpropenes. At concentrations below 1 M, the results in Figure 4 agree well with those of Hammond and coworkers.[8] Their value at 1 M of $G_{t\to c} = 5.48$, which gives with their $G_{c\to t} = 4.45$ a sum of 9.93, is considerably larger than our value of $G_{t\to c} = 4.2$, from which a sum of 7.7 is calculated. Nevertheless, in contrast with results for *trans*-stilbene,[2] it is evident that the values of $G_{t\to c}$ in Figure 4 do not reach an upper limit near 0.1 M solute but continue to increase (though at a much diminished rate) with increase in solute concentration. Absence of such a continued increase in the case of *trans*-stilbene is attributed plausibly to self-quenching of excited singlets of *trans*-stilbene for which Saltiel, *et al.*,[9] report $k_q\tau = 3.0\ M^{-1}$.

Present and published results for radiation-induced isomerization of the stilbenes[2,6,17] and 1,2-diphenylpropenes[4] suggest the following conclusions. Because of sensitivity to catalysis, *cis*-stilbene isomerization is likely to provide a reliable measure of the yield of *solute* excited states only at concentrations below 0.01 M in cyclohexane and 0.2 M in benzene. Isomerization of *trans*-stilbene provides a direct measure of the yield of *solute* excited states only at concentrations below ~0.1 M in both cyclohexane and benzene. Isomerizations of the 1,2-diphenylpropenes provide a direct measure of the yield of *solute* excited states at all concentrations that have been studied in cyclohexane and in benzene.

Precursors in Cyclohexane. As noted in the Introduction, previous work with *trans*-stilbene in cyclohexane[2,6] indicates that the yield of solute excited states is related to the yield of scavenged electrons. Yields of solute excited states obtained from the results in Figure 5 are somewhat larger than those calculated from $G_{t\to c}$ for *trans*-stilbene;[2,6] for 0.1 M solute the results in Figure 5 give $G_{t\to c} + G_{c\to t} = 3.1$ as compared to 2.3 calculated from $G_{t\to c}$ at 0.1 M *trans*-stilbene. Complexity of the isomerization mechanism in cyclohexane is such that detailed speculation on the causes of such a difference is not justified. However, it should be noted that the model used for interpretation of *trans*-stilbene results (*cf.* ref 6) can be accommodated to the results for the 1,2-diphenylpropenes (*e.g.*, by use of 1.35 as the average number of diphenylpropene molecules excited *per* electron scavenged at 0.1 M). Self-quenching of excited singlets of *trans*-stilbene may be partially responsible for the lower yield calculated from $G_{t\to c}$ for 0.1 M *trans*-stilbene.

Precursors in Benzene. Results in Figure 4 show that, with increase in solute concentration, a rather large initial rate of increase in $G_{t\to c}$ is followed by an apparent approach to an upper limit (near 0.1 M) which merges into a gradual increase above 0.1 M. For each value of $G_{t\to c}$ in Figure 4 a yield of solute excited states, G^*, can be calculated from eq I. However, estimation of yields for precursors of the solute

$$G^* = G_{t\to c}(1 + \phi_{c\to t}/\phi_{t\to c}) = (11/6)G_{t\to c} \qquad \text{(I)}$$

excited states is a complex problem. Discussion of the problem is facilitated by separate consideration of the results for solute concentrations above and below 0.1 M.

A number of factors may contribute to the gradual increase in $G_{t\to c}$ with increase in solute concentration above 0.1 M. Results of Hentz and Sherman[7] indicate that ~20% of the electrons of geminate ion pairs are captured by a solute such as 1,2-diphenylpropene at 0.1 M in benzene. Positive-charge transfer to the solute also occurs and with a probability that may be enhanced by electron capture.[18] Thus, with increase in solute concentration above 0.1 M, cations and anions of the solute are increasingly involved in charge-neutralization processes. In 1 M solutions the benzene cation and thermalized electron of each geminate pair will, on the average, be adjacent to a solute molecule, and involvement of solute molecules in charge-neutralization processes should be essentially complete. Participation of 1,2-diphenylpropene ions in the charge-neutralization processes may enhance G^* and, thereby, contribute to the growth in $G_{t\to c}$ above 0.1 M. In addition, because internal conversion from upper excited singlet states to the lowest excited singlet occurs with low efficiency in benzene,[19] an increased probability of excitation transfer from upper excited states of benzene at higher solute concentrations, certainly near 1 M, will enhance G^*. The growth in $G_{t\to c}$ above 0.1 M also may include contributions from subexcitation electrons and direct higher-energy depositions in

(17) E. Fischer, H. P. Lehmann, and G. Stein, *J. Chem. Phys.*, **45**, 3905 (1966).

(18) S. J. Rzad, R. H. Schuler, and A. Hummel, *ibid.*, **51**, 1369 (1969).

(19) C. W. Lawson, F. Hirayama, and S. Lipsky, *ibid.*, **51**, 1590 (1969).

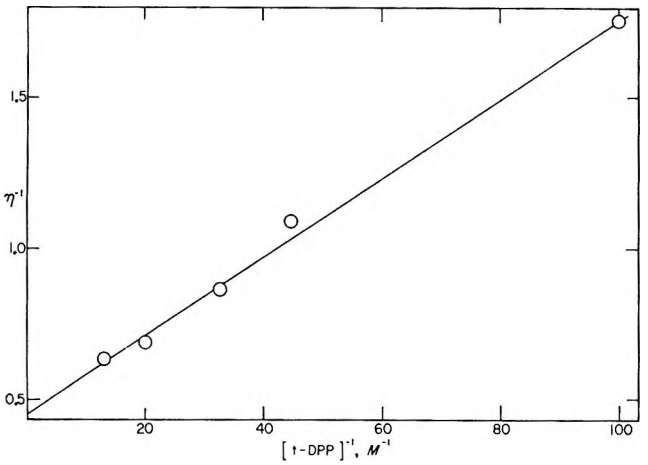

Figure 6. Plot of η^{-1} *vs.* reciprocal of the concentration of *trans*-1,2-diphenylpropene (*cf.* eq II).

the solute, and possibly, as suggested by Hammond and coworkers,[8] from scavenging of spur triplets. All things considered, it does not seem possible to establish a correlation between G^* and a yield of solvent excited states for solute concentrations greater than ~0.1 M.

Results for solute concentrations below 0.1 M do permit estimation of yields for the lowest excited singlet and triplet states of benzene. A value of $^1G_0 = 1.5$ has been obtained for the lowest excited singlet in studies of scintillation[20] and sensitized decomposition[21] of solutes at low concentrations in benzene. From $^1k^1\tau = 1200\ M^{-1}$ for transfer from the lowest excited singlet of benzene to *trans*-DPP, it follows that such transfer is essentially complete at 0.01 M *trans*-DPP. Consequently, as *trans*-DPP concentration increases from 0.01 M to 0.08 M, the increase in $G_{t\to c}$ (*cf.* Figure 4) is attributable almost entirely to scavenging of the lowest triplet of benzene by the solute. Therefore, results for the concentration range 0.01–0.08 M are well represented by eq II, in which $^3G_0$ is the yield of

$$\eta \equiv G_{t\to c} - 1.5(6/11) = (6/11)^3G_0{}^3k^3\tau[t]/(1 + {}^3k^3\tau[t]) \quad \text{(II)}$$

benzene triplets which do not have the lowest excited singlet as a precursor. A plot of η^{-1} *vs* $[t]^{-1}$ is shown in Figure 6. Values of $^3G_0 = 4.1$ and $^3k^3\tau = 34\ M^{-1}$ are calculated from the reciprocal of the intercept and the ratio of intercept to slope, respectively. Thus, a value of $G_0^* \equiv {}^1G_0 + {}^3G_0 = 5.6$ is obtained.

The value of $G_0^* = 5.6$ is in remarkably good agreement with estimates obtainable from previous work with the stilbenes. Our work[2] and that of Fischer, *et al.*,[17] with *trans*-stilbene suggest that transfer to stilbene from both the lowest excited singlet and triplet states of benzene must be near completion at 0.1 M stilbene. With $^1G_0 = 1.5$ and $k_q\tau = 3.0\ M^{-1}$ for self-quenching of excited singlets of *trans*-stilbene,[9] a correction of 0.2 is calculated for addition to values of 2.8[2] and 2.5[17] measured for $G_{t\to c}$ at 0.1 M. Assuming that electron scavenging by 0.1 M stilbene causes a negligible error in the calculation of G_0^*, use of $\phi_{t\to c}/\phi_{c\to t} = 1.31$ for the stilbenes[12] gives $G_0^* = 5.3$ and $G_0^* = 4.8$ from the corrected values of $G_{t\to c} = 3.0$ and $G_{t\to c} = 2.7$, respectively. Concordant values of G_0^* can be calculated directly from measured values of $G_{c\to t}$. Multiplication of our value[2] of $G_{c\to t} = 2.4$ at 0.1 M *cis*-stilbene by 2.31 gives $G_0^* = 5.5$. Results presented as $2.4 \times G_{c\to t}$ in Figure 2 of Hammond and coworkers[8] show scatter about an apparent plateau over a concentration range of 0.09–0.3 M *cis*-stilbene. The average of nine values within this concentration range is $G_{c\to t} = 2.3$ which multiplied by 2.31 gives $G_0^* = 5.3$.

Values of $^1G_0 = 1.5$ and $^3G_0 = 4.1$ also are in accord with results obtained in studies of the radiation-induced isomerization of olefins in benzene.[22,23] Under the conditions of such work, only transfer from the lowest triplet of benzene to the olefin occurs. Intersystem crossing from the lowest excited singlet to the triplet occurs with a probability of $\chi = 0.60$ in liquid benzene.[21,22] Therefore, in radiation-induced isomerization of olefins in benzene, the limiting yield obtained for solute triplets, corresponding to the total yield of lowest triplets in neat benzene, should be $^3G = 5.0$ (*i.e.*, $1.5 \times 0.60 + 4.1$). A value of $^3G = 5.0$ has been obtained by Golub, *et al.*,[23] with 2-pentene, 2-hexene, 2-heptene, and 2-octene. Cundall and Tippett[22] report $^3G = 4.7$ for 2-butene.

It is possible, then, to interpret much of the work on radiation-induced isomerizations in benzene in terms of $^1G_0 = 1.5$, $^3G_0 = 4.1$, and $\chi = 0.60$. However, a major problem remains in reconciliation of such yields with the considerably lower yields (by a factor of ~2) obtained for triplets of various solutes in pulse radiolysis of benzene solutions.[24–26] Though a number of suggestions could be offered and some suggestions have been presented,[22,26] there is at present no really satisfactory explanation for the discrepancy.

(20) P. Skarstad, R. Ma, and S. Lipsky, *Mol. Cryst.*, **4**, 3 (1968).

(21) L. M. Perkey, Ph.D. Thesis, University of Notre Dame, 1969; to be published.

(22) R. B. Cundall and W. Tippett, Advances in Chemistry Series, No. 82, American Chemical Society, Washington, D. C., 1968, p 387.

(23) M. A. Golub, C. L. Stephens, and J. L. Brash, *J. Chem. Phys.*, **45**, 1503 (1966).

(24) R. Cooper and J. K. Thomas, *ibid.*, **48**, 5097 (1968).

(25) E. J. Land and A. J. Swallow, *Trans. Faraday Soc.*, **64**, 1247 (1968).

(26) R. B. Cundall, G. B. Evans, P. A. Griffiths, and J. P. Keene, *J. Phys. Chem.*, **72**, 3871 (1968).

Thermally Stimulated Depolarization. A Method for Measuring the Dielectric Properties of Solid Substances

by T. Nedetzka, M. Reichle, A. Mayer, and H. Vogel

Physik Department der Technischen Hochschule München, Munich, Germany *(Received February 10, 1969)*

Thermally stimulated depolarization (TSD) of a polarized dielectric provides a method for measuring its dielectric properties. All mechanisms contributing to the dielectric constant which are temperature dependent can be measured separately by this method, namely orientational polarization of permanent dipoles or of dipoles induced by the electric field, space charge polarization, and electrode effects. The principal features of this method are described and a general theory of TSD is presented.

Introduction

The investigation of the dielectric properties of matter by the alternating field method[1-4] is in general complicated by two facts. (a) The contributions of different polarization mechanisms can be distinguished in the dispersion curve only if the corresponding relaxation times differ considerably. (b) In case of nonvanishing electric conductivity within the sample, space charge phenomena on the interfaces between sample and electrodes can simulate an additional polarization mechanism superimposed with the true dielectric dispersion. Those difficulties are effective in particular when studying the dielectric properties of hydrated lyophilized proteins.[1,4,5]

A new promising method for the investigation of dielectric properties is presented here in which the cited complications are eliminated. The principal features of the method of "thermally stimulated depolarization"—an analogous method has been applied in thermoluminescence studies[6,7]—are the following. The sample is mounted between the plates of a condenser to which an electric field of about 1 kV/cm is applied at room temperature so that a polarization is produced in the material. The sample is then cooled down to a temperature such that the polarization is frozen in; *i.e.*, the thermal energy is not large enough to reorientate the dipoles even after removal of the electric field. Only when the sample is subsequently heated according to a given temperature program, the frozen polarization gets liberated. This process can be followed by connecting the condenser plates through a resistance R_A and measuring the voltage U_m which is proportional to the time derivative of the induction charges on the condenser plates liberated by the decreasing polarization (Figure 1). The frozen polarization will be liberated at certain temperatures, corresponding to the special type of polarization mechanism, and will appear as a voltage peak over the temperature axis (Figure 2). Position and shape of those thermally stimulated depolarization curves give information on activation energy and relaxation time of the respective polarization mechanism and on the magnitude of the susceptibility. In the following a general theory of thermally stimulated depolarization is presented.

Theory of Thermally Stimulated Depolarization (TSD)

(This theory is based on electrostatic units.) In an electric polarizable medium several different mechanisms can in general contribute to the macroscopically observed polarization P, namely electronic and atomic displacement polarization, orientational polarization of dipoles, and space charge polarization.[8] P is proportional to the strength of the electric field F

$$P = P_{el} + P_{at} + P_{or} + P_{sp} = \chi F \qquad (1)$$

χ being the macroscopic susceptibility. Electronic and atomic polarizations are not temperature dependent since they are pertinent to deformation of the electronic shell and displacement of ions, respectively. Therefore those polarization contributions cannot be frozen in and do not appear in TSD measurement. Orientational polarization of permanent dipoles or of dipoles induced by internal electric fields is temperature dependent owing to the temperature dependence of both the equilibrium polarization and the relaxation time τ.[9] Space charge polarization is temperature dependent since its decrease takes place by compensation of the space charge *via* the resistance of the sample R_I which is temperature dependent (2). Orientational and

(1) W. Goebel and H. Vogel, *Z. Naturforsch.*, **19**, 292 (1964).

(2) G. Brausse, A. Mayer, T. Nedetzka, P. Schlecht, and H. Vogel, *J. Phys. Chem.*, **72**, 3098 (1968).

(3) N. Dannhauser, *J. Chem. Phys.*, **48**, 1918 (1968).

(4) T. Nedetzka, Diplomarbeit, Technische Hochschule München, 1964.

(5) H. P. Schwan, *Phys. Tech. Biol. Res.*, **6**, 323 (1963).

(6) W. Hoogenstraten, *Philips Res. Rep.*, **13**, 515 (1958).

(7) L. Mader and N. Riehl, *Z. Phys.*, **206**, 319 (1967).

(8) A. Hippel, "Dielectric and Waves," John Wiley and Sons, New York, N. Y., 1954.

(9) W. Kauzmann, *Rev. Mod. Phys.*, **14**, 12 (1942).

$$R_I = R_I^0 \exp\left(\frac{E}{kT}\right) \quad (2)$$

space-charge polarization therefore both can be frozen in if the sample is cooled down to sufficiently low temperature. The theory of TSD of both polarization mechanisms is described in the following sections.

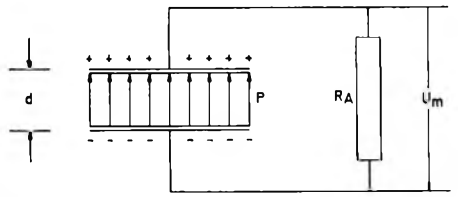

Figure 1. Experimental diagram of the TSD method.

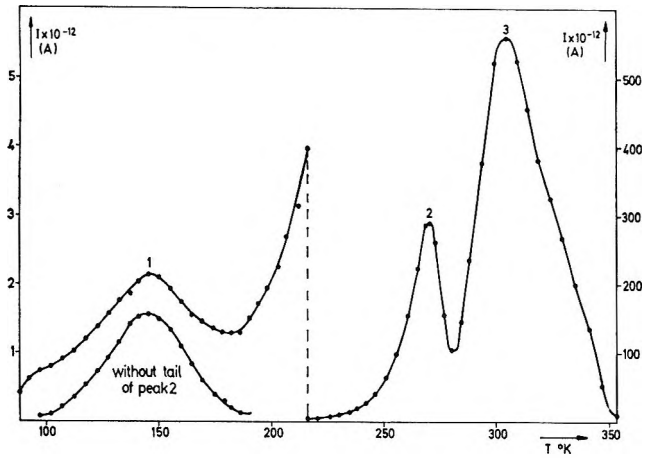

Figure 2. Depolarization peaks gained with a sample of lyophilized hemoglobin. Peaks 1 and 2 belong to orientational polarization; peak 3 belongs to space charge polarization.

1. Orientational Polarization and Its TSD. In substances with a large static dielectric constant $\epsilon_s(\epsilon_s > 3)$, permanent molecular dipoles largely determine the dielectric properties.[9] A theory of the relaxation behavior of dipoles has been given by Debye[10] on the basis of rotational diffusion. The application of this theory is limited as it has been derived under the following conditions: (a) no dipole–dipole interaction, (b) the equilibrium state is attained only by a single process (by transition over a potential barrier or rotational friction), (c) all dipoles behave in the average equally. Unfortunately, those conditions are seldom fulfilled simultaneously in practical situations. An alternative theory of dielectric relaxation is that of Kauzmann[9] which is based on the theory of chemical reaction rates and which is more general than the theory of Debye. In the following we shall therefore make use of the Kauzmann theory.

In Kauzmann's theory the time rate of change of the macroscopic polarization is expressed in terms of the motions of the individual molecular dipoles which are rotated from an element of solid angle $d\Omega$ to another $d\Omega'$ in an interval of time dt. For the transition probability, w_I (in the case of no electric field) follows from chemical rate theory

$$w_1 = \frac{svkT}{h} \exp\left(\frac{\Delta S}{k}\right) \exp\left(-\frac{E}{kT}\right) = \frac{w_0}{4\pi} T \exp\left(-\frac{E}{kT}\right) \quad (3)$$

where w_0 is the temperature independent factor, s is a sterical factor for hindered rotation, v is a transmission factor expressing the fraction of activated dipoles which accomplish the transition. Normally v is close to unity. ΔS is the entropy change upon transition, E is the activation energy, k is the Boltzmann factor, and T is the absolute temperature. Calculating the dipole transitions according to Boltzmann statistics and integrating over all dipoles and orientations, the following basic equations are obtained:[9] equilibrium polarization

$$P_{eq} = \frac{N_0 \mu_{eff}^2 aF}{3kT} = \chi F \quad (4)$$

where N_0 = number of dipoles/cm³, μ_{eff} = effective dipole moment of a molecule, F = external electric field, aF = internal electric field operating on the dipole[11] where

$$a = \frac{3\epsilon_s}{2\epsilon_s + 1}$$

and χ = the dielectric suceptibility; relaxation equation

$$\frac{dP}{dt} = 4\pi w_1 (P_{eq} - P) \quad (5)$$

where P is the instantanous polarization; relaxation time

$$\tau = \frac{1}{4\pi w_1} = \frac{1}{w_0 T} \exp\left(\frac{E}{kT}\right) \quad (6)$$

Equation 5 describes the time rate of change of the macroscopic polarization P in terms of the transition probability w_1 of the individual dipoles and is valid for continuous and discrete possibilities of dipole orientation. In the case of thermally stimulated depolarization we are concerned not with the time dependence of the polarization but with its temperature dependence. To keep calculations simpler in the theory and for better realization in the experiment, the relation between temperature and time is chosen linear; that means the sample is heated with constant rate q (deg/sec).

$$T = T_0 + qt \quad (7)$$

(10) P. Debye, *Phys. Ber.*, 15, 777 (1913).

(11) W. Weizel, "Lehrbuch der Theoretischen Physik," Springer-Verlag, West Berlin, 1963.

where T_0 is the initial temperature. Equation 5 can then be rewritten with the new variable T, using eq 3

$$\frac{dP}{dT} = \frac{4\pi w_1}{q}(P_{eq} - P) \tag{8}$$

Inserting w_1 from eq 3 gives

$$\frac{dP}{dT} = \frac{w_0}{q} T(P_{eq} - P) \exp\left(-\frac{kT}{E}\right) \tag{9}$$

Equation 9 expresses the temperature dependence of the macroscopic polarization. To find the temperature dependence of the polarization, eq 9 must be integrated.

The polarized sample by induction binds charges on the surface of the condenser plates. If the polarization decays (due to thermal activation) these charges are liberated and will flow through the resistance R_A producing a voltage U_m (Figure 1). This voltage on its part produces again a polarization P_{eq} in the sample which is opposed to the change of the polarization and which tends to maintain the original polarization

$$P_{eq} = \frac{N_0 \mu_{eff}^2 a U_m}{3kTd} \tag{10}$$

The Maxwell equations give the connection between the polarization change dP/dT and the voltage U_m

$$U_m = IR_A = -R_A f q \frac{dP}{dT} \tag{11}$$

where f is the area of the condenser plates in cm^2. Inserting eq 10 and 11 in eq 9 and solving for dP/dT gives

$$\frac{dP}{dT} = -\frac{w_0 TP \exp\left(-\frac{E}{kT}\right)}{q\left[1 + w_0 \exp\left(-\frac{E}{kT}\right) N_0 \mu_{eff}^2 a R_A f \frac{1}{3kd}\right]} \tag{12}$$

Denoting

$$\frac{N_0 \mu_{eff}^2 a R_A f}{3kdT} = \chi R_A C = c \tag{13}$$

where χ is the macroscopic susceptibility of the sample (eq 4) and $C = f/d$ the capacitance of the empty condenser, eq 13 reads

$$\frac{dP}{dT} = -\frac{4\pi w_1 P}{q(1 + 4\pi w_1 c)} \tag{14}$$

Equation 14 can be integrated only for two limiting cases: $4\pi w_1 c \ll 1$ and $4\pi w_1 c \gg 1$

(*a*) $4\pi w_1 c \ll 1$. This condition is certainly fulfilled for low temperatures due to the exponential dependence of the transition probability w_1 on $(-1/T)$. The physical meaning of the condition is—as can be realized from comparing eq 9 and 15—that the equilibrium polarization P_{eq} is much smaller than the initial polarization P_0 which is to be depolarized thermally. In fact, in practical cases the external voltage applied to the sample producing the initial polarization is by orders of magnitude larger than the voltage U_m which is measured. In the limiting case $4\pi w_1 c \ll 1$ eq 14 becomes

$$\frac{dP}{dT} = -\frac{w_0}{q} PT \exp\left(-\frac{E}{kT}\right) \tag{15}$$

Integrating eq 15 gives

$$\ln\left(\frac{P}{P_0}\right) = -\frac{w_0}{q}\int_{T_0}^{T} T' \exp\left(-\frac{E}{kT'}\right) dT' \tag{16}$$

The integral in eq 16 can be solved by partial integration

$$\ln\left(\frac{P}{P_0}\right) = -\frac{w_0}{q}\left\{\left[\frac{T'^2}{2}\exp\left(-\frac{E}{kT'}\right)\right]_{T_0}^{T} - \frac{E}{2k}\int_{T_0}^{T} \exp\left(-\frac{E}{kT'}\right) dT'\right\} \tag{17}$$

and developing into a series of products

$$\int \exp\left(-\frac{E}{kT'}\right)\frac{d(kT')}{E} = \exp\left(-\frac{E}{kT'}\right) B\left(\frac{E}{kT'}\right) \tag{18}$$

where

$$B\left(\frac{E}{kT'}\right) = \sum_{i=2}^{\infty} (-1)^i (i-1)! \left(\frac{E}{kT'}\right)^{-i} \tag{19}$$

which, although it is semiconvergent, can be chopped off after some of the dominant first terms, according to Debye's method of steepest descent[12,13] for $EkT \gg 1$.

This finally gives the polarization P explicitly as a function of temperature

$$P = P_0 \exp\left\{-\frac{w_0}{q}\left[\frac{T^2}{2}\exp\left(-\frac{E}{kT}\right) - \frac{T_0^2}{2}\exp\left(-\frac{E}{kT_0}\right)\right] + \frac{w_0 E^2}{2qk^2}\left[B\left(\frac{E}{kT}\right)\times \exp\left(-\frac{E}{kT}\right) - B\left(\frac{E}{kT_0}\right)\exp\left(-\frac{E}{kT_0}\right)\right]\right\} \tag{20}$$

where P_0 is the initial polarization frozen in at temperature T_0. Under the condition $kT \ll E$ (this condition is always valid for relaxation processes as known from chemical rate processes) the series B in eq 19 can be broken off after the second term and eq 20 is then simplified to the approximation

$$P = P_0 \exp\left\{-\frac{w_0 k}{qE_0}\left[T^3 \exp\left(-\frac{E}{kT}\right) - T_0^3 \exp\left(-\frac{E}{kT_0}\right)\right]\right\} \tag{21}$$

(12) H. Poincaré, *Acta Math.*, **8**, (1886).
(13) P. Debye, *Math. Ann.*, **67**, (1909).

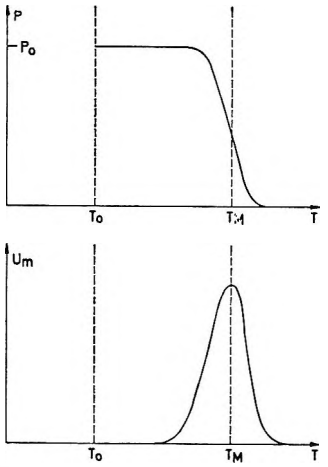

Figure 3. Calculated dependence of the polarization P and the measuring voltage U_m from the temperature. This picture is valid when the temperature I_0, to which the sample was cooled down, is low enough to prevent spontaneous depolarization.

Equation 21 describes the course of the polarization during the process of linear heating. This function has no extremum but only a point of inflection

$$T_w = \frac{E}{k}\left[\ln\left(\frac{w_0 k T_w^3}{q(E + kT_w)}\right)\right]^{-1} \tag{22}$$

This expression for T_w has been derived directly from eq 14, independently from the approximation that leads to eq 21. The point of inflection T_w of the approximation 21 is slightly shifted in relation to that of the exact equation.[20] For $T < T_w$ the polarization is nearly constant: $P = P_0$, for $T > T_w$ the polarization is zero: $P = 0$. In the surrounding of the point of inflection T_w the polarization $P(T)$ decreases rapidly. The qualitative behavior of the polarization as a function of temperature is shown in Figure 3. Inserting eq 15 and 20 in eq 11, one obtains for the measuring voltage U_m

$$U_m = R_A f w_0 P_0 T \exp\left\{-\frac{E}{kT} - \frac{w_0}{2q}\left[T^2 \exp\left(-\frac{E}{kT}\right) - T_0^2 \exp\left(-\frac{E}{kT_0}\right)\right] + \frac{w_0 E^2}{2qk^2}\left[B\left(\frac{E}{kT}\right)\exp\left(-\frac{E}{kT}\right) - B\left(\frac{E}{kT_0}\right)\exp\left(-\frac{E}{kT_0}\right)\right]\right\} \tag{23}$$

In the same approximation as in the case of eq 21 one obtains from eq 23

$$U_m = R_A f w_0 T P_0 \exp\left\{-\frac{E}{kT} - \frac{w_0 k}{Eq} T^3 \exp\left(-\frac{E}{kT}\right) + \frac{w_0 k}{Eq} T_0^3 \exp\left(-\frac{E}{kT_0}\right)\right\} \tag{24}$$

From eq 11 it follows at once that the maximum of U_m coincides with the point of inflection of the polarization P

$$T_M = T_W \tag{25}$$

Equation 24 can also be written as

$$U_m = U'T \exp\left\{-\frac{E}{kT} - \frac{w_0 k}{Eq} T^3 \exp\left(-\frac{E}{kT}\right)\right\} \tag{26}$$

where U' contains all the terms which do not depend on temperature T. To investigate the course of the measuring voltage U_m depending on T eq 26 shall be rewritten

$$U_m = U'T \exp\left(-\frac{E}{kT}\right) \exp\left\{-\frac{w_0 k}{Eq} T^3 \exp\left(-\frac{E}{kT}\right)\right\} \tag{27}$$

Equation 27 contains a product of two exponential functions. It is well known that in such a case the temperature dependence of U_m is mainly governed by that exponential function from which the exponent changes more with temperature. Differentiating the two exponents gives their temperature dependence. It can be seen that the first exponent is weakly temperature dependent. Its absolute value decreases slowly with temperature. The second exponent is strongly temperature dependent. At low temperature it remains nearly zero. Then its absolute value and its derivative increase very rapidly with increasing temperature. At a certain temperature T' the derivatives of the two exponents are equal

$$T' = \frac{E}{k}\left\{\ln\left[\frac{w_0 k T'^3}{Eq}\left(1 + 3\frac{kT'}{E}\right)\right]\right\}^{-1} \tag{28}$$

Since in practice $kT_M \ll E$, the comparison between T_M and T' yields

$$T' = \frac{T_M}{1 - \frac{4k^2 T_M^2}{E^2}} \tag{29}$$

which for reasonable values means a difference of about 4%. For $T < T' \approx T_M$ the first exponential function of eq 27 dominates the temperature course of U_m.

$$U_m \sim T \exp\left(-\frac{E}{kT}\right) \tag{30}$$

For $T > T_M \approx T'$ the second term of eq 27 dominates and depresses U_m.

The measured voltage U_m is seen to increase with increasing temperature T in the range $T < T_M$ and to decrease in the range $T > T_M$. Figure 3 shows qualitatively the dependence of U_m on T. The activation energy can be determined from the temperature dependence of the measured voltage U_m approximately by plotting the log of the increase of U_m over $1/T$ according to eq 30. In first approximation a straight line is obtained, the slope of which gives the activation energy E (eq 31). The activation energy E can also be

$$E = -k\frac{\mathrm{d}(\ln U_m)}{\mathrm{d}(1/T)} \tag{31}$$

determined from the peak temperature at different heating velocities q from eq 22

$$E = \frac{k\left\{\ln\left(\frac{T_{M1}^3}{q_1}\right) - \ln\left(\frac{T_{M2}^3}{q_2}\right)\right\}}{1/T_{M1} - 1/T_{M2}} \tag{32}$$

From eq 22 the temperature independent jump constant can be computed.

$$w_0 = \frac{q}{kT_M^3}(E + kT_M)\exp\left(\frac{E}{kT_M}\right) \tag{33}$$

With the aid of eq 3 the entropy change ΔS upon reorientation of the dipoles can in principle be determined, provided that the sterical factor s is known or can be estimated.

(*b*) $4\pi w_1 c \gg 1$. This condition means that the temperature T_0 to which the sample was cooled down was not low enough in order to make the transition probability w_1 sufficiently small. w_1 is still so large that the reorientation of dipoles can be achieved at that temperature. The polarization then decays at this temperature in a short time. In this limiting case eq 12 becomes

$$\frac{\mathrm{d}P}{\mathrm{d}T} = \frac{-P}{q\chi R_A C} \tag{34}$$

The susceptibility of the orientational polarization has the temperature dependence[9,14] (see also eq 4)

$$\chi = \frac{\chi'}{T} \tag{35}$$

Therefore eq 34 is replaced by

$$\frac{\mathrm{d}P}{\mathrm{d}T} = \frac{-TP}{q\chi' R_A C} \tag{36}$$

integration of eq 36

$$P = P_0 \exp\left\{-\frac{T^2 - T_0^2}{2q\chi' R_A C}\right\} \tag{37}$$

Inserting eq 34 and 37 in eq 11 gives for the measured voltage U_m

$$U_m = \frac{fP_0}{\chi' C} T \exp\left(-\frac{T^2 - T_0^2}{2q\chi' R_A C}\right) \tag{38}$$

For $(T^2/2q\chi' R_A C) < 1$ U_m increases proportional to T and for $(T^2/2q\chi' R_A C) > 1$ U_m decreases rapidly proportional to $\exp(-T^2)$. The maximum of U_m occurs at the temperature T_M

$$T_M = (q\chi' R_A C)^{1/2} \tag{39}$$

Figure 4 shows schematically the dependence of U_m on T.

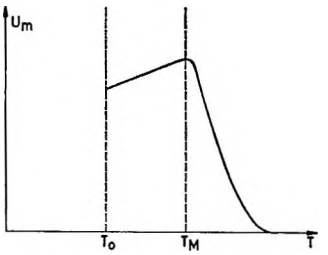

Figure 4. Calculated relation between the measuring voltage U_m and the temperature T in the case when the starting temperature T_0 is high enough for spontaneous depolarization.

2. Relationship between the Area A of the Depolarization Peak, Susceptibility χ, *Static Dielectric Constant* ϵ, *and Dipole Moment* μ_{eff}. The initial polarization P is, according to eq 11, equal to the charges Q induced on the condensor plates divided by the area f of the condensor plates

$$P_0 = \frac{Q}{f} \tag{40}$$

The polarization gets liberated upon heating up the samples and the induced charge Q can flow off

$$Q = \int I(t)\mathrm{d}t = mA \tag{41}$$

If the electric current I is flowing only through the external resistance R_A (Figure 1) then

$$I(t) = I_A(t) = \frac{U_m(t)}{R_A} \tag{42}$$

In case that the resistance R_I of the samples is not considerably greater than R_A, the following equation must be used

$$I(t) = \frac{I_A(t)}{R_I}(R_A + R_I) = U_m(t)\frac{R_A + R_I}{R_A R_I} \tag{43}$$

The resistance R_I can be determined very simply by changing R_A during the measurement. In case that U_m changes proportional to R_A, then $R_I \gg R_A$. In the other case with eq 43 and 24, the magnitude of R_I can be determined and the total discharge current $I(t)$ can be calculated. The integral of eq 41 is proportional to the registered area A of the dipolarization peak. The depolarization curves are recorded by a charge recorder and the factor m can be computed from the sensitivity and the feed velocity of the recorder. The area A of the depolarization peak is determined by planimetry. P_0 then can be computed according to eq 1

$$P_0 = \chi F_0 = \frac{mA}{f} \tag{44}$$

where F_0 is the electric field applied to the sample during

(14) W. Fröhlich, "Theory of Dielectric," Oxford at the Clarenden Press, 1958.

freezing in the polarization. From eq 40, 41, 42, and 43 one gets for the susceptibility

$$\chi = \frac{mA}{fF_0} \tag{45}$$

Susceptibility χ and dielectric constant ϵ are related by

$$\epsilon = 1 + 4\pi\chi = 1 + 4\pi\frac{mA}{fF_0} \tag{46}$$

In the case of a substance made up of permanent dipoles we have $\epsilon \gg 1$. From eq 4 and 44 then follows for the effective dipole moment μ_{eff}

$$\mu_{eff} = \sqrt{\frac{2P_0kT}{N_0F_0}} = \sqrt{\frac{2mAkT}{N_0F_0f}} \tag{47}$$

The effective dipole moment μ_{eff} can deviate from the dipole moment μ of a free molecule.[14] This deviation is due to (a) electronic polarizability of the molecule, (b) short-range interaction between the dipoles, (c) nonsphericity of the molecule, and (d) existence of an additional quadrupole moment.

Fröhlich[14] considers the influences of (a) and (b) introducing relation 48 where the factor $3/(n^2 + 2)$

$$\mu = \frac{3\mu_{eff}}{(n^2 + 2)\sqrt{1 + z\langle\cos\vartheta\rangle}} \tag{48}$$

is due to the electronic polarizability and the factor $(1 + z\langle\cos\vartheta\rangle)^{1/2}$ is due to the short-range interaction. $n = \sqrt{\epsilon}$ is the refractive index, z the number of the nearest neighbors of the dipole molecule, $\langle\cos\vartheta\rangle$ is spatial average cosine of the angle between two adjacent dipoles. This angle ϑ strongly depends on the kind of interaction between the two dipoles (*i.e.*, electrostatic interaction, chemical binding, sterical hindrance, etc.). $\langle\cos\vartheta\rangle$ is negative for antiparallel alignment of the dipoles and positive for parallel alignment.

3. Space Charge Polarization and Its TSD. Dielectric materials often exhibit some small electric conductivity. This produces in general a space charge cloud on the interface between sample and electrode[5,15,16] (Figure 5). The space charge simulates a polarization which can be frozen in and can be heated out. This process can be described as shown in Figure 6. C_E is the capacitance between space charge cloud and electrode and R_E is the resistance. C_I and R_I are the capacitance and the resistance between the space charge clouds. For simplicity, C_E and R_E are assumed to be the same for the two electrodes; in fact the results are qualitatively not altered if different capacitances and resistances are assumed. In dielectric materials the following relation holds.

$$R_I = R_{I0}e^{E/kT} \tag{2}$$

In the following we shall compute the discharge of the capacitances as function of a linear temperature change

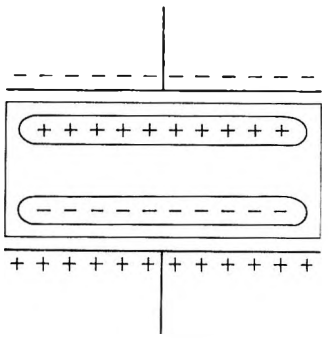

Figure 5. Schematic representation of the space charge at the interfaces between sample and electrodes.

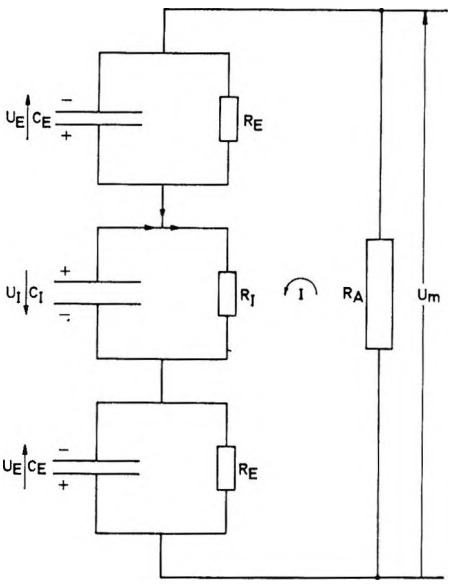

Figure 6. Diagram of connections for the depolarization of the space charges.

of the sample which will give us the measured voltage U_m. Since the differential equation of the total system cannot be integrated only the limiting cases will be discussed.

(*a*) $R_E \ll R_I$, R_A *Variable.* In this case space charges are produced only if there exists a contact voltage between sample and electrodes. Compensation of charges takes place through R_E. No electric current flow through R_A. The measured voltage U_m is zero.

(*b*) $R_E \gg R_I$, R_A *Variable.* No electric current flows through R_E. The discharge of the capacitance over R_I is coupled with a flow-off of charges through R_A. The following relation then holds

$$I_A = \frac{U_m}{R_A} = -C_E\dot{U}_E \tag{49}$$

With the aid of function and network equations the two differential equations can be set up

(15) W. Goebel, Dissertation, Technische Hochschule München, 1963.

(16) E. Potter, "Electrochemistry," Cleaver-Hume, London, 1956.

$$\dot{U}_E + 2\frac{U_E}{R_A C_E} - \frac{U_I}{R_A C_E} = 0 \quad (50)$$

$$\dot{U}_I + \frac{U_I}{R_I C_I} + \frac{C_E \dot{U}_E}{C_I} = 0 \quad (51)$$

Introducing a linear relation of temperature and time according to eq 7 and inserting eq 2 gives

$$\frac{dU_E}{dT} + \frac{2U_E}{qR_A C_E} - \frac{U_I}{qR_A C_E} = 0 \quad (52)$$

$$\frac{dU_I}{dT} + \frac{U_I}{qR_{I_0} C_I} \exp\left(-\frac{E}{kT}\right) + \frac{C_E}{C_I}\frac{dU_E}{dT} = 0 \quad (53)$$

Equations 52 and 53 lead to a differential equation of second order in U_E which cannot be solved analytically. Therefore additional approximations have to be made. According to Potter[16] the electrode capacitance C_E is considerably larger than the sample capacitance C_I.

$$C_E \gg C_I \quad (54)$$

We also assume that the changes of U_I and U_E with T are not to different

$$\frac{dU_E}{dT} \approx \frac{dU_I}{dT} \quad (55)$$

Equations 52, 53, 54, and 55 then gives

$$\frac{dU_E}{dT} = \frac{-2U_E}{qC_E\left[R_A + R_{I0} \exp\left(\frac{E}{kt}\right)\right]} \quad (56)$$

Integration of eq 56 is possible for two cases (α) $R_A \ll R_I$ and (β) $R_A \gg R_I$: (α) $R_A \ll R_I$ yields

$$\frac{dU_E}{dT} = -\frac{2U_E}{qC_E R_{I0}} \exp\left(-\frac{E}{kT}\right) \quad (57)$$

The solution of eq 57 is possible by the same development into a series of products as used in eq 19. Breaking off after the first term of the series we get

$$U_E = U_{E0} \exp\left\{-\frac{2T^2 k}{qR_{I0}C_E E} \exp\left(-\frac{E}{kT}\right) + \frac{2T_0^2 k}{qR_{I0}C_E E} \exp\left(-\frac{E}{kT_0}\right)\right. \quad (58)$$

combining all temperature independent terms to a factor U'_{E0} and making use of eq 49 gives

$$U_m = \frac{2U'_{E0}R_A}{R_{I0}} \exp\left\{-\frac{E_0}{kT} - \frac{2kT^2}{qR_{I0}C_E E} \exp\left(-\frac{E}{kT}\right)\right\} \quad (59)$$

Equation 59 has a maximum at

$$T_M = \frac{E}{k \ln\left(2kT_M{}^2 \frac{2kT_M + E}{qR_{I0}C_E E^2}\right)} \quad (60)$$

(β) $R_A \gg R_I$. The flow-off of the charges is determined only by the large resistance R_A

$$\frac{dU_E}{dT} = \frac{-2U_E}{qR_A C_E} \quad (61)$$

Integration of eq 61 and inserting in eq 49 gives for the measured voltage U_m

$$U_m = 2U_{E0} \exp\left\{-\frac{2(T - T_0)}{qR_A C_E}\right. \quad (62)$$

Equation 59 is similar to eq 26 and eq 62 similar to eq 38. The main difference is the factor T being present in eq 26 and 38 and the power of T in the exponential function of eq 26 and 38, being larger by 1 than that of the respective eq 59 and 62. This indicates that space charge polarization exhibits similar depolarization curves as true orientational polarization. Varying C_E and R_E by taking different electrode materials, the space charge peak changes its magnitude and width, but orientational polarization peaks do not. Thus one can distinguish between the two different kinds of peaks.

Conclusion

To simplify calculations the theory of TSD was developed for one mechanism at a time. With several mechanisms—for instance, different kinds of dipole molecules plus space charge—one can show that every mechanism can be calculated separately, if only the respective activation energies differ sufficiently to separate the different depolarization peaks.

Orientational polarization and space charge polarization produce similar depolarization curves. It is possible, however, to distinguish between them by variation of the electrode material that changes the space charge polarization. The method presented allows one to compute and to explain the activation energy, relaxation time, and effective molecular dipole moment of orientational polarization from the shape and position of the TSD curves more exactly and clearly than by the alternating field method, because every mechanism shows its own peak. The usefulness of this method has been demonstrated by an investigation of the dielectric properties of lyophilized hemoglobin. Figure 2 shows a TSD measurement of hemoglobin. Peaks 1 and 2 can be attributed to differ-

(17) M. Reichle, T. Nedetzka, A. Mayer, and H. Vogel, *J. Phys. Chem.*, **74**, 2659 (1970).

(18) NOTE ADDED IN PROOF. Under unfavorable conditions the TSD peaks can overlap, so that they cannot be separated exactly. The following method can be applied to overcome this difficulty. During cooling the polarizing voltage is only applied in that temperature range in which the peak to be investigated appears in heating. In this case mechanisms yielding TSD peaks at higher temperatures cannot contribute because the thermal energy is not sufficient to overcome the activation energy. Mechanisms yielding peaks at lower temperatures will depolarize during further cooling with shorted sample. Thus only the interesting TSD peak will occur. This method confirmed experimentally will be described in detail in a separate paper.[19]

(19) T. Nedetzka, in preparation.

ent orientational polarization and peak 3 to space charge polarization. These measurements are discussed in detail in the following paper.[17-19]

Acknowledgment. This work was supported by a grant from Stiftung Volkswagenwerk. We are much indebted to Prof. N. Riehl for stimulating discussions.

Dielectric Properties of Hydrated Lyophilized Hemoglobin as Determined with the Method of Thermally Stimulated Depolarization

by M. Reichle, T. Nedetzka, A. Mayer, and H. Vogel

Physik Department der Technischen Hochschule München, Munich, Germany *(Received February 10, 1969)*

The dielectric properties of hydrated lyophilized hemoglobin have been measured by the TSD method.[1] Three distinct TSD peaks were observed in the temperature range from 85 to 350°K. Their dependence on the degree of hydration, on the magnitude of the applied electric field, and on the electrode material were investigated. Susceptibility, activation energy, and relaxation time of the respective polarization mechanism were calculated from the temperature position, shape, and magnitude of the TSD peaks. The three peaks were identified as caused by orientational polarization of polar amino acid residues, orientational polarization of the total hemoglobin molecule, and electrode polarization, respectively.

Introduction

In the preceding paper[1] a method has been described for the determination of the dielectric properties of a solid material. The sample is polarized by an applied high electric field. This polarization is subsequently frozen in by cooling the sample down to a temperature sufficiently low to prevent depolarization by thermal energy. This of course holds only for processes with an activation energy, like dipole orientation and space charge. If the frozen sample is heated up linearly the polarization will be liberated at characteristic temperatures. In a circuit containing the sample capacity and a resistance the charges bound by induction on the electrode can go away. Thus for each polarization mechanism an inherent current peak can be measured. From the position of the peak on the temperature scale and its size and shape, the magnitude of the polarization and its activation energy and relaxation time can be calculated. The theoretical background and the equations used for calculating these quantities have been discussed in detail in the preceding paper.[1] Here, we repeat only the principal formula, which are given in electrostatic units.

The temperature dependence of the current peak for dipole orientation mechanism is expressed as

$$I_m = fw_0TP_0 \exp\left\{-\frac{E}{kT} - \frac{w_0k}{Eq}T^3 \exp\left(-\frac{E}{kT}\right) + \frac{w_0k}{Eq}T_0^3 \exp\left(-\frac{E}{kT_0}\right)\right\} \quad (1)$$

f = surface area of the electrodes, P_0 = the frozen polarization, E = activation energy for dipole orientation, k = Boltzmann constant, T_0 = initial temperature, w_0 = temperature-independent part of the transition probability of the dipoles w_1.

$$w_1 = \frac{w_0}{4\pi} T \exp\left(-\frac{E}{kT}\right) \quad (2)$$

According to eq 1, E can be obtained in the ascending flank of the peak from the slope of a straight line in a log I *vs.* $1/T$ plot: activation energy

$$E = -k\frac{\mathrm{d} \ln I}{\mathrm{d}(1/T)} \quad (3)$$

temperature-independent part of w_1

$$w_0 = \frac{q}{kT_M^3}(E + kT_M) \exp\left(\frac{E}{kT_M}\right) \quad (4)$$

T_M = the temperature at the current maximum; the relaxation time

$$\tau = \frac{1}{4\pi w_1} \quad (5)$$

and susceptibility

$$\chi = \frac{mA}{fF_0} \quad (6)$$

(1) T. Nedetzka, M. Reichle, A. Mayer, and H. Vogel, *J. Phys. Chem.*, **74**, 2652 (1970).

m = normalization factor, A = peak area, F_0 = electric field strength of the initial polarization; the dielectric constant

$$\epsilon = 1 + 4\pi\chi \tag{7}$$

effective dipole moment

$$\mu_{eff} = \sqrt{\frac{2mAkT'}{N_0F_0f}} \tag{8}$$

N_0 is the number of molecules/cm³ and T' is the temperature for which the relaxation time is still sufficiently short in order to let the polarization corresponding to the temperature T' adjust during the time of the applied electric field. T' can be computed from eq 4 and 5. The effective dipole moment μ_{eff} deviates from the dipole moment of the free molecule μ:

$$\mu = \frac{3\mu_{eff}}{(n^2 + 2)\sqrt{1 + z\langle\cos\vartheta\rangle}} \tag{9}$$

n is the refractive index of the substance, z is number of nearest neighbors to the molecule, and $\langle\cos\vartheta\rangle$ is the spatial average of the cosine of the angle between two adjacent dipoles.

Dipole–dipole interaction energy between two adjacent dipoles is given by

$$E = \frac{\mu_{eff}^4}{3kTa^6} \tag{10}$$

where a = mean distance between the dipoles. It is well known that the dielectric behavior of lyophilized protein strongly depends on the degree of hydration.[2-7] Measurement with alternating electric field techniques is subject to difficulties with electrode or space charge polarization effects which obscure the bulk dielectric properties of the material. With the TSD method these effects can be separated and it is to this end that the method has been applied to continue the previous studies[2] of the dielectric properties of lyophilized hydrated hemoglobin.

Material

Horse hemoglobin has been prepared as described elsewhere.[2] The lyophilized material was pressed to pellets of 13 mm diameter and 1–3 mm thickness. The degree of hydration was adjusted by exposing the pellets to a water vapor pressure in sealed tubes over H_2SO_4 solutions.[2] The hydration $h = 0$ is defined here as the hydration left after heating under vacuum at 105° for a longer time.[2]

It was not possible to investigate salt-free material because the surface of those pellets splitted when moistened. Lyophilized hemoglobin powder consists apparently of fibers of approximately 5000 Å thickness; if pressed to pellets, the surface contains coiled fibers, as observed with a microscope. Lyophilized hemoglobin appears to be amorphous, *i.e.*, the hemoglobin molecules do not form microcrystallites; there are, however, indications that regions with a certain close-range order are formed.[7] Freshly lyophilized hemoglobin is denatured to 5–10%. The dry material is rather resistant toward denaturation, over a long period of time (month), while partially hydrated material is denatured considerably during the same period of time. In the average the degree of denaturation of the hemoglobin pellets—determined after the TSD measurements—was about 25%. Freshly lyophilized hemoglobin powder consists of about 60% met–hemoglobin and 40% oxyhemoglobin. The percentage of met-hemoglobin is increasing with time up to nearly 100%. With increasing degree of hydration the volume of the hemoglobin pellet is increasing, as also mentioned in reference 2. Weight and volume of the pellets were determined for each experiment. Degrees of hydration are defined as grams of H_2O per gram of protein and they have been varied between 0 and 30%.

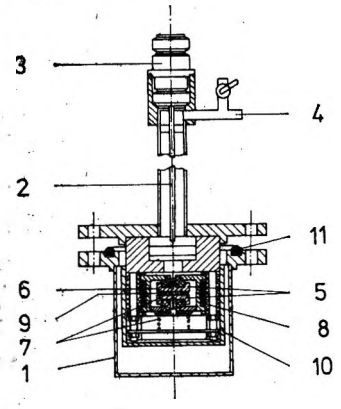

Figure 1. Measuring cell: 1, cell tube; 2, coaxial line; 3, coupling; 4, tubing; 5, electrodes; 6, fixed electrode; 7, springy electrode; 8, heating coil; 9, sample; 10, Teflon cylinder; 11, sealing ring.

Method

The measuring cell (Figure 1) was enclosed in a vacuum-tight tube. The coaxial line for the applied voltage and the electrometer consisted of a copper tube with an inner polyvinyl chloride insulated cable. This device proved to be better than a shielded cable, since bending or twisting of such a cable produces changes of capacitance and induced currents. A tubing for introducing a protecting gas (N_2 or He) into the tube and ducts for the heating and thermoelectric wires are installed. The upper electrode of the cell was fixed while

(2) G. Brausse, A. Mayer, T. Nedetzka, P. Schlecht, and H. Vogel, *J. Phys. Chem.*, **72**, 3098 (1968).

(3) D. D. Eley and D. I. Spivey, *Nature*, **188**, 725 (1960).

(4) D. Rosen, *Trans. Faraday Soc.*, **59**, 2178 (1962).

(5) S. Maricic, G. Pivat, and V. Pravdic, *Biochim. Biophys. Acta*, **79**, 293 (1964).

(6) S. Takashima and H. P. Schwan, *J. Phys. Chem.*, **69**, 4176 (1965).

(7) U. Wehnelt, P. Schlecht, A. Mayer, and T. Nedetzka, in preparation.

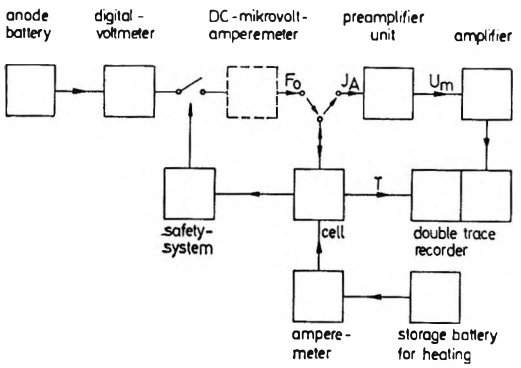

Figure 2. Block diagram of apparatus.

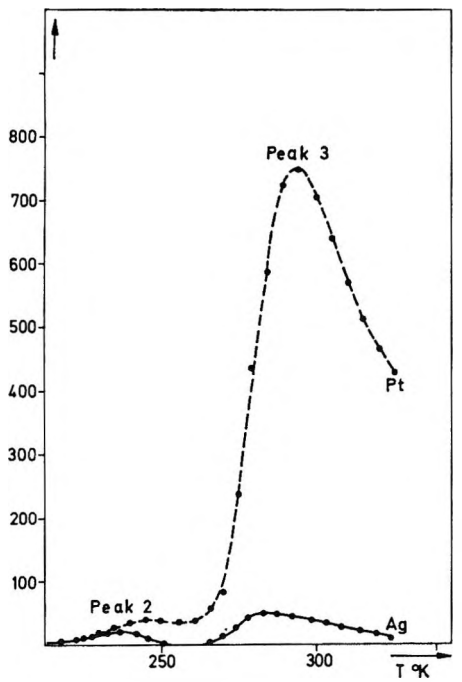

Figure 3. TSD peak 3 for two different electrode materials: Ag and Pt; $h = 12\%$, $F_0 = 550$ V/cm, $q = 0.2$ deg/sec.

the lower electrode was pressed on the pellet by a spring. Near this spring the thermoelectric wires were soldered. The cell is enveloped by a heating coil—a brass tube on which thermo-coaxial heating wire was soldered. Ag electrodes were used. In order to investigate electrode effects foils of several other materials were put on the electrodes (Pt, polyester, etc.).

The measurements were performed as follows. A pellet was introduced into the cell. The tube was cooled with liquid nitrogen. By heating, a temperature of 290°K was maintained. The voltage was applied to the cell. A safety system switched off the voltage in case of a current increasing to 10^{-6} A, in order not to destroy the sample in the cell by electrolysis or breakdown. After *ca.* 20 min the heating was interrupted and the sample was cooled down to *ca.* 85°K during about 1 hr. The voltage was switched off and the vibrating reed electrometer was connected. The sample was heated up linearly with a heating velocity of usually 0.2 deg/sec. The electrometer measured the liberated charges. With a double-trace recorder the TSD peaks and the temperature were plotted simultaneously. A polarizing electric field of up to 1800 V/cm was used.

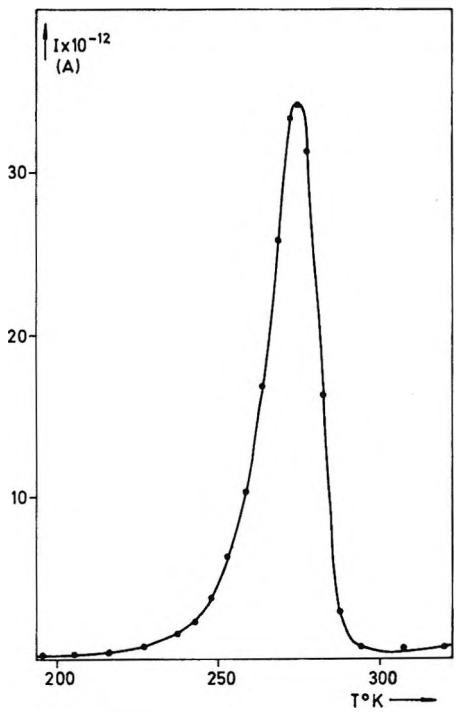

Figure 4. TSD peak 2; $h = 7\%$, $F_0 = 563$ V/cm, $q = 0.2$ deg/cm.

Results

With lyophilized hydrated horse hemoglobin three distinct TSD peaks were observed in the temperature range from 85 to 350°K, as shown in[1] Figure 2. Their dependence on the degree of hydration, on the magnitude of the applied electric field, and on the electrode material was investigated. The TSD peaks are denoted 1, 2, and 3 in the same order as they appear when starting at low temperatures. The shape of the peaks is in agreement with the equations derived in reference 1. In a control experiment it was ascertained that without a polarizing field there are no TSD peaks. There is also no polarization left in the sample after the measurement.

Peak 3. Peak 3 cannot be observed at degrees of hydration lower than 7%. But then this peak is growing quite rapidly with increasing hydration and for $h > 10\%$ it is overlapping peak 2, so that this peak can no longer be separated. The magnitude of peak 3 depends strongly on the electrode material. As shown in Figure 3 this magnitude is about 50 times larger for platinum electrodes than for silver electrodes. If insulating electrodes are used—4-μ polyester foils put in between sample and electrode—peak 3 disappears completely. This effect was used in order to investi-

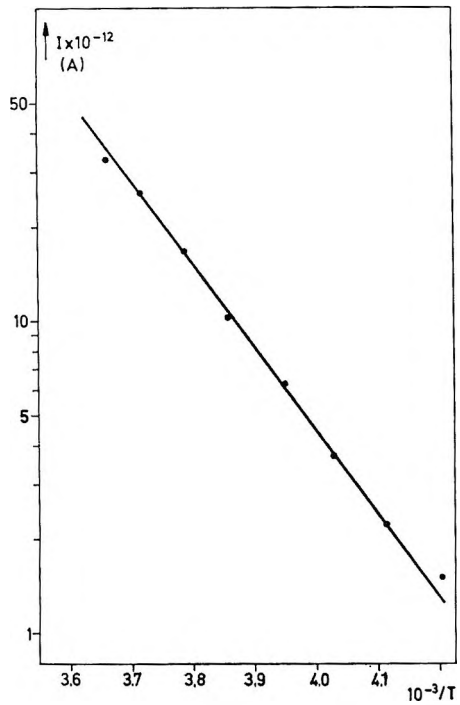

Figure 5. Logarithmic plot of the ascent of TSD peak 2 of Figure 5 *vs.* $1/T$.

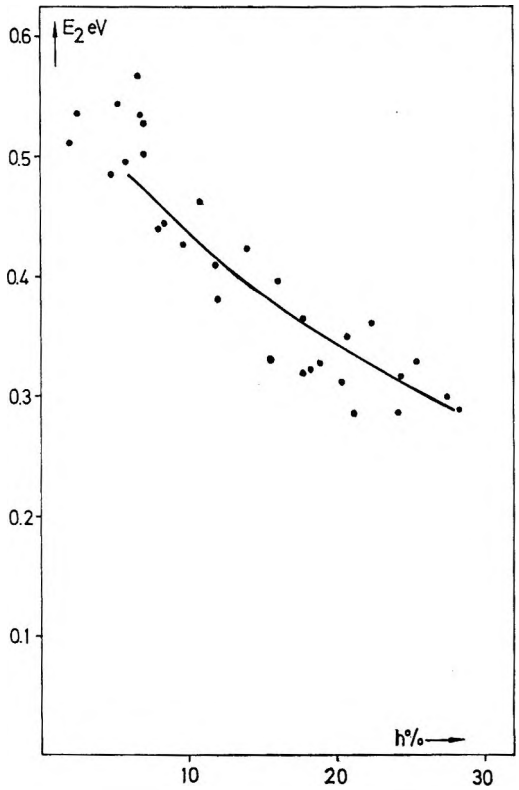

Figure 6. Dependence of the activation energy E_2 of TSD peak 2 on hydration degee h; 0, experimental data; solid line, theoretical curve calculated on the basis of dipole—dipole interaction.

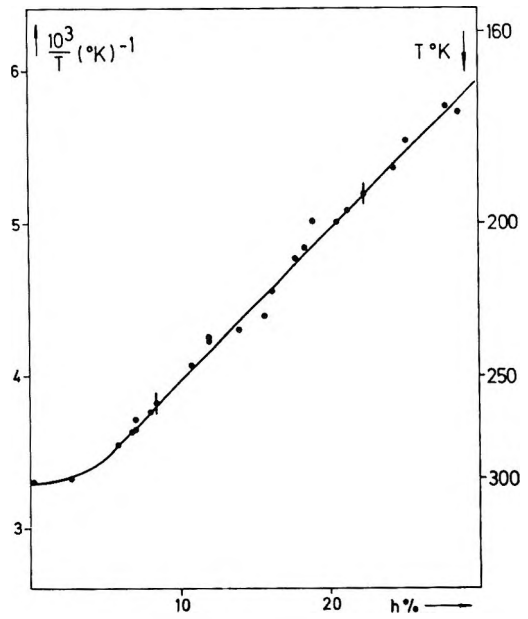

Figure 7. Dependence of the temperature of the peak maximum of TSD peak 2 on hydration degree h.

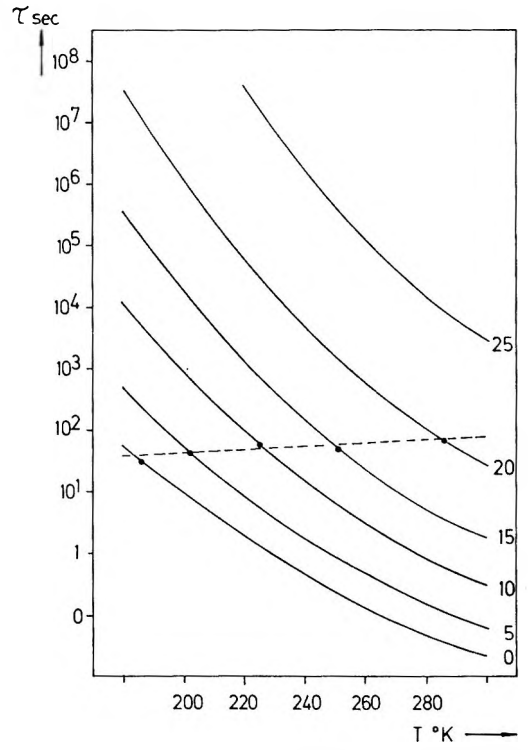

Figure 8. Dependence of relaxation times of TSD peak 2 on temperature for different hydration degrees.

gate peak 2 at $h > 10\%$. We believe that peak 3 is caused by electrode polarization, probably by the accumulation of hydrogen and oxygen by the polarization near the respective electrodes. Its magnitude therefore depends on the transfer resistance between sample and electrode. As this peak is not reflecting properties of the protein material, it is omitted from discussion.

Peak 2. Peak 2 (Figure 4) does not depend on electrode material and is therefore certainly not due to electrode polarization effects. It depends, however, strongly on the degree of hydration. The first inter-

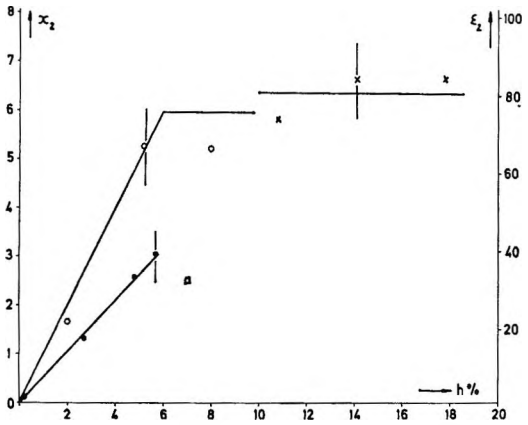

Figure 9. Dependence of susceptibility χ and dielectric constant ϵ of TSD peak 2 on hydration degree h for different samples.

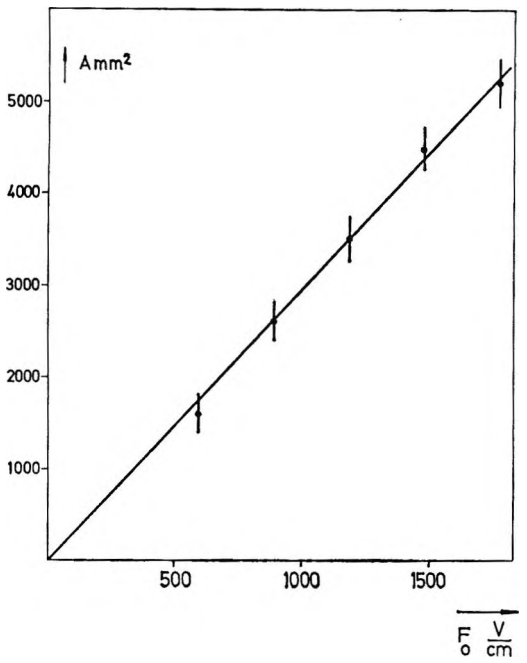

Figure 10. Dependence of peak area A of TSD peak 2 on polarizing field strength F_0.

esting quantity we can calculate from this peak is the activation energy. It can be obtained according to eq 3 from the rising part of the peak using a log I *vs.* $1/T$ plot. This plot yields a straight line as shown in Figure 5. The activation energy depends on the degree of hydration, as shown in Figure 6. We believe the scattering of the measuring points to be due to different sample conditions as similar variations have been obtained by Maricic, *et al.*,[5] too. There is also a second way for obtaining the activation energy. Different heating velocities result in a shift of the temperature position of the peak maximum. Because of experimental difficulties inherent in our apparatus this method is not as accurate as the previous one; the results, however, are in good agreement with the values obtained from eq 3.

The position of the peak, as measured by the maximum temperature T_M, depends on hydration. We obtain in a $1/T$ *vs.* h plot (Figure 7) a straight line. From the maximum temperature and other magnitudes appearing in eq 2 and 5 we can calculate the relaxation time of the polarization process. This is plotted in Figure 8 as a function of temperature with the degree of hydration as a parameter. It seems interesting that while the position of the maximum changes considerably with hydration, the relaxation time at the maximum temperature remains constant. This is also indicated in Figure 8.

From the area of the peak the susceptibility χ and the dielectric constant ϵ (eq 6 and 7) can be computed. In Figure 9 χ and ϵ are plotted for 4 different samples depending on the hydration. Here again the variation of the data is probably due to different sample conditions, but all samples show the same characteristic pattern: the susceptibility increases linearly up to $h = 5.8\%$ while it is constant for larger hydration values. The characteristic hydration $h = 5.8\%$ corresponds to the first BET layer of hemoglobin corresponding to 1 H_2O molecule per ionizable group. The most reasonable value of the susceptibility for high hydration is $\chi = 6.3$, which means $\epsilon = 80.2$ and $\mu_{eff} = 200$ D. For one sample we examined the dependence of the peak area on the applied polarizing electric field. Figure 10 shows proportionality between A and F_0 as required by eq 6. As space charge polarization and orientational polarization are the only two mechanisms which can give TSD peaks in these experiments, space charge effects being, however, not proportional to the field strength, this proportionality strongly suggests dipole orientation as the polarization mechanism of peak 2.

Peak 1. Peak 1 (Figure 11) is smaller than peak 2 by about two orders of magnitude. It can be observed only for hydration values lower than 7% because at higher values it is overlapped by peak 2 and cannot be separated. Therefore, only qualitative statements can be made. The peak does not depend on electrode effects. Its dependence on the degree of hydration is similar to peak 2. The activation energy, obtained in the same way as for peak 2 from eq 3, decreases with hydration (Figure 12). $1/T_M$ plotted *vs.* h again gives a straight line, similar to peak 2. From the area of the peak, again the susceptibility χ and the dielectric constant ϵ can be obtained. They are plotted *vs.* h in Figure 13. Similar to the behavior of peak 2, χ is linearly increasing with h until $h = 5.8\%$, whereas at higher degrees of hydration it remains constant and is $\chi = 0.47$, corresponding to $\mu_{eff} = 38$ D per molecule of hemoglobin. In contrast to peak 2, we obtain a finite value of $\chi = 0.22$ (corresponding to $\mu_{eff} = 26$ D) even with maximally dehydrated material at $h = 0$. The proportionality of the peak area A and the strength of the polarizing field again suggests an orientational polarization mechanism for this peak.

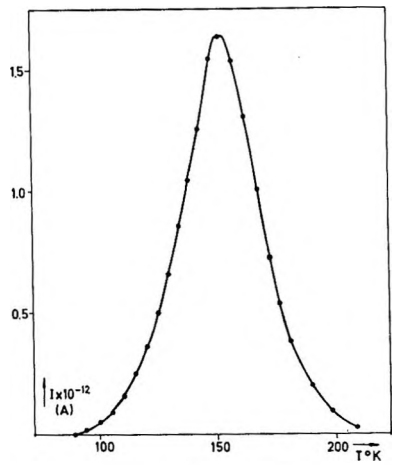

Figure 11. TSD peak 1; $h = 4.8\%$; $F_0 = 582$ V/cm, $q = 0.2$ deg/sec.

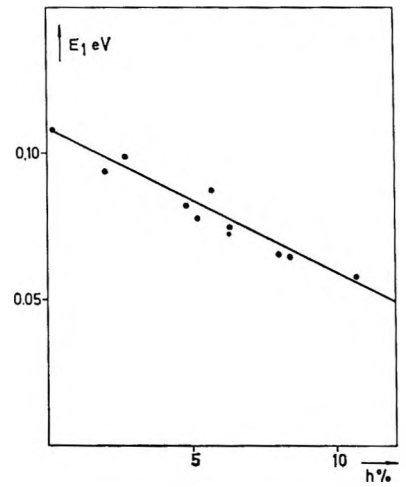

Figure 12. Dependence of the activation energy E_1 of TSD peak 1 on hydratation degree h.

Discussion

Peak 2. As already pointed out in the preceding section, peak 2 is due to an orientational polarization mechanism. The effective dipole moment calculated from the susceptibility data is 200 D and therefore we are forced to believe that it is the dipole moment of the hemoglobin molecule which is oriented. Since the susceptibility of a completely dehydrated sample is zero, the activation energy however finite, one has to conclude that the dipole moment of hemoglobin is zero at $h = 0$ and is only formed in the presence of water. It has been shown by Schlecht[8] that in the case of myoglobin in solution, the dipole moment is determined merely by the ionized groups. If that is assumed to be true also in our case, the following relation is valid

$$\chi \sim \frac{N_0 \mu_{eff}^2}{3kT} \qquad (11)$$

Since χ increases apparently linearly with increasing

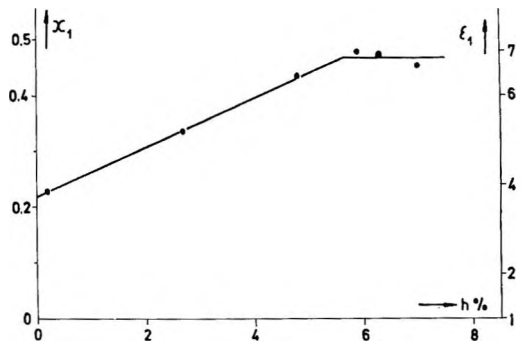

Figure 13. Dependence of susceptibility and dielectric constant ϵ of TSD peak 1 on hydratation degree h for different samples.

degree of hydration, one has to conclude that the pellet gets hydrated not uniformly, but rather that the water adsorbed by the pellet is used to hydrate and ionize completely a certain amount of hemoglobin molecules which, then, by orientation contribute to the susceptibility. The number of dipoles N_0 therefore increases proportionally to h. If the pellet were hydrated uniformly, μ_{eff} instead of N_0 would increase with increasing h and the susceptibility would not be a linear function of h. The susceptibility data indicate (Figure 9) that the maximum dipole moment of a hemoglobin molecule is formed when a degree of hydration is attained which corresponds to the first BET layer[9] of hemoglobin,[2] *i.e.*, when in the average one H_2O molecule has been bound per ionizable group. At hydrations higher than 5.8% the water is distributed uniformly in the pellet. As the activation energy depends on the degree of hydration (Figure 6) one would obtain a very broadened peak, if h were not uniform in the whole pellet. The dipole moment of hemoglobin as determined in aqueous solution by alternating field technique[10,11] is between 300 and 350 D, while measured in lyophilized state in the TSD experiments it was found to be about 200 D. This discrepancy might be due to (a) the fact that with the static TSD method one sees only the permanent dipole moment and not the fluctuational dipole moment which in alternating field measurements might give a contribution;[10] (b) the effect of dipole–dipole interaction between adjacent molecular dipoles (eq 9) in the tight package of the lyophilized state, thus apparently in our case diminishing the effective dipole moment. Since peak 2 is due to the orientation of molecular dipole moments, the activation energy corresponds to the potential barrier between adjacent favorable positions of the molecule. If there is dipole–dipole interaction in a substance and

(8) P. Schlecht, "Proceedings of the Symposium on Protides and Fluids," Brugge, Ed., Pergamon Press, Oxford, 1969.

(9) S. Brunauer, P. H. Emmet, and E. Teller, *J. Amer. Chem. Soc.*, **60**, 309 (1938).

(10) W. Goebel and H. Vogel, *Z. Naturforsch. B*, **19**, 292 (1964).

(11) P. Schlecht, A. Mayer, G. Hettner, and H. Vogel, *Biopolymers*, in press.

some short-range order, eq 10 holds, giving a relation between activation energy, mean distance between neighboring dipoles, and dipole moment. The distance $a(h)$ between the hemoglobin molecules in dependence on degree of hydration h has been determined previously.[2] Substituting this $a(h)$ together with μ_{eff} and T as obtained in these experiments gives the curve shown in Figure 6, which approximates the experimental data rather well. This analysis suggests that there is some short-range order in the lyophilized material and that the activation energy is due to dipole–dipole interaction between adjacent hemoglobin molecules.

Peak 1. As pointed out above, peak 1 must also be caused by an orientational polarization mechanism. Though no definitive statements can be made about its origin it seems probable that this peak is pertinent to the orientation of the polar amino acid residues of the hemoglobin molecule. The polar amino acid residues do have a dipole moment even if they are not ionized and they should have some freedom of orientation. Thus they can contribute to the susceptibility already at zero hydration. With increasing hydration these polar amino acid side chains become ionized and their dipole moment is increasing. In this case the susceptibility is made up of two contributions

$$\chi \sim \frac{N}{3kT}\left[(1-x)\mu_{eff}^{(0)2} + x\mu_{eff}^{(i)2}\right] \qquad (12)$$

a first one $(1 - x)\ \mu_{eff}^{(0)2}$ which is present already at $h = 0$ and which is decreasing with the fraction of ionized residues x, and a second one $x\mu_{eff}^{(i)2}$ characteristic for the hydrated material. N is the total number of ionizable residues.

Equation 12 together with the experimental data plotted in Figure 13 suggest that the number of ionized groups increases linearly with the degree of hydration up to $h = 5.8\%$ and that at this degree of hydration all available ionizable groups are dissociated and charged. This agrees very well with the conclusions drawn for peak 2.

In context with the discussion of our TSD measurements on lyophilized hemoglobin the work of Engelhardt and Riehl[12] must be mentioned; they observed a TSD peak in single crystal ice at 115°K with an activation energy of 0.19 eV. They attributed the origin of this peak to space charge polarization of trapped protons. (See Table I.)

Concluding Remarks

A comparison of the results obtained here by TSD measurements with those obtained by conventional dielectric measurements with alternating field[5,13,14] shows some discrepancies. The characteristics of the dependence of χ and ϵ on hydration are different for the two methods. Figure 14 shows the curve for ϵ *vs.* h as obtained by Brausse, *et al.*,[2] in alternating field measurements. Also the relaxation times τ differ

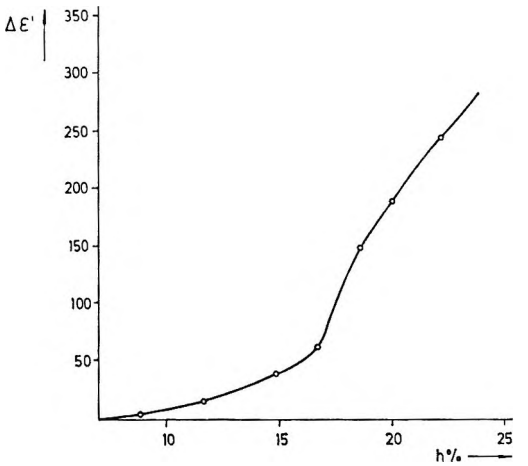

Figure 14. Dependence of the susceptibility on hydratation degree h as obtained from alternating field method (data from Brausse[2]).

considerably. The relaxation time τ obtained by TSD measurements is about 100 sec; τ obtained by alternating field[2] is 10^{-5} to 10^{-6} sec.

At least a great part of this discrepancy is due to difference in observation temperatures for TSD and ac measurements. Since the relaxation time is governed by a law (see ref 1 eq 6)

$$\tau \sim \frac{1}{T}\exp\left(\frac{E}{kT}\right) \qquad (13)$$

with typical values of $E = 0.33$ eV, peak temperature $T_M = 200$°K (*cf.* Figures 6 and 7 at $h = 20\%$), the TSD relaxation time would be reduced at room temperature by a factor of 2×10^3 as compared with the peak temperature T_M.

Thus if we want to contend that peak 2 of a TSD plot describes orientational polarization, we have to propose that ac results for dry samples need a reinterpretation. Unfortunately, in none of the above mentioned papers of alternating field measurements was the dependence of ϵ on the electric field strength measured. This was done, however, in the TSD measurements described above. Also, in the TSD measurements, the dependence of the activation energy of peak 2 on hydration is excellently fitted by eq 10 which describes a dipole–dipole interaction with a mean distance directly determined from the volume increase of the pellet on hydration (*cf.* Figure 6).

There are some arguments in the above mentioned papers that the susceptibility χ measured with the alternating field method is not due to an orientational process: χ has there not the temperature dependence $1/T$ as required for orientational polarization, but

(12) H. Engelhardt and N. Riehl, *Phys. kondens. Materie*, 5, 73 (1966).

(13) D. D. Eley and R. B. Leslie, *Advan. Chem. Phys.*, 7, 238 (1964).

(14) S. Takashima and H. P. Schwan, *J. Phys. Chem.*, 69, 4176 (1965).

Table I: Characteristic Data of the TSD Peaks of Lyophilized Hemoglobin

	Peak 1	Peak 2	Peak 3
Origin of the TSD peak	Orientation of polar amino acid residues	Orientation of the macromolecule	Electrode polarization
Temp position of the TSD peak $T_M(h)$	$1/T$ increases linearly with increasing h		
	$T_{M1}(0) = 164°K$	$T_{M2}(0) = 286°K$	T_{M3} *ca.* 300°K
	$T_{M1}(10\%) = 143°K$	$T_{M2}(25\%) = 164°K$	
Activation energy $E(h)$	E decreases with increasing h		
	$E_1(0) = 0.1$ eV	$E_2(0) = 0.5$ eV	
	$E_1(10\%) = 0.05$ eV	$E_2(25\%) = 0.3$ eV	
		Dipole–dipole interaction	
Relaxation time τ at $T_M(h)$	~100 sec	~50 sec	
Susceptibility $\chi(h)$	χ increases linearly with increasing h in the range $0 < h < 5.8\%$		
	χ is constant for $h > 5.8\%$		
	$\chi(0) = 0.22$	$\chi(0) = 0$	
	$\chi(>5.8\%) = 0.47$	$\chi(>5.8\%) = 6.3$	
Effective dipole moment $\mu(h)$	$\mu(0) = 26$ D	$\mu = 200$ D	
	$\mu(5.8\%) = 36$ D		
Dependence on electric field	Linear	Linear	
Dependence on electrode polarization	No	No	Yes

rather increases with increasing temperature,[2] similar to the electric conductivity. In the alternating field measurements the relaxation times τ of lyophilized hemoglobin are the same (10^{-5} to 10^{-6} sec[2]) as for hemoglobin in aqueous solutions.[9] However, one should rather expect longer relaxation times for pressed pellets of dry hemoglobin due to the sterically hindered rotation, compared with relatively free rotation in dilute hemoglobin solutions. In the TSD measurements, in fact, a relaxation time of about 100 sec was obtained.

From the data of Brausse, *et al.*,[2] a saturation behavior of $\epsilon(h)/h$ *vs.* h can be deduced which would suggest a polarization mechanism specific to the hydration water but not specific to the hemoglobin. The increase of χ at $h = 17\%$ observed with the conventional alternating field method (Figure 14) occurs obviously at the same hydration where the beginning of protonic conductivity was observed by Maricic, *et al.*[5]

These arguments strongly suggest that the susceptibility χ measured with the alternating field method is not due to orientational polarization, but rather due to a polarization mechanism based upon electric conductivity, for example Maxwell–Wagner effect. A more careful analysis of the results obtained with the alternating field method and new experimental data with this method will be given in a separate paper (in preparation).[7]

Acknowledgment. We are greatly indebted to Professor Riehl for his constant interest in this work and for numerous stimulating discussions. This work was supported by a grant from Stiftung Volkswagenwerk.

The Frequency Extrapolation of Conductance Data for Aqueous Salt Solutions

by Thomas B. Hoover[1a]

Institute for Materials Research, National Bureau of Standards, Washington, D. C. 20234 *(Received January 5, 1970)*

Polarization phenomena in conductivity measurements were investigated in order to reduce systematic error in the standardization of solutions intended for the calibration of conductivity cells and salinometers. Data for demal potassium chloride solutions and for Standard Sea Water were obtained with two cells having constants of 37 and 86, respectively, both with bright platinum and with palladium black-coated electrodes. Four empirical and three theoretical functions of resistance *vs.* frequency were fitted to the data. Correctness of the extrapolation was judged by the agreement of the limiting resistance obtained with bright electrodes with that obtained with coated electrodes. All of the empirical formulas predicted limiting values for the bright electrodes that were lower by 0.02 to 0.15%. Equations based on the model of Grahame[1b] for the faradaic process, as well as a simplified model, agreed within 0.01% while a third theoretical equation was intermediate in accuracy.

Introduction

Systematic sources of error in conductivity measurements are being sought as part of a program for standardizing and certifying solutions for use in the calibration of conductivity cells and salinometers. One such source of error is the frequency-dependent polarization impedance that inevitably accompanies the measurement of the ac conductance of solutions in conventional cells.

The present study deals with various mathematical means for extrapolating resistance *vs.* frequency data in order to remove polarization effects. Various experimental techniques for accomplishing the same objective were ruled out for reasons given below. Seven empirical and theoretical equations that have been used or proposed for the reduction of conductivity data are critically compared, using data for aqueous salt solutions in cells with bright platinum electrodes and with electrodes coated with palladium black. The comparable situation for fused salts has been reviewed recently[2] but there has been no such analysis of aqueous systems. Robinson and Stokes[3] discuss polarization models qualitatively and emphasize that the functional form of the resistance–frequency curve must be determined whenever polarization is not negligible.

Test Equations

The equations to be compared and their historical or theoretical bases follow. R represents the observed resistance of a parallel R–C bridge arm having the same impedance as the conductivity cell, R_1 is the high-frequency limit of R (assumed to correspond to the electrolytic resistance of the cell), f is the frequency in Hz, and ω is the angular frequency ($2\pi f$).

Two-Parameter Equations

$$R = R_1 + af^{-1/2} \qquad \text{(A)}$$

Jones and Christian,[4] in a classical study of polarization in conductivity measurements, recommended eq A as a practical expedient although it was recognized that this function led to R_1 values somewhat smaller than the true electrolytic resistance.

$$R = R_1 + af^{-1} \qquad \text{(B)}$$

Several workers[3,5] have found empirically that eq B better represented their data than did eq A.

Three-Parameter Equations

$$R = R_1 + af^{-1/2} + bf^{-1} \qquad \text{(C)}$$

Nichol and Fuoss[6] found that the simpler eq A and B were inadequate to represent their data for dipping electrode designs and used this quadratic function of $f^{-1/2}$

$$R = R_1 + af^b \qquad \text{(D)}$$

Because of uncertainty as to the best exponent for f in eq A and B, eq D was proposed.[7] Although this equation can provide an excellent fit to experimental data, it will be seen below that it can introduce a large error in extrapolation. Accordingly, the use of eq D is not recommended.

Theoretical Equations. These are based on the model[1b] for the conductivity cell shown in Figure 1, where C_0 is the geometric capacity of the cell and C_1 is the

(1) (a) Southeast Water Laboratory, Athens, Ga. 30601; (b) D. C. Grahame, *J. Electrochem. Soc.*, **99**, 370C (1952).

(2) (a) G. D. Robbins, *J. Electrochem. Soc.*, **116**, 813 (1969); (b) G. J. Hills and S. Djordjevic, *Electrochim. Acta*, **13**, 1721 (1968); (c) G. D. Robbins and J. Braunstein in "Molten Salts: Characterization and Analysis," G. Mamantov, Ed., Marcel Dekker, New York, N. Y., 1969, pp 445–477.

(3) R. A. Robinson and R. H. Stokes, "Electrolyte Solutions," 2nd ed, Butterworth Publications Ltd., London, 1959, pp 93–95.

(4) G. Jones and S. M. Christian, *J. Amer. Chem. Soc.*, **57**, 272 (1935).

(5) J. C. Nicol and R. M. Fuoss, *ibid.*, **77**, 198 (1955).

(6) J. C. Nichol and R. M. Fuoss, *J. Phys. Chem.*, **58**, 696 (1954).

(7) T. B. Hoover, *ibid.*, **68**, 876 (1964).

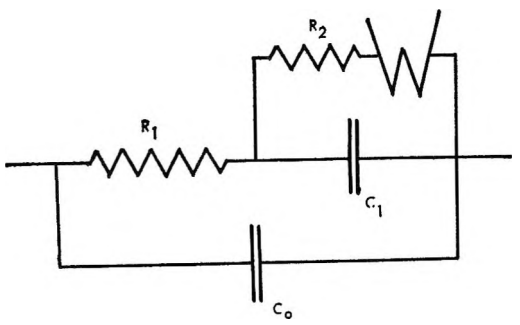

Figure 1. Equivalent circuit for conductance cell, according to ref 8.

double-layer capacity at the electrode surface. R_2 is the frequency-independent part of the faradaic impedance and W represents the Warburg impedance. The complex impedance of W is assumed to be represented by

$$Z_W = k(1 - i)\omega^{-1/2} \quad (1)$$

R_2 arises from the rate of oxidation or reduction at the electrode and W from the diffusion of the electroactive species. Feates, Ives, and Pryor[8] solved the bridge balance conditions for this model with the restriction that W is negligible and obtained the equation

$$R = R_1 + \frac{R_2}{1 + a\omega^2} \quad (E)$$

where

$$a = R_1R_2^2C_1^2/(R_1 + R_2) \quad (2)$$

These authors used an empirical extrapolation formula equivalent to eq B for reduction of their data.

The alternate solution for the model of Figure 1 for the simplifying condition that $R_2 = 0$ was given by Hills and Djordjevic.[2b] Their corrected eq 4 in the notation of the present report is test eq F.

$$R_s = R_1 + \frac{k}{\omega^{1/2}(1 + 2kC_1\omega^{1/2} + 2k^2C_1^2\omega)} \quad (F)$$

Note that R_s is the resistance of an equivalent *series* R–C bridge arm. The solution in terms of the parallel combination is much less tractable.

The bridge balance conditions for the model of Figure 1, including both the R_2 and Warburg impedance, are derived in Appendix A. These lead to the result

$$R = R_1 + [R_2(R_1 + R_2) + k(R_1 + 2R_2)\omega^{-1/2} + 2k^2\omega^{-1}]/[R_1R_2^2C_1^2\omega^2 + 2kR_1R_1C_1^2\omega^{3/2} + 2k^2R_1C_1^2\omega + 2kR_1C_1\omega^{1/2} + R_1 + R_2 + k\omega^{-1/2}] \quad (3)$$

In order to fit eq 3 to experimental data it has been expanded in powers of $\omega^{-1/2}$ with the result

$$R = R_1 + a\omega^{-2} + b\omega^{-5/2} + c\omega^{-7/2} + \ldots \quad (G)$$

where the coefficients have the theoretical values

$$a = (R_1 + R_2)/R_1R_2C_1^2 \quad (4)$$

$$b = -k/(R_2C_1)^2 \quad (5)$$

$$c = [2k^3R_1C_1 - 2kR_2(R_1 + R_2)]/R_1R_2^4C_1^3 \quad (6)$$

Because of the omission of higher negative powers of ω, eq G is expected to be asymptotically correct at higher frequencies.

Chang and Jaffé[9] examined the faradaic process in detail but did not obtain an explicit function for R in terms of f. Because of the difficulty of applying their results to conductivity data, the Chang–Jaffé model is not considered further here.

The essential requirement of an extrapolation formula is that the high-frequency limit R_1 correspond closely to the true resistance of the electrolyte in the cell. This condition was judged by the agreement between the value of R_1 obtained for the same cell and solution whether the electrodes were bright platinum or coated with palladium black. The coating should change the double-layer parameters greatly without affecting R_1. Since the palladium black has a finite thickness, any effect on the cell constant was reduced by using capillary cells with relatively large constants (37 and 86). The extrapolation formula should also provide a close fit to the experimental measurements over an appreciable range of frequencies. It is also desirable that the theoretically based equations yield plausible values for the double-layer parameters.

Although the use of platinum or palladium black is a familiar and effective means of reducing polarization effects on conductivity measurements, bare metallic electrodes have some advantages for checking standard solutions. We prefer to introduce the sample to a clean, dry cell, when only a limited specimen is available, since there may not be enough to rinse the cell to constant composition as would be required with the highly adsorptive blacked electrodes. Potentiometric[10] and inductive[11] cells have been used to avoid polarization effects completely but these require specialized measuring instruments and are not suitable to our ultimate objective of redetermining the Jones and Bradshaw[12] standards on an absolute basis.

Experimental Section

Apparatus. Two cells of the conventional Jones design were used. These had circular platinum elec-

(8) F. S. Feates, D. J. G. Ives, and J. H. Pryor, *J. Electrochem. Soc.*, **103**, 580 (1956).

(9) H. C. Chang and G. Jaffé, *J. Chem. Phys.*, **20**, 1071 (1952).

(10) F. P. Anderson, H. C. Brookes, M. C. B. Hotz, and A. H. Spong, *J. Sci. Instrum.*, **2**, 499 (1969).

(11) S. R. Gupta and G. J. Hills, *ibid.*, **33**, 313 (1956).

(12) G. Jones and B. C. Bradshaw, *J. Amer. Chem. Soc.*, **55**, 1780 (1933).

trodes 7.0 cm^2 in area in enlarged bulbs connected by a sufficient length of 4-mm i.d. tubing to give constants of 37.050 and 86.096. Two bare copper leads were soldered to each electrode support close to the outside of the cell for use with the 4-terminal method of measurement. The uncompensated lead resistance was calculated from the materials of construction (copper, tungsten, and platinum) to be 0.002 ohm.

A Jones–Dike bridge was modified for use in the 4-terminal mode by providing auxiliary switches for reversing leads and connecting the active potential lead directly to the detector. In this configuration the entire slide-wire circuit of the bridge was in the "Standard" arm and 26.181 ohms was determined to be the correction to be added to the dial readings to compensate for this modification.

The parallel capacitance required for balance was provided by an external calibrated 1400-pF variable air capacitor, supplemented as needed by mica capacitors up to 0.06 μF. The thermostat was a self-lagging oil bath equipped with proportional, rate, and reset controls. Temperatures were measured with two calibrated platinum resistance thermometers of different time constants (6 and 11 sec). In 28 measurements the maximum difference between the readings of the two thermometers was 3.6×10^{-3} °K, while the standard deviation of the difference was 1.6×10^{-3} °K and the mean difference was less than $^1/_5$ the standard deviation.

Solutions and Filling of Cells. Two solutions were used: demal potassium chloride[12] sealed in 100-cm^3 ampoules and Standard Sea Water, Lot P50, which is supplied in double-necked 250-cm^3 ampoules.[13] Our experience has confirmed the observation that a major source of random error is in the filling of cells.[14] We have obtained standard deviations less than 50 ppm for the measurements of conductivities of sets of four or five ampoules of Standard Sea Water and attribute the high degree of precision largely to the ability to drain the sample directly from the ampoule into the cell. The potassium chloride solution was prepared from specially purified and dried salt and contained 71.1435 g of KCl/kg of solution (corrected to vacuum weights). Borosilicate ampoules were filled in a 5° cold room, having first been flushed with nitrogen presaturated with the same solution. The filled ampoules were immersed in an ice bath above the solution level while the necks were sealed off.

Cells with bright electrodes were rinsed thoroughly with distilled water, followed by three portions of spectrographic grade acetone, dried with nitrogen and filled from freshly opened ampoules. At the end of this series of measurements, each electrode was palladized for 4.5 min at 50 mA, using a solution prepared by electrolytically dissolving 0.1 g of palladium in 20 cm^3 of constant-boiling hydrochloric acid and diluting to 100 cm^3. Palladium black is advantageous in that it can be stripped completely from the electrode. The coated electrodes were rinsed thoroughly and electrolyzed in dilute sulfuric acid for 1.5 hr with frequent reversals of polarity. The palladized electrodes were never allowed to become dry but were kept wet with water or aqueous electrolyte. Before filling, the cells were rinsed several times with a solution of the approximate composition as that to be measured, and finally with a small portion from the freshly opened ampoule. After the resistance measurement the cell was emptied and immediately refilled from another ampoule of the same solution and the measurements were repeated. The resistances for the second series were 0.01 to 0.07% lower than the first and are the ones reported here.

Fitting Equations to Data.[15] After applying bridge calibration corrections and adjusting the data to exactly 25° (on the International Practical Temperature Scale of 1948), the seven equations were fitted by computer programs. The linear eq A and B were fitted by conventional least-square methods. The polynomials of a degree higher than first (eq C and G) were fitted by orthogonal polynomials.[16] The nonlinear forms (eq D, E, and F) were fitted by an iteration technique that varied one parameter until the sum of the squares of deviations was minimized. For each value of the independently adjusted parameter the other two parameters were set by a least-squares fit of a linearized form of the equation.[17] The step size for the iteration was varied in a way that guaranteed that the sum of squares of deviations passed through the minimum at least once and convergence was accepted when successive iterations reduced the sum of squares less than 0.01%.

Results and Discussion

The results are summarized in Table I, where the calculated values of R_1 according to the seven equations are compared for two solutions and two cells, each with bright and with palladized electrodes. Also included for comparison are the data of Jones and Christian[4] for 0.1 *M* silver nitrate with silver electrodes, and the data of Jaffé and Rider[18] for 10^{-3} *M* potassium

(13) Available from I. A. P. O. Standard Sea-Water Service, Charlottenlund Slot, Charlottenlund, Denmark.

(14) R. W. Bremner, T. G. Thompson, and C. L. Utterback, *J. Amer. Chem. Soc.*, **61**, 1219 (1939).

(15) The original data, in the form of a table of frequency and observed equivalent parallel resistance and capacitance, have been deposited as Document No. 00925 with the National Auxiliary Publications Service, c/o CCM Information Corp., 909 3rd Ave., New York, N. Y. 10022.

(16) J. W. Bright and G. S. Dawkins, *Ind. Eng. Chem. Fundam.*, **4**, 93 (1965).

(17) For example, in eq D, R_1 was adjusted by trial to give a best fit when a and b were determined by least-squares fit of $\log (R - R_1) = \log a + b \log f$. In eq F, the product kC_1 was adjusted and R_1 and k were fitted by linear least squares.

(18) G. Jaffé and J. A. Rider, *J. Chem. Phys.*, **20**, 1077 (1952).

Table I: Limiting Resistance R_l and Standard Deviation of Fit for Seven Test Equations Applied to Experimental Data

	Cell constant 37				Cell constant 86				0.1 *M* $AgNO_3$, Ag electrodes[a]	10^{-3} *M* KCl, Ni electrodes[b]
	KCl		SSW		KCl		SSW			
	Bright	Coated	Bright	Coated	Bright	Coated	Bright	Coated		
Freq range (kHz)	0.25–15.0	0.25–10.0	0.25–15.0	0.25–10.0	0.25–10.0	0.25–8.0	0.25–10.0	0.25–2.0	0.5–4.0	0.018–18.0
Eq A										
R_l	332.422	332.875	697.539	698.255	773.116	773.411	1621.37	1621.98	220.07	(52)
s.d.[c]	0.046	0.007	0.161	0.004	0.029	0.006	0.13	0.005	0.31	145
Eq B										
R_l	332.902	332.885	698.172	698.263	773.474	773.423	1621.90	1621.99	227.34	198
s.d.	0.141	0.009	0.073	0.003	0.10	0.007	0.10	0.005	0.65	48
Eq C										
R_l	332.480	332.859	698.006	698.260	773.102	773.408	1621.701	1621.99	222.355	281
s.d.	0.038	0.005	0.049	0.003	0.026	0.005	0.075	0.004	0.025	17
Eq D										
R_l	332.597	262.640	698.134	698.258	773.143	773.370	1621.871	1621.99	223.531	241.5
s.d.	0.039	0.005	0.058	0.003	0.027	0.005	0.091	0.004	0.015	8.3
Eq E										
R_l	332.895	332.874	698.277	698.265	773.457	773.421	1621.921	1621.99	225.6	253
s.d.	0.067	0.005	0.058	0.004	0.046	0.006	0.048	0.005	1.4	27
Eq F										
R_l	332.644	332.875	697.922	698.264	773.151	773.421	1621.79	1622.00	224.930	242.9
s.d.	0.036	0.006	0.020	0.003	0.038	0.001	0.06	0.002	0.013	1.1
Eq G										
R_l	332.872	332.883	698.227	698.264	773.434	773.421	1621.931	1621.99	227.30	253
s.d.	0.047	0.008	0.015	0.004	0.037	0.007	0.021	0.007	0.12	10

[a] Reference 4. [b] Reference 18. [c] The square root of the mean squared difference between experimental and calculated resistance is designated by s.d. (ohms).

chloride with nickel electrodes. The latter results are of interest because of the very wide range of frequencies that was investigated.

With respect to the requirement that the equations yield the same value for R_l for either bright or coated electrodes, both theoretical eq E and G are very satisfactory. The relative differences for all eight comparisons are less than 70 ppm, That these values of R_l represent the true resistance of the electrolyte is supported not only by the prediction from the theoretical models, but also by the fact that nearly all the extrapolation formulas yield the same results for the palladium-blacked electrodes. A notable exception is the exponential equation *D* in the case for the cell (constant 37) with demal potassium chloride. Here the best fit yielded a large exponent ($B = -1.47$) and a value of R_l some 70 ohms too low.

The simple, 2-parameter equation in reciprocal frequency (eq B) provides very satisfactory agreement between the measurements obtained with bright and coated electrodes but this agreement appears to be the result of a cancellation of errors. The comparison of several of these functions in Figure 2 shows that eq B actually reproduces the experimental data quite poorly. Over a limited range of frequencies (approximately 1 to 10 kHz) a good fit can be obtained with equation *B* but it then extrapolates to too low a value for R_l.

The equations that provide the best extrapolation do not necessarily fit the data most closely. In Figure 3, deviations from equation E are plotted as a function of $f^{-1/2}$. This scale expands the high-frequency region where the extrapolation behavior is crucial. It appears that none of the functions fits the data within experimental precision although eq C gives the smallest standard deviation of fit (Table I). Equation D yields essentially the same result as eq C. It is well known that the close fit of an empirical equation to a set of data does not provide a sound basis for extrapolating beyond the range of the measurements and this caution applies to the four empirical forms considered in the present report.

Equation F has not been mentioned in the foregoing discussion because it was not tested on a strictly comparable basis. The measurements were made with a parallel *R–C* bridge arm and had to be recalculated to the equivalent series values by eq 7 and 8

$$R_s = R_p/(1 + \omega^2 R_p^2 C_p^2) \quad (7)$$

$$C_s = C_p[1 + 1/(\omega^2 R_p^2 C_p^2)] \quad (8)$$

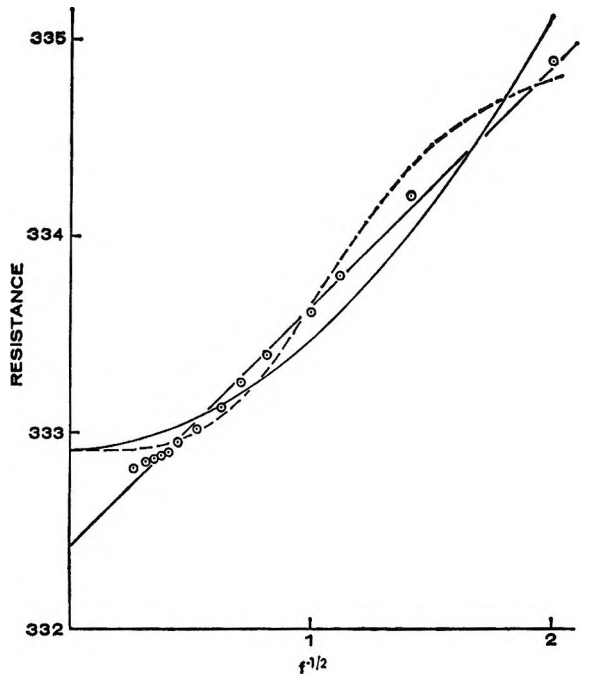

Figure 2. Comparison of test equations. Data points are for demal KCl, bright platinum electrodes, cell constant 37. Key: eq A, straight line; B, solid curve; E, broken curve.

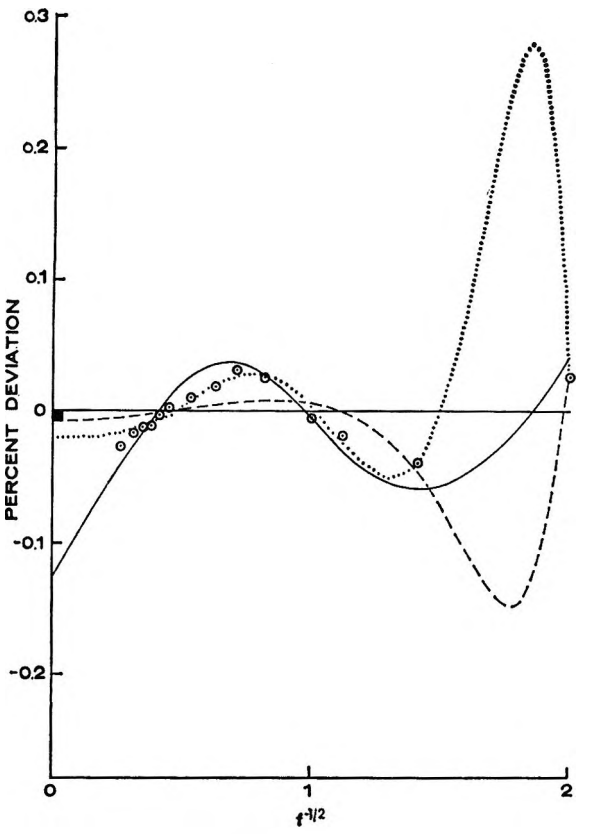

Figure 3. Percentage deviations from test eq E. Data points are for demal KCl, bright platinum electrodes, cell constant 37. The solid rectangle at the origin of the coordinates represents the probable limiting resistance for palladized electrodes. Key: eq C, solid; G, broken; G plus next higher term, dotted.

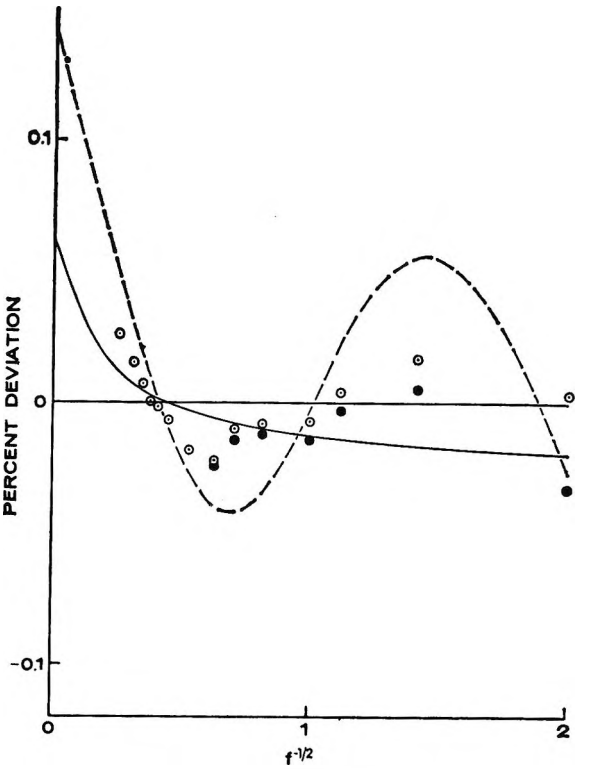

Figure 4. Percentage deviations from test eq A. Data points are for demal KCl, bright platinum electrodes, cell constant 37. Key: R_p, open circles; R_s, filled circles; eq E, broken line; F, solid curve.

in order to apply eq F. Capacitances were measured with much less accuracy than resistances and the application of eq 7 and 8 introduced an undetermined error. Although equation F is a fit of R_s *vs.* ω, points were omitted when the corresponding value of the series capacitance appeared clearly discordant. Equation F reproduces the data points more closely than equation E but extrapolates to R_1 values that seem uniformly nearly 0.2 ohm too low. These functions (E and F) are compared in Figure 4. It should be noted that eq F provides the best fit to the data of Jaffé and Rider.[18]

It is apparent from Figure 3 that eq G behaves very poorly at the lower frequencies, probably due to the neglect of higher terms in the polynomial expansion of eq 3. The next higher term is $d\omega,^{-4}$ where

$$d = -\left[\frac{4k^4}{R_2^5 C_1^{::}} - 2k^2\frac{(3R_1 + R_2)}{R_1 R_2^4 C_1^3} + \frac{(R_1 + R_2)^2}{R_1^2 R_2^3 C_1^4}\right] \quad (9)$$

Inclusion of the term in ω^{-4} improves the fit appreciably reducing the standard deviation from 0.047 to 0.015 ohm. However, the behavior between the two lowest experimental frequencies is even more extreme, as shown in Figure 3.

The fundamental parameters of the faradaic impedance and double layer for the theoretical models

Table II: Fundamental Parameters of Conductance Cell Derived from Frequency Dependence of Resistance

	Eq E	Eq F	Eq G	G plus higher term
Demal KCl, Bright Platinum Electrodes, Cell Constant 37				
R_1, ohms	332.895	332.644	332.872	332.826
R_2, ohms	2.107	...	8.44	4.17
C_1, μF	102.8	15.58	35.3	34.5
k, ohm-sec$^{-1/2}$	...	96.3	476	324
0.1 M $AgNO_3$, Ag Electrodes (ref 4)				
	Eq E	Eq F	Ref 18	Eq G
R_1, ohms	225.6	224.93	(223.2)	227.3
R_2, ohms	19.1	...	...	40.0
C_1, μF	5.49	1.96	1	3.73
k, ohm-sec$^{-1/2}$	...	1302.4	1230	3434

are compared in Table II. Evaluation of these parameters from the empirically determined constants of eq E and F is straightforward. The corresponding evaluation for the Grahame model of Figure 1 from the coefficients of eq G is outlined in Appendix B. The parameters are at least plausible in magnitude although it is questionable how much physical significance should be attached to them. The coefficients for one example are shown in Table III. Their standard deviations

Table III: Polynomial Coefficients and Their Standard Deviations. Test Equation G Fitted to Data for Demal KCl, Bright Platinum Electrodes, Cell Constant 37

	4-Term eq	5-Term eq
Constant	332.872 ± 0.019	332.828 ± 0.008
2nd	$(97.6 \pm 7.8) \times 10^6$	$(20.4 \pm 1.2) \times 10^7$
3rd	$-(58.1 \pm 5.7) \times 10^8$	$-(18.2 \pm 1.3) \times 10^9$
4th	$(33.6 \pm 4.2) \times 10^{11}$	$(41.9 \pm 4.1) \times 10^{12}$
5th	...	$-(10.2 \pm 1.1) \times 10^{14}$

are sufficiently large to suggest considerable uncertainty in any derived parameters. It is interesting that the inclusion of an additional term to eq G greatly changes the polynomial coefficients but appreciably affects only the R_2 parameter. For comparison, the values reported by Hills and Djordjevic[2b] for the data of Jones and Christian[4] are included in Table II. The procedure used to solve the equation is not clear from the authors' description but their value for C_1 corresponds closely to the result of a graphical extrapolation of the experimental C_s. The simultaneous determination of the three parameters of eq F yields a value for C_1 more in conformity with the other equations.

Recommendations

Although the frequency dependence of the measured resistance should be determined when polarization is not negligible, this step is not sufficient to ensure accuracy. The Grahame model of Figure 1 and its simplifications predict that the limiting resistance is approached horizontally. Consequently, any of the simple extrapolation formulas that have been proposed will give low results. In many cases, an experimental value in the range 5 to 10 kHz is more accurate than an empirical extrapolation. Equation E can be solved by a relatively simple program[19] and is sufficiently accurate for extrapolation purposes. Since the theoretical model of polarization that has been used is a general one it may be inferred that the eq E, F, and G based upon it may be generally valid. This inference has been tested experimentally only for aqueous and molten salt electrolytes.

Appendix A

Bridge Balance Conditions for the Grahame[1b] Model of the Conductance Cell. Let a and b represent the real and imaginary parts of the complex faradaic impedance, where

$$a = R_2 + k\omega^{-1/2} \tag{A1}$$

$$b = k\omega^{-1/2} \tag{A2}$$

By the usual procedures, the real and imaginary parts of the complex admittance of the circuit of Figure 1 yield the equations

$$1/R_p = \frac{R_1 + a + 2\omega bR_1C_1 + \omega^2R_1C_1^2(a^2 + b^2)}{[R_1(1 + \omega bC_1) + a]^2 + [\omega aR_1C_1 - b]^2} = \frac{[A]}{[D]} \tag{A3}$$

$$C_p - C_0 = \frac{C_1(a^2 + b^2) + b\omega^{-1}}{[R_1(1 + \omega bC_1) + a]^2 + [\omega aR_1C_1 - b]^2} = \frac{[B]}{[D]} \tag{A4}$$

where the numerators and denominator are designated by [A], [B], and [D].

Elimination of [D] between eq A3 and A4 gives

$$[B] = [A]R_p(C_p - C_0) \tag{A5}$$

From A3

$$[D] - R_1[A] = a^2 + b^2 + aR_1 \tag{A6}$$

Since $[D] = R_p[A]$

$$[A] = \frac{a^2 + b^2 + aR_1}{R_p - R_1} \tag{A7}$$

Substituting A7 in A5

$$R_p(C_p - C_0) = \frac{(R_p - R_1)[B]}{a^2 + b^2 + aR_1} \tag{A8}$$

The value of [A] from eq A3 is substituted in eq A5, split in two parts, one of which is multiplied by $R_p(C_p -$

(19) A copy of the program, written in BASIC language, may be obtained from the author.

C_0) and the other by the right side of eq A8. After rearrangement

$$[B]\left[1 - \frac{(R_p - R_1)(R_1 + a + 2\omega bR_1C_1)}{a^2 + b^2 + aR_1}\right] = \omega^2R_1R_pC_1^2(C_p - C_0)(a^2 + b^2) \quad \text{(A9)}$$

For $k = 0$ ($a = R_2$, $b = 0$), eq A9 reduces to balance condition IV of ref 8.

From eq A7

$$R_p - R_1 = \frac{a^2 + b^2 + aR_1}{R_1 + a + 2\omega bR_1C_1 + \omega^2R_1C_1^2(a^2 + b^2)} \quad \text{(A10)}$$

Substitution for a and b and polynomial expansion in powers of $\omega^{-1/2}$ yields test eq G.

Feates, Ives, and Pryor[8] eliminate ω to obtain a second balance condition but that approach is neither practicable nor useful in the present case. Instead, we use eq A5 in the form

$$R_p(C_p - C_0) = \frac{[B]}{[A]}$$

Substitution for [A] and [B] and polynomial expansion in powers of $\omega^{-1/2}$ leads to the asymptotic expression

$$\omega^2R_p(C_p - C_0) = \frac{1}{R_1C_1} - \frac{k}{R_1R_2^2C_1^2}\omega^{-1/2} + \frac{2k^2R_1C_1 - R_1R_2 - R_2^2}{R_1^2R_2^3C_1^3}\omega^{-2} - \frac{2k^3R_1C_1 + 2kR_1R_2 - kR_2^2}{R_1^2R_2^4C_1^3}\omega^{-5/2} + \frac{8k^2}{R_1R_2^4C_1^3}\omega^{-3} + \ldots \quad \text{(A11)}$$

Appendix B

Evaluation of Fundamental Conductance Cell Parameters from the Coefficients of Equation G. Since the coefficients have the theoretical values given in eq 4, 5, and 6, the following relations may be derived

$$C_1^2 = (R_1 + R_2)/aR_1R_2 \quad \text{(B1)}$$

$$R_2^2 = (2abC_1 - c)/2b^3C_1^4 \quad \text{(B2)}$$

$$R_2 = R_1/(aR_1C_1^2 - 1) \quad \text{(B3)}$$

$$-k = bR_2^2C_1^2 \quad \text{(B4)}$$

R_1 is available as the constant term and an estimate of R_2 (*e.g.*, from eq E) gives an initial estimate of C_1 by eq B1. Successive approximations for C_1 are made until the same value of R_2 is obtained from eq B2 and eq B3. From these final values, k is calculated from eq B4.

Nuclear Magnetic Resonance Measurements of Proton Exchange in Aqueous Thiourea

by R. L. Vold and Adolfo Correa

Department of Chemistry, University of California, La Jolla, California *(Received December 17, 1969)*

The semiclassical line shape expression of Hahn, Maxwell, and McConnell for chemical exchange between two unequally populated sites is extended to the case where spin $^1/_2$ nuclei in one site are coupled to a relaxing nucleus of spin I. The line shape expression is written in closed algebraic form for spin $I = 1$ and $I = {}^3/_2$. Experimental results are reported for acid-catalyzed protolysis of aqueous thiourea. Possible exchange reactions are discussed. Water line widths are used to derive rate parameters. The rate law for acid-catalyzed protolysis of aqueous thiourea is found to be $R = (1.0 \pm 0.2) \times 10^5$ [thiourea] $[H_3{}^+O]^{0.98\pm0.02}$ M sec^{-1}. Protolysis of thiourea N–H protons is concluded to be catalyzed about 60 times more efficiently than N-methyl acetamide N–H protons.

Introduction

Nmr line shape methods have been widely used to measure proton transfer reaction rates in aqueous solutions of amines,[1] amides,[2] and amino acids.[3] In most of these studies, less than the maximum possible information was obtained from both the water resonance and the N–H resonance, due to the complication of line broadening by scalar coupling to relaxing nitrogen nuclei.

In this paper the semiclassical line shape expression of Hahn, Maxwell, and McConnell[4] for chemical exchange between two unequally populated sites is extended to the case where spin $^1/_2$ nuclei in one site are coupled to a relaxing nucleus of spin I. The line shape expression is written in closed algebraic form for spin $I = 1$ and $I = {}^3/_2$.

Experimental results are reported for aqueous thiourea. A large number of proton transfer reactions are *a priori* possible for this molecule. Also, it is a rather effective protein denaturing agent, by mechanisms which may involve alterations of water structure by thiourea.[5] The possibility exists that effects of water structure may be revealed in detailed studies of proton transfer kinetics of urea and substituted ureas. Thiourea is particularly suitable for initial investigations because the thiourea–water chemical shift is large, which allows reaction rates to be measured over a wide range of concentrations.

Theory

Consider the case of two sites, A and B, distinguished by their chemical shifts ω_a and ω_b, with equilibrium populations of spin $^1/_2$ nuclei p_a and p_b, respectively. Assume that nuclei in site B are spin coupled ($\mathcal{A}$ radians/sec) to a nucleus of spin I, resulting in $(2I + 1)$ subsites of B, with chemical shifts $\omega_b + I\mathcal{A}$, $\omega_b + (I - 1)\mathcal{A}, \ldots \omega_b - I\mathcal{A}$. Assume also that spin $^1/_2$ nuclei transfer from A to B at rate k_{ab} and from B to A at rate k_{ba}. Then k_{ab} and k_{ba} are related by the principle of detailed balancing

$$p_a k_{ab} = p_b k_{ba} \tag{1}$$

The rate of transfer of magnetization from A to any particular subsite of B is $k_{ab}/(2I + 1)$ and the rate of transfer from any subsite of B into A is k_{ba}. Assume that the spin I nucleus relaxes at rate R_1 (due to the quadrupole mechanism), and that spin $^1/_2$ nuclei can be scrambled with equal probability among the $(2I + 1)$ subsites of B alone by a reaction with specific rate k_s. It is shown in the Appendix that the exact line shape expression for this model system is

$$I(\omega) = -Re\{[p_a(\beta + \eta) + p_b\alpha - 4\bar{k}p_a p_b]/[\alpha(\beta + \eta) - 4\bar{k}^2 p_a p_b]\} \tag{2}$$

where $I(\omega)$ is the absorption intensity at ω radians/sec from the first moment of the spectrum.

$$\alpha = -R_2{}^0 - k_{ab} + i(\omega_a - \omega) \tag{3}$$

$$\beta = -R_2{}^0 - k_{ba} + i(\omega_b - \omega) \tag{4}$$

$$\bar{k} = {}^1/_2(k_{ab} + k_{ba}) \tag{5}$$

$$\eta = {}^2/_3\mathcal{A}^2(\beta - 0.6R_1 - k_s)/[(\beta - 0.6R_1 - k_s) \times (\beta - R_1 - k_s) + \mathcal{A}^2/_3] \tag{6}$$

Except for the addition of η, eq 2 is identical with the Hahn–Maxwell–McConnell expression.[4] Limiting expressions for slow or fast chemical exchange ($\bar{k}$) or quadrupole relaxation (R_1) can readily be obtained from eq 2.

(1) E. Grunwald, C. F. Jumper, and S. Meiboom, *J. Amer. Chem. Soc.*, **84**, 4664 (1962).

(2) C. Y. S. Chen and C. A. Swenson, *ibid.*, **91**, 234 (1969).

(3) M. Sheinblatt, *J. Chem. Phys.*, **39**, 2005 (1963).

(4) E. L. Hahn and D. E. Maxwell, *Phys. Rev.*, **88**, 1070 (1952); H. M. McConnell, *J. Chem. Phys.*, **28**, 430 (1958).

(5) M. Abu-Hamdiyyah, *J. Phys. Chem.*, **69**, 2720 (1965).

· The fast quadrupole relaxation limit is obtained by expanding eq 6 in powers of $\mathcal{A}/(\beta - R_1 - k_s)$ to second order and neglecting small imaginary terms. It is found that

$$\eta \approx -{}^2/_3\mathcal{A}^2/(R_1 + k_{ba} + k_s) \quad (7)$$

Equation 7 has sometimes been employed in (2) to correct for quadrupole relaxation effects on an *ad hoc* basis without including k_{ba} or k_s in the denominator of η. This procedure can lead to serious errors, particularly in the fast chemical exchange limit where the exchange broadened, single peak has width R_2'/π Hz, where

$$R_2' = R_2^0 + p_a p_b(\omega_a - \omega_b)^2/2\bar{k} + {}^2/_3 p_b\mathcal{A}^2/(R_1 + k_{ba} + k_s) \quad (8)$$

As expected, the slow chemical exchange–slow quadrupole relaxation limit of eq 2 yields four lines, broadened by the appropriate uncertainty in the lifetime of the spin states. The slow chemical exchange/fast quadrupole relaxation limit of eq 2 yields two lines, centered at ω_a and ω_b, respectively. In this limit the A resonance is broadened by k_{ab}/π Hz, independent of quadrupole effects but the B resonance is broadened by $(k_{ba} - \eta)$, with η given by eq 7. In this limit, by contrast to that of eq 8, $(k_{ba} + k_s)$ may be ignored relative to k_1 in the denominator of η.

The limiting expressions are presented here not because they are useful in evaluating experimental data (errors in such procedures are well documented[6]) but because they provide physical insight into effects of the various rate processes on $I(\omega)$ which is lacking from numerical computation.

Experimental Procedures

Thiourea (Matheson Coleman and Bell) was recrystallized from methanol, mp 180.0–181.4°. Kinetic studies were done on 0.5 M thiourea (this concentration gives the minimum accurately measurable exchange broadening), 0.75, 1.0, and 1.4 thiourea (solubility limit) in the pH range 1 to 5 at 35°. All solutions were made up no more than 2 hr prior to use.

Acid concentration in the samples was adjusted using small quantities of strong hydrochloric acid, while monitoring the pH with a Corning Model 10 pH meter equipped with a Corning Model 476050 combination electrode. The measured pH values were found to be within ±0.02 unit of −log [HCl] by calibration for each thiourea concentration with known volumes of standard acid, prepared from constant boiling HCl.

Solution pH was maintained constant by use of McIlvaine's buffer[7] above pH 2 and by Clark and Lubs's buffer[8] between pH 1 and 2. Preliminary experiments demonstrated that the pH remained constant within ±0.01 unit for at least 2 hr for each solution, and that line widths were reproducible within ±0.1 Hz independent of buffer concentration. Therefore catalysis by buffer components of those reactions which influence nmr lineshape is negligibly slow. As further evidence for this fact, all the data presented here for 1.4 M thiourea were obtained in unbuffered solutions. Although the precision of these data is less than that for the other thiourea concentrations, the rate constant derived from it does not differ significantly from that for the other thiourea concentrations.

Nmr spectra were obtained using a Varian T-60 spectrometer operating at 60 MHz with ambient probe temperature of 35°. For all solutions studied, the resonance consisted either of a single averaged resonance or two lorentzian resonances, the weaker being due to thiourea N–H protons. The internal chemical shift was found to be 150 Hz ± 2 Hz, independent of thiourea concentration. Precalibrated frequency scales were used, checking the calibration periodically by the sideband method. The precision of the shift measurement is low because the N–H resonance was much wider and weaker than the water proton resonance. The width of the water resonance above pH 5 was found to be 2.0 ± 0.1 Hz for all thiourea concentrations, and equal to the width of the single peak observed at very low pH values. This value was taken to be the line width in absence of exchange. It is larger than the line width (~0.5 Hz) due to field inhomogeneity because of radiation damping. The T-60 employs a small, single coil in its probe circuitry.

Recording accurate complete line shapes is the method of choice for accurate nmr kinetic studies, but it could not be done in this case because of the great disparity in relative populations (p_w = 0.96 in 1.4 M thiourea). Minor misalignment of the rf phase control introduces significant distortions in the wings of the very intense water line which interfere with the wing of the weaker and wider N–H resonance. Therefore the lines were recorded separately, with a sweep rate of 0.2 Hz/sec for peaks less than 15-Hz wide and 2.0 Hz/sec for wider peaks. At least four measurements of each peak were made, at rf levels well below saturation. The intense (water) line was found to be lorentzian ($\Delta_{1/2} = \sqrt{3}\Delta_{3/4}$) in all cases; only full widths at half-maximum intensity ($\Delta_{1/2}$) are reported here. The urea peak was found to be about 50 Hz wide in solutions with pH >5, but the precision of the measurement is low, particularly for the lower urea concentrations, due to phase adjustment problems. Therefore the N–H line widths were not extensively used in deriving rate parameters (see below).

(6) A. Allerhand, H. S. Gutowsky, J. Jones, and R. A. Meinzer, *J. Amer. Chem. Soc.*, **88**, 3185 (1966).

(7) "Handbook of Chemistry and Physics," 39th ed, Chemical Rubber Publishing Co., p 1615.

(8) "Handbook of Chemistry and Physics," 47th ed, Chemical Rubber Publishing Co., p D-79.

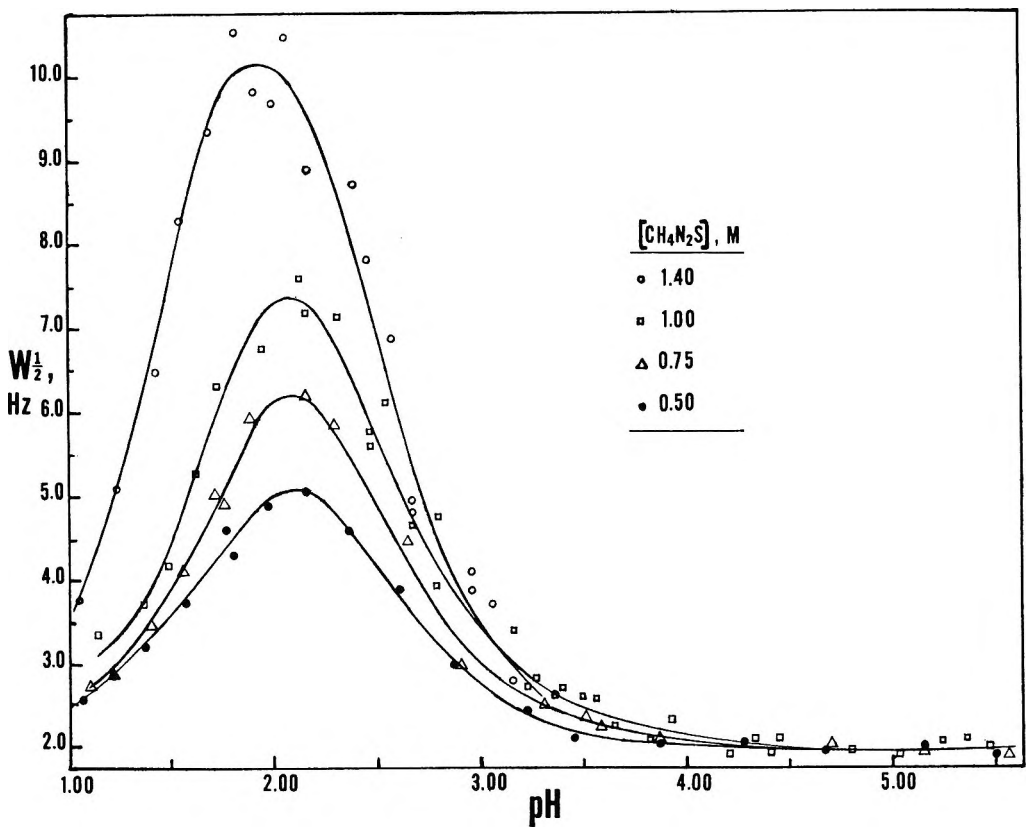

Figure 1. Water line widths (full width/half height) for aqueous thiourea. All line widths except those for 1.4 *M* thiourea were measured with buffered solutions.

Results and Discussion

The following proton transfer reactions were considered

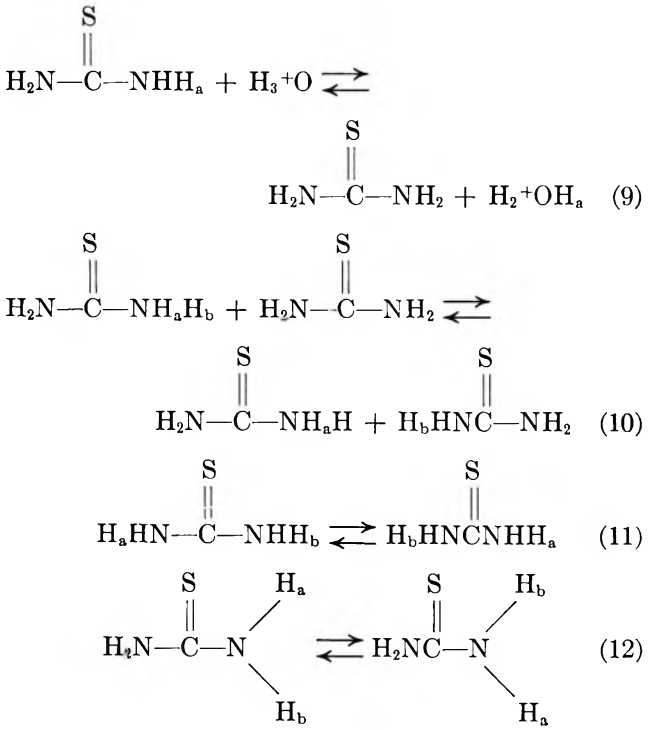

Reaction 9 is a schematic representation of acid-catalyzed proton transfers from thiourea to water. Its forward rate R is related to the pseudo-zero-order rate k_{ba} of eq 2 by the relation

$$k_{ba} = \frac{1}{[\text{thiourea}]}\frac{d}{dt}[\text{thiourea}] = R/[\text{thiourea}] \quad (13)$$

Reactions 10 and 11 together give the total rate of transfer of protons among different N–H groups not involving water as an intermediate. Reaction 12 represents internal rotation, which in principle renders the representation of (9)–(11), as well as the line shape expression (eq 2), incomplete. We have ignored internal rotation in the data analysis described below for two reasons. Firstly, at most a single N–H resonance was observed. Thus if hindered internal rotation is present, the rate of reaction 12 is sufficiently fast to average the resonance parameters of H_a and H_b. Some of the observed N–H line width could, however, be due to incomplete averaging of these differences. Secondly, theoretical calculations were made by numerical solution of Alexander's density matrix equations,[9] allowing H_a and H_b in eq 12 to be chemically shifted by up to 20 Hz. For values of the N–H coupling constants less than 100 Hz, *any* value of the internal rotation rate, and *all* values of the thiourea–water exchange rates, the computed water line widths were found to be

(9) S. Alexander, *J. Chem. Phys.*, **37**, 967 (1962).

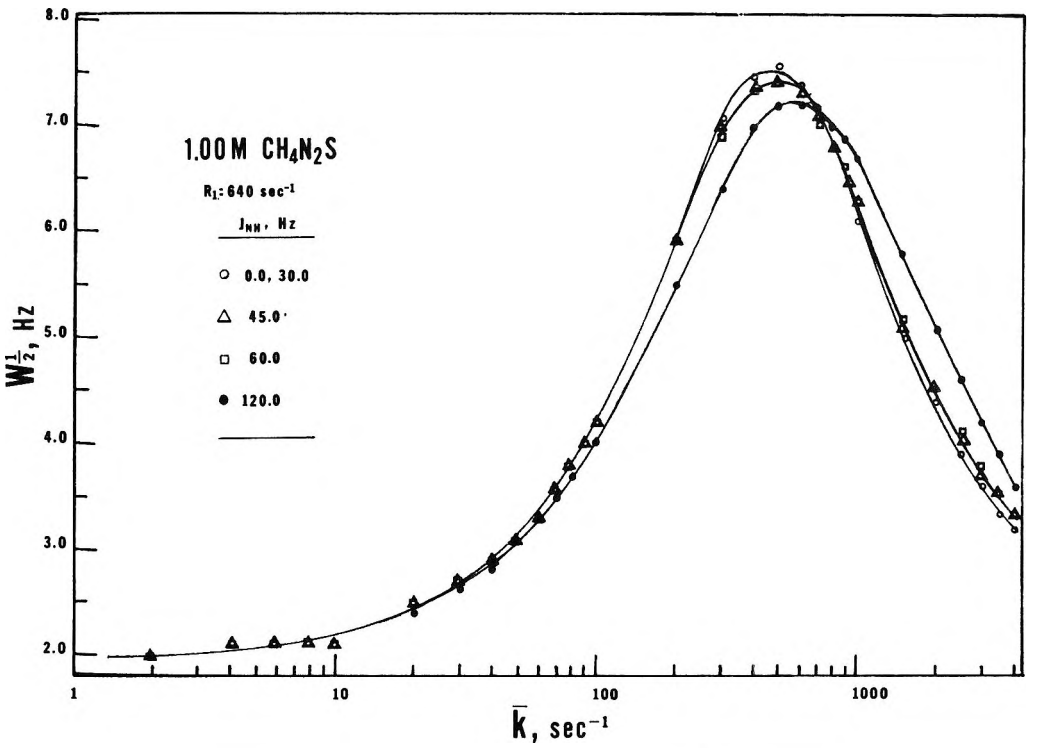

Figure 2. Exact computed water line widths as a function of average exchange rate $\bar{k}$. Curves similar to this were calculated using eq 2 of the text for other thiourea concentrations and for values of R_1 between 200 sec^{-1} and 1000 sec^{-1}.

independent of the parameters used to describe internal rotation, as long as the quadrupole relaxation rate R_1 was chosen large enough to partially collapse the N–H resonance.

Water line widths measured as a function of pH are shown in Figure 1. Equation 2 was used to compute water line widths as a function of the average exchange rate $\bar{k}$ and the results are shown in Figure 2 for thiourea concentration of 1.0 M. Similar curves were calculated for the other thiourea concentrations. In these calculations, the relative populations were chosen to correspond to the known sample composition and the chemical shift was taken as 150 Hz. Since the scalar coupling constant α_{NH} is not known for thiourea, the value of 60 Hz (compared with 63.4 Hz for urea[10]) was used, and R_1 was chosen to yield a computed thiourea line width of about 50 Hz. The direct exchange rate k_s was arbitrarily set equal to zero, because eq 7 is at least approximately valid for aqueous thiourea, and so only the sum $(R_1 + k_s)$ is relevant. As can be seen from Figure 2, the "quadrupole parameters" R_1 and α_{NH} have very little effect on the water line widths. Nevertheless, those curves in Figure 2 which predict less than the maximum observed line width in Figure 1 cannot correspond to reality. We used the curve in Figure 2 which does predict the correct maximum line width together with the line widths of Figure 1 to estimate $\bar{k}$ (and hence k_{ba}) *via* eq 1 and 5 as a function of pH for each thiourea concentration. The results are shown in Figure 3. Values of α_{N-H} and R_1 used in this computation may be significantly in error, but their ratio predicts the correct thiourea line width in absence of proton exchange, and possible errors in the individual parameters do not affect the accuracy of the thiourea–water proton exchange rate measurement.

In the calculations leading to Figure 3, the value of R_2^0 was varied slightly from 2.0 Hz found by direct measurement. The linearity and slope of Figure 3 was found to be dependent on the value used for R_2^0; typically the slope varied by 10% for a 7% change in R_2^0. Such behavior is expected when the natural line width

Table I: Rate Law of Protolysis of Aqueous Thiourea

$[CH_4N_2S]$, M	Slope of Figure 3[a]	Y intercept of Figure 3[b]	$k \times 10^{-5}$, M^{-1} sec^{-1}
0.50	−0.95	4.95	0.9
0.75	−1.00	5.07	1.2
1.00	−0.99	5.04	1.1
1.40[c]	−0.97	4.85	0.7

[a] The general form of the rate law is Rate = $k[CH_4N_2S]^m \cdot [H^+]^n$, from which it follows that, $\log k_{ba} = \log k[CH_4N_2S]^{m-1} - n$pH. The slope of a plot of $\log k_{ba}$ *vs.* pH (Figure 3) indicates that the order of the rate law with respect to hydrogen ion concentration is 0.98 ± 0.02. [b] The Y intercept indicates that the rate law is first order with respect to thiourea concentration. [c] No buffer was used for this thiourea concentration.

(10) J. B. Lambert, J. W. Roberts, G. Binsch, and J. D. Roberts, *J. Amer. Chem. Soc.*, 86, 5564 (1964).

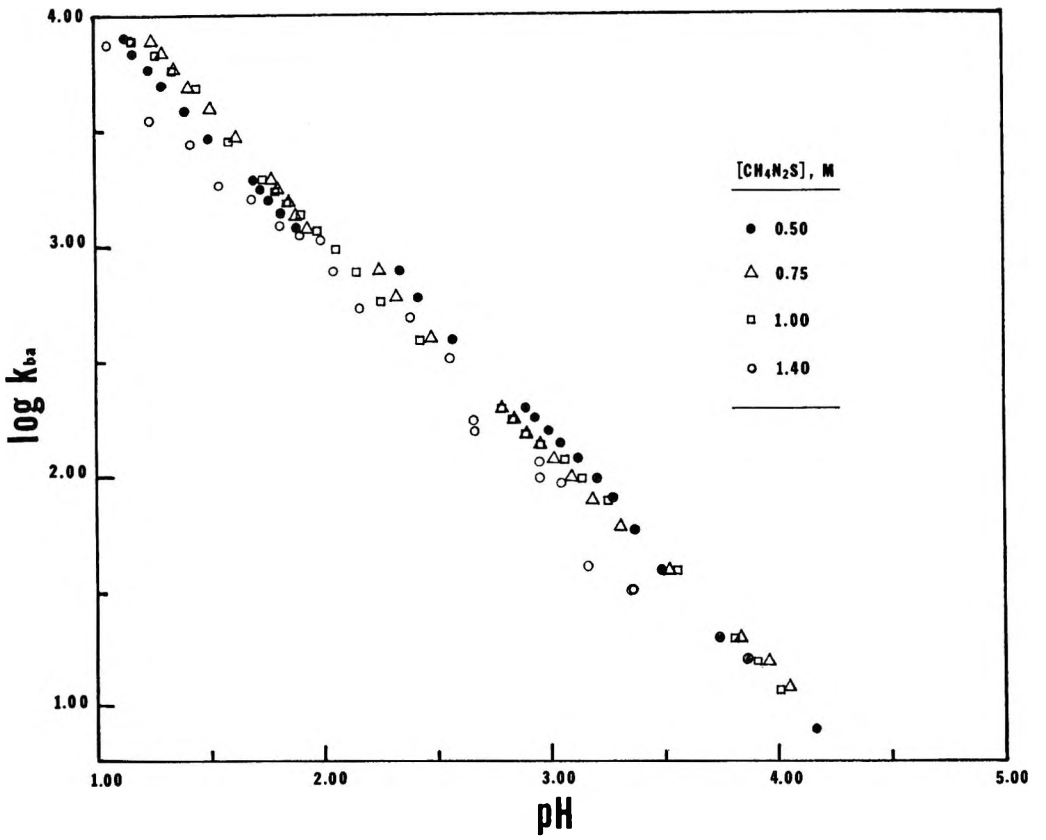

Figure 3. Logarithm of k_{ba}, the inverse lifetime of a proton on thiourea nitrogen, plotted against pH, for various thiourea concentrations.

contributes at least 20–25% of the maximum observed line width. The slope and intercept for each thiourea concentration shown in Figure 3 are listed in Table I, from which the rate law for protolysis is found to be

$$R = (1.0 \pm 0.2) \times 10^5[\text{thiourea}][H_3{}^+O]^{0.98 \pm 0.02} \quad (14)$$

Errors of the type just discussed for $R_2{}^0$ lead to larger errors in estimating the order of the reaction as well as its rate constant; analogous errors in enthalpies and entropies of activation have been pointed out for variable temperature studies.[6] For the present case the slope of the curves in Figure 3 is most certainly either integral or half integral, and probably should be 1.00. Use of this fact has allowed us to estimate $R_2{}^0$ properly, and also to conclude that the thiourea–water chemical shift does not vary significantly with pH, for if it did, the slopes in Figure 3 would not have been close to unity.

The use of *water* line widths to compute lifetimes of protons on thiourea ($1/k_{ba}$ from measured values of k_{ab}) depends crucially on the validity of eq 1, and one situation where this relation could fail is if protonation of sulfur as opposed to nitrogen were slow enough to produce extra broadening of the water peak. From the slow exchange limit of eq 2, if eq 1 is valid, the ratio of *exchange* broadening of the thiourea and water resonance should be p_a/p_b. The water peak exchange broadening can be estimated by subtracting the natural line width from the observed line width. The thiourea peak exchange broadening can be estimated by subtracting the thiourea line width at neutral pH from that observed at lower pH. Although eq 7 shows that this procedure is not exact, in the present case if the slow exchange condition is met, $R_1 \gg k_{ba}$ and little error is made. For 1 M thiourea, p_a/p_b is 26, and the ratio of thiourea to water exchange broadening was found to vary randomly between 22 and 32 at pH between 3.6 and 4.0. For lower pH values (larger rates), this ratio is significantly smaller, but calculations using eq 2 indicate that the slow exchange approximation, rather than eq 1, is breaking down. Therefore we conclude that the rate law of eq 14 is an accurate representation of acid-catalyzed protolysis in aqueous thiourea.

For N-methylacetamide,[11] the protolysis rate constant for acid catalysis is 400 M^{-1} sec^{-1}, and for base catalysis, 2×10^5. The acid-catalyzed reaction is supposed to be slow because protonation occurs preferentially on oxygen rather than nitrogen,[11] and the latter process only is observed by nmr. The mechanism for base catalysis is thought to be a bimolecular collision. Correcting the rate constant for acid-cata-

(11) A. Berger, A. Loewenstein, and S. Meiboom, *J. Amer. Chem. Soc.*, **81**, 62 (1959).

lyzed protolysis of thiourea by a statistical factor of 4 (for one of the four equivalent N–H protons the rate constant is $2.5 \times 10^4\ M^{-1}\ \text{sec}^{-1}$), its value is much closer to the base-catalyzed rate constant of N-methylacetamide than to the acid rate constant. However, thiourea is known to protonate preferentially on sulfur[12] and not on nitrogen. We therefore conclude that the protolysis of thiourea N–H protons is catalyzed by acid about 60 times more efficiently than N-methylacetamide N–H protons.

Conclusions

Proton lifetimes on aqueous thiourea have been determined from measurements of water and N–H nmr line widths. Effects of quadrupole relaxation of nitrogen may be separated experimentally from chemical exchange effects. Acid-catalyzed protolysis of thiourea N–H groups is about 60 times more efficient than acid-catalyzed protolysis of N-methylacetamide N–H groups. Factors responsible for this difference could perhaps be determined by studies of substituted ureas and thioureas.

Acknowledgment. We gratefully acknowledge partial support of this work by the National Science Foundation and the Office of Naval Research. Mr. Thomas DiGennaro provided many useful suggestions leading to the closed form of the line shape expression.

Appendix

A general expression for the nmr line shape $I(\omega)$ is given by

$$I(\omega) = -Re\{\mathbf{1A} - i\omega\mathbf{I})^{-1}\mathbf{W}\} \qquad \text{(A1)}$$

where **1** and **I** are the unit matrix and the unit vector, respectively, **W** is a vector of relative weights, ω is the frequency offset in radians/sec from the first moment of the spectrum, and **A** is a complex, nonhermitian matrix. For the case discussed in the text, all the matrices and vectors in (A1) are of dimension $2I + 2$ where I is the spin of the nucleus to which spin $^1/_2$ nuclei are coupled in subsite B. The vector **W** is given by

$$\mathbf{W} = (p_a, p_b/(2I+1), p_b/(2I+1), \cdots p_b/(2I+1)) \qquad \text{(A2)}$$

An analytical formula for $I(\omega)$ can be obtained by obtaining an explicit expression for the inverse $(\mathbf{A} - i\omega\mathbf{I})^{-1}$ in terms of elements of **A**. **A** consists of submatrices as follows

$$\mathbf{A} = \mathbf{R}_2^0 + \mathbf{K} + \mathbf{K}_s + \mathbf{R}_1 + i\mathbf{\Omega} + i\mathbf{J} \qquad \text{(A3)}$$

$\mathbf{R}_2^0$ refers to the width of each transition in absence of the exchange processes included in the other matrices. We assume for simplicity that $\mathbf{R}_2^0$ is diagonal and proportional to the unit matrix, the proportionality constant being R_2^0 of eq 3 and 4 of the text. **K** refers to the thiourea–water proton exchange; its elements can readily be obtained from the discussion following eq 1 of the text. $\mathbf{K}_s$ describes the scrambling of thiourea protons among themsleves. $\mathbf{R}_1$ describes quadrupole relaxation of spin S. It consists of the quadrupolar matrices obtained previously,[13] bordered by a row and column of zeroes. $\mathbf{\Omega}$ is a diagonal matrix whose first entry is ω_a, the resonant frequency of spins in site A, and all other diagonal elements are ω_b, the site B resonant frequency. **J** describes scalar coupling of spins in site B to the quadrupolar nucleus. Its diagonal elements are $0, I\mathcal{a}, (I-1)\mathcal{a}, \ldots -I\mathcal{a}$. Off-diagonal elements of **J** are due to the nonsecular part of the heteronuclear scalar coupling. They are neglected in this work, limiting validity of eq 2 to situations where the rates are less than the difference in resonant frequency of protons from nitrogen.

In order to explicitly calculate the inverse required by eq A1, it is useful to transform (A1) by a similarity transformation. For any nonsingular matrix **P**

$$I(\omega) = -Re\{\mathbf{1P}\{\mathbf{P}^{-1}\mathbf{AP} - i\omega\mathbf{I}\}^{-1}\mathbf{P}^{-1}\mathbf{W}\} \qquad \text{(A4)}$$

Equation A4 may be used successively choosing **P** each time to accomplish any desired simplification. $\mathbf{R}_1$ and $\mathbf{K}_s$ commute, and P may be chosen to diagonalize them simultaneously. For spin $I = 1$

$$P = \begin{bmatrix} 1 & 0 & 0 & 0 \\ 0 & 1/\sqrt{3} & 1/\sqrt{2} & 1/\sqrt{6} \\ 0 & 1/\sqrt{3} & 0 & -2/\sqrt{6} \\ 0 & 1/\sqrt{3} & 1-/\sqrt{2} & 1/\sqrt{6} \end{bmatrix} \qquad \text{(A5)}$$

and for spin $I = {}^3/_2$

$$P = \begin{bmatrix} 1 & 0 & 0 & 0 & 0 \\ 0 & {}^1/_2 & 3/2\sqrt{5} & -1/2\sqrt{5} & {}^1/_2 \\ 0 & {}^1/_2 & 1/2\sqrt{5} & 3/2\sqrt{5} & -{}^1/_2 \\ 0 & {}^1/_2 & -1/2\sqrt{5} & -3/2\sqrt{5} & -{}^1/_2 \\ 0 & {}^1/_2 & -3/2\sqrt{5} & 1/2\sqrt{5} & {}^1/_2 \end{bmatrix} \qquad \text{(A6)}$$

For arbitrary spin I, the first three eigenvectors (columns of **P**) are

$$\mathbf{P}_1 = \text{col}(1,0,0,\ldots 0)$$

$$\mathbf{P}_2 = \text{col}(0,1,1,1,\ldots 1)\sqrt{2I+1}$$

$$\mathbf{P}_3 = \text{col}(0,I,(I-1)\ldots. -I)/\sqrt{{}^1/_3 I(I+1)(2I+1)} \qquad \text{(A7)}$$

Equation A7 and the facts that **P** is orthonormal, and R_1 itself is symmetric about the diagonal and the antidiagonal, allow additional relations to be obtained among the elements P_{ij}. For example, since any column P_j of **P** is orthogonal to $\mathbf{P}_2$

(12) T. Birchall and R. J. Gillespie, *Can. J. Chem.*, **41**, 2642 (1963).

(13) H. L. Gutowsky, R. L. Vold, and E. J. Wells, *J. Chem. Phys.*, **43**, 4107 (1965).

$$\sum_{j=1}^{2I+2} P_{ij} = 0 \qquad (j = 1,3,4,\ldots 2I+2) \qquad \text{(A8)}$$

After transforming (A1) to a form in which $\mathbf{R}_1$ and $\mathbf{k}_s$ are diagonal, it is convenient to further transform the result by the diagonal matrix diag($\sqrt{(2I+1)P_a}$, $\sqrt{P_b}$'1,1,...1). This procedure symmetrizes the upper 2 × 2 block of **A**, and yields the result

$$I(\omega) = -Re\{L_e(\mathbf{B} - i\omega\mathbf{I})^{-1}L_r\} \qquad \text{(A9)}$$

where

$$\begin{aligned} L_e &= (\sqrt{p_a},\sqrt{p_b},0,\ldots 0\sqrt{2I+1} \\ L_r &= (\sqrt{p_a},\sqrt{p_b},0,\ldots 0)/\sqrt{2I+1} \end{aligned} \qquad \text{(A10)}$$

and

$$B = \begin{bmatrix} \mathbf{A}_2 & \mathbf{X} \\ \mathbf{Y} & \mathbf{A}_{2I} \end{bmatrix} \qquad \text{(A11)}$$

The matrix $\mathbf{A}_2$ is precisely the matrix form of the HMM equations[13] obtained previously. The rectangular matrix **X** is given by

$$\mathbf{X} = \begin{bmatrix} 0 & 0\ldots 0 \\ 2iA\sqrt{I(I+1)/3P_b} & 0\ldots 0 \end{bmatrix} \qquad \text{(A12)}$$

and **Y** is given by

$$Y = \begin{bmatrix} 0 & X_{2I}p_b \\ \cdot & \\ \cdot & 0 \\ \cdot & \cdot \\ 0 & \cdot \\ & \cdot \\ & 0 \end{bmatrix} \qquad \text{(A13)}$$

The elements of $\mathbf{A}_{2I}$ cannot be explicitly determined without knowledge of all the eigenvectors of **P**.

Nevertheless eq A9–A13 suffice to yield eq 2 of the text, where η is the only nonvanishing element of the matrix

$$Q = XA_{2I}^{-1}Y \qquad \text{(A14)}$$

For the case of spin $I = 1$, we obtain eq 6 of the text while for $I = 3/2$

$$\eta = {}^5/_4\mathfrak{A}^2(\beta - R_1)(\beta - 2R_1)/[(\beta - R_1)^2(\beta - 2R_1) + {}^4/_5\mathfrak{A}^2)] \qquad \text{(A15)}$$

This derivation could be extended to cases of $I > 3/2$ by using a computer to calculate the eigenvalues and eigenvectors of $\mathbf{R}_1$, but the resulting expression for η would be very cumbersome. The derivation can also be applied to cases of line broadening caused by scalar coupling to nuclei relaxing by other mechanisms than quadrupole coupling to permanent field gradients.

Carbon-13 Nuclear Magnetic Resonance Spectra of Monosubstituted Cyclopropanes

by K. M. Crecely, R. W. Crecely, and J. H. Goldstein

Chemistry Department, Emory University, Atlanta, Georgia 30322 *(Received February 9, 1970)*

High-resolution ^{13}C spectra have been obtained and analyzed for cyclopropane and its monosubstituted –Cl, –Br, –I, $-NH_2$, and –COCl derivatives. The long-range ^{13}C–H coupling constant in cyclopropane has been found to be −2.55 Hz. Relationships between the long-range ^{13}C–H couplings and the H–H couplings in these cyclopropanes are discussed.

Introduction

There have been numerous nmr studies of cyclopropane and its monosubstituted derivatives.[1-13] The proton chemical shifts and H–H coupling constants have been reported for many of these compounds.[1-8] In several cases the ^{13}C–H satellite spectra have been analyzed.[7,8] Such analyses yield the ^{13}C–H directly bonded couplings and information about the differences between long-range ^{13}C–H coupling constants. The ^{13}C spectra of cyclopropane and several monosubstituted derivatives have appeared in the literature,

(1) H. M. Hutton and T. Schaefer, *Can. J. Chem.*, **41**, 2774 (1963).
(2) K. B. Wiberg and B. J. Nist, *J. Amer. Chem. Soc.*, **85**, 2788 (1963).
(3) T. Schaefer, F. Hruska, and G. Kotowycz, *Can. J. Chem.*, **43**, 75 (1965).

but only the ^{13}C chemical shifts and directly bonded couplings were determined from these studies.[9-11] The C–C coupling constants in several of the cyclopropanes have been obtained by observing the ^{13}C satellites of the ^{13}C spectra with complete proton decoupling.[12,13] In no cases have the long-range ^{13}C–H couplings been reported.

In the present study high-resolution ^{13}C spectra have been obtained and analyzed for cyclopropane and five of its monosubstituted derivatives. The long-range ^{13}C–H couplings and the ^{13}C chemical shifts have been determined for these compounds. The couplings have been compared to long-range ^{13}C–H couplings in other compounds and relationships have been investigated between the ^{13}C–H couplings and the H–H couplings in cyclopropanes.

Experimental Section

All of the compounds were obtained from commercial sources except cyclopropyl iodide, which was prepared by adding iodine to cyclopropyl magnesium bromide in tetrahydrofuran. The samples were prepared in 13-mm nmr tubes. For the substituted compounds ~15% benzene was added to serve as an internal proton lock. Cyclopropane itself was run as a ~15% solution in benzene. The CS_2 sample used for referencing purposes also contained ~15% benzene.

The ^{13}C spectra were obtained using a Bruker HFX-90 spectrometer operating in the frequency sweep mode. Sweep widths of 1.0 and 0.4 Hz/cm were used depending on the complexity of the patterns. Normally ~130 scans were accumulated using a Fabri-Tek 1074 signal averaging system. The spectra were initially calibrated relative to the benzene lock and then converted to ppm relative to CS_2. At a field setting which caused resonance of the benzene protons to occur at 90 MHz, CS_2 was found to resonate at 22.631891 MHz.

The proton spectra were taken on a Varian A-60A spectrometer using ~15% benzene as an internal reference. Calibrations were performed by the usual sideband technique.

Calculations and Results

The ^{13}C spectra were analyzed using H–H coupling values obtained previously.[7] Since the calculated ^{13}C spectra were found to be dependent on the proton chemical shifts, the proton spectra were rerun and analyzed to obtain the shifts when the sample contained ~15% benzene. These proton chemical shifts were then converted to their values at 90 MHz for use in the analyses. The ^{13}C spectra of the monosubstituted cyclopropanes were analyzed as ABB'CC'X spin systems where X = ^{13}C. The spectral parameters were obtained with the aid of PROSPECT I, an iterative least-squares program modeled after LAOCOON II.[14] Initial trial values of the long-range ^{13}C–H couplings were adjusted to conform to the differences in these parameters, which were available from previous analyses of the corresponding satellite spectra.[7,15]

In the analysis of the $\alpha^{13}C$ pattern of cyclopropyl chloride and cyclopropyl bromide two sets of parameters were found which were consistent with the differences obtained from satellite spectra. In one set the CCH couplings were positive and in the other negative. However, in the case of cyclopropyl iodide and cyclopropane carboxylic acid chloride, the α patterns could be fit only with negative values. It has therefore been assumed that the long-range couplings to the α carbon are negative in all the compounds studied. For the iodide and the acid chloride the differences between the CCH coupling values determined from the ^{13}C spectra deviate slightly (0.6 and 1.0 Hz) from those obtained from the satellites. However, trial calculations show that changes of this magnitude in the differences have no effect on the predicted satellite spectra.

The $\alpha^{13}C$ spectrum of cyclopropylamine was broad and could not be analyzed. The long-range ^{13}C–H couplings were estimated from the observed width of the pattern and the difference obtained from the satellite analysis.

In analyzing the $\beta^{13}C$–H satellite patterns it was not necessary to introduce differences between the long-range ^{13}C–H couplings. Trial calculations of these satellite spectra showed that the difference between the two long-range couplings from the β carbon to the β protons has to be nearly zero. Changes in the coupling from the β carbon to the α proton had no effect on the satellites. With this information it was possible in most cases to obtain a unique set of parameters which characterize the $\beta^{13}C$ spectra. In these cases the ^{13}C–H long-range couplings to the β carbon were also found to be negative. In one case (cyclopropylamine) changing the sign of the coupling from the β carbon to the α proton caused very minor changes in the predicted spectrum. Slightly better agreement between observed

(4) V. S. Watts and J. H. Goldstein, *J. Chem. Phys.*, **46**, 4165 (1967).

(5) P. A. Scherr and J. P. Oliver, *J. Mol. Spectrosc.*, **31**, 109 (1969).

(6) M. S. Gopinathan and P. T. Narasimhan, *Indian J. Pure Appl. Phys.*, 7, 178 (1969).

(7) K. M. Crecely, V. S. Watts, and J. H. Goldstein, *J. Mol. Spectrosc.*, **30**, 184 (1969).

(8) G. Schrumph and W. Luettke, *Tetrahedron Lett.*, **31**, 2635 (1969).

(9) J. J. Burke and P. C. Lauterbur, *J. Amer. Chem. Soc.*, **86**, 1870 (1964).

(10) G. E. Maciel and G. B. Savitsky, *J. Phys. Chem.*, **69**, 3925 (1965).

(11) P. H. Weiner and E. R. Malinowski, *ibid.*, **71**, 2791 (1967).

(12) F. J. Weigert and J. D. Roberts, *J. Amer. Chem. Soc.*, **89**, 5962 (1967).

(13) F. J. Weigert, Dissertation, California Institute of Technology, 1968.

(14) S. Castellano and A. A. Bothner-By, *J. Chem. Phys.*, **41**, 3863 (1964).

(15) In the paper cited, subscripts 2 and 3 in footnote *b* to Table II should be interchanged.

Table I: ^{13}C Chemical Shifts[a] and Long-Range ^{13}C–H Coupling Constants[b] for Cyclopropanes

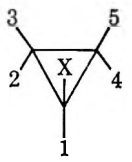

X	δC_α	δC_β	$J_{C_\alpha H_3}$	$J_{C_\alpha H_5}$	$J_{C_\beta H_1}$	$J_{C_\beta H_4}$	$J_{C_\beta H_5}$
H	195.7	195.7	−2.55	−2.55	−2.55	−2.55	−2.55
I	213.0	182.5	−2.3	−5.5	−1.1	−2.75	−2.85
Br	178.9	183.9	−1.55	−5.35	−0.75	−2.9	−2.85
Cl	165.5	183.9	−1.15	−5.05	−0.55	−3.05	−2.75
COCl	169.1	180.5	−2.2	−3.2	−1.25	−2.35	−2.5
NH_2	168.9	185.5	−1.0	−4.0	+0.65	−2.9	−2.7

[a] Values are in ppm relative to CS_2. [b] Values are in Hz.

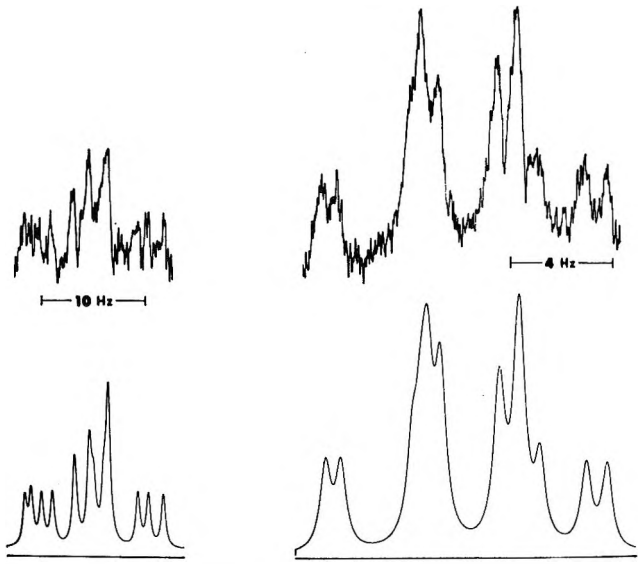

Figure 1. Observed and computer calculated ^{13}C spectra of of cyclopropyl iodide. The high-frequency half of the spectrum of the α carbon is shown on the left and the center region of the spectrum of the β carbon is shown on the right.

and calculated frequencies was obtained with a positive sign for this coupling.

The ^{13}C spectrum of cyclopropane was analyzed as a seven-spin system. A satisfactory prediction of the observed spectrum was obtained only with a negative value for J_{CCH}.

Figure 1 shows the observed and calculated ^{13}C spectra of cyclopropyl iodide. The high-frequency half of the spectrum of the α carbon and the center region of the spectrum of the β carbon are illustrated. These spectra are representative of those obtained in this study. The ^{13}C chemical shifts and the long-range ^{13}C–H couplings for the cyclopropanes are given in Table I. The estimated uncertainty is judged to be ± 0.1 Hz for the long-range couplings and ± 0.1 ppm for the chemical shifts. Since the directly bonded ^{13}C–H couplings obtained in this study do not differ significantly from those reported previously,[7] they are not included with the present results.

Discussion

The ^{13}C chemical shifts obtained in this study for the cyclopropanes agree with those reported previously.[9,11] The α ^{13}C chemical shifts of the substituted cyclopropanes correlate with the ^{13}C chemical shifts of similarly substituted methanes, as was noted by Weiner and Malinowsky.[11]

The coupling constants obtained in this study are of interest since they provide information on the effects of substituents on the long-range ^{13}C–H couplings in a system where the geometry is fixed. However, interpretation of the long-range couplings in the three-membered rings presents some difficulty. An ambiguity arises in that these couplings can be viewed as either two-bond or three-bond couplings, the latter having been found to be of larger magnitude than the former in several cases.[16,17]

One striking aspect of the present results is that $J_{C_\alpha H_3}$ is uniformly more negative than $J_{C_\alpha H_2}$. Somewhat similar observations have been reported for vinyl bromide,[18] but in this case the difference between the two analogous couplings was even larger ($J_{C_\alpha H_{cis}} = -8.5$, $J_{CH_{\alpha trans}} = +7.5$). It is interesting to note that $J_{C_\alpha H_2}$ correlates with electronegativity of the substituent,[19] as shown in Figure 2, while $J_{C_\alpha H_3}$ does not. The unusually small values of $J_{C_\alpha H_3}$ in the halogen compounds is reminiscent of the trends observed in the $^{13}CCCH$ couplings in $(CH_3)_3C$–$^{13}CH_2$–X.[20,21] In both

(16) G. J. Karabatsos, *J. Amer. Chem. Soc.*, **83**, 1230 (1961).

(17) G. J. Karabatsos, J. D. Graham, and F. M. Vane, *ibid.*, **84**, 37 (1962).

(18) R. M. Lynden-Bell, *Mol. Phys.*, **6**, 537 (1963).

(19) P. R. Wells, *Progr. Phys. Org. Chem.*, **6**, 127 (1968).

(20) G. J. Karabatsos and C. E. Orzech, Jr., *J. Amer. Chem. Soc.*, **86**, 3574 (1964).

(21) G. J. Karabatsos and C. E. Orzech, Jr., *ibid.*, **87**, 560 (1965).

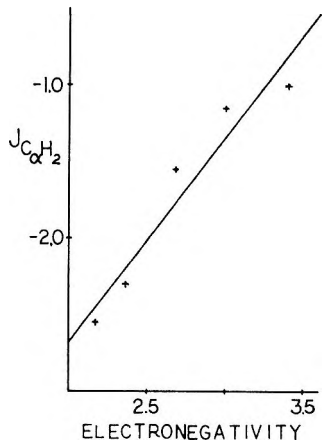

Figure 2. Electronegativity of the substituent *vs.* $J_{C_\alpha H_2}$.

cases the coupling values increase in the order opposite to that expected from halogen electronegativity. It has been suggested that there could be spin-dipole or electron-orbital contributions through space to these ^{13}CCCH couplings which might be enhanced by the close promixity between the halogen and the methyl group in the $(CH_3)_3C-^{13}CH_2-X$ compounds.[21] Geometrically the difference between H_2 and H_3 in the substituted cyclopropanes is determined by their relation in space to the substituent. The unusual behavior of $J_{C_\alpha H_3}$ is consistent with possible spin-dipole or electron-orbital contributions to this coupling, since H_3 is closer to the substituent than is H_2.

The coupling between the β carbon and the α proton in the monosubstituted cyclopropanes is more positive than the coupling in cyclopropane itself. The analogous coupling in the ethyl halides[22] and in vinyl bromide[18] is also more positive than the coupling in the corresponding parent compounds.[23] However, since the sign of this coupling in the ethyl halides has not been determined, it is not known whether the difference with respect to ethane is $\sim$2 or $\sim$7 Hz. This coupling in the cyclopropanes varies monotonically with electronegativity of the substituent as does $J_{C_\alpha H_2}$, although the magnitude of $J_{C_\alpha H_2}$ in the substituted compounds is about twice that of $J_{C_\beta H_1}$. The couplings from the β carbon to the β protons change very little through the series of cyclopropanes.

Assuming that the Fermi contact term is the only coupling mechanism, Karabatsos has developed relationships between C–H and H–H coupling constants over the same number of bonds. He has had limited success in applying these relationships to experimental data.[17] Weigert and Roberts have applied the Karabatsos formulation to intermolecular comparisons of C–H and H–H couplings. They have had some success in relating long-range ^{13}C–H couplings in benzene and in the five-membered aromatic heterocycles to H–H couplings in substituted ethylenes and other suitable model compounds.[24,25]

In the present study trends have been observed between $J_{H_\alpha H_\beta}$ and two of the long-range ^{13}C–H couplings ($J_{C_\alpha H_2}$ and $J_{C_\alpha H_1}$). However, such correlations are not linear. The ^{13}C–H long-range couplings fail to correlate with the geminal H–H couplings. In addition there are no suitable model compounds with which to make intermolecular comparisons. Since the pathway of the ^{13}C–H long-range couplings in the cyclopropanes can be over two bonds or three bonds, multiple correlations involving a vicinal and the geminal H–H coupling seemed reasonable. Linear regressions showed that $J_{C_\alpha H_2}$ and $J_{C_\beta H_1}$ could be predicted to within experimental error with two such parameters. For $J_{C_\alpha H_3}$ the correlation was good but the residuals were larger than the estimated experimental errors in the parameters. Table II gives the regression equations obtained along with the corresponding correlation coefficients and standard errors.

Table II: Multiple Regression Parameters Relating ^{13}C–H and H–H Coupling Constants in Cyclopropanes

Regression eq	Correlation coeff	Std error of est
$J_{C_\alpha H_2} = -20.42 + 2.51J_{24} + 1.09J_{23}$	0.995	0.08
$J_{C_\beta H_1} = 11.01 - 1.35J_{12} - 0.34J_{23}$	0.998	0.07
$J_{C_\alpha H_3} = -3.44 + 0.58J_{12} + 1.00J_{23}$	0.973	0.36

Since the uncertainty in the CCH coupling values obtained for the amine are considerably larger than those for the remaining compounds, the regressions were also run omitting this data point. The regression equations obtained in this way for $J_{C_\alpha H_2}$ and $J_{C_\beta H_1}$ were very similar to those obtained previously and predicted coupling values for the amine that were within 0.3 Hz of the experimental values. For $J_{C_\alpha H_3}$, omitting the amino point caused considerable changes in the regression coefficients. The resulting expression failed to predict a reasonable value for $J_{C_\alpha H_3}$ in this compound.

The vicinal H–H coupling (J_{24}) required to predict $J_{C_\alpha H_2}$ was not the same as the coupling (J_{12}) which predicted $J_{C_\beta H_1}$. It is interesting to note that if the long-range ^{13}C–H couplings are considered to be three-bond couplings, the coupling paths of $J_{C_\alpha H_2}$ and J_{24} share two bonds as do those of $J_{C_\beta H_1}$ and J_{12}.

As mentioned previously, the correlation obtained for $J_{C_\alpha H_3}$ was not as good as those for $J_{C_\alpha H_2}$ and $J_{C_\beta H_1}$. The regression expression fails to predict the correct

(22) G. Miyazima, Y. Utsumi, and K. Takahashi, *J. Phys. Chem.*, **73**, 1370 (1969).

(23) R. M. Lynden-Bell and N. Sheppard, *Proc. Roy. Soc., Ser. A*, **269**, 385 (1962).

(24) F. J. Weigert and J. D. Roberts, *J. Amer. Chem. Soc.*, **89**, 2967 (1967).

(25) F. J. Weigert and J. D. Roberts, *ibid.*, **90**, 3543 (1968).

order for $J_{C_\alpha H_\beta}$ in the halogen compounds. The largest residual occurred for the iodide, where the deviation between the observed and calculated coupling was ~0.5 Hz.

The relations found here between the long-range ^{13}C–H couplings and H–H couplings in substituted cyclopropanes show considerable promise. However, data for additional compounds will be necessary to test the validity of such correlations.

Acknowledgment. This work was supported in part by a grant from the National Institutes of Health.

Carbon-13 Magnetic Resonance. XVIII.[1] Selected Nucleosides

by Alan J. Jones,[2a] David M. Grant,[2b] Michael W. Winkley,[2b] and Roland K. Robins[2b]

Department of Chemistry, Colorado State University, Fort Collins, Colorado 80521, and the Department of Chemistry, University of Utah, Salt Lake City, Utah 84112 *(Received January 26, 1970)*

The natural abundance carbon-13 magnetic resonance spectra of 23 pyrimidine nucleosides are reported. A wide variety of structural variations in both the pyrimidine and ribose moieties have been considered. The carbon-13 shifts of the sugar carbon atoms in the ribosides, deoxyribosides, arabinosides, and anhydronucleosides enable their distinction. Substituent effects on the pyrimidine shifts are of the same order though of different magnitude than those reported for monosubstituted benzenes and pyridines. Contributions from keto-tautomeric structures are evidenced in the spectra of 6-hydroxycytidine and 1-(β-D-ribofuranosyl)-barbituric acid.

In previous papers we have described the natural abundance carbon-13 magnetic resonance spectra of the naturally occurring nucleosides[3] and a variety of their derivatives (29 in all), which enabled total spectral assignments to be made.[1] Dorman and Roberts[4] have similarly reported the spectra of the corresponding naturally occurring nucleotides. The apparent independence of the ribose carbon atom resonances from those of the heterocyclic base was emphasized by both groups of workers.[3,4] Clear distinction was made between the ribosides and deoxyribosides based primarily on the chemical shift observed at the carbon atom C-2′. Further, the chemical shifts of the heterocyclic bases were shown to correlate reasonably well with calculated MO parameters.[1,3] It was suggested[1,3] that this gross correlation further emphasizes the fact that the carbon-13 chemical shift reflects the important electronic features even in these relatively complex molecules. A qualitative correlation of the shifts with the known chemical reactivities of these compounds was also noted.[1,2]

In the present paper we report the natural abundance carbon-13 spectra of the variety of nucleosides in which structural variations relatively common to the area of synthetic nucleoside chemistry are found. The structures of the 23 nucleosides studied are summarized in Figure 1. Structural variations in the heterocyclic base (pyrimidine) and the ribose moiety have been considered. These data, along with those previously reported,[1,3,4] should provide an index for structural identification using carbon-13 magnetic resonance techniques in nucleoside chemistry.

Experimental Section

Carbon-13 spectra were obtained using a Varian AFS-60 analog frequency sweep spectrometer in the manner described previously.[1] All of the nucleosides studied were either obtained from commercial sources or prepared using standard procedures and were purified and dried prior to spectral determination. Maximum concentrations (at 40°) of the nucleosides in dimethyl sulfoxide were employed. All chemical shifts were calculated relative to the internal reference (DMSO) and converted to the benzene scale.

Results and Discussion

The observed carbon-13 shifts in the nucleosides studied are presented in Table I. For comparison we also include the data for uridine (U), thymidine (T), cytidine (C), and 6-methylcytidine for which unequiv-

(1) Previous paper in this series: A. J. Jones, D. M. Grant, M. W. Winkley, and R. K. Robins, *J. Amer. Chem. Soc.*, in press.

(2) (a) Colorado State University; (b) University of Utah.

(3) A. J. Jones, D. M. Grant, M. W. Winkley, and R. K. Robins, *Proc. Natl. Acad. Sci. U. S.*, **65**, 27 (1970).

(4) D. E. Dorman and J. D. Roberts, *ibid.*, **65**, 19 (1970).

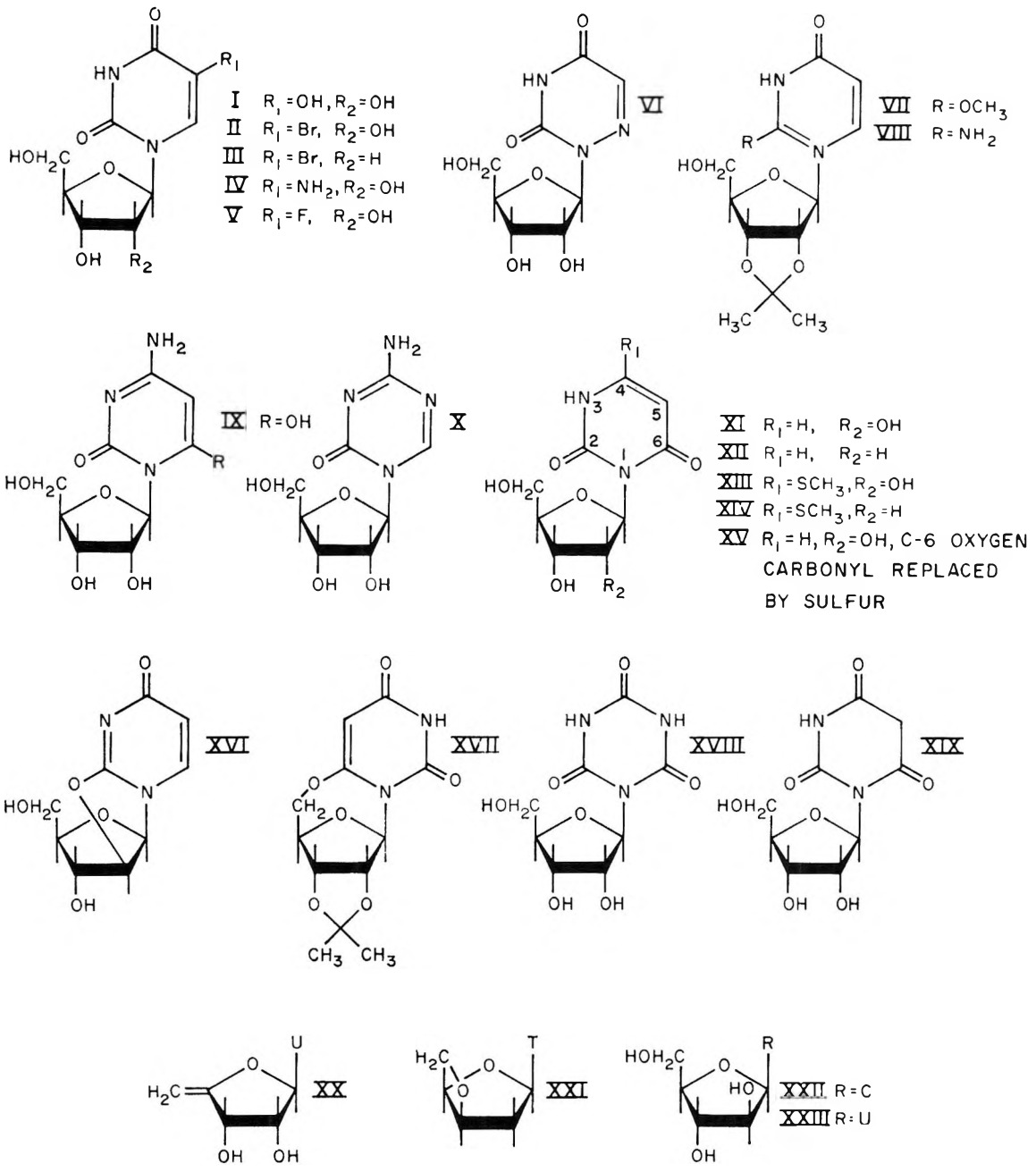

Figure 1. Structures of the nucleosides studied.

ocal assignments have been made.[1] The resonances attributable to the ribose carbon atoms are, as noted in earlier examples,[1,4] relatively invariant to changes in the nitrogen base, with the exception of some 2,6-disubstituted pyrimidine ribosides studied. Assignments of the ribose and heterocyclic carbon resonances in all of the compounds studied rely on the observation of changes in shifts corresponding to specific structural modifications in the molecule. Many of the fundamental arguments for these assignments have been discussed earlier.[1] Consequently, we will discuss here only those structural features which provide differences from those presented previously.

Ribose Carbon Atoms. The ordering of the shifts C-1′, C-4′, C-3′, C-2′, C-5′, and C-4′, C-1′, C-3′, C-5′, C-2′, in the direction of increasing field, in the ribosides and deoxyribosides, respectively, has been established.[1,4] The present data provide no exceptions to the ordering though several variations in absolute shifts resulting from structural changes are to be noted. Thus in the 2′,3′-*O*-isopropylidene derivatives VII, VIII, and XVII the range of shifts for C-1′ to C-4′ is considerably reduced (12 ppm compared with 20 ppm). Unequivocal assignments for these lines have not been obtained. It is clear that the geometrical changes produced by isopropylidenation are reflected in the changes

Table I: Carbon-13 Chemical Shifts in Selected Pyrimidine Nucleosides[a]

Nucleoside	Carbon positions								
	C-2	C-4	C-5	C-6	C-1′	C-2′	C-3′	C-4′	C-5′
I	−22.09	−33.18	+7.45	−5.05	+39.94	+57.18	+54.33	+42.66	+66.17
II	−22.35	−31.50	+31.77	−12.84	+38.85	+58.20	+53.49	+42.79	+67.21
III	−22.11	−31.52	+31.97	−12.68	+42.58	(+88)[b]	+57.67	+40.05	+66.67
IV	−22.10	−33.35	+11.71	+4.48	+39.87	+57.01	+54.47	+42.72	+65.82
V	−21.79	...	...	...	+39.01	+57.90	+53.62	+42.59	+67.08
VI	−20.91	−29.06	−8.85	...	+37.88	+57.11	+54.95	+42.83	+65.53
VII[c]	−27.66	−42.02	+20.28	−11.46	(+35.15	+47.49	+43.30	+40.76)	+66.54
VIII[d]	−26.86	−42.43	+20.93	−11.79	(+33.93	+47.63	+45.37	+42.63)	+66.87
IX	−27.15	−36.34	+8.75	−23.64	+40.23	+56.91	+52.64	+43.03	+64.71
X	−26.05	−38.30	...	−29.00	+37.93	+58.35	+53.48	+43.23	+67.21
XI	−23.60	−13.89	−27.35	−35.84	+40.09	+57.30	+56.49	+43.04	+65.12
XII	−23.49	−13.45	+27.25	−35.67	+46.97	+91.62	+56.63	+41.68	+66.06
XIII	−22.82	−28.96	+33.36	−33.62	+40.09	+57.31	+56.52	+43.22	+65.18
XIV	−23.01	−28.75	+33.19	−34.01	+46.43	+90.62	+56.30	+41.20	+65.71
XV	−20.72	−8.22	+14.10	−65.42	+34.56	+57.74	+55.96	+43.00	+65.35
XVI[e]	−32.23	−44.04	+19.02	−9.25	+38.65 (3)		+52.73 (1)		+66.78
XVII[f]	−22.17	−35.33	+37.86	−33.32	(+38.76	+43.06	+44.29	+45.85)	+50.35
XVIII	−21.76	−20.84	...	−21.76	+39.14	+57.43	+56.12	+42.90	+65.17
XIX	−38.89	−39.52	+87.21	−24.00	+39.03	+57.19	+55.46	+42.75	+64.78
XX	−22.91	(−35.47)	+25.03	−13.11	+38.02	+58.27	+55.53	(−34.33)	+42.17
XXI	−23.48	−36.02	+17.99	−8.83	+39.34	+90.41	+47.78	+40.71	+52.33
XXII	−31.90	−42.87	+34.86	−19.13	+41.01	+52.61	+52.61	+41.48	+66.80
XXIII	−22.91	−14.97	+27.56	−36.05	+42.42	+52.09	+52.09	+42.89	+66.81
Uridine	−23.38	−36.20	+25.46	−13.68	+39.42	+57.42	+53.66	+42.58	+66.30
Thymidine[g]	−23.06	−36.37	+18.02	−8.80	+43.47	+88.10	+56.87	+40.10	+66.17
Cytidine	−28.42	−38.17	+32.85	−14.29	+38.41	+57.96	+53.40	+43.16	+66.65
6-Methylcytidine[h]	−28.82	−37.66	+31.99	−26.83	+35.62	+57.39	+56.63	+42.36	+65.23

[a] Shifts given in ppm relative to benzene and positive values indicate higher field. [b] Approximate shift for C-2′: obscured by DMSO peak. [c] Isopropylidene carbons at +14.75, +100.79, and +102.56 ppm; methoxy carbon at +72.50 ppm. [d] Isopropylidene carbons at +13.81, +100.85, and +102.49 ppm. [e] Numbers in parentheses indicate intensities. [f] Isopropylidene carbons at +16.10, +101.74, and +103.33 ppm. [g] Methyl group at +115.28 ppm. [h] Methyl group at 10+7.65 ppm.

noted in the shifts. The downfield shift at C-5′ (*ca.* −16 ppm) in 5′,6-anhydro-2′3′-*O*-isopropylidene-6-hydroxyuridine (XVII) reflects the effect of the bridge structure at this position. A similar downfield shift (*ca.* −14 ppm) is also noted at C-5′ in 3′,5′-anhydrothymidine (XXI), while the effect at C-3′ is smaller in magnitude (*ca.* −9.0 ppm with respect to the resonance of C-3′ in thymidine). In the cycloside, 2,2′-anhydrouridine (XVI), the uncertainties in the geometrical features prevent absolute assignment of the triple and single intensity lines corresponding to C-1′ through C-4′. It is apparent that geometry does play an important role in determining the shifts of the ribose carbon atoms.

In 1-(5-deoxy-β-D-erythropent-4-enofuranosyl)uracil (XX) the resonances at +38.02, +58.27, and +55.53 are similar enough to those regularly observed for the C-1′, C-2′, and C-3′ carbons, respectively, to suggest their assignment. The lines at +42.17 and −34.33 ppm must therefore be assigned to C-4′ and C-5′ (note that the remaining lines in the spectrum are in positions corresponding to those found in uridine). The lower field line of this pair is assigned to C-4′ due to the enolic structure (CH_2=C–O–) now found about C-4′. The shift at C-4′ is thus downfield −76.9 ppm, while that at C-5′ is downfield −14.1 ppm from the corresponding lines in uridine. In 1-(2,3-dideoxy-β-D-glyceropent-2-enofuranosyl)thymine, described previously,[1] the shifts at C-2′ and C-3′ are downfield −55.8 and −61.3 ppm, respectively.

In 1-(β-D-arabinofuranosyl)cytosine (XXII) and 1-(β-D-arabinofuranosyl)uracil (XXIII) the resonances corresponding to the carbon atom pairs C-1′, C-4′, and C-2′, C-3′ are almost coincident. The spectral similarity in the ribose carbon region for both of these compounds suggests that the observed resonances are characteristic of a β-D-arabinofuranoside. Thus the carbon-13 chemical shifts enable characterization of ribosides, deoxyribosides, arabinosides, and a variety of anhydronucleoside structures. Figure 2 shows typical spectra of the riboside carbon atoms in these characteristic environments.

Pyrimidine Carbon Atoms. The ordering of the chemical shifts in uridine and cytidine, of which many of the present compounds are derivatives, have been established.[1] Consequently, we are interested here only in the modification of these shifts occurring upon substitution. Carbon-13 substituent effects have been

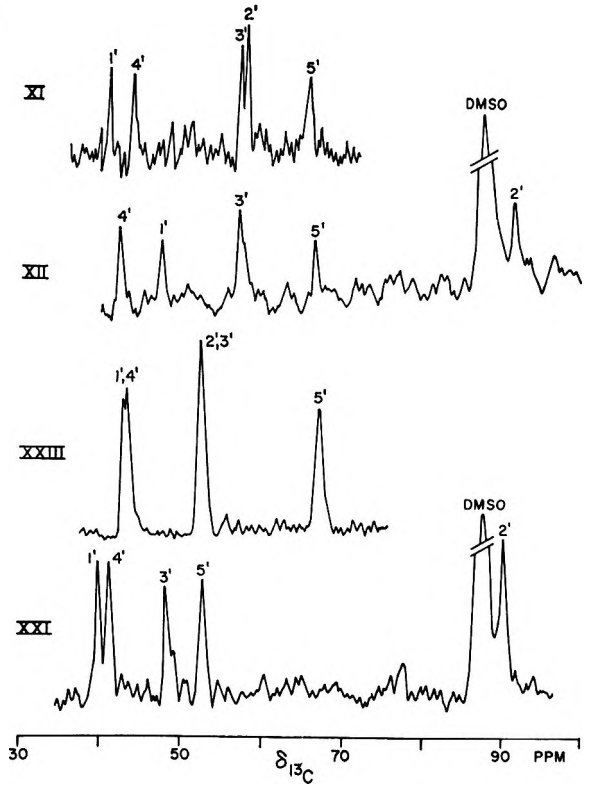

Figure 2. Typical spectra of the sugar carbon atoms in a riboside, deoxyriboside, arabinoside, and deoxyanhydronucleoside.

measured in monosubstituted benzenes[5] and in 2-, 3-, and 4-substituted pyridines.[6] In the present limited pyrimidine series the substituent effects observed are clearly in the same direction as previously noted.[5,6] The magnitudes of these effects, however, differ from those previously reported suggesting that modified sets of parameters are necessary for each type of ring system studied.

Thus in thymidine a downfield shift (−7.4 ppm) was reported[1] at the position of substitution (C-5), while at C-6 an alkene β-substituent effect (+5.3 ppm) occurred, compared with uridine. Negligible shifts were observed at C-4 and C-2. In 5-hydroxyuridine (I) the line assigned to C-5 is also shifted downfield (−18 ppm) relative to that in uridine, while at C-6 an upfield shift of 8.6 ppm is observed. In this case not only are the shifts at C-5 and C-6 relatively larger but also those at C-2 (downfield −1.3 ppm) and C-4 (upfield 3 ppm) are not negligible. No contributions from tautomeric structures in this compound were evidenced. In 5-aminouridine (IV), C-5 is shifted downfield (−13.7 ppm), C-6 upfield (18.2 ppm), while the shifts at C-2 and C-4 resemble those in the 5-hydroxyuridine. The shifts in the 5-bromouridine (II) and 5-bromo-2′-deoxyuridine (III) provide an interesting contrast. An upfield shift of 6.4 ppm is observed at C-5 while C-2 and C-4 shift downfield −1.0 and −4.7 ppm, respectively, and C-6 upfield 1 ppm. In 5-fluorouridine the coupling between fluorine and C-5, C-4, and C-6 prevented observation of these resonances even after prolonged scanning.

In general, the observed substituent effects on the carbon-13 shifts in 5-substituted pyrimidines provide no particular exceptions in direction, although they do differ in magnitude, to those generally observed on substitution of aromatic[5] or heterocyclic[6] ring systems. It might therefore be expected that similar electronegativity relationships, substituent parameter, and related effects would equally apply in these cases.

It should be noted that similar substituent effects are observed in 6-methylcytidine[1] and 6-hydroxycytidine (IX) in which C-6 is shifted downfield −12.8 and −9.4 ppm, respectively. However, the shift at C-5 in 6-hydroxycytidine (IX) is downfield (−24.1 ppm) (compare with the upfield shift of +8.6 ppm observed in 5-hydroxyuridine). This shift is presumably attributable to the expected contribution from the tautomeric form (XXIV) in this compound and suggests that the equilibrium lies strongly toward this form.

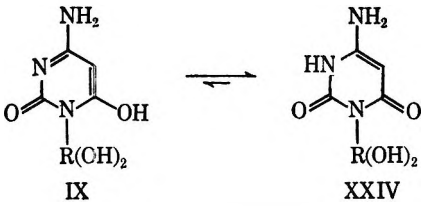

($R(OH)_2$ is used for β-D-ribofuranosyl)

The spectrum of 6-azauridine (VI) has only three carbon-13 resonances in the pyrimidine region. Only one of these lines is substantially different in position compared with the parent to suggest its assignment to C-5. In 5-azacytidine (X), however, the resonance due to C-6 is shifted to lowest field (−29.0 ppm) as shown by observation of the coupled spectrum in which only the lines due to the quaternary carbon atoms C-2 and C-4 were observed in the pyrimidine region. The shifts at C-5 in VI (−34.3 ppm) and C-6 in X (−14.7 ppm) are substantially different in magnitude and serve to emphasize the important electron density contribution to the C-5 shift in uridine.

The structural modifications of an anhydronucleoside have been discussed so far in terms of the ribose carbon shifts. The shifts of the pyrimidine ring carbons involved in anhydronucleoside formation are also modified considerably. Thus in 2,5′-anhydro-2′,3′-*O*-isopropylideneuridine[1] all the carbon resonances shift downfield relative to uridine as shown in Table II. Similarly, the shifts observed in the 2-methoxy and 2-amino compounds VII and VIII and the other anhydronucleosides studied show the same effect (see

(5) H. Spiesecke and W. G. Schneider, *J. Chem. Phys.*, **35**, 731 (1961).

(6) H. L. Retcofsky and R. A. Friedel, *J. Phys. Chem.*, **71**, 3592 (1967); **72**, 290, 2619 (1968).

Table II). The similarity in the majority of the shifts (Table II) observed in VII compared with 2,5′-anhydro-2′,3′-*O*-isopropylideneuridine emphasizes the relative absence of interactions between the sugar and pyrimidine moieties in the nucleosides. Further, the shifts in VIII suggest that the amino substituent is almost identical in its electronic effects to the methoxyl substituent. In 2,2′-anhydrouridine (XVI) these effects differ slightly in magnitude but are in the same direction.

Table II: Carbon-13 Shifts in Some Cyclosides and Related Compounds

Compound	δ_{13C} relative to corresponding shifts in uridine			
	C-2	C-4	C-5	C-6
2,5′-Anhydro-2′,3′-*O*-isopropylideneuridine (ref 1)	−5.60	−6.42	−6.60	−1.61
VII	−4.28	−5.82	−5.16	+2.22
VIII	−3.48	−6.23	−4.51	+1.89
XVI	−8.85	−7.84	−6.42	+4.43
XVII	+1.26	+0.87	+12.86	−19.64

It is therefore apparent that the majority of the shifts occurring on anhydronucleoside formation can be reconciled in terms of substituent effects. All of the results suggest a correlated polarization of charge throughout the ring system.

The assignment of the resonances due to C-2 and C-4 in 5′6-anhydro-2′,3′-*O*-isopropylidene-6-hydroxyuridine (XVII) are based on the structural similarity at these positions compared with uridine. The chemical shifts at C-5 and C-6 in XVII compared with uridine and the 2,5′-anhydronucleosides (Table II) provides a contrast. A downfield shift would be expected at C-6, the position of substitution in XVII, but the upfield shift at C-5 is less readily accounted for. It is probable that this shift arises from an "ortho-substituent contribution" of the electron donor at C-6. These effects were also observed in the 4-methylthio derivatives of 5′,6- and 2,5′-anhydronucleosides described in an earlier communication.[7] The effect of electron donation from a group adjacent to C-5 is also apparent in the shift of C-5 in cytidine (+32.85 ppm) compared with the derivative of its isomer, 2′,3′-*O*-isopropylidene isocytidine (VIII), +20.93 ppm. The remaining shifts at C-2, C-4, and C-6 in these compounds are remarkably similar.

The 3-ribosyl uracils XI–XV provide further structural variations to the nucleoside series. For convenience we have numbered these systems from the nitrogen atom attached to the sugar (see Figure 1) and, therefore, for the sake of clarity we refer to these compounds by Roman numerals instead of by name. The

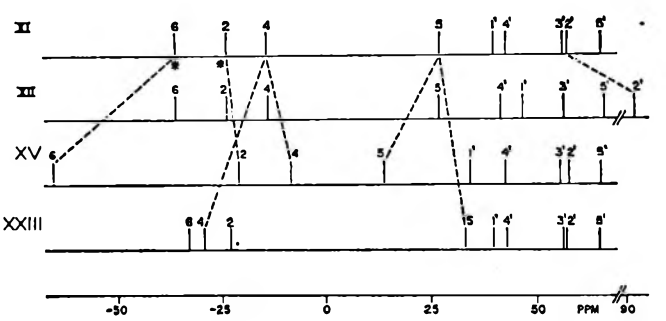

Figure 3. Carbon-13 chemical shift correlations showing the assignments in the 3-(β-D-ribofuranosyl)uracils. Asterisk indicates lines observed in the coupled spectra.

carbonyl carbons are numbered C-2 and C-6. The spectra of this group of compounds exhibit four carbon resonances, which have been assigned from consideration of substituent effects as shown in Figure 3. In the coupled spectrum of XI only the lines at -23.6_0 and -35.8_4 ppm are observed and must therefore be assigned to the carbonyl carbons C-2 and C-6. Substitution of sulfur for oxygen in the carbonyl group at C-6 (XV) in XI provides a significant downfield shift (−29.58 ppm) for the lowest field line in this pyrimidine group. On this basis this line is attributed to C-6, while that at -23.6_0 ppm must be assigned to C-2. The resonance due to C-2 in XV is shifted upfield (2.88 ppm) while that at $+27.3_5$ ppm is shifted downfield (-13.2_5 ppm) and that at −13.89 ppm is shifted upfield (5.67 ppm). This pattern of shifts is similar to that characteristically observed in the uridines and cytidines upon thiation[1] and suggests that the highest field line be attributed to C-5. The assignment of the carbon atom C-4 was confirmed by the downfield shift (-15.0_7 ppm) for this position observed in the 4-methylthio derivative (XIII). The chemical shift order C-6, C-2, C-4, and C-5 is thus established in the 3-(β-D-ribofuranosyl)-uracil derivatives. The large upfield shifts at C-5 (6.0_1 ppm) in the 4-methylthio derivatives XIII and XIV reflect an increase in electron density at this position, presumably because of the electron donor (SCH_3) adjacent to it.

It has been noted that the chemical shifts of the sugar carbon atoms observed in all the ribosides studied have been relatively invariant to the nitrogen heterocycle. However, in (XV) the C-1′ ribose carbon atom resonance is shifted downfield (-5.5_3 ppm) while the other carbons are relatively unaffected. Similar downfield shifts were noted at C-1′ in 2,4-dithiouridine (−5.21 ppm) and 2-thiocytidine (−4.32 ppm) compared with the parent systems.[1] These shifts appear to be characteristic of substitution of a highly polarized group at C-2 and C-6 and therefore may be attributed to an

(7) A. J. Jones, M. W. Winkley, and D. M. Grant, *Tetrahedron Lett.*, 5197 (1969).

inductive withdrawal of electrons at C-1′ through three-bonds.

Assignment of the carbon-13 shifts in 1-(β-D-ribofuranosyl)cyanuric acid (XVIII) are relatively unambiguous. As shown in Figure 4 the two equivalent carbonyl carbon atoms C-2 and C-6 give rise to a resonance at −21.76 ppm having twice the intensity of that due to C-4 at −20.84 ppm. However, in 1-(β-D-ribofuranosyl)barbituric acid (XIX) only three pyrimidine carbon resonances were observed for a solution in dimethyl sulfoxide. XIX may be best represented in its triketo form and evidence presented here indicates that the triketo form is predominant.

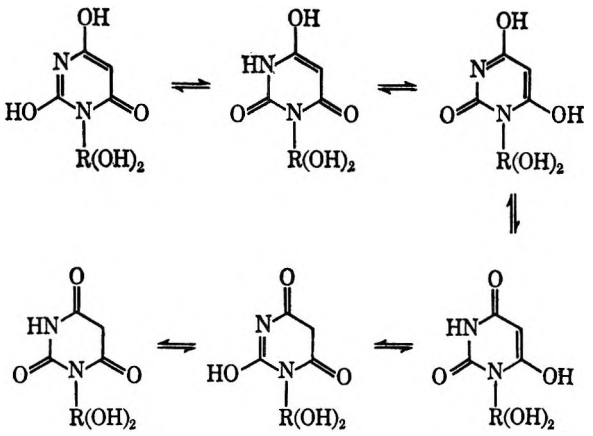

($R(OH)_2$ is used for β-D-ribofuranosyl)

A line which is obscured by the dimethyl sulfoxide peak was observed for the solution in N,N-dimethylformamide as shown in Figure 4. It is clear that the three carbonyl shifts are not abnormal but that the resonance attributable to C-5 (+87.21 ppm) is not only in the region typical for a methylene carbon but is also less intense compared with the other pyrimidine or ribose carbon resonances in the spectrum. The low intensity at C-5 is indicative of the tautomerism represented above. In previous pmr studies Fox, *et al.*,[8] have reported that the methylene proton resonances cannot be seen readily. For further comparison of the chemical shifts the spectrum of uridine is included in Figure 4.

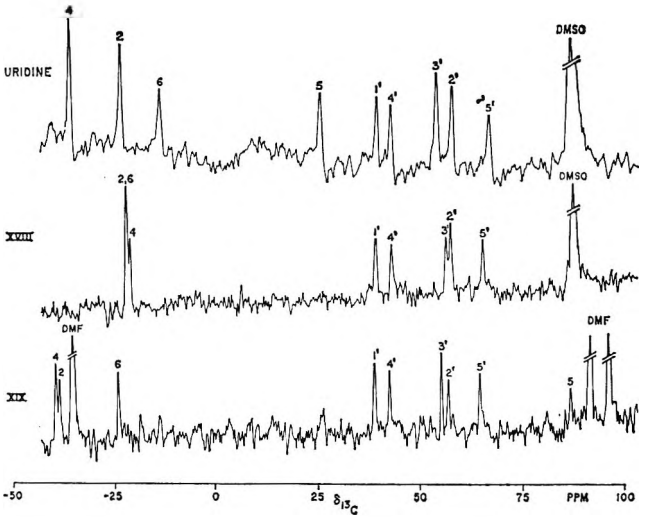

Figure 4. The natural abundance carbon-13 spectra of uridine, 1-(β-D-ribofuranosyl) cyanuric acid, and 1-(β-D-ribofuranosyl)-barbituric acid. Note the high-field resonance due to the methylene carbon C-5 in the latter.

Conclusions

In the present paper we have outlined some of the characteristic carbon-13 shifts observed in nucleosides. A wide variety of structural changes have been considered but spectral assignments have been possible in all but a few cases. It is clear from the results presented that a number of problems in nucleoside and nucleotide chemistry are susceptible to solution using carbon-13 magnetic resonance techniques. We have considered to date only the neutral species in highly polar media. Dorman and Roberts[4] have shown in the naturally occurring nucleotides there is also some dependence on pH. Possible temperature effects are also suggested from the above results on 1-(β-D-ribofuranosyl)barbituric acid. The future of carbon-13 studies in this most important area of bio-organic chemistry therefore seems certain.

Acknowledgment. This work was supported by Grants GM-08521-09 and CA-08109-04, National Institutes of Health, U. S. Public Health Service.

(8) B. A. Otter, E. A. Falco, and J. J. Fox, *J. Org. Chem.*, **34**, 1390 (1969).

Studies of Surface Reactions of Nitric Oxide by Nitrogen-15 Isotope Labeling. I. The Reaction between Nitric Oxide and Ammonia over Supported Platinum at 200–250°

by K. Otto, M. Shelef, and J. T. Kummer

Scientific Research Staff, Ford Motor Company, Dearborn, Michigan 48121 *(Received February 9, 1970)*

The catalytic interaction between NO and NH_3 is an undesirable side reaction in the oxidation of NH_3 to nitric acid, and an important selective reaction for the removal of NO from waste effluents. Details of this reaction were investigated by circulating mixtures of $^{15}NH_3$, ^{14}NO, and Ar in a gradientless batch reactor over a sample of Pt supported on alumina. The reaction products and their relative ratios were $^{14}N^{15}N:{}^{15}N^{14}NO:{}^{14}N_2O:{}^{14}N_2 = 50:13:32:6$. A corresponding product distribution was obtained when switching the ^{15}N-isotope label from NH_3 to NO. A change of the partial pressure of NH_3 or an increase of the temperature from 200 to 250° had little effect on the product distribution. Nitrogen is formed predominantly from the interaction of one molecule of NH_3 and one molecule of NO, while nitrous oxide, in contrast, is formed mainly by the interaction of a pair of NO molecules, presumably with chemisorbed hydrogen obtained from dissociative chemisorption of NH_3. The results can be described by two generalized sets of reactions. In the first set either $^{14}N^{15}N$ or $^{15}N^{14}NO$ is formed. Chemisorbed hydrogen, liberated thereby, is consumed in the second set of reactions to reduce ^{14}NO to $^{14}N_2O$ or $^{14}N_2$. The experimentally observed distribution agrees well with the distribution of the reaction products as given by the balance of the hydrogen intermediate.

Introduction

The interaction of ammonia and nitric oxide, resulting in nitrogen and water, is considered as an undesirable side reaction when ammonia is oxidized industrially to nitric acid and as the cause of the "defixation" of nitrogen.[1-4] Obviously, in practice, conditions are chosen so as to minimize the extent of this reaction. With the industrial gauze catalysts of Pt and Pt-base alloys, employed at high space velocities and temperatures of 750–950°, the defixation of nitrogen can be largely avoided. Oxygen chemisorption is believed to inhibit the reaction in the case of Pt catalysts at high temperatures.[1,3]

Under different conditions, namely at lower temperatures, the reaction between NO and NH_3 takes place on a wide variety of catalytic surfaces; now it proceeds selectively in the presence of oxygen. This process has formed the basis for a series of patents dealing with the purification of industrial and automotive effluents containing NO, prior to their release into the atmosphere. Among these are patents assigned to Engelhard Industries[5] employing supported catalysts containing metals of the platinum group, Co, Ni, and Fe; to Ethyl Corp.[6] employing catalysts containing Cu promoted by Pd; to BASF[7] employing the oxides of V, Mo, and W; and to Hamburger Gaswerke[8] employing a mixture of Cr and Fe oxides. The selective reduction of NO by NH_3 in the presence of oxygen has also been documented in the open literature.[9-12]

At the same time it is well known that under most circumstances the catalytic reduction of NO with reducing agents not containing nitrogen lacks such a selectivity in the presence of oxygen, and, on the contrary, the oxygen reacts in preference to the nitric oxide. The products of NO reduction, N_2 or N_2O, require for their formation the close proximity of two nitrogen atoms, and intuitively it appears that this difficult formation of the N–N bond may be facilitated by supplying one N atom each from either of the reactants, as is the case in the reaction between NO and NH_3. Some indirect evidence that this indeed may be the case has been brought by Michailova,[1] but direct proof is lacking.

(1) E. A. Michailova, *Acta Physicochim. URSS*, **10**, 653 (1939).

(2) V. S. Yakovlev, *Ukr. Khim. Zh.*, **30**, 289 (1964).

(3) Ya. M. Fogel, B. T. Nadykto, V. I. Shvachko, V. F. Rybalko, and I. E. Korobchanskaya, *Kinet. Katal.*, **5**, 942 (1964).

(4) S. N. Ganz and A. M. Vashkevich, *Khim. Tekhnol.*, **9**, 89 (1967).

(5) (a) J. G. E. Cohn, D. R. Steele, and H. C. Andersen, U. S. Patent 2,975,025 (1961); (b) H. C. Andersen and C. D. Keith, U. S. Patent 3,008,796 (1961); (c) H. C. Andersen, J. G. E. Cohn, and R. C. Glogau, U. S. Patent 3,032,387 (1962); (d) H. C. Andersen, U. S. Patent 3,053,613 (1962); (e) C. D. Keith and P. M. Kenah, U. S. Patent 3,328,115 (1967).

(6) M. E. Griffing, F. W. Lamb, and R. E. Stephens, U. S. Patent 3,449,063 (1969).

(7) H. Nonnenmacher and K. Kartte, U. S. Patent 3,279,884 (1966).

(8) K.-H. Schmidt and V. Schulze, German Patent 1,259,298 (1968).

(9) H. C. Andersen, W. J. Green, and D. R. Steele, *Ind. Eng. Chem.*, **53**, 199 (1961).

(10) (a) M. Markvart and V. Pour, *J. Catal.*, **7**, 279 (1967); (b) *Chem. Prum.*, **19**, 8 (1969).

(11) S. Jaros and J. Krizek, *ibid.*, **17**, 581 (1967).

(12) M. Shelef and J. T. Kummer, Preprint 13f, 62nd Annual Meeting of The American Institute of Chemical Engineers, Washington, D. C., Nov 1969.

. As will be demonstrated below, the elucidation of this question is a problem well suited for the use of reactants NO and NH_3 alternately labeled by the stable ^{15}N isotope. The investigation has revealed that under the conditions of the experiment the reaction products, besides water, consist roughly of equimolar amounts of nitrogen and nitrous oxide. The nitrogen molecules are predominantly derived by combining nitrogen atoms from both reactants. Simultaneously, another very important and apparently faster process takes place, leading mainly to nitrous oxide. In this case both of the nitrogen atoms are derived, in the main, from nitric oxide molecules.

Experimental Section

A. Catalyst. A platinum catalyst was prepared by impregnating crushed Al_2O_3 pellets (Kaiser alumina) with a solution of platinum black dissolved in aqua regia. The catalyst was dried for several hours at 125° and then calcined in air at 600° for 8 hr. The levels of impurities in the alumina, evaluated by spectrographic analysis, were within the following limits (in ppm) $1 < Fe < 100$, $1 < Si < 100$, $1 < Mg < 10$, $1 < Cu < 10$, $Ga < 1$. The size of the catalyst granules ranged from 1200 to 1500 μ. The bulk density was 0.7 g/cm^3; the average pore radius was 30 Å.

Chemical analysis showed that the platinum content of the catalyst was 0.81 wt %, which is equivalent to 2.5×10^{19} Pt atoms per gram of catalyst. A reduced platinum surface was prepared by exposing the catalyst to hydrogen at 450° for 3 hr and subsequently removing adsorbed water and hydrogen by evacuating it for several hours at the same temperature. The platinum surface was characterized by its capacity to adsorb at room temperature oxygen on a reduced bare surface and hydrogen both on an oxidized and a reduced bare surface. The adsorption of oxygen on a reduced surface, followed by evacuation, also at room temperature, produced the oxidized state of the platinum surface. All three adsorption isotherms were measured in a pressure range from 100 to 300 Torr. The chemisorbed quantities of oxygen and hydrogen, respectively, were calculated by extrapolating the isotherms to zero pressure. These amounts at $p \to 0$ yielded the ratio O_2 (bare surface): H_2 (bare surface):H_2 (oxidized surface) = 1:2:4, within 4 %.

Assuming that each platinum atom in the surface adsorbed one atom of oxygen on a reduced bare surface,[13] it followed that there were 4.07×10^{18} platinum atoms present on the surface per gram of catalyst which is ~16% of the total number of Pt atoms. The total surface area was determined by argon adsorption at the temperature of liquid nitrogen, using the BET method, as 194 m^2/g. Only ~0.2% of the total surface was occupied by Pt atoms.

B. Purity of Gases. Nitric oxide was purified by vacuum distillation as described in a previous publication.[14] Great care was taken to remove nitrous oxide completely. Small amounts of nitrogen were tolerated, since nitrogen appeared as a stable reaction product and was included in the gas analysis. Other ordinary gases used in the reaction or in calibrating the mass spectrometer were purified by standard methods until extra mass spectrometric peaks caused by contaminants were completely eliminated. Nitric oxide and ammonia labeled by ^{15}N (Isomet Co.), contained, according to mass spectrometric analysis, 4.0% ^{14}NO and 11.5% $^{14}NH_3$, respectively, as isotopic impurities.

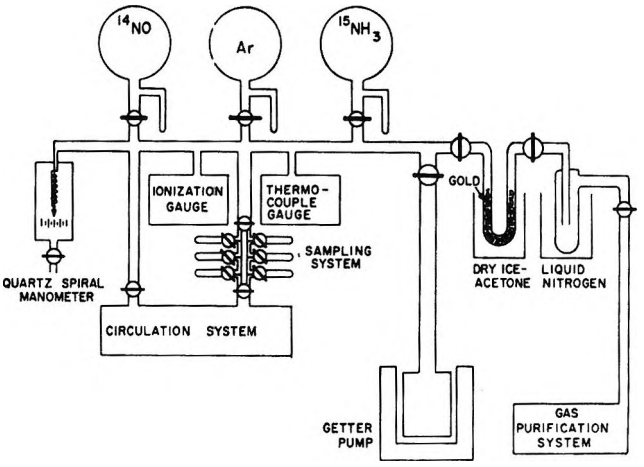

Figure 1. The experimental setup.

C. Apparatus. A diagram of the vacuum apparatus employed is given in Figure 1. The important parts of this system were kept free from mercury vapor by using a quartz spiral manometer for pressure measurements and a VacIon getter pump to evacuate the system. Mercury present in adjacent parts was kept out by two cold traps; one of them was kept in liquid nitrogen, the second one, containing gold bits, was immersed in a Dry Ice–acetone bath. Ammonia, labeled by the ^{15}N isotope, was released slowly from a storage vessel into the circulation system. After the desired ammonia pressure had been reached, the circulation system was closed. Then ^{14}NO was admitted to the circulation system, where the ammonia was kept temporarily at a cold spot. The ammonia temperature was low enough to keep its pressure below one Torr, but high enough so as not to condense out the admitted NO. A pressure of 300 Torr of argon was finally added and the cold spot removed to vaporize the ammonia. The three components were mixed thoroughly for at least 1 hr by the pumping unit of the circulation system which is shown in detail in Figure 2. The unidirectional magnetic pump employed a glass piston filled with iron filings and made tight by Teflon tape wrapping. The adjustable pumping speed was measured by a flow meter. The flow rate was 300–400 cm^3/min and the

(13) D. E. Mears and R. C. Hansford, *J. Catal.*, 9, 125 (1967).
(14) K. Otto and M. Shelef, *ibid.*, in press.

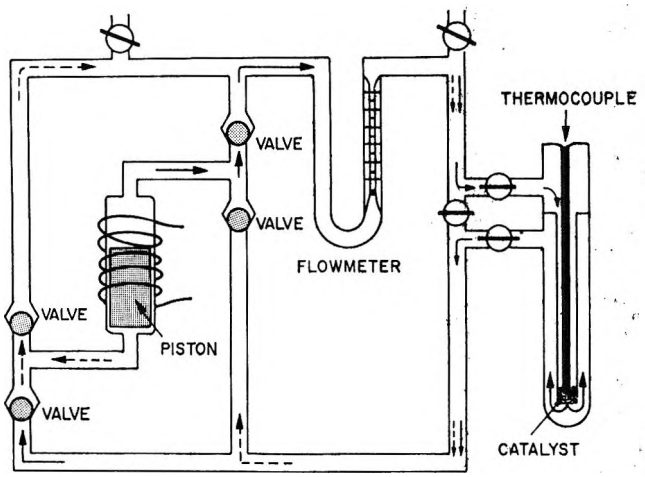

Figure 2. Details of the circulation system.

volume of the circulation system, including the reactor, was 303 cm^3. Thus, the gas volume was completely recirculated approximately once every minute. The reaction was started by opening the two stopcocks at the reaction vessel, while closing at the same time the stopcock located between them. The well-mixed reactants were pushed through the center tube of the reactor to contact the catalyst which was sitting on a fritted disk. Only 0.25 g of the catalyst was used for most of the experiments. The reactor was provided with a thermocouple well for measuring the catalyst temperature. From time to time a small gas volume was released into a detachable sampling system, shown in Figure 1.

D. Gas Analysis. The gas samples were analyzed by a CEC 21-103 mass spectrometer, using a gas pressure of 0.05 Torr, an ionization voltage of 70 V, and a current of 50 μA. A strict time schedule was obeyed. Mass peaks were examined at least up to mass number m/e 90. The mass spectrometer was calibrated with chemically pure Ar, $^{14}N_2$, $^{14}N_2O$, ^{14}NO, H_2O, and H_2, correcting for nitrogen contamination in case of nitric oxide. The presence of isotopic impurities was taken into account. A distinction had to be made between doubly ionized nitrogen molecules and nitrogen atoms with a single charge produced in the mass spectrometer. These two species fall on the same m/e ratio when derived from either $^{14}N_2$ or $^{15}N_2$ but on different m/e ratios when derived from a $^{14}N^{15}N$ parent molecule. The discrimination was possible after calibrating the mass spectrometer with a nitrogen mixture containing large amounts of $^{14}N^{15}N$.

It is also interesting to note that analysis by the mass spectrometer makes it possible to distinguish between isotopic molecules $^{14}N^{15}NO$ and $^{15}N^{14}NO$. The reason is that the nitrous oxide molecule has a large probability of being fractured in the mass spectrometer, under the influence of the electron beam, to form ions of NO and N. This NO fragment falls on m/e 30 in case of $^{15}N^{14}NO$, but on m/e 31 in case of $^{14}N^{15}NO$, the oxygen atom being attached at one end of the nitrous oxide molecule. During the course of this work it was found that the oxygen atom in the nitrous oxide produced by the reaction remained attached to the nitrogen atom to which it was bonded before the reaction in the NO molecule. A complete scheme of the pertinent fragmentation pattern is given in Table I. As each of the isotopic species must be taken into account as a separate compound, there are 14 different components which have to be considered. Correspondingly, 14 mass peaks are needed for analysis. Those which are listed in Table I were found to give the most consistent results. The corresponding relative sensitivities, with respect to nitrogen, of the mass spectrometer are given in the last line of Table I for each compound.

The mathematical analysis is straightforward, using those constants which determine, together with the observed peaks heights, up to 14 simultaneous equations, whose solution is easily obtained by computer. It is seen that most of the mass peaks have contributions from several compounds; *e.g.*, at m/e 15 the peak may be composed of up to eight different fragments. It is obvious that in such a multicomponent system, with many of the components present at a low concentration level, the accuracy of the analyses is considerably limited.

The analyses were complicated by the fact that the reaction was accompanied by a decrease in the total number of moles during the reaction. This decrease was amplified by some adsorption of water and ammonia on the alumina support. The loss was taken into account by using the constant amount of argon as a reference. The absolute amount of any component in the system was calculated by multiplying the amount which was derived from the mass spectrometric analysis by the ratio of the Ar peak heights at the beginning and at the end of a given time interval.

Corrections were also applied to account for the isotopic impurities present in the reactants, and the results given refer to reactants which are isotopically pure.

Experimental Results

The primary concern of this investigation was the reduction of ammonia by nitric oxide. However, a few other reactions which were considered as being possibly involved in the overall catalytic process were also cursorily studied. Since ammonia is known to be chemisorbed dissociatively on many catalytic sufaces, Pt among them, it is of interest to study the effect of additional hydrogen. A second point of concern was the reduction of N_2O by NH_3 as a possible secondary reaction. Finally, it had to be ascertained that the support material did not add significantly to the reaction. A listing of the experiments performed is given in Table II.

Table I: Mass Spectrometer Fragmentation Patterns and Relative Sensitivities of the System Components

No.	m/e	1 Ar	2 $^{14}N_2$	3 $^{14}N^{15}N$	4 $^{15}N_2$	5 $^{14}N^{15}NO$	6 $^{15}N^{14}NO$	7 $^{14}N_2O$	8 $^{15}N_2O$	9 ^{14}NO	10 ^{15}NO	11 $^{14}NH_3$	12 $^{15}NH_3$	13 H_2O	14 H
1	2											0.01025	0.01025	0.0076	1
2	14		0.1046	0.0394		0.1308		0.1308		0.0825		0.0289			
3	15			0.0394	0.1046		0.1308		0.1308	0.02115	0.0825	0.0918	0.0289		
4	16					0.0438	0.0438	0.0438	0.0438	0.01445	0.01445	0.9087	0.0918	0.0328	
5	17											1	0.9087	0.2807	
6	18											0.0102	1	1	
7	28		1					0.1085							
8	29			1		0.1085	0.1085								
9	30				1		0.3215	0.3215	0.1085	1					
10	31					0.3215			0.3215		1				
11	40	1													
12	44							1							
13	45					1	1								
14	46								1						
Relative sensitivities		0.727		1.000				1.267		0.928		1.550		1.502	2.018

Table II: Initial Conditions of the Performed Experiments

Run no.	Reactants[a,b]	Temp, °C
1	60 ^{14}NO + 60 $^{14}NH_3$	200
2	60 ^{14}NO + 60 $^{15}NH_3$	200
3[c]	60 ^{15}NO + 60 $^{14}NH_3$	200
4	120 ^{14}NO + 30 $^{15}NH_3$	200
5	120 ^{15}NO + 30 $^{14}NH_3$	200
6	120 ^{14}NO + 30 $^{15}NH_3$	225
7	120 ^{15}NO + 30 $^{14}NH_3$	250
8	120 ^{14}NO + 30 $^{15}NH_3$	250
9	90 $^{14}N_2O$ + 60 $^{14}NH_3$	200
10	60 ^{14}NO + 30 H_2	200
11	60 ^{14}NO + 30 H_2 + 40 $^{15}NH_3$	200
12	60 ^{14}NO + 60 $^{15}NH_3$	250

[a] The numbers in front of the reactants represent absolute initial pressures (in Torr). [b] The reactants were always diluted by approximately 300 Torr of Ar. [c] Weight of the Pt catalyst was 0.25 g, except for run 3 which was studied with 0.5 g. The influence of the support material on the NO reduction was evaluated on 2.5 g of the bare alumina support (run 12).

A. The Reaction between NO and NH_3. The distributions of the reaction products observed during the reaction between NO and NH_3 for two different concentrations and at different temperatures are listed in Tables III to VI. Water is excluded from the listed reaction products; its quantitative analysis is considered unreliable because considerable amounts of water disappear from the gas phase by adsorption mostly on the inert support surface. The only reaction products besides water were found to be nitrogen and nitrous oxide. It is therefore possible to describe the overall reaction by a linear combination of the two equations

$$4NH_3 + 6NO = 5N_2 + 6H_2O \quad (1)$$

and

$$2NH_3 + 8NO = 5N_2O + 3H_2O \quad (2)$$

The water formed can be calculated correspondingly and the losses of ammonia by adsorption, again apparently on the support surface, can also be assessed. The nitrogen-containing reaction products consisted of the four species $\overline{N}N$, $\overline{N}NO$, N_2, and N_2O, where $\overline{N}$ refers to the nitrogen atom introduced initially with the ammonia, N to that with the NO molecule. Other possible species, *i.e.*, $N\overline{N}O$, $\overline{N}_2O$, and $\overline{N}_2$ were not detected beyond the limits of experimental error.

The analyses were checked by performing a material balance of the nitrogen isotope N which was introduced with the NO molecules. A material balance of $\overline{N}$ could not be obtained, as a portion of the ammonia was always unaccounted for due to adsorption as mentioned above. In a few instances when the balance showed a discrepancy of more than 10%, the data were rejected.

The distribution of reaction products for a mixture containing equimolar amounts of $^{15}NH_3$ and ^{14}NO (run 2 in Table II) is given in the upper half of Table III for $T = 200°$. As the reaction proceeded, the gas was analyzed at discrete time intervals, starting at time zero with the unreacted mixture. The points t_1 and t_2 indicate two of these times and the distribution of the reaction products refers to the reaction which took place within the corresponding interval $t_1 \rightarrow t_2$ given in the table.

Since the analysis is complicated, the results have been checked by switching the ^{15}N label from the ammonia molecule to the nitric oxide molecule (run 3 in Table II). The results are given in the lower half of Table III. The agreement between corresponding percentages in these tables illustrates the reliability of the analysis. The distribution of the products does not show a marked change as a function of time. The largest fraction—almost 50%—consists of the mixed nitrogen, containing one nitrogen atom from $\overline{N}H_3$ and one from NO. Nitrogen which is derived completely

Table III: Distribution of the Reaction Products for the Initial Conditions, 60 Torr of $\overline{N}H_3$ + 60 Torr of NO at 200°

Reactants	$t_1 \rightarrow t_2$, min	$\overline{N}N$, %	$\overline{N}NO$, %	N_2O, %	N_2, %	$\frac{(N_2 + \overline{N}N)}{(N_2O + \overline{N}NO)}$	$\frac{(\overline{N}N + \overline{N}NO)}{(N_2 + N_2O)}$	$\frac{(H_1)}{(H_0)}$
60 Torr of $^{15}\overline{N}H_3$								
60 Torr of ^{14}NO	0–90	48.0	13.8	35.6	2.7	1.03	1.61	1.09
	3–30	42.8	14.6	35.6	7.0	0.99	1.35	0.87
	10–30	48.3	14.2	32.3	5.2	1.15	1.67	1.06
	10–90	49.2	14.3	32.1	4.3	1.15	1.75	1.13
Av values		47.1	14.2	33.9	4.8	1.08	1.59	1.04
60 Torr of $^{14}\overline{N}H_3$								
60 Torr of ^{15}NO	0–90	49.6	13.2	33.5	3.8	1.14	1.68	1.08
	0–270	50.0	13.5	30.5	6.0	1.27	1.74	1.06
	14–270	48.4	15.8	29.3	6.6	1.22	1.79	1.13
	30–270	51.1	11.5	29.8	7.6	1.42	1.67	0.95
Av values		49.8	13.5	30.8	6.0	1.26	1.72	1.06

Table IV: Distribution of the Reaction Products for the Initial Conditions, 30 Torr of $\overline{N}H_3$ + 120 Torr of NO at 200°

Reactant	$t_1 \rightarrow t_2$, min	$\overline{N}N$, %	$\overline{N}NO$, %	N_2O, %	N_2, %	$\frac{(N_2 + \overline{N}N)}{(N_2O + \overline{N}NO)}$	$\frac{(\overline{N}N + \overline{N}NO)}{(N_2 + N_2O)}$	$\frac{(H_1)}{(H_0)}$
30 Torr of $^{15}\overline{N}H_3$								
120 Torr of ^{14}NO	20–300	49.5	11.9	34.8	3.7	1.14	1.60	1.01
	20–1251	48.6	12.2	33.1	6.0	1.21	1.56	0.94
	50–300	49.1	13.5	32.5	4.9	1.17	1.67	1.06
	50–1215	48.4	13.0	31.9	6.8	1.23	1.59	0.96
	110–200	48.6	11.1	34.9	5.4	1.17	1.48	0.90
	110–1215	48.0	11.9	32.8	7.3	1.24	1.49	0.88
	200–300	54.5	7.2	34.0	4.3	1.43	1.61	0.89
Av values		49.5	11.5	33.4	5.5	1.23	1.57	0.95
30 Torr of $^{14}\overline{N}H_3$								
120 Torr of ^{15}NO	20–110	50.9	12.3	29.0	7.8	1.42	1.72	0.99
	20–200	54.6	10.6	29.9	4.9	1.47	1.87	1.08
	20–1165	54.9	10.7	26.0	8.4	1.72	1.91	1.02
	50–300	51.4	12.2	28.2	8.2	1.47	1.75	0.99
Av values		52.9	11.5	28.3	7.3	1.52	1.81	1.02

from NO accounts only for about 5%. About 33% is nitrous oxide which contains only N atoms which were present in the NO molecules, while approximately 14% consists of nitrous oxide containing both types of the two nitrogen isotopes.

The accuracy of the analysis is illustrated more clearly in Figure 3 by plotting the absolute amounts of the reaction products and also the remaining amount of NO as a function of time. The data shown in Figure 3 produce linear plots as a function of $t^{1/2}$, and this is the only reason for representing them in this fashion, and no kinetic implications should be associated at this stage with the chosen manner of representation.

The reaction products are divided into two parts. The first part, indicated by squares, gives the reaction products which contain nitrogen from the NO molecule only. The second part, represented by circles, gives the sum of the reaction products with mixed nitrogen atoms.

In the previous cases there was enough ammonia present to reduce the given amount of NO completely to nitrogen, in accordance with eq 1. In another case the conditions were chosen to supply only enough ammonia for reducing the given amount of NO to nitrous oxide (runs 4 and 5, Table II). These results are listed in Table IV. Within the limits of experimental error the same product distribution observed for equimolar amounts of nitric oxide and ammonia is also found here. An overall average of the percentages obtained at 200° (Tables III and IV) is

$$\overline{N}N:\overline{N}NO:N_2O:N_2 = 49.8:12.7:31.6:5.9 \quad (3)$$

Table V shows that no marked change in the product distribution occurs upon increasing the temperature by 25°. However, at 250° (Table VI) nitrogen derived from NO is approximately doubled, which is associated with an equivalent decrease of the corresponding N_2O; the mixed nitrogen $\overline{N}N$ does not show such an increase.

B. The Influence of Additional Hydrogen. A mixture of 30 Torr of H_2, 60 Torr of NO, and 300 Torr of Ar reacted at 200° over the same catalyst which had been used for studying the reaction between NO and NH_3. The reaction was very fast initially, raising the catalyst temperature by 20°. Within 5 min more than 50% of

Table V: Distribution of the Reaction Products for the Initial Conditions, 30 Torr of $^{15}\bar{N}H_3$ + 120 Torr of ^{14}NO at 225°

$t_1 \rightarrow t_2$, min	$\bar{N}N$, %	$\bar{N}NO$, %	N_2O, %	N_2, %	$\frac{(N_2 + \bar{N}N)}{(N_2O + \bar{N}NO)}$	$\frac{(\bar{N}N + \bar{N}NO)}{(N_2 + N_2O)}$	$\frac{(H_1)}{(H_0)}$
0–60	51.2	8.9	38.7	1.1	1.10	1.51	0.95
0–180	49.7	11.4	33.6	5.4	1.22	1.57	0.94
5–60	51.4	10.9	35.3	2.3	1.16	1.66	1.05
5–180	49.6	12.4	32.0	6.0	1.25	1.63	0.99
12–180	48.9	13.4	32.3	5.4	1.19	1.65	1.03
25–180	47.8	14.6	30.6	6.9	1.21	1.66	1.03
60–180	48.5	13.2	29.8	8.5	1.33	1.61	0.94
Av values	49.6	12.1	33.2	5.1	1.21	1.61	0.99

Table VI: Distribution of the Reaction Products for the Initial Pressures, 30 Torr of $^{15}\bar{N}H_3$ + 120 Torr of ^{14}NO at 250°

$t_1 \rightarrow t_2$, min	$\bar{N}N$, %	$\bar{N}NO$, %	N_2O, %	N_2, %	$\frac{(N_2 + \bar{N}N)}{(N_2O + \bar{N}NO)}$	$\frac{(\bar{N}N + \bar{N}NO)}{(N_2 + N_2O)}$	$\frac{(H_1)}{(H_c)}$
0–12	48.4	14.9	26.4	10.4	1.42	1.72	0.99
0–25	47.8	14.9	26.4	10.8	1.42	1.69	0.96
0–60	46.6	15.4	26.3	11.7	1.40	1.63	0.93
0–135	46.2	15.5	26.5	11.8	1.38	1.61	0.93
5–12	48.4	14.7	25.5	11.4	1.49	1.71	0.96
5–25	47.4	14.9	25.8	11.9	1.46	1.65	0.93
12–25	45.7	15.3	26.4	12.6	1.40	1.56	0.89
Av values	47.2	15.1	26.2	11.5	1.42	1.65	0.94

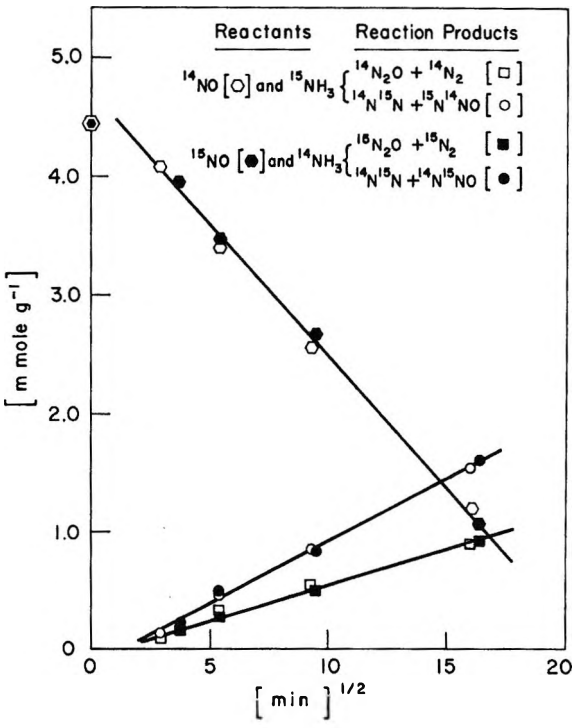

Figure 3. The decrease in the nitric oxide reactant and the formation of the nitrogen-containing products as a function of $\sqrt{t}$, in the NO + NH_3 reaction (runs 2 and 3, Table II).

the admitted hydrogen had reacted and the temperature had returned to 202°. The product distributions for this are given in Table VII, again excluding water. It is seen that the ratio of nitrogen to nitrous oxide is

Table VII: Reduction of NO by H_2 for the Initial Conditions 60 Torr of NO + 30 Torr of H_2, 200°[a]

$t_1 \rightarrow t_2$, min	Disappearance of (NO), mmol/g	Formation of —N-containing products— (N_2), mmol/g	(N_2O), mmol/g	$(N_2)/(N_2O)$
0–5	2.35	0.25	0.77	0.32
0–20	2.46	0.30	0.81	0.37
0–120	2.89	0.47	0.95	0.49
0–1100	3.31	0.60	1.09	0.55
5–20	0.11	0.05	0.04	1.25
20–120	0.43	0.17	0.14	1.21
120–1100	0.42	0.13	0.14	0.93

[a] Amount of NO at start of reaction—4.10 mmol/g of catalyst.

about 1:3 in the interval from 0 to 5 min. This ratio shows a considerable increase with time; *e.g.*, from 120 to 1100 min about equal amounts of N_2 and N_2O were formed as shown in the last column of the table.

It is worth noting at this juncture that the formation of NH_3 is completely absent in the case of the NO–H_2 reaction. Kokes[15] noted the formation of copious amounts of NH_3 when using a similar Pt catalyst in a comparable temperature range, but there was a vastly different ratio of reactants (large excess of hydrogen). Our conclusion on the absence of the ammonia formation is substantiated by the good material balance for nitrogen which can be noted in Table VII.

(15) R. J. Kokes, *J. Phys. Chem.*, **70**, 296 (1966).

Table VIII: Distribution of the Reaction Products for the Initial Conditions, 60 Torr of ^{14}NO + 40 Torr of $^{15}NH_3$ + 30 Torr of H_2 at 200°[a]

$t_1 \rightarrow t_2$, min	(NO) reacted, mmol/g	$\bar{N}N$, %	$\bar{N}NO$, %	N_2O, %	N_2, %	$\frac{(N_2 + \bar{N}N)}{(N_2O + \bar{N}NO)}$	$\frac{(\bar{N}N + \bar{N}NO)}{(N_2 + N_2O)}$
0–9	2.33	9.7	0	82.0	8.3	0.220	0.108
0–50	2.40	11.6	0	80.1	8.3	0.248	0.131
0–200	2.75	19.5	0	71.8	8.8	0.393	0.241
0–1135	3.86	28.4	8.8	45.4	17.4	0.845	0.591

[a] Amount of NO at start of reaction—3.85 mmol/g of catalyst.

In another experiment (run 11, Table II) a mixture of 60 Torr of NO, 40 Torr of $^{15}NH_3$, 30 Torr of H_2, and 300 Torr of Ar reacted at 200° until the NO was used up. Table VIII shows the percentages of the nitrogen-containing products as a function of time. A fast initial reaction was accompanied by a temperature increase of 10°, the temperature had dropped to its original value within 9 min.

C. The Reduction of N_2O by Ammonia. This reaction was studied at 200° with a mixture containing 90 Torr of N_2O, 60 Torr of NH_3, and 300 Torr of Ar. The ratio of nitrogen formed to nitrous oxide disappearing was 4:3, in accordance with the overall stoichiometry $3N_2O + 2NH_3 \rightarrow 4N_2 + 3H_2O$. Comparison of the reaction rate with that of the NO–NH_3 reaction as presented in Figure 3 showed that the reduction of one mole of NO to N_2 and N_2O is nine times faster than the reduction of one mole of N_2O to N_2.

D. Effect of the Support Material. The contribution of the relatively large area of the alumina surface to the catalytic reaction was evaluated in a blank run. The reaction rate for a sample of the bare alumina support measured at 250° was less than 1% of the rate of reaction between NO and NH_3 measured at 200°.

Discussion

At the outset of the discussion we should make it clear that the main object of the study was to measure the product distributions and to deduce therefrom the possible reaction paths. To this end the isotopic study lends itself admirably. No attempt at a kinetic analysis was made at this stage. It is appropriate to point out that, at least during the initial stages of the reaction, the reaction system was not entirely free of mass-transfer limitations. This is shown by applying the criteria of Walker, *et al.*[16]

The condition for which diffusional constraints in the pores of the catalyst can be neglected is given as

$$\frac{dc}{dt} \leq \frac{0.1 C_R D_{eff}}{2R} \qquad (4)$$

where, dc/dt is the reaction rate, C_R is the reactant concentration, D_{eff} is the effective diffusion coefficient, and R is the characteristic diffusion dimension. Our measured initial reaction rate in the time interval from 0 to 25 min for the NH_3–NO reaction is 1.78×10^{-8} mol of NO/sec cm² (external catalyst area), while the calculated right-hand side of eq 4 at 500°K is 2.75×10^{-9} mol/sec cm², *i.e.*, smaller by a factor ~6.5. This means that the diffusional limitations cannot be neglected altogether. Pure Knudsen diffusion and a tortuosity factor of 3 were assumed for this estimation. The diffusion limitations were, of course, more serious for the faster NO–H_2 reaction, and, most probably, insignificant for the slower NH_3–N_2O reaction. This possible involvement of mass transfer does not affect the validity of our subsequent deductions.

The evaluation of the product distribution results is considerably facilitated by the total absence of nitrogen or nitrous oxide molecules containing both N atoms derived from NH_3. This excludes the reaction between two ammonia molecules. Further, in the mixed nitrous oxide the original N–O bond was preserved. This permits the omission of processes which involve bond formation between oxygen and $\bar{N}$.

The following sequence of four overall reaction paths, each of which can be split further into elementary steps, can be postulated, which leads to the observed reaction products of eq 3 (where water was omitted). We write them down for the case of labeled ammonia

$$^{14}NO + {}^{15}NH_3 \longrightarrow {}^{14}N{}^{15}N + H_2O + (H)_{ads} \qquad (5)$$

$$^{14}NO + {}^{15}NH_3 \longrightarrow {}^{15}N{}^{14}NO + 3(H)_{ads} \qquad (6)$$

$$2{}^{14}NO + 2(H)_{ads} \longrightarrow {}^{14}N_2O + H_2O \qquad (7)$$

$$2{}^{14}NO + 4(H)_{ads} \longrightarrow {}^{14}N_2 + 2H_2O \qquad (8)$$

Comparing the set of paths to eq 3 we notice that (5) and (7) are, respectively, major and (6) and (8) minor paths under the reaction conditions of this work. We will show here that the experimentally observed product distribution is in accord with this scheme and try to visualize some of the elementary steps involved.

One can, for instance, subdivide the major path (5) plausibly as

$$^{15}NH_3 \longrightarrow (^{15}NH_3)_{ads} \qquad (5a)$$

$$^{14}NO \longrightarrow (^{14}NO)_{ads} \qquad (5b)$$

(16) P. L. Walker, Jr., F. Rusinko, Jr., and L. G. Austin in *Advan. Catal.*, XI, 170 (1959).

$$(^{15}NH_3)_{ads} \longrightarrow (^{15}NH_2)_{ads} + (H)_{ads} \quad (5c)$$

$$(^{15}NH_2)_{ads} + (^{14}NO)_{ads} \longrightarrow [\text{surface complex I}] \longrightarrow {}^{14}N^{15}N + (H_2O)_{ads} \quad (5d)$$

$$(H_2O)_{ads} \longrightarrow H_2O \quad (5e)$$

The important primary step in this sequence which is relevant to the overall scheme is (5c), the surface dissociation of ammonia.

There is strong evidence that it is the predominant mode of interaction with the surface on a variety of metals.[17-19] We need not invoke, to justify our results, further dissociation such as $(NH_2)_{ads} \rightarrow (NH)_{ads} \rightarrow (N)_{ads}$. This process takes place on Pt only at higher temperatures (>1150°K)[20] and is probably absent in our system.

The overall path (5) is the same as postulated by Schwab[21] and Fogel.[3] The surface complex (I) containing one $\overline{N}$, one N, one O, and two H atoms, could well be the same in the major path (5) and the minor path (6), splitting into a water molecule and a nitrogen molecule in the former case, and as

$$(^{15}NH_2)_{ads} + (^{14}NO)_{ads} \longrightarrow [\text{surface complex I}] \longrightarrow {}^{15}N^{14}NO + 2(H)_{ads} \quad (6a)$$

in the latter.

Incorporation of (6a) into the sequence of the elementary reactions instead of (5d), will lead to (6). The elementary steps must of course include the desorption of the $^{15}N^{14}NO$ product.

Paths 7 and 8 should be in essence the same as those in the reduction of NO by hydrogen. However, there is a paucity of mechanistic studies concerning this process as well. Whenever the formation of N_2O is encountered in a system containing hydrogen, oxygen, and nitrogen, the species HNO (actually a pair or a dimer of the species) is postulated as an intermediate. This is so in the surface oxidation of NH_3,[22,23] gas-phase oxidation of NH_3,[24,25] gas-phase reduction of NO by H_2,[26] and finally also in the surface reduction of NO by H_2.[15,27] Being aware that the actual presence of the HNO intermediate has not been observed in any of these reactions, we nevertheless assume here the formation of HNO groups on the surface

$$(NO)_{ads} + (H)_{ads} \longrightarrow (HNO)_{ads} \quad (7a)$$

and their further clustering into pairs to form the surface intermediate leading to both paths 7 and 8. In the case of path 7 the surface complex is assumed to split according to

$$2(HNO)_{ads} \longrightarrow [\text{surface complex II}] \longrightarrow (N_2O)_{ads} + (H_2O)_{ads} \quad (7b)$$

In path 8 the complex is reduced further by removal of another oxygen atom by a pair of chemisorbed hydrogen atoms.

$$[\text{surface complex II}] + 2(H)_{ads} \longrightarrow N_2 + 2(H_2O)_{ads} \quad (8a)$$

The same scheme for NO reduction by H_2 was proposed by Gonzalez and Audette.[27] We do not enumerate for paths 7 and 8 the obvious adsorption and desorption steps. The proposed surface steps are not considered to be the unique detailed path but only a plausible representation. One could, for instance, postulate a surface complex containing one $(HNO)_{ads}$ and one $(NO)_{ads}$ which then splits into $(N_2O)_{ads}$ and $(OH)_{ads}$, the $(OH)_{ads}$ further recombining with $(H)_{ads}$.

The possibility of the N_2O being readsorbed, and subsequently reduced to N_2, as a major reaction path is eliminated in our system by the following experimental facts. Firstly, N_2O reduction by NH_3 is slower by about one order of magnitude than that of NO. Secondly, there is no change with time in the product distribution toward the decrease of N_2O and increase in N_2. Finally, there is no marked difference in the distribution product when the initial ratios of the reactants are widely varied (compare Tables III and IV). At higher temperatures one would expect the N_2O catalytic decomposition to become more important.

The ratios of the total nitrogen produced to nitrous oxide and that of isotopically mixed products to the products derived wholly from the nitric oxide reactant serve as indicators of the constancy of the product distribution. No consistent changes are observed and the scatter is thought to be associated with the precision of the experiment.

At 250° the internal distribution changes somewhat but both ratios still remain within the bounds of the scatter at lower temperatures. The examination of the distribution shows that at 250°, the relative importance of the minor processes, (6) with respect to (5), and especially (8) with respect to (7), has increased.

The other deviation in the experimental data from this apparent constancy of product distribution is the

(17) C. E. Melton and P. H. Emmett, *J. Phys. Chem.*, **68**, 3318 (1964).

(18) R. E. Mardaleishvili, H. C. Hu, and Ya. Zh. Smorodinskaya, *Kinet. Katal.*, **8**, 786 (1967).

(19) J. W. May, R. J. Szostak, and L. H. Germer, *Surface Sci.*, **15**, 37 (1969).

(20) C. W. Nutt and S. Kapur, *Nature*, **224**, 169 (1969).

(21) G. M. Schwab, H. Noller, and J. Block, in "Handbuch der Katalyse," Vol. 5, G. M. Schwab, Ed., "Heterogene Katalyse II," Springer, Vienna, 1957, p 376.

(22) J. Zawadzki, *Discuss. Faraday Soc.*, **8**, 140 (1950); (see also references therein).

(23) W. Krauss, *Z. Elektrochem.*, **53**, 320 (1949).

(24) D. C. Bull, *Combust. Flame*, **12**, 603 (1968).

(25) D. Husain and R. G. W. Norrish, *Proc. Roy. Soc., Ser. A*, **273**, 145 (1963).

(26) K. A. Wilde, *Combust. Flame*, **13**, 173 (1969).

(27) R. D. Gonzalez and D. E. Audette, *J. Catal.*, in press.

lower value of the unmixed N_2 at short reaction times. This being a minor product, its effect on the above ratios is also minor. At this time only speculative rationalizations of this fact could be offered.

A simple hydrogen balance, assuming a steady state on the surface, affords a reliable experimental check of the proposed scheme. Thus, hydrogen liberated in (5) and (6) is consumed in (7) and (8). There is one H atom liberated for every $\bar{N}\bar{N}$ molecule and three for every $\bar{N}\bar{N}O$, two are consumed for every N_2O formed and four for every N_2. Denoting the hydrogen liberated by H_l and that consumed by H_c, we write at steady state

$$\frac{H_l}{H_c} = \frac{\bar{N}\bar{N} + 3\bar{N}\bar{N}O}{2N_2O + 4N_2} = 1 \qquad (9)$$

The examination of the last column (H_l/H_c) in Tables III–VI, shows this ratio to be fairly close to unity, the averaged values of runs being always within a 5% deviation and the individual measurements within a 10% deviation. This is taken as a direct confirmation of the overall scheme.

The reaction of NO with hydrogen on the Pt catalyst is faster than that with NH_3, notwithstanding the necessity of the N–N bond formation between atoms of two NO molecules. This is witnessed by the rapid initial decrease in H_2 concentration and the concomitant temperature rise. At short times the product distribution is lower in N_2, which is quite similar to that observed in the products from paths 7 and 8 in the overall scheme. In the absence of chemisorbed (NH_2) groups the path leading to N_2 is not a minor one, as seen in Table VII. This may be associated with denser coverage of the surface by H atoms. The possibility of the subsequent N_2O reduction must also be checked under these conditions.

As expected, the fast reaction with hydrogen predominates in the ternary reactant mixture (Table VIII) in the initial stages. The main product initially is N_2O (path 7). This explains both the low ratios of nitrogen to nitrous oxide and of mixed to pure products. As the hydrogen becomes exhausted, the mixed nitrogen $\bar{N}\bar{N}$ formed in path 5 becomes more prominent, increasing both ratios. In the early stages path 6 is totally suppressed, which could plausibly be explained by hampering of the splitting of surface complex I according to (6a), the chemisorbed hydrogen being supplied mainly by the dissociative chemisorption of the gas-phase hydrogen molecules.

While we do not propose a limiting stage for the overall process, it appears that the consumption of the chemisorbed hydrogen atoms is faster than their formation and the limiting step is one of the elementary steps entering the paths 5 and 6. It might well be the dissociative chemisorption of NH_3; if so one could expect noticeable isotopic effects when using deuterated ammonia.[18] This is worthy of further study as well as is the behavior of other catalysts in this interesting surface reaction.

Acknowledgment. The coaching of J. C. Neerman in the use of the mass spectrometer has been paramount to the success of this work. We wish to thank A. G. Piken for help in the literature search.

The Activity Coefficients of *p*-Nitroanilinium Chloride and Bromide in Concentrated Aqueous Salt Solutions at 25°

by Michel Lucas

Section d'Etudes Chimiques et Radioactives, Centre d'Etudes Nucléaires de Fontenay-aux-Roses, France

and Joseph Steigman[1]

Department of Chemistry, Polytechnic Institute of Brooklyn, Brooklyn, New York 11201 *(Received December 15, 1969)*

The molal activity coefficients of *p*-nitroanilinium chloride in dilute acid aqueous solutions containing the alkali chlorides and tetramethylammonium and tetraethylammonium chlorides were determined indirectly. The activity coefficient of the neutral base was calculated from its solubility in the various salt solutions, and the coefficient of the acid was calculated from emf measurements in cells without liquid junctions. The indicator ratio was measured spectrophotometrically, and the stoichiometric concentration of strong acid was known. Several bromide systems were also investigated. The activity coefficient of the indicator salt was highest in LiCl solutions and decreased in the order: NaCl > KCl > CsCl > $(CH_3)_4NCl$ > $(C_2H_5)_4NCl$ over the approximate concentration range 1–5 *m*. In bromide solutions the order was NaBr > KBr > $(C_2H_5)_4NBr$. Some of the results were analyzed by means of the equation $-\log \gamma^{\pm} = [+0.509\sqrt{I}/(1 + \sqrt{I})] - bm$, in which *m* is the molality of neutral salt, and *b* is an empirical coefficient. The *b* coefficient for *p*-nitroanilinium chloride decreased in the order: LiCl > NaCl > KCl. 2,4-Dichloroanilinium chloride and diphenylammonium chloride did not show the same variation.

Introduction

The H_0 value of a dilute aqueous acid solution is changed by the addition of neutral salts.[2-4] If B represents a suitable basic indicator (for example, *p*-nitroaniline) and BH^+ is its conjugate acid, eq 1–3 show the reaction, the equilibrium constant, and the definition which are involved. In eq 2, pK_A^0 is the negative

$$BH^+ \rightleftarrows B + H^+ \quad (1)$$

$$pK_A^0 = \log \frac{[BH^+]}{[B][H^+]} + \log \frac{f_{BH^+}}{f_B f_{H^+}} = pK' + \log \frac{f_{BH^+}}{f_B f_{H^+}} \quad (2)$$

$$H_0 = pK_A^0 + \log \frac{[B]}{[BH^+]} \quad (3)$$

logarithm of the thermodynamic dissociation constant of BH^+, pK' is the corresponding mass action or simple concentration equilibrium constant, and the last term shows the logarithm of the ratio of the molar activity coefficients of the three species of eq 1. The changes produced by neutral salts in the H_0 of an acid solution reflect changes in the activity coefficient term in eq 2. The values of f_B, the activity coefficient of the neutral base, have been estimated—for relatively insoluble indicators—from solubility measurements in the various salt solutions.[2,3,5,6]

$$\log \frac{S^0}{S} = kC_s = \log f_B \quad (4)$$

In this equation, S_0 is the solubility of the base in water, S is its solubility in the salt solution of concentration C_s, k is the Setschenow constant, and f_B is the desired molar activity coefficient (assuming that its value in water is unity). The more critical part of the problem is the interpretation of the ratio of the coefficients f_{BH^+}/f_{H^+} in the salt solutions. In general, the change in the ratio has been attributed to a change in the hydration of the hydronium ion, or to the difference in the change of hydration of the two cations.[4,6-8] The particle hydration, in turn, has been related to the activity of water in the electrolyte solutions. The formulation by Rosenthal, *et al.*, for uncharged bases, which shows an excellent fit for the experimental data, is typical.[4,9]

$$\log \frac{f_B f_{H^+}}{f_{BH^+}} = B\bar{M} + n \log a_w \quad (5)$$

$\bar{M}$ represents the salt molarity, a_w is the measured water activity, and B and n are constants.

(1) To whom inquiries regarding this paper should be addressed.

(2) M. A. Paul, *J. Amer. Chem. Soc.*, 76, 3236 (1954).

(3) M. A. Paul and F. A. Long, *Chem. Rev.*, 57, 1 (1957).

(4) D. Rosenthal and J. S. Dwyer, *J. Phys. Chem.*, 66, 2687 (1962).

(5) F. A. Long and D. McIntyre, *J. Amer. Chem. Soc.*, 76, 3243 (1954).

(6) M. Ojeda and P. A. H. Wyatt, *J. Phys. Chem.*, 68, 1857 (1964).

(7) K. N. Bascombe and R. P. Bell, *Discuss. Faraday Soc.*, 24, 158 (1957).

(8) M. Lucas, *Bull. Soc. Chim.*, 2767 (1966).

(9) D. Rosenthal, I. T. Oiwa, A. D. Saxton, and L. R. Lieto, *J. Phys. Chem.*, 69, 1588 (1965).

The present research is based on a different approach: it is the calculation, by difference, of the activity coefficient of the species BH^+X^- in a dilute solution of the strong acid H^+X^- in the presence of a high concentration of alkali and other monovalent salts M^+X^-. The activity coefficient of H^+X^- has been, or can be, evaluated in solutions of its alkali metal salts from emf measurements of cells without liquid junction. Hence, this approach is much more limited than that described in the preceding paragaph. The present work is confined largely to HCl and HBr solutions of *p*-nitroaniline in the presence of neutral chlorides and bromides. The activity coefficient of the neutral base, f_B, is taken from solubility measurements, as before. For the salt BH^+X^-, a suitable expression (based on eq 2) is

$$\log f_{BH^+}f_{X^-} = 2 \log f^{\pm}(BHX) = pK_A^0 - pK' + \log f_B + \log f_{H^+}f_{X^-} \quad (6)$$

The molar activity coefficients $f_{BH^+}f_{X^-}$ were then changed to molal activity coefficients. The method of calculation is described below.

Experimental Section

Chemicals. The quaternary ammonium salts were of polarographic grade (Carlo Erba). The other reagents were of the highest obtainable commercial purity.

Measurements. Values of pK' of *p*-nitroanilinium halides were determined spectrophotometrically, following Rosenthal and Dwyer.[4] A Maroc spectrophotometer (Jobin and Yvon) equipped with a photomultiplier was used. The solubility of *p*-nitroaniline in a number of salt solutions was measured by the method of Ojeda and Wyatt.[6] Potentiometric measurements were made with a glass electrode and either an Ag–AgCl or Ag–AgBr electrode, in a double-walled cell maintained at 25 ± 0.2°, using a Metrohm E 338 instrument. From duplicate measurements, it is estimated that the values of pK' which we measured are reliable to ±0.05 unit. This applies to measurements in CsCl, NaBr, KBr, and quaternary ammonium halide solutions. The potentiometric measurements in 4 *m* NaBr, 4 *m* KBr, and in the organic salt solutions were reproducible to 1.5 mV.

Calculations. In most H_0 studies the salt concentrations are expressed in molar units, whereas concentrations in emf studies are usually given as molalities. It was therefore necessary to interconvert these differently based concentrations. The term 2 log ($m/\bar{M}$) (m represents salt molality, and $\bar{M}$, the corresponding molarity) was added to 2 log $\gamma^+(H^+X^-)$, (twice the mean molal activity coefficient of H^+X^-). This gave 2 log $f^{\pm}$·(H^+X^-) (twice the mean molar activity coefficient of H^+X^- in the same solution).[10] The resulting molar concentration of salt was now somewhat different from that used in the H_0 measurements. The values of 2 log $f^{\pm}(H^+X^-)$ were then changed by interpolation to those of the salt molarity which was used in the H_0 (or pK') measurement. The values of 2 log $f^{\pm}(BH^+X^-)$ were subsequently calculated by difference, according to eq 6. Finally, these were reconverted to the molal scale by adding the quantity 2 log ($\bar{M}/m$).

The results recorded below for $(C_2H_5)_4NBr$ are uncertain and rest on several assumptions. It has been known for many years that quaternary ammonium iodides and other organic iodide salts form some type of solid compound with AgI in water.[11] It was found that $(C_4H_9)_4NBr$ in concentrated aqueous solution reacts with AgBr.[12] In the present research it was observed that at 25° solutions of $(C_2H_5)_4NBr$ from 0.1 to 0.4 *M* produced no change in solid AgBr, but that from 0.64 *M* to 3.3 *M*, a white compound was formed. This compound was not discolored in visible light. Its composition was $2[(C_2H_5)_4NBr]\cdot 3AgBr$. Because of its apparent dissociation to AgBr in $(C_2H_5)_4NBr$ solutions more dilute than 0.45 ± 0.02 *M*, it was not possible to calculate (by extrapolation in dilute solution) the value of E^0 for the reaction

$$3Ag + 5Br^- + 2(C_2H_5)_4N^+ - 3e \rightleftarrows 3AgBr\cdot 2(C_2H_5)_4NBr \quad (7)$$

Accordingly, the following equation was used for 0.01 *M* solutions of HBr in the various $(C_2H_5)_4NBr$ solutions

$$E_{expt} = E^0_{AgBr-Ag} + 0.0592 \log f_{H^+}f_{Br^-} + 0.0592 \log [H^+][Br^-] + {}^2/_3 \times 0.0592 \log f_{(C_2H_5)_4N^+} \times f_{Br^-}[Br^-][(C_2H_5)_4N^+] \quad (8)$$

The activity coefficients of the quaternary ammonium salt solutions were taken from the paper by Lindenbaum and Boyd.[13] The estimated standard deviation for the calculated values of log $f_{H^+}f_{X^-}$ in this system is ±0.10. The measured emf readings were stable for weeks. The main problem in the interpretation of the measurements arises from the chemical purity and composition of the solid compound. Hence, the derived values of log $\gamma^{\pm}(BH^+Br^-)$ must be taken as tentative.

Most of the H_0 measurements of *p*-nitroaniline in salt solutions were made in 0.1 *M* HCl. It is assumed that the activity coefficient of 0.1 *M* HCl or HBr in concentrated salt solutions has the same value as in more dilute acid solutions in the same salt medium.[14] The acid activity coefficients reported in this paper were measured for 0.01 *M* HCl or HBr solutions.

(10) H. S. Harned and B. B. Owen, "The Physical Chemistry of Electrolytic Solutions," Reinhold, New York, N. Y., 1958, p 11. The original equation includes the term d_0, the density of water. At 25°, this is 0.997, which was rounded off to unity, in view of the much larger errors associated with eq 6.

(11) R. L. Datta and T. Gosh, *J. Amer. Chem. Soc.*, **36**, 1017 (1914).

(12) H. Lilenfeld, B. S. Thesis, Polytechnic Institute of Brooklyn, N. Y., 1966.

(13) S. Lindenbaum and G. E. Boyd, *J. Phys. Chem.*, **68**, 911 (1964).

(14) Reference 10, p 598.

Table I: Values of 2 log $f^{\pm}$(HCl) and 2 log $f^{\pm}$(HBr) in Concentrated Aqueous Salt Solutions at 25°

Salt	Concn, m	2 log $\gamma^{\pm}(H^+X^-)$	$\bar{M}$	2 log $m/\bar{M}$	2 log $f^{\pm}$(HX), interpolated	$\bar{M}$, interpolated
LiCl	1	−0.19[a]	0.98	0.02	−0.17	1
	2	−0.01[a]	1.92	0.04	+0.05	2
	3	+0.22[a]	2.82	0.06	0.33	3
	4	+0.47[a]	3.70	0.07	0.67	4
	5	+0.80[b]	4.53	0.09	1.08	5
NaCl	1	−0.25[a]	0.98	0.02	−0.23	1
	2	−0.11[a]	1.92	0.04	−0.06	2
	3	0.06[a]	2.83	0.06	+0.16	3
	4	0.25[b]	3.69	0.07	0.40	4
	5	0.44[b]	4.51	0.09	+0.67	5
KCl	1	−0.29[a]	0.97	0.03	−0.26	1
	2	−0.21[a]	1.90	0.05	−0.15	2
	3	−0.13[a]	2.74	0.08	−0.01	3
	4	−0.02[b]	3.55	0.10	+0.16	4
CsCl	1	−0.36[a]	0.96	+0.04	−0.32	1
	2	−0.39[a]	1.84	0.07	−0.31	2
	3	−0.35[a]	2.65	0.11	−0.21	3
	4	−0.28[b]	3.40	0.14	−0.05	4
NaBr	1	−0.19[a]	0.97	0.03	−0.16	1
	2	−0.02[a]	1.90	0.05	+0.06	2
	3	+0.18[a]	2.77	0.07	+0.32	3
	4	0.40	3.66	0.10	+0.58[c]	4
KBr	1	−0.28[a]	0.96	0.04	−0.24	1
	2	−0.18[a]	1.86	0.06	−0.10	2
	3	−0.07[a]	2.70	0.09	+0.07	3
	4	+0.01	3.47	0.12	+0.18[c]	4
$(CH_3)_4NCl$	2	−0.55	1.66	−0.16	−0.39[c]	1.66
	3	−0.60	2.30	−0.23	−0.38[c]	2.30
	5	−0.67	3.30	−0.36	−0.41[c]	3.30
$(C_2H_5)_4NCl$	1	−0.48	0.86	−0.13	−0.35[c]	0.86
	2	−0.62	1.50	−0.25	−0.37[c]	1.50
	4	−0.83	2.42	−0.43	−0.40[c]	2.42
$(C_2H_5)_4NBr$	1.21	−0.51	1	0.16	−0.35[c]	1
	3.12	−0.86	2	0.39	−0.47[c]	2
	4.31	−1.02	2.5	0.47	−0.55[c]	2.5
	7.50	−1.48	3.33	0.71	−0.77[c]	3.33

[a] Reference 10, pp 748–750. [b] Harned's rule: see Experimental Section. [c] Present work.

Harned's rule[15] was applied to 5 m LiCl (α_{12} = −0.0055), 5 m NaCl (α_{12} = 0.030), 4 m KCl (α_{12} = 0.066), and 4 m CsCl (α_{12} = 0.097). This last coefficient may be slightly in error because in solutions of CsCl more concentrated than 3.21 M, a solid compound, CsCl·AgCl, is formed.[16] The value of pK_A^0 for *p*-nitroaniline at 25° in water is 0.99.[3]

Results and Discussion

Table I shows the values of 2 log $f^{\pm}$(HCl) and 2 log $f^{\pm}$(HBr) in various aqueous salt solutions at 25°, together with the molal activity coefficients from which they were calculated. The data taken from the literature are rounded off to the second decimal place, although they are more precise. The uncertainty in $\gamma^{\pm}$ in our measurements is about ±0.03.

Table II shows the values of 2 log $f^{\pm}(BH^+X^-)$ and of 2 log $\gamma^{\pm}(BH^+X^-)$ in the salt solutions listed in Table I. The activity coefficients of the neutral base are also listed. The literature values are rounded off to the second decimal place. The uncertainty in the value based on the measurements reported here is of the order of ±0.05 in log $\gamma^{\pm}(BH^+X^-)$ for CsCl, KBr, and NaBr, and somewhat greater for the quaternary ammonium salt solutions.

Table III shows the values of 2 log $f^{\pm}(BH^+X^-)$ and of 2 log $\gamma^{\pm}(BH^+X^-)$ of 2,4-dichloroanilinium chloride (DCA) and diphenylammonium chloride (DPA) in LiCl, NaCl, and KCl solutions. The calculations are based on Paul's measurements,[2] and on the data of Table I. The values of $pK_A^0 - pK'$ and of log f_B are rounded off to the second decimal place.

Some of the relationships which can be seen in Tables II and III were anticipated by Paul.[2] Thus, he had shown that there was a constant increment per unit molarity change in the term $\Delta \log f_{H^+}/f_{BH^+}$ for LiCl, NaCl, and KCl solutions of PNA, a similar

(15) Reference 10, p 600.

(16) M. Lucas, *Bull. Soc. Chem.*, 1792 (1969).

Table II: Values of 2 log $f^{\pm}(BH^+X^-)$ and of 2 log $\gamma^{\pm}(BH^+X^-)$ for PNA in Concentrated Aqueous Salt Solutions at 25°, and Some Related Quantities

Salt	$\bar{M}$	$pK_A^0 - pK'$	log f_B	2 log $f^{\pm}$ (H^+X^-)	2 log $f^{\pm}$ (BH^+X^-)	2 log $\bar{M}/m$	2 log $\gamma^{\pm}$ (BH^+X^-)	
LiCl	1	−0.24[a]	0.09[c]	−0.17	−0.32	−0.02	−0.34	1.02
	2	−0.48[a]	0.18[c]	+0.05	−0.25	−0.04	−0.29	2.09
	3	−0.74[a]	0.26[c]	+0.33	−0.15	−0.06	−0.21	3.20
	4	−1.05[a]	0.33[c]	+0.67	−0.05	−0.07	−0.12	4.36
	5	−1.30[a]	0.40[c]	+1.08	+0.18	−0.09	+0.09	5.58
NaCl	1	−0.20[b]	0.08[b]	−0.23	−0.36	−0.02	−0.38	1.02
	2	−0.41[b]	0.16[b]	−0.06	−0.31	−0.04	−0.35	2.09
	3	−0.62[b]	0.24[b]	+0.16	−0.22	−0.06	−0.28	3.19
	4	−0.82[b]	0.32[b]	+0.40	−0.10	−0.07	−0.17	4.33
	5	−1.03[b]	0.40[b]	+0.67	+0.04	−0.09	−0.05	5.58
KCl	1	−0.15[b]	0.024[b]	−0.26	−0.39	−0.03	−0.42	1.03
	2	−0.29[b]	0.05[b]	−0.15	−0.39	−0.05	−0.44	2.13
	3	−0.44[b]	0.07[b]	−0.01	−0.37	−0.08	−0.45	3.31
	4	−0.58[b]	0.10[b]	+0.16	−0.32	−0.10	−0.42	4.59
CsCl	1	−0.09[c]	−0.05[c]	−0.32	−0.46	−0.04	−0.50	1.05
	2	−0.18[c]	−0.10[c]	−0.31	−0.59	−0.07	−0.66	2.19
	3	−0.27[c]	−0.14[c]	−0.21	−0.62	−0.11	−0.73	3.47
	4	−0.36[c]	−0.19[c]	−0.05	−0.60	−0.14	−0.74	4.87
NaBr	1	−0.20[c]	0.02[c]	−0.16	−0.34	−0.03	−0.37	1.03
	2	−0.40[c]	0.05[c]	+0.06	−0.29	−0.05	−0.34	2.11
	3	−0.60[c]	0.07[c]	+0.32	−0.21	−0.07	−0.28	3.30
	4	−0.78[c]	0.09[c]	+0.58	−0.11	−0.10	−0.21	4.50
KBr	1	−0.18[c]	−0.02[c]	−0.24	−0.44	−0.04	−0.48	1.04
	2	−0.38[c]	−0.05[c]	−0.10	−0.53	−0.06	−0.59	2.18
	3	−0.56[c]	−0.07[c]	+0.07	−0.56	−0.09	−0.65	3.38
	4	−0.74[c]	−0.10[c]	+0.18	−0.66	−0.15	−0.81	4.75
$(CH_3)_4NCl$	1.66	+0.19[c]	−0.30[c]	−0.39	−0.50	−0.16	−0.66	2
	2.30	+0.28[c]	−0.42[c]	−0.38	−0.52	−0.23	−0.75	3
	3.30	+0.43[c]	−0.59[c]	−0.41	−0.57	−0.36	−0.93	5
$(C_2H_5)_4NCl$	0.86	+0.25[c]	−0.37[c]	−0.35	−0.47	−0.13	−0.60	1
	1.50	+0.41[c]	−0.58[c]	−0.37	−0.54	−0.25	−0.79	2
	2.42	+0.72[c]	−1.01[c]	−0.40	−0.69	−0.43	−1.12	4
$(C_2H_5)_4NBr$	1	+0.35[c]	−0.44[c]	−0.35	−0.44	−0.16	−0.62	1.21
	2	0.70[c]	−0.88[c]	−0.47	−0.65	−0.38	−1.03	3.12
	2.50	0.81[c]	−1.14[c]	−0.55	−0.88	−0.46	−1.35	4.31
	3.33	1.12[c]	−1.55[c]	−0.77	−1.14	−0.71	−2.00	7.50

[a] D. Rosenthal and J. S. Dwyer, *Anal. Chem.*, **35**, 161 (1963). [b] Reference 2. [c] Present work.

increment in LiCl solutions of DCA and DPA, but practically none in NaCl and KCl solutions of the latter indicators. The value of the increment per unit molarity change in the term 2 log $f^{\pm}(BH^+X^-)$ − 2 log $f^{\pm}(H^+X^-)$ in the present paper is different from his because of a difference in the value of the Setschenow constant of PNA in LiCl. These increments in the various alkali halide solutions are: about 0.21 for KBr, 0.18 for NaBr, 0.14 for CsCl, 0.19 for LiCl, and 0.12 for NaCl, and KCl. The quaternary ammonium salt solutions showed no regular increment in this term, either on a molality or molarity basis.

Considering the molal activity coefficients of the indicator salts themselves, it appears that there is a regular order in the coefficients of PNA, but not in those of DCA and DPA. The decreasing order of 2 log $\gamma^{\pm}$ for PNA is: in LiCl > NaCl > KCl > CsCl > $(CH_3)_4NCl$ > $(C_2H_5)_4NCl$, and in NaBr > KBr > $(C_2H_5)_4NBr$. In addition, the coefficient is approximately the same in NaBr as in NaCl, but in KCl, it is greater than in KBr. These trends can be seen in Figure 1. On the other hand, the order of 2 log $\gamma^{\pm}$ for DCA is: in KCl > LiCl > NaCl, and for DPA it is: in NaCl > LiCl ≈ KCl. Furthermore, the values of the coefficients for the latter two indicators are consistently higher than those of PNA, and do not show much variation in the solutions of the three salts which were examined. Thus, there appears to be a considerably greater specificity of interaction of the PNA chloride with added inorganic electrolytes than of the DCA and DPA salts.

The difference between the chloride of PNA and those of DCA and PNA in concentrated LiCl, NaCl, and KCl solutions is made more evident in the following equation

$$-\log \gamma^{\pm}(BH^+X^-) = \frac{0.59\sqrt{I}}{1+\sqrt{I}} - bm \qquad (9)$$

Table III: Values of 2 log $f^{\pm}(BH^+X^-)$ and of 2 log $\gamma^{\pm}(BH^+X^-)$ for DCA and DPA in Concentrated Aqueous Salt Solutions at 25°, and Some Related Quantities

Salt	$\bar{M}$	$pK_A^0 - pK'$	log f_B	2 log $f^{\pm}$ (H^+X^-)	2 log $f^{\pm}$ (BH^+X^-)	2 log $\gamma^{\pm}$ (BH^+X^-)	m
				DCA			
LiCl	1	−0.25	0.15	−0.17	−0.27	−0.29	1.02
	2	−0.50	0.29	+0.05	−0.13	−0.20	2.09
	3	−0.74	0.44	+0.33	+0.03	−0.03	3.20
	4	−0.99	0.58	+0.67	+0.26	+0.19	4.36
NaCl	1	−0.20	0.20	−0.23	−0.23	−0.25	1.02
	2	−0.41	0.39	−0.06	−0.08	−0.12	2.09
	3	−0.61	0.59	+0.16	+0.14	+0.08	3.19
	4	−0.81	0.78	+0.40	+0.37	+0.30	4.33
KCl	1	−0.18	0.17	−0.26	−0.27	−0.30	1.03
	2	−0.35	0.34	−0.15	−0.16	−0.21	2.13
	3	−0.53	0.50	−0.01	−0.04	−0.12	3.31
	4	−0.71	0.67	+0.16	+0.12	+0.02	4.59
				DPA			
LiCl	1	−0.29	0.20	−0.17	−0.23	−0.28	1.02
	2	−0.58	0.40	+0.05	−0.13	−0.17	2.09
	3	−0.88	0.60	+0.33	+0.05	−0.01	3.20
	4	−1.17	0.80	+0.67	+0.30	+0.23	4.36
NaCl	1	−0.25	0.27	−0.23	−0.21	−0.23	1.02
	2	−0.50	0.54	−0.06	−0.02	−0.06	2.09
	3	−0.75	0.81	+0.16	+0.22	+0.16	3.19
	4	−1.00	1.08	+0.40	+0.48	+0.41	4.33
KCl	1	−0.18	0.22	−0.26	−0.22	−0.25	1.03
	2	−0.36	0.44	−0.15	−0.07	−0.12	2.13
	3	−0.54	0.66	−0.01	+0.11	+0.05	3.31
	4	−0.72	0.88	+0.16	+0.32	+0.22	4.59

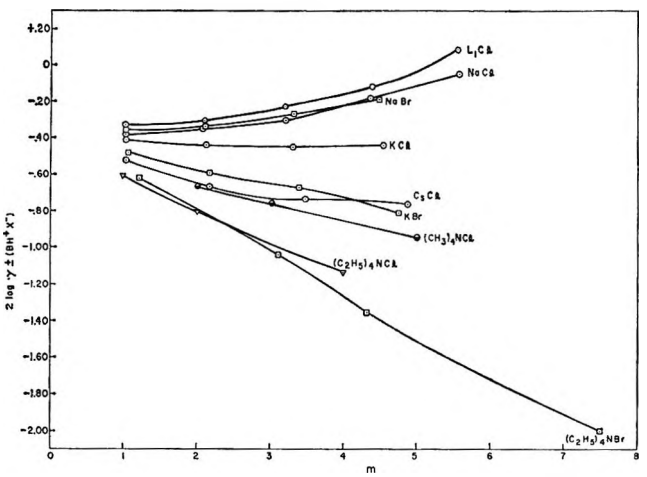

Figure 1. 2 log $\gamma^{\pm}$ of *p*-nitroanilinium chloride and bromide in various aqueous salt solutions plotted against molality of salt.

In this equation, I is the ionic strength, m is the salt molality, and b is a constant. Table IV shows the values of b for the three indicator salts in LiCl, NaCl, and KCl solutions. The data are taken from Tables II and III.

There was a trend to lower values of b with increasing salt concentration in a number of systems, suggesting that a better fit would have been found with an additional parameter. However, the relative magnitudes of the b coefficients for 1 m and 2 m salt solutions were not very different from the mean values shown in Table IV.

Table IV: Values of the b Coefficient for PNA, for DCA and for DPA in LiCl, NaCl, and KCl Solutions

Salt	$b(PNA^+X^-)$	$b(DCA^+X^-)$	$b(DPA^+X^-)$
LiCl	0.073 ± 0.007	0.101 ± 0.005	0.105 ± 0.006
NaCl	0.061 ± 0.002	0.117 ± 0.007	0.130 ± 0.005
KCl	0.038 ± 0.008	0.088 ± 0.012	0.112 ± 0.005

It can be seen that the order of the empirical b coefficients for PNA is: in LiCl > NaCl > KCl. For DCA the order is: in NaCl > LiCl > KCl, and for DPA it is: in NaCl > KCl ≈ LiCl. At the same time, the b coefficients of the two latter indicator salts are consistently higher than those of PNA^+Cl^-, and show much less variation in the different electrolyte solutions. There are evidently structural effects operating which may be due to the nitro group. It is known that this group exerts effects on the activity coefficients of neutral benzenoid molecules in aqueous salt solutions which are quite different from those of other substituents.[17] It appears to exert a specific effect on the activity coefficient of the conjugate acid of PNA as well.

(17) F. A. Long and W. F. McDevit, *Chem. Rev.*, 51, 119 (1952).

Bi-ionic Potential across Charged Membranes

by Yoshinori Toyoshima and Hiroshi Nozaki

Institute of Industrial Science, Tokyo University, Roppongi, Tokyo, Japan *(Received January 28, 1970)*

Theoretical equations were derived for the bi-ionic potential which arises between two uni-univalent electrolyte solutions with different cations separated by a negatively ionizable membrane and for the membrane potential which arises between two solutions of the uni-univalent electrolyte of different concentrations separated by the membrane. In the derivations, it is most critical to assume that the activity coefficients and mobilities of small ions in the membrane are given by the expressions proposed from the expanded "additivity rule" which are usable in multi-ionic systems and to take into account the difference of the standard chemical potential of single-ion species in the membrane phase and in the bulk solution. The theoretical equation for the bi-ionic potential contains four parameters. In order to determine the values of them, the membrane potential data obtained with the corresponding membranes were analyzed by the theoretical equation for the membrane potential. To check the theory for the bi-ionic potential, data are determined with oxidized collodion membranes in three pairs of electrolyte solutions, KCl–NaCl, KCl–LiCl, and NaCl–LiCl. It is demonstrated that these data are fitted accurately by the equation derived.

Introduction

A steady electromotive force of a bi-ionic cell containing two electrolytes AP and BP separated by a membrane is called the bi-ionic potential (BIP).[1] This potential is a measure for the selectivity of a membrane for the ions of the same sign and has been the subject of many theoretical and experimental studies,[2-7] but it appears that no satisfactory results have as yet been established. The mathematically rigorous equations were derived on the basis of the thermodynamics of irreversible processes by Scatchard[8] and Helfferich.[6] In their derivations, however, they considered only a perfectly cation-selective (anion-selective) membrane separating two mixtures of uni-univalent electrolytes with a common anion (cation); *i.e.*, they neglected the effect of flow of anion on the BIP. Moreover, these types of treatment did not provide information about the actual mechanism which produces observed BIP. For the membrane potential which arises between solutions of an electrolyte of different concentrations separated by a uniform membrane, Teorell[9] and Meyer and Sievers[10] derived a first theoretical equation based on a fixed-charge membrane model. Also, recently we[11] integrated flow equations provided by the thermodynamics of irreversible processes under the appropriate assumptions for the mobilities and activity coefficients of small ions in the membrane phase to derive an equation for the membrane potential and found the derived equation agreed with typical experimental data with porous membranes covering wide ranges of concentrations of the external solutions. On the other hand, any theoretical equation for the BIP which would clarify the mechanism which produces the corresponding experimental data has never been given with regard to the moderately selective membrane through which the common anions can partially migrate.

In our previous treatment for the membrane potential, the difference of the standard chemical potential for small ion species in the membrane phase and in the bulk solution was assumed to be negligible for any ion species, since we considered the very porous membrane.

The defects of this assumption become apparent when we study about membranes that are so compact that they have a selectivity not only for ions of the opposite sign but also for ions of the same sign. For a compact membrane, the effective charge density evaluated by analyzing the experimental data of membrane potential according to our previous theory[11] was strongly dependent on the kind of electrolyte used.

In the present paper, we first describe a derivation of the equation for the BIP and membrane potential by integrating the flow equation for anion species which is common in the solutions placed on the both sides of membrane using the appropriate assumptions for the mobilities and activity coefficients of small ions in the

(1) J. R. Wilson, "Demineralization by Electrodialysis," Butterworths, London, 1960.

(2) F. Bergsma and A. J. Staverman, *Discuss. Faraday Soc.*, **21**, 61 (1956).

(3) F. Michaelis, *Kolloid-Z.*, **62**, 2 (1933).

(4) K. Sollner, *J. Phys. Chem.*, **49**, 47, 171 (1945).

(5) C. E. Marshall and C. A. Krinbill, *J. Amer. Chem. Soc.*, **64**, 1814 (1942).

(6) F. Helfferich, *Discuss. Faraday Soc.*, **21**, 83 (1956).

(7) F. Helfferich, "Ion Exchange," McGraw-Hill, New York, N. Y., 1962, p 378.

(8) G. Scatchard, *J. Amer. Chem. Soc.*, **75**, 2883 (1953); *Discuss. Faraday Soc.*, **21**, 30 (1956).

(9) T. Teorell, *Proc. Soc. Exp. Biol. Med.*, **33**, 282 (1935); *Progr. Biophys. Biophys. Chem.*, **3**, 305 (1953); *Z. Elektrochem.*, **55**, 460 (1951).

(10) K. H. Meyer and J. F. Sievers, *Helv. Chim. Acta*, **19**, 649, 665, 987 (1936).

(11) Y. Toyoshima, M. Yuasa, Y. Kobatake, and H. Fujita, *Trans. Faraday Soc.*, **63**, 2803 (1967).

membrane phase. In the derivation, we take into account the effect of the differences of the standard chemical potentials of single ions in the membrane phase and in the bulk solution. Second, we present the bi-ionic potential data which we have determined with oxidized collodion membranes in three pairs of uni-univalent electrolytes covering wide ranges of concentration and show that these data are fitted well by the theoretical equation with the parameters predetermined by the measurements of membrane potentials.

Theory

We consider a system (Figure 1) in which two large compartments contain the aqueous solutions composed of two simple uni-univalent electrolytes AP and BP with different compositions. Here A and B represent the cationic species and P is the common anion. It is assumed that the system is isothermal and there is no electric field applied externally across the membrane. For simplicity, we confine ourselves to the fact that the electric charges carried by the membrane matrix are negative charges and they distribute uniformly with a density X. The solutions are so vigorously stirred that the concentration in each compartment is maintained uniformly except in a thin layer adjacent to the membrane surfaces. These thin layers exert considerable effect for a quantitative interpretation of the phenomena considered. We, however, ignore the stagnant layers in this study only for simplicity. The flow of all components in the membrane is considered to occur only in the direction of membrane thickness. We take the space coordinate x in this direction, its origin being placed on the membrane surface which is in contact with solution 1 (see Figure 1). The value of x for the other membrane surface is denoted by L.

Neglecting interacting flows between ions of different species and the effect of mass flow, the fluxes of ions A, B, and P are given by

$$J_N = -u_N C_N(RT \, \mathrm{d} \ln a_N/\mathrm{d}x + F\mathrm{d}\varphi/\mathrm{d}x) \quad (N = A, B) \quad (1)$$

$$J_P = -u_P C_P(RT \, \mathrm{d} \ln a_P/\mathrm{d}x - F\mathrm{d}\varphi/\mathrm{d}x) \quad (2)$$

where J_i (i = A, B, P) is the flux of ionic species i relative to the frame of reference fixed to the membrane, u_i, C_i, and a_i are the mobility (relative to the local center of mass), molar concentration, and activity of ion i. For the unidimensional flows considered above, the law of mass conservation gives the equation

$$\mathrm{d}J_i/\mathrm{d}x = 0 \quad (i = A, B, C) \quad (3)$$

when the flows are stationary. Hence we have J_N = constant with respect to the axial direction. Rearranging eq 2, the gradient of the electrochemical potential of the anion is represented in terms of J_P, a_P, and $u_P C_P$ as

$$\mathrm{d}\tilde{u}_P/\mathrm{d}x = RT \, \mathrm{d} \ln a_P/\mathrm{d}x - F\mathrm{d}\varphi/\mathrm{d}x = -J_P/u_P C_P \quad (4)$$

The integration of eq 4 between two bulk solutions across the membrane leads to

$$\Delta\tilde{u}_P = -J_P \int_0^L (1/u_P C_P)\mathrm{d}x = -F\Delta\varphi + RT \ln (a_P^{II}/a_P^{I}) \quad (5)$$

where I and II indicate the values in the external solutions 1 and 2 and $\Delta\varphi$ is the difference of the electric potential between two bulk solutions, $\varphi^{II} - \varphi^{I}$, *i.e.*, the BIP in question. Using the steady-state condition, J_P = constant with respect to x, eq 5 may be written to give

$$\Delta\varphi = (J_P/F)\int_0^L (1/u_P C_P)\mathrm{d}x + (RT/F) \ln (a_P^{II}/a_P^{I}) \quad (6)$$

Our problem now is to obtain the steady-state values of J_P and $(1/u_P C_P)$ as functions of the concentrations in the external solutions and of x. It is one of the unsolved problems in the field of polyelectrolyte study to derive exact theoretical expressions for the activities and mobilities of small ions in polyelectrolyte solution.

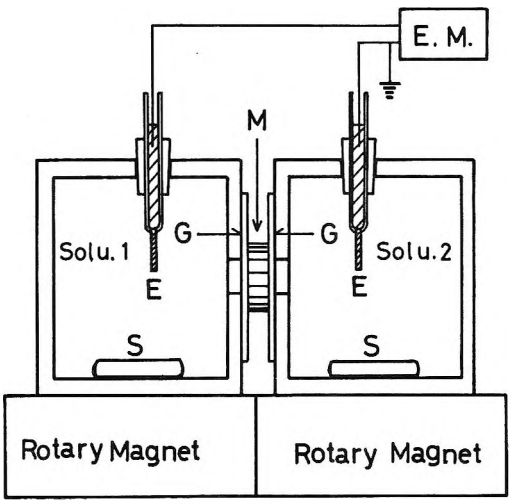

Figure 1. Schematic diagram of the cell used for measurements of the membrane potential and bi-ionic potential: E, Ag–AgCl electrode; E.M., electrometer; M, membrane; G, gasket; S, stirrer.

In the system of negatively ionizable membrane and a uni-univalent electrolyte, however, we had proposed recently the following assumptions for the concentration dependences of u_i and a_i of ion i (i = +,−) in the membrane phase

$$u_+C_+ = u_+^0(C_- + \phi' X)$$
$$u_-C_- = u_-^0 C_- \quad (7)$$

$$a_+ = \gamma_+^0(C_- + \phi X)$$
$$a_- = \gamma_-^0 C_- \quad (8)$$

and succeeded in explaining the experimental data for various transport phenomena occurring through charged membranes by the corresponding theoretical equations derived under these assumptions quantitatively. Here u_i° and γ_i° are the mobility and activity coefficient of ion i in the polyelectrolyte free solution. The quantity ϕX is often called the "thermodynamically effective" concentration of the counterions dissociated from the ionizable groups fixed on the membrane matrix and it is assumed to be independent of the concentration of the added salt. Likewise, $\phi' X$ is taken as the effective concentration of the counterions which can contribute to the diffusion process and also it is assumed to be independent of the concentration of the added salt. For the system of oxidized collodion membrane and uni-univalent electrolyte, we found the values of ϕ and ϕ' were equal to each other.

One of our proposals here is to extend eq 7 and 8 to the system containing two kinds of uni-univalent electrolytes AP and BP with common species as anion. This system is composed of the following four kinds of electrolytes AP, BP, AM, and BM, where M represents the negatively ionizable groups fixed on the membrane skeleton. Following to eq 7 and 8, we propose the expressions for the activities and mobilities for small ions in the membrane.

$$a_A = \gamma_A^0(C_{AP} + C_{AM}\phi)$$
$$a_B = \gamma_B^0(C_{BP} + C_{BM}\phi) \quad (9)$$
$$a_P = \gamma_P^0(C_{AP} + C_{BP})$$

$$u_A C_A = u_A^0(C_{AP} + C_{AM}\phi)$$
$$u_B C_B = u_B^0(C_{BP} + C_{PM}\phi) \quad (10)$$
$$u_P C_P = u_P^0(C_{AP} + C_{BP})$$

Here C_{AP}, C_{BP}, C_{AM}, and C_{BM} are the concentrations of the electrolytes AP, BP, AM, and BM, respectively, and ϕ is a constant characteristic of the given membrane. In addition to these assumptions we assume that the ratio of C_{AM} to C_{BM} is equal to that of C_{AP} to C_{BP}

$$C_{AM}/C_{BM} = C_{AP}/C_{BP} \quad (11)$$

and that the all ions behave idealy in the polyelectrolyte free solution, *i.e.*, $\gamma_i^0 = 1$ (i = A, B, P). The requirement that the electric neutrality must be realized in any element of the membrane gives the relation

$$C_{AM} + C_{BM} = X \quad (12)$$

Solving C_{AM} and C_{BM} from eq 11 and 12 and introducing the resulting expressions into eq 9 and 10, we obtain

$$a_A = C_{AP}[1 + \phi X/(C_{AP} + C_{BP})]$$
$$a_B = C_{BP}[1 + \phi X/(C_{AP} + C_{BP})] \quad (13)$$
$$a_P = C_{AP} + C_{BP}$$

$$u_A C_A = u_A^0 a_A$$
$$u_B C_B = u_B^0 a_B \quad (14)$$
$$u_P C_P = u_P^0 a_P$$

We wish to propose here to use eq 13 and 14 for the activities and mobilities of small ions in charged membranes.

Since in the system considered here no electric field is applied externally across the membrane, no net electric charge is transported from one side of the membrane to the other. This means that the electric current density, I, must be zero at any cross section of the membrane; that is

$$I = F(J_A + J_B - J_P) = 0 \quad (15)$$

Eliminating $(d\varphi/dx)$ from eq 1, 2, and 15 and introducing eq 13 and 14 into $u_i C_i$ and a_i (i = A, B, P) appearing in the resulting expressions, respectively, the following equations for the reduced fluxes of ion species A and B are obtained

$$j_A = \frac{v_B\eta + 2\xi - 1}{v_A\xi + v_B\eta - 1}(d\xi/dx) - \frac{\xi(v_B - 2)}{v_A\xi + v_B\eta - 1}(d\eta/dx) \quad (16)$$

$$j_B = -\frac{\eta(v_A - 2)}{v_A\xi + v_B\eta - 1}(d\xi/dx) + \frac{v_A\xi + 2\eta - 1}{v_A\xi + v_B\eta - 1}(d\eta/dx) \quad (17)$$

Here j_N (N = A, B) is the reduced flux of ion species N defined by $j_N = -(1/RTu_N^0\phi X)J_N$, v_N is defined by $v_N = 1 + u_N^0/u_P^0$ and ξ and η are the reduced concentrations defined by $\xi = C_{AP}/\phi X + C_{AP}/(C_{AP} + C_{BP})$ and $\eta = C_{BP}/\phi X + C_{BP}/(C_{AP} + C_{BP})$. Even in the bulk solution the mobility of a single ion is dependent on its concentration, but we prefer to neglect the concentration dependency of u_N^0 as a first approximation. Taking this assumption into account, we may regard j_A and j_B to be independent of the space coordinate x and hence ξ and η may be obtained as functions of x by solving the simultaneous differential equations, eq 16 and 17, if the values of ξ and η at both membrane surfaces are given as boundary conditions. In order to simplify the calculations, we introduced the following new variables I_1, I_2, ϵ_1, and ϵ_2

$$I_1 = j_1 + j_2 \qquad I_2 = v_1 j_1 + v_2 j_2 \quad (18)$$
$$\xi_1 = \xi + \eta \qquad \epsilon_2 = v_1\xi + v_2\eta \quad (19)$$

Rewritting eq 16 and 17 by using the above variables and solving the resulting equations for $d\epsilon_1/dx$ and $d\epsilon_2/dx$, we obtain

$$d\epsilon_1/dx = I_2(\xi_1 - j)/(2\epsilon_1 - 1) \quad (20)$$
$$d\epsilon_2/dx = I_2[\epsilon_2(1 - 2j) + (2\epsilon_1 - 1)]/(2\epsilon_1 - 1) \quad (21)$$

Combination of eq 20 and eq 21 reads

$$d\epsilon_2/d\epsilon_1 = [\epsilon_2(1 - 2j) + (2\epsilon_1 - 1)]/(\epsilon_1 - j) \quad (22)$$

This equation is easily solved to give the following relation

$$(2j - 1) \ln \left(\frac{\xi_L + \eta_L - j}{\xi_0 + \eta_0 - j}\right) = \frac{j(v_A\xi_0 + v_B\eta_0) - (\xi_0 + \eta_0)}{j(v_A\xi_L + v_B\eta_L) - (\xi_L + \eta_L)} \quad (23)$$

where $j = I_1/I_2$ and ξ_0 and ξ_L are the values of ξ in the membrane phase at $x = 0$ and $x = L$ and η_0 and η_L are the corresponding values of η.

Now let us go back to eq 6 for the BIP. Using the reduced variables, the equation may be rewritten in the following form

$$\Delta\varphi = -(RT/F)I_2(1 - j)\int_0^L \frac{1}{\epsilon_1 - 1}dx \quad (24)$$

Introducing eq 20 into eq 24 and integrating the resulting expression over the membrane thickness, we may easily obtain for $\Delta\varphi$

$$\Delta\varphi = -\left(\frac{RT}{F}\right)\left[\ln\left(\frac{\xi_L + \eta_L - 1}{\xi_0 + \eta_0 - 1}\right) - (2j - 1)\ln\left(\frac{\xi_L + \eta_L - j}{\xi_0 + \eta_0 - j}\right)\right] \quad (25)$$

Following previous workers,[9,12] we assume that at both membrane surfaces the equilibrium distribution for every ion species is maintained between the membrane phase and the external bulk solutions. Neglecting the effect of osmotic pressure produced between the two phases, we may give

$$K_N^2(a_{NP})_1^2 = (a_N)_0(a_P)_0$$
$$K_N^2(a_{NP})_2^2 = (a_N)_L(a_P)_L \quad (26)$$

where $(a_{NP})_1$ and $(a_{NP})_2$ are the mean activities of the electrolyte NP (N = A, B) in bulk solutions 1 and 2, respectively, defined by

$$(a_{NP})_1^2 = a_N^I a_P^I$$
$$(a_{NP})_2^2 = a_N^{II} a_P^{II} \quad (27)$$

$(a_i)_0$ and $(a_i)_L$ (i = A, B, P) are the single-ion activities of species i in the membrane phase at $x = 0$ and $x = L$ and K_N (N = A, B) is defined by

$$1/K_N = \exp[(\mu_N^{om} - \mu_N^{ob} + \mu_P^{om} - \mu_P^{ob})/2RT] \quad (28)$$

In eq 28, μ_N^{om} is the standard chemical potential of cation N in the membrane phase and μ_N^{ob} is that in the external bulk solution and μ_P^{om} and μ_P^{ob} are the corresponding values of anion P. Introducing eq 13 into eq 26 and rewriting the resulting expressions using the reduced quantities, we obtain

$$\xi_0 = (1 + \tau_A^I)/2\delta_A^I \qquad \eta_0 = (1 + \tau_B^I)/2\delta_B^I$$
$$\xi_L = (1 + \tau_A^{II})/2\delta_A^{II} \qquad \eta_L = (1 + \tau_B^{II})/2\delta_B^{II} \quad (29)$$

where τ_A, τ_B, δ_A and δ_B are defined by

$$\tau_A = \sqrt{1 + \left(\frac{2K_A}{\phi X}\right)^2 C_A^2\delta_A} \qquad \tau_B = \sqrt{1 + \left(\frac{2K_B}{\phi X}\right)^2 C_B^2\delta_B} \quad (30)$$

$$\delta_A = \frac{K_B^2C_B^2}{K_A^2C_A^2} + 1 \qquad \delta_B = \frac{K_A^2C_A^2}{K_B^2C_B^2} + 1$$

and I and II indicate the values in solution 1 and 2. In eq, 30 C_N is the concentration of cation N in the external solution. Introduction of eq 30 into eq 23 and 25 leads to

$$(2j - 1)\ln[\{2 + (\tau_A^{II}/2\delta_A^{II}) + (\tau_B^{II}/2\delta_B^{II}) - j\}/\{2 + (\tau_A^I/2\delta_A^I) + (\tau_B^I/2\delta_B^I) - j\}] = \ln[(jv_1 - 1)\{1 + (\tau_A^I/2\delta_A^I)\} + (jv_2 - 1)\{1 + (\tau_B^I/2\delta_B^I)\}] - \ln[(jv_1 - 1)\{1 + (\tau_A^{II}/2\delta_A^{II})\} + (jv_2 - 1)\{1 + (\tau_B^{II}/2\delta_B^{II})\}] \quad (31)$$

$$-\left(\frac{F}{RT}\right)\Delta\varphi = \ln\frac{(1 + \tau_A^{II})/\delta_A^{II} + (1 + \tau_B^{II})/\delta_B^{II} - 2}{(1 + \tau_A^I)/\delta_A^I + (1 + \tau_B^I)/\delta_B^I - 2} - (2j - 1)\ln\frac{(1 + \tau_A^{II})/\delta_A^{II} + (1 + \tau_B^{II})/\delta_B^{II} - 2j}{(1 + \tau_A^I)/\delta_A^I + (1 + \tau_B^I)/\delta_B^I - 2j} \quad (32)$$

In order to compare eq 32 under eq 31 with the corresponding experimental data, it is required that the parameters, K_A, K_B, ϕX, v_A, and v_B can be evaluated by other experiments.

A steady electromotive force which arises between solutions of an electrolyte NP of different concentrations at constant temperature and pressure when they are separated by a membrane has been called the membrane potential, $\Delta\varphi_m$. Using the same basic flow equations and assumptions for the mobilities and activities of the movable ions in the membrane phase as used above, we may easily derive a theoretical equation for $\Delta\varphi_m$, eq 32.

(12) Y. Toyoshima, Y. Kobatake, and H. Fukita, *Trans. Faraday Soc.*, 63, 2814 (1967).

$$(F/RT)\Delta\varphi_m = -\ln\gamma - (1 - 2/\nu_N)\ln\frac{\sqrt{1 + (2C_N^{II}K_N/\phi X)^2} + (1 - 2/\nu_N)}{\sqrt{1 + (2C_N^{I}K_N/\phi X)^2} + (1 - 2/\nu_N)} + \ln\frac{\sqrt{1 + (2C_N^{II}K_N/\phi X)^2} + 1}{\sqrt{1 + (2C_N^{I}K_N/\phi X)^2} + 1} \quad (33)$$

where $\gamma = C_N^{II}/C_N^{I}$. In the derivation of eq 33, the effect of the stagnant layers was neglected. Expansion of eq 33 in powers of $(1/C_N^{I})$ with the concentration ratio being kept constant yields

$$(F/RT)\Delta\varphi_m = -(1 - 2/\nu_N)\ln\gamma - 2(1 - 1/\nu_N)(1/\nu_N)(1 - 1/\gamma) \times (\phi X/K_N)(1/C_N^{I}) + O[(1/C_N^{I})^2] \quad (34)$$

We define the apparent transference number t_- for anion by the Nernst equation

$$-(F/RT)\Delta\varphi_m = (1 - 2t_-)\ln\gamma \quad (35)$$

Introducing eq 34 into eq 35 and expanding $1/t_-$ as a power series in $1/C_N^{I}$, we obtain

$$1/t_- = \nu_N + (\nu_N - 1)[(\gamma - 1)/\gamma \ln\gamma] \times (\phi X/K_N)(1/C_N^{I}) + O[(C_N^{I})^{-2}] \quad (36)$$

Using eq 36, the values of ν_N and $\phi X/K_N$ can be determined from the ordinate intercept and initial slope of a plot for $1/t_-$ against $1/C_N^{I}$ at a given γ.

Experimental Section

Three oxidized collodion membranes having different charge densities and porosities numbered S-1, S-2, and S-3 were prepared by the method of Sollner and Gregor.[13] The charge densities and porosities of the membranes were controlled by adjusting the time of drying and oxidation. Water contents of these membranes are listed in Table I.[14] For measurements of the membrane potential and bi-ionic potential we used each membrane repeatedly with different electrolytes, but no significant change occurred in the measured values of the membrane potential and of the bi-ionic potential when the experimental conditions were identical. Uni-univalent electrolytes examined were KCl, NaCl, and LiCl. Before use, KCl and NaCl were purified by repeated recrystallizations, and LiCl (of analytical grade) was used as delivered. The water used as solvent was prepared by treating distilled water with both cation and anion exchangers.

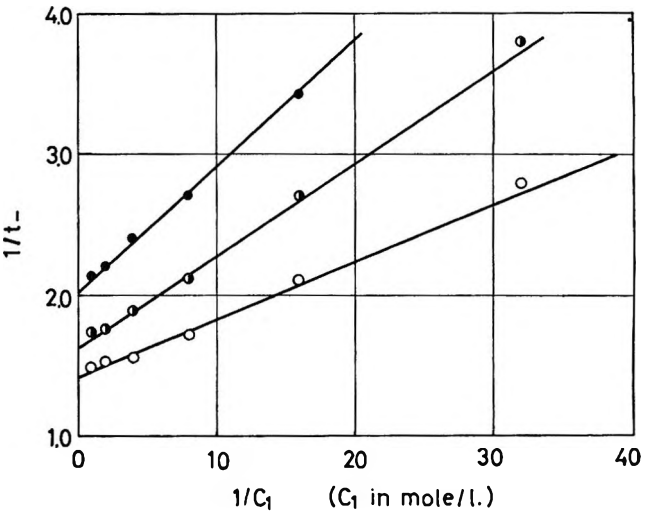

Figure 2. Plots of $1/t_-$ against $1/C_1$ for the systems of membrane S-2 and the three kinds of electrolytes at $\gamma = 2$: ●, KCl; ◑, NaCl; ○, LiCl.

Figure 1 shows a schematic diagram of the apparatus used for measuring the membrane potential and bi-ionic potential. The electromotive force which arose between the bulk solutions was conducted by silver–silver chloride electrodes or by calomel electrodes through saturated KCl bridges and measured by an electrometer (Keithley Instruments 610B Type). The bulk solutions were stirred by a pair of magnetic stirrers in order to be maintained uniform in each concentration. In measurements of the BIP, we confined ourselves that each solution placed in the both compartments involved a kind of electrolyte differs from each other and its concentration was equal to each other, C, in order to simplify the comparison of the theory and experiments. At first, the solutions were left as they were for 1 hr at least till the fluxes of the all species reached to steady state. Then we exchanged them for new identical solutions and measured the emf. On each system five determinations of emf were made. The results agreed with 0.1 mV and their average was taken as a desired result. All measurements were made in an air bath at 30°. The procedure used for mea-

Table I: Some Characteristics of Membrane–Electrolyte Pairs Studied

Membrane	Electrolyte	$\phi X/K_N$,[a] equiv/l.	ν_N	Water content, wt %	$(\nu_N)_{bulk}$[b]	$(K_N/K_{K^+})^2$
S-1	KCl	0.0417	1.95	87.3	1.96	1.000
	NaCl	0.0406	1.65	87.3	1.62	1.051
	LiCl	0.0403	1.48	87.3	1.45	1.070
S-2	KCl	0.120	2.03	29.0	1.96	1.000
	NaCl	0.128	1.62	29.0	1.62	0.820
	LiCl	0.139	1.41	29.0	1.45	0.712
S-3	KCl	0.0372	2.08	21.1	1.96	1.000
	NaCl	0.0405	1.65	21.1	1.62	0.775
	LiCl	0.0451	1.39	21.1	1.45	0.600

[a] Determined by the measurements of membrane potentials in the concentrated regions of electrolyte. [b] The values of ν_N are in the concentration of 0.2 *m*.[14]

(13) K. Sollner and H. P. Gregor, *J. Phys. Chem.*, **50**, 407 (1946); **51**, 299 (1947).

(14) R. A. Robinson and R. H. Stokes, "Electrolyte Solutions," Butterworths, London, 1959, p 465.

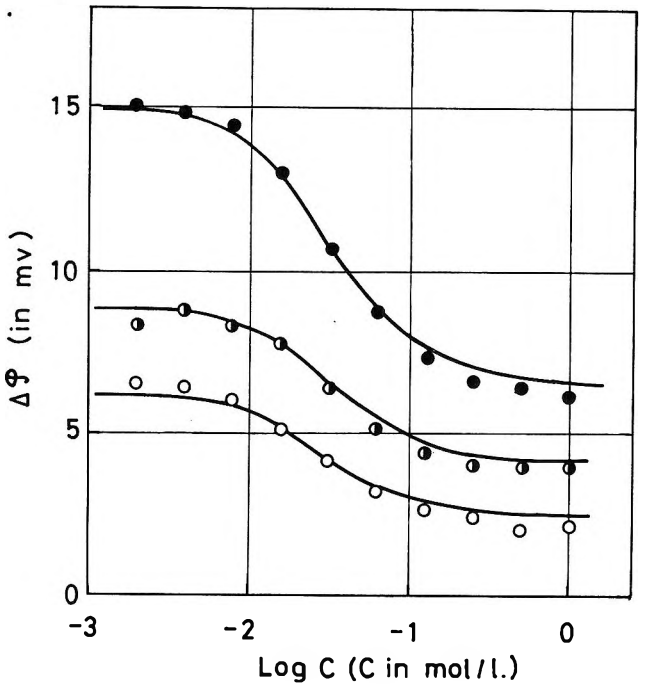

Figure 3. Comparison of eq 38 (together with eq 39) with experimental data of bi-ionic potential for the systems of membrane S-1 and the three pairs of electrolytes. ◑, KCl-NaCl; ●, KCl-LiCl; ○, NaCl-LiCl.

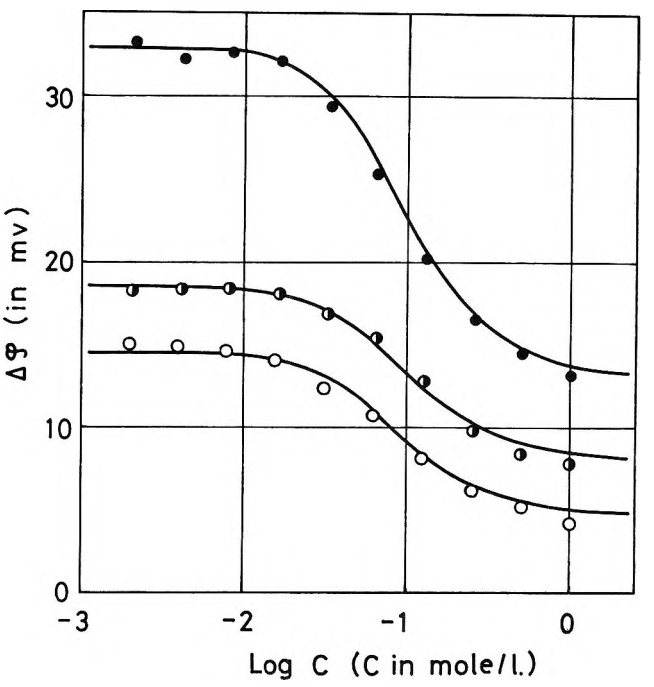

Figure 4. Comparison of eq 38 (together with eq 39) with experimental data of bi-ionic potential for the systems of membrane S-2 and the three pairs of electrolytes. Notations are the same as in Figure 4.

surements of the membrane potential was essentially the same as employed in our previous reports.[12,15] Data were taken as a function of C_N^I at $\gamma = 2$.

Result and Discussion

Figure 2 shows plots for $1/t_-$ against $1/C_N^I$ at $\gamma = 2$ for membrane S-2 with three electrolytes. The results for the other membranes were essentially similar to this graph. The intercepts and slopes of the straight lines indicated in the figures have been used to evaluate the parameters v_N and $\phi X/K_N$ (N = K^+, Na^+, Li^+). Table I summarizes the values of parameters v_N and $\phi X/K_N$ and the water contents for various membrane electrolyte pairs. The $(v_N)_{bulk}$ in the table refers to the ionic mobility in free solution at 2.0 M.[14] Table I shows that for a given electrolyte the values of v_N would hardly depend on the membrane used, and the values agree with the corresponding value of $(v_N)_{bulk}$. Also Table I indicates that $\phi X/K_N$ depends on the pair of membrane electrolyte used. These are the results that might be expected. In our previous work[12,14] for membrane potentials, the difference of the standard chemical potential of single-ion species between the membrane phase and in the bulk solution was neglected. Therefore we can put K_N equal to unity for all ionic species. As a result, the effective charge density, ϕX determined was slightly dependent on the electrolyte used, but we had no explanation for this effect in that stage. However, the dependency of ϕX on the kind of electrolyte was insignificant, since the membranes studied were very porous. The defects of the above

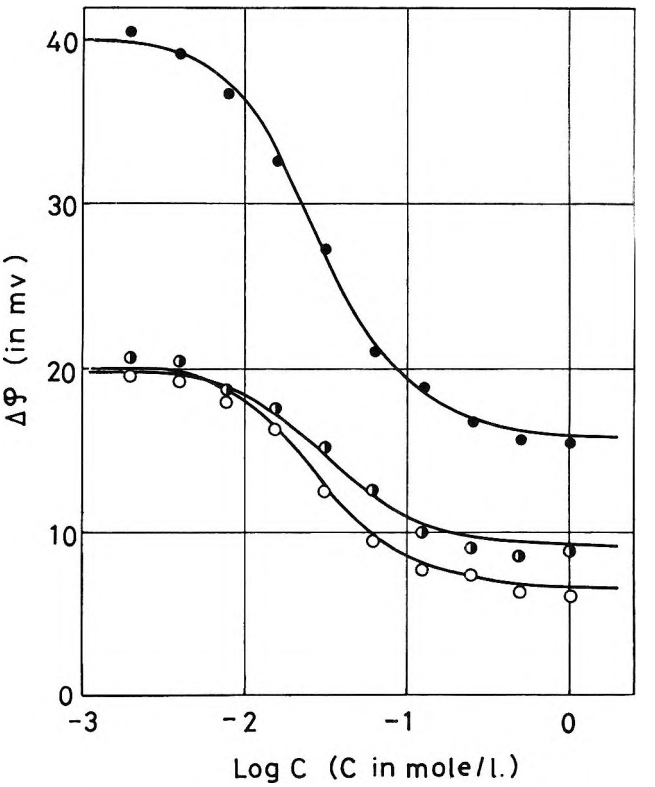

Figure 5. Comparison of eq 38 (together with eq 39) with experimental data of bi-ionic potential for the systems of membrane S-3 and the three pairs of electrolytes. Notations are the same as in Figure 4.

(15) Y. Kobatake, N. Takeguchi, Y. Toyoshima, and H. Fujita, *J. Phys. Chem.*, 69, 3981 (1965).

assumptions became apparent when we studied the compact membranes as used here. Therefore, we prefer to regard $\phi X/K_N$ as a parameter characteristic for the membrane and electrolyte pair in this study.

According to the definition of K_N, $(K_A/K_B)^2$ may be regarded as the selectivity constant of a membrane for positive ion species A to B. The last column of Table I shows that membrane S-1 has no specific selectivity for any cation studied here; however, S-2 and S-3 are more selective for K^+ than Na^+ and Li^+, $K_{K^+} > K_{Na^+} > K_{Li^+}$. It is indicated in Table I that the selectivity of the membranes for the specific cation increases with the compactness of the membranes.

Bi-ionic Potential

Once the values of the parameters v_N, $\phi X/K_N$ for a given membrane–electrolyte system have been determined by measurements of the membrane potential, one may calculate the theoretical $\Delta\varphi$ *vs.* C curve for any system and then compare it with the corresponding experimental data. Considering the experimental condition that each compartment involves a kind of electrolyte different from each other with the same concentration, eq 31 and 32 are reduced to

$$(2j + 1) \ln \{(g_A + 2j)/(g_B + 2j)\} - \ln \{(jv_A + 1)/(jv_B + 1)\} - \ln (g_A/g_B) = 0 \quad (37)$$

$$\Delta\vartheta = [2 \ln (K_A/K_B) + \ln \{(jv_A + 1)/(jv_B + 1)\}](F/RT) \quad (38)$$

where

$$g_N = 1 + \{1 + (2K_N C/\phi X)^2\}^{1/2} \qquad (N = A, B) \quad (39)$$

In Figures 3, 4, and 5, BIP data obtained are plotted against log C (C is the concentration of the external bulk solutions) for the three membranes studied with three pairs of electrolytes and compared to the corresponding theoretical curves calculated from eq 38 and eq 37 using values listed in Table I for parameters. These figures indicate that the calculated curves of $\Delta\varphi$ follow the experimental data satisfactorily down to a relatively small value of C for all systems shown. On the other hand, the theoretical curves of $\Delta\varphi_m$ calculated from eq 33 follow the experimental data only in a range of relatively large values of C_1 and deviate systematically above the latter as C_1 becomes smaller. This disagreement points to some unknown defect of the assumptions or approximations incorporated in the present theory. We shall discuss the disagreement between the theory and experimental data for membrane potentials in the following report.

Acknowledgments. The help of Mr. K. Nakamaru and Mr. T. Takahashi of this laboratory in the meaurements of the BIP is acknowleged.

A Study of the Nature of Active Sites on Zeolites by the Measurement of Heat of Immersion. I. Electrostatic Field of Calcium-Substituted Y Zeolite

by Kazuo Tsutsumi and Hiroshi Takahashi

Institute of Industrial Science, The University of Tokyo, Roppongi, Minato-ku, Tokyo, Japan *(Received June 30, 1969)*

The electrostatic field strengths of Na- and Ca-substituted Y zeolites were determined by the measurements of heats of immersion into various organic liquids. By exchanging Na of Na–Y zeolite for Ca, the field strength increases when the molar exchange ratio exceeds 40%. This fact can be explained by the difference of the cation sites in zeolite. The field strengths are 1.3×10^5 esu/cm^2 for Na–Y and 6.5×10^5 esu/cm^2 for Ca–Y zeolites. These values suggest that the electrostatic field can be the source of the catalytically active center for carbonium ion type reactions of Ca-substituted zeolite.

Introduction

Zeolite is a kind of hydrated aluminosilicate and its ion exchange and adsorption ability have been applied to various uses such as softening hard water, dehydrating, and deodorizing. These years zeolite has been known also to be useful as a catalyst and, since 1960 when Rabo, *et al.*,[1] and Weisz and Frilette[2] reported the reaction data on hydrocarbons and their derivatives on isomerization, cracking, and dehydration by

(1) J. A. Rabo, D. N. Stamires, and J. E. Boyle, *Actes Congr. Int. Catal., 2nd*, 2055 (1960).

(2) P. B. Weisz and V. J. Frilette, *J. Phys. Chem.*, **64**, 382 (1960).

using Linde molecular sieve as catalyst, much investigation has been done into this subject.

There are three kinds of active sites to be useful as catalysts. First, zeolite has pores consisting of 4-, 5-, 6-, 8-, 10-, and 12-oxygen rings, which are of molecular size and act as molecular sieves. Take the ester exchange reaction for example.

$$RCO_2R' + R''OH \rightleftharpoons RCO_2R'' + R'OH \quad (1)$$

If the zeolite adsorbs R'OH selectively, the ester exchange occurs easily because of sieve action when it is added during the above reaction as a cocatalyst besides alkoxide catalyst.[3] Secondly, the zeolite conceivably has acid sites like silica–alumina. They are recognized from amine titration by the Benesi method,[4] esr study of organic ion radicals which adsorb to Lewis acid,[5-7] and ir study of interaction between acid site and base.[8-12] The third is due to the electrostatic field on the zeolite surface which was advocated by Rabo, *et al.*[1,13,14] They calculated the field strength of X- and Y-type zeolite cation sites and showed Y type is stronger. Recently, Boudart, *et al.*,[15] estimated the field strength of the zeolite from the heat adsorption of krypton. In that case, they determined the heat of adsorption by using Clausius–Clapeyron's equation.

The carbon atoms of C–C and C–H bonds of hydrocarbon are polarized by this field into carbonium ions, which act as an intermediate to promote the reaction.

In this paper the quantitative field strength on zeolite surface is obtained by direct calorimetric measurement of heat of immersion into organic liquids, and the change of field strength when exchanging Na of Na-Y type zeolite for Ca is examined.

Theory

The heat of immersion is defined by the difference of energy between solid surface and solid–liquid interface

$$H_i = E_{SL} - E_S \quad (2)$$

where H_i is the heat of immersion, E_{SL} the solid–liquid interface energy, and E_S the surface energy of the solid. The additivity of intermolecular forces being assumed, the experimentally determined heat of immersion per unit surface area can be expressed as the sum of the dispersion force contribution (E_i^d), a polarization force contribution (E_i^α), and a contribution due to the interaction of the permanent dipole of the liquid with the electrostatic field of the solid (E_i^μ).

$$H_i = E_i^d + E_i^\alpha + E_i^\mu \quad (3)$$

The term E_i^μ is given by

$$E_i^\mu = -n\mu F \quad (4)$$

where n is the number of the adsorbed molecules, μ the dipole moment of the liquid, and F the average electrostatic field of solids.

From eq 3 and 4, as the liquid's dipole moment affects the heat of immersion when the solid has electrostatic field on its surface, the field strength F is known by measuring heats of immersion into various kinds of liquids with different dipole moments.

Experimental Section

Faujasite type Na–Y zeolite was synthesized from silica–alumina gel. Its SiO_2/Al_2O_3 mole ratio was 3.25 by chemical analysis and measurement of unit cell dimension by X-ray analysis. Its purity was proved to be 100% by X-ray analysis and water adsorption capacity. The exchange of Na for Ca was made by stirring an aqueous suspension of Na–Y zeolite plus a proper amount of $CaCl_2$ for several hours at 90°. High-exchange species were obtained by repeating the treatment several times with a concentrated $CaCl_2$ solution. Ion-exchange ratio was measured from quantitative analysis by flame photometry for Na and by the EDTA titration method for Ca.

The liquids used were the guaranteed reagents purified by usual methods with dehydrating agents and dried with Linde molecular sieve 4A.

Heat of immersion was measured as follows. After zeolite was put into a glass ampoule and evacuated for 10 hr at 450° under 10^{-5} mm, the ampoule was sealed off and set in the twin conduction type microcalorimeter (Applied Electric Laboratory Co.) with the liquid, until they reached thermal equilibrium at 25°. Then the ampoule was broken and the zeolite was immersed into the liquid. The heat liberated was recorded and calibrated by the known amount of heat.

The BET specific surface area was measured by nitrogen adsorption at liquid nitrogen temperature and calculated from the finite layer adsorption isotherm by use of the BET equation for narrow capillaries.

Results

Table I shows heats of immersion of each zeolite into various organic liquids. The weight of zeolite was

(3) D. P. Roelofsen, J. A. Hagendoorn, and H. van Bekkum, *Chem. Ind.*, 1622 (1966).

(4) A. E. Hirschler, *J. Catal.*, **2**, 428 (1963).

(5) D. N. Stamires and J. Turkevich, *J. Amer. Chem. Soc.*, **86**, 749 (1964).

(6) J. T. Richardson, *J. Catal.*, **9**, 172 (1967).

(7) F. R. Dollish and W. K. Hall, *J. Phys. Chem.*, **71**, 1005 (1967).

(8) J. B. Uytterhoeven, L. G. Christner, and W. K. Hall, *ibid.*, **69**, 2117 (1965).

(9) T. R. Hughes and H. M. White, *ibid.*, **71**, 2192 (1967).

(10) J. W. Ward, *J. Catal.*, **9**, 225, 396 (1967); **10**, 34 (1968); **11**, 238, 251 (1968).

(11) P. E. Eberly, Jr., *J. Phys. Chem.*, **72**, 1042 (1968).

(12) F. R. Cannings, *ibid.*, **72**, 4691 (1968).

(13) P. E. Pickert, J. A. Rabo, E. Dempsey, and V. Schomaker, *Proc. 3rd Intern. Congr. Catal.*, 714 (1964).

(14) J. A. Rabo, C. L. Angell, P. H. Kasai, and V. Schomaker, *Discuss. Faraday Soc.*, **41**, 328 (1966).

(15) Yun-Yang Huang, J. E. Benson, and M. Boudart, *Ind. Eng. Chem. Fundam.*, **8**, 346 (1969).

represented by that of dehydrated species. The heat of immersion into *n*-hexane and *n*-octane, whose dipole moments are 0, is almost constant irrespective of Ca exchange, and any effect expected from the difference in field strength F is not noticed. In case of *n*-butyl alcohol, $\mu = 1.65$ D, the heat of immersion is almost the same as that of Na type when the exchange ratio is low, but Z-IV and Z-V with high exchange ratios show fairly high heats of immersion. In the case of 1-nitropropane, $\mu = 3.57$ D, the heat of immersion becomes remarkably high when the exchange ratio exceeds 40% and the effect of field strength is distinguished. As eq 3 clearly shows, the heat of immersion into the liquid with $\mu = 0$ is decided by E_i^d and E_i^α, but when μ becomes larger and F stronger, E_i^μ becomes dominant and causes higher heat values.

Table I: Heats of Immersion of Zeolites into Organic Liquids at 25°

Sample	Ca exchange, mole %	Heat of immersion, cal/g: *n*-Hexane (0[b])	*n*-Octane (0)	*n*-Butanol (1.65 D)	1-Nitropropane (3.57 D)
Z-I[a]	0	28 0	22.2	54.0	65.4
Z-II	22.5	27.2	21.4	55.4	62.0
Z-III	41.5	27.0	...	...	67.1
Z-IV	60.1	28.5	22.6	61.4	97.2
Z-V	87.8	33.1	24.2	66.8	162.6
Z-VI	95.7	33.2	...	...	197.8

[a] Original Sample Z-I, Na-Y Faujasite Type Zeolite $SiO_2/Al_2O_3 = 3.25$. [b] Dipole moment.

Table II shows heats of immersion per unit specific surface area measured by the BET method. The heat of immersion is almost constant for *n*-hexane, while the effect of exchange ratio is notable for 1-nitropropane. As the difference in immersional heats between 1-nitropropane and *n*-hexane corresponds to $n\mu F$, the field strength is obtainable from these values. The result is given in Table II, column 5. For this calculation, the cross-section area of the absorbed molecule is supposed to be 25 Å^2.

Table II: Heats of Immersion and Field Strengths of Zeolites

Sample	Ca exchange, mole %	Heat of immersion, ergs/cm^2: *n*-Hexane	1-Nitropropane	Field strength ($\times 10^{-5}$ esu/cm^2)
Z-I	0	143.8	334.8	1.3
Z-II	22.5	130.9	298.3	1.2
Z-III	41.5	130.2	323.5	1.4
Z-IV	60.1	140.9	480.4	2.4
Z-V	87.8	161.1	791.2	4.4
Z-VI	95.7	168.2	1001.5	5.8

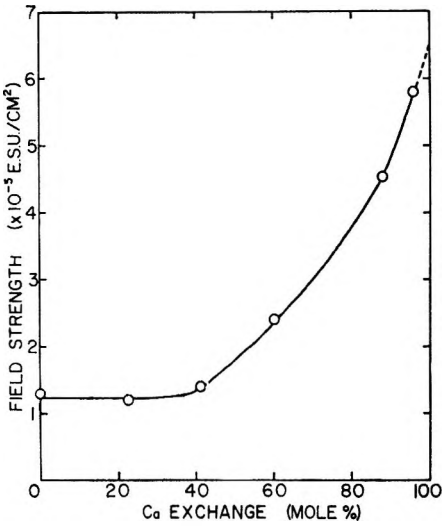

Figure 1. Change of field strengths *vs.* zeolite composition.

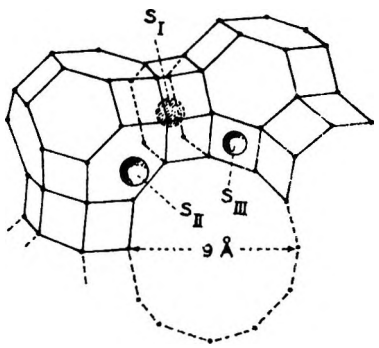

Figure 2. Schematic drawing of cation positions in faujasite.

The change of F with ion exchange is given in Figure 1. It is observed that F is almost constant until the exchange ratio reaches 40%, and increases at higher exchanges. By extrapolation, F is 5 times greater than that of Na type when Na is completely replaced for Ca.

It is interesting to distinguish three contributions to interaction between zeolite surface and adsorbates, but since it is impossible owing to the pore structure to neglect the influence of steric hindrance on the heat of immersion when adsorbates have only low or no dipole moment but high polarizability, the discrimination is rather difficult.

Discussion

According to Breck,[16] Shoemaker, *et al.*,[17] faujasite type zeolite has three kinds of cation sites as follows (Figure 2): site 1, in the centers of the hexagonal prism joining truncated cuboctahedrons (S_I); site 2, neighboring to the unjoined hexagonal face (S_{II}); site 3, neighboring to the tetragonal face inside a channel (S_{III}).

(16) D. W. Breck, *J. Chem. Educ.*, **41**, 678 (1964).

(17) G. R. Eulenberger, D. P. Shoemaker, and J. G. Keil, *J. Phys. Chem.*, **71**, 1812 (1967).

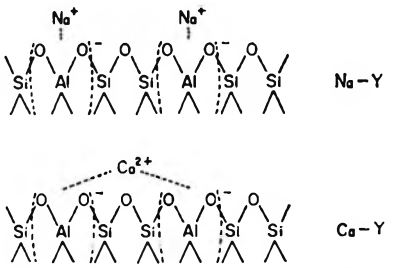

Figure 3. Schematic drawing of Na–Y and Ca–Y zeolites.

Per unit cell there are 16 cations in site 1 and 32 in site 2. The cations in site 2 and site 3 interact with all molecules sorbed in the channel, while the cations in site 1 interact only with molecules which can pass through a pore of 2.0 Å consisting of a six-oxygen ring. The zeolite, whose SiO_2/Al_2O_3 ratio is 3.25, has 73 monovalent cations per unit cell, but if replaced with divalent Ca ions, the number of cations reduces to half. Supposing that cation exchange begins at site 1, Ca does exist only in site 1 until molar exchange ratio is 43.8%, and therefore the field strength measured from the immersional heat will be the same as Na type's. This prediction agrees completely with the present results. It may result from the chemical stability of the cation site that exchanging ions enter preferably into site 1.

From the Gauss theorem, the field strength of the solid related to the charge density (σ) per unit surface area by the equation

$$F = 2\pi\sigma \tag{5}$$

The quantity σ is given by the expression

$$\sigma = eN \tag{6}$$

where e is the electronic charge and N is the effective number of charge per unit surface area.

From (5), (6), and the field strength F observed, N_{obsd} of Na–Y type is

$$N_{obsd} = 4.4 \times 10^{13} \tag{7}$$

By using the field strength F obtained by extrapolation to 100% exchange in Figure 1, N_{obsd} of Ca–Y type is

$$N_{obsd} = 2.2 \times 10^{14} \tag{8}$$

When the SiO_2/Al_2O_3 ratio is 3.25, the number of cations in site 2 and site 3 per unit surface area (N_{calcd}) is calculated as follows

$$N_{calcd} = 3.2 \times 10^{14} \quad \text{Na–Y} \tag{9}$$

$$N_{calcd} = 1.1 \times 10^{14} \quad \text{Ca–Y} \tag{10}$$[18]

From these figures the ratio of effective cation sites is

$$N_{obsd}/N_{calcd} = 0.14 \quad \text{Na–Y} \tag{11}$$

$$N_{obsd}/N_{calcd} = 2.0 \quad \text{Ca–Y} \tag{12}$$

Figure 3 explains that the field strength increases with Ca exchange. An anion in zeolite structure is tetrahedrally coordinated aluminum, $(AlO_4)^-$, and each Na ion is joined to an $(AlO_4)^-$ ion one by one. Ca ion, however, is joined to two $(AlO_4)^-$ ions so that the bond distance becomes large and the bond strength is lowered. Thus, a Ca ion, replacing two Na ions electrovalencewise, tends to join energetically only to one site, leaving the other $(AlO_4)^-$ ion almost free. Under this situation there exist one positive charge at the filled site and one negative charge at the empty site and a stronger electrostatic field would result. Furthermore, the longer the bonding distance, the easier it will be for the molecules to approach.

Thus it was proved from these examinations that a stronger electrostatic field is generated by exchanging Na ion for Ca ion, and this is consistent to the model of Rabo and others. Among some discussions about active sites, the second and the third points on solid acid and electrostatic field do not oppose each other. The result of measurement on the acidity and the acid strength of Ca-exchanged Y zeolite by Benesi's method is closely related to the present result on electrostatic field strength.[19] It is suggested that the solid acid character is caused from the polarization of water molecules and the proton formation resulting from the electrostatic field on the surface.

Acknowledgment. The authors are grateful to Professor Hideo Akamatu for valuable discussions. They wish to thank Mrs. Setsuko Horikoshi for her secretarial help during the preparation of the manuscript.

(18) This value is calculated by assuming that 16 Ca ions are, located in S_I.

(19) M. Ikemoto, K. Tsutsumi, and H. Takahashi, *Seisan Kenkyu* **21**, 453 (1969).

Dissociation Energy of Vanadium and Chromium Dicarbide and Vanadium Tetracarbide

by Fred J. Kohl and Carl A. Stearns

Lewis Research Center, National Aeronautics and Space Administration, Cleveland, Ohio 44135 *(Received January 20, 1970)*

The Knudsen effusion method was used in conjunction with a double focusing mass spectrometer to study the vaporization of the vanadium–carbon and chromium–carbon systems over the temperature ranges 2417–2603°K and 2083–2176°K, respectively. The molecular species VC_2, VC_4, CrC_2 were identified and experimentally determined third-law enthalpies were combined with published thermodynamic data to yield the dissociation energies: $VC_2(g) = V(g) + C_2(g)$, $D_0^0(V-C_2) = 570 \pm 20$ kJ mol^{-1}; $VC_4(g) = V(g) + 2C_2(g)$, $D_0^0(C_2-V-C_2) = 1193 \pm 22$ kJ mol^{-1}; $CrC_2(g) = Cr(g) + C_2(g)$, $D_0^0(Cr-C_2) = 445 \pm 18$ kJ mol^{-1}. Atomization energies were also calculated. Results are discussed in terms of the metal oxide–metal dicarbide bond strength analogy.

Introduction

Only a few vaporization studies of the vanadium–carbon and chromium–carbon systems have been reported in the literature.[1-5] Two of these studies suggest or present evidence for the existence of gaseous metal carbon molecular species. Drowart, *et al.*,[1] gave no details of their study but did report an atomization energy of 1167 ± 21 kJ mol^{-1} for VC_2. Doan[2] used spark source mass spectrometry to study the Cr–C system and reported peaks that correspond to the CrC^+ and CrC_2^+ molecular ions. His ratios of metal carbide to metal for these two species were 1×10^{-5} and 3×10^{-4}, respectively. The other investigators[3-5] report vapor pressures of the metal atoms over various metal carbon condensed phases.

Recent identifications of gaseous dicarbide and tetracarbide molecules of high stability in equilibrium over condensed phases of various rare earth carbon systems[6-11] and transition metal carbon systems[12,13] prompted us to investigate the V–C and Cr–C systems. Knudsen effusion molecular-beam mass spectrometric methods appeared to be ideally suited to these studies. Our objectives were to use this method to identify metal carbide molecules and to measure their dissociation energy. The study was limited in both cases to compositions of condensed phase metal carbide in equilibrium with excess carbon at each temperature.

Procedure

The Knudsen cell–mass spectrometer system and experimental method used in this study were the same as described previously.[6,12,14] The tungsten Knudsen cell had an orifice of 0.076 cm diameter and zero length (knife edge); it was fitted with a graphite liner made from Ultra Carbon UFS graphite rod. A 0.25-cm diameter hole in the wall of the liner was arranged to line up with the effusion orifice.

For the study of the V–C system, a homogeneous mixture of graphite (Ultra Carbon UFS-4) and vanadium, in the atomic ratio of 2.1 to 1.0, was loaded into a new cell liner. The vanadium was 99% pure as obtained from Cerac Inc. The mixture was heated in the Knudsen cell to 2330°K. Eight hours was required to reach this temperature with the pressure maintained at less than 1×10^{-5} Torr. The cell was kept at temperature for an additional 16 hr before measurements were started. At the conclusion of the experiment, X-ray diffraction analysis showed that the residue was a mixture of graphite and cubic vanadium carbide with a lattice parameter of 416.5 ± 0.2 pm. According to Storms,[4] this lattice parameter corresponds to a composition of approximately $VC_{0.88}$ which is close to the upper phase limit for the VC phase.

For each of the two experiments (I and II) on the Cr–C system, the cell liners were loaded with a homo-

(1) J. Drowart, A. Pattoret, and S. Smoes, *Proc. Brit. Cer. Soc.*, **8**, 67 (1967).

(2) A. S. Doan, Jr., presented at the First National Bureau of Standards Materials Research Symposium, Gaithersburg, Md., Oct 3–7, 1966; NASA TM X-52216, 1966.

(3) S. Fujishiro and N. A. Gokcen, *J. Electrochem. Soc.*, **109**, 835 (1962).

(4) E. K. Storms, "The Refractory Carbides," Academic Press, New York, N. Y., 1967, pp. 1–17.

(5) S. Fujishiro and N. A. Gokcen, *Trans. AIME*, **221**, 275 (1961).

(6) F. J. Kohl and C. A. Stearns, NASA TN D-5646, 1970; *J. Chem. Phys.*, in press.

(7) G. Balducci, A. Capalbi, G. DeMaria, and M. Guido, *ibid.*, **48**, 5275 (1968).

(8) G. Balducci, *et al.*, *ibid.*, **50**, 1969 (1969).

(9) G. Balducci, *et al.*, *ibid.*, **43**, 2136 (1965).

(10) G. Balducci, *et al.*, *ibid.*, **51**, 2871 (1969).

(11) G. Balducci, G. DeMaria, and M. Guido, *ibid.*, **51**, 2876 (1969).

(12) C. A. Stearns and F. J. Kohl, NASA TN D-5653, 1970; *High Temp. Sci.*, in press.

(13) T. S. Starostina, L. N. Sidorov, P. A. Akishin, and N. M. Karasev, *Izv. Akad. Nauk SSSR*, **3**, 647 (1967).

(14) C. A. Stearns and F. J. Kohl, NASA TN D-5027, 1969.

geneous mixture of Cr_3C_2 and graphite (Ultra Carbon UFS-4) in the weight ratio of 10 to 1. The Cr_3C_2, of unspecified purity, was purchased from Astro Metals Inc. Spectrographic analysis for metallic impurities revealed moderate amounts of Al plus trace amounts of B, Cu, Fe, V, Ni, Si, and Ti. Each Cr_3C_2-C mixture was heated in a Knudsen cell to 1400°K over a period of 24 hr prior to the start of the ion intensity measurements. For the last 10 hr of the preheating period the pressure was maintained at less than 2×10^{-6} Torr. X-ray diffraction analysis of the sample residue from experiment II showed that the solid was a mixture of graphite, Cr_3C_2 and a small amount of Cr_7C_3.

The ion species were identified by their mass to charge ratio (m/e) and isotopic abundances. Shutter profile measurements were used to establish which species were originating from the Knudsen cell. Because the intensities of the carbide species under investigation were extremely low, all intensity measurements were made with ionizing electrons of 20-eV energy and an anode current of 150 μA. Appearance potentials were measured by recording the ionization efficiency curve and applying the linear extrapolation method.

Results and Calculations

The only pertinent ion species detected were V^+, VC_2^+, VC_4^+, Cr^+, and CrC_2^+. A careful search at the maximum temperature of each experiment failed to reveal any monocarbides or higher carbides other than those noted above.

In the vanadium experiment, ion intensities were measured at 13 temperatures in the range from 2417 to 2603°K. Below 2417°K the intensity of the carbide species were too low to measure and above 2603°K the intensity of V^+ became high enough to indicate that the pressures were approaching the point where the conditions of effusive flow no longer applied. The shutter effect for V^+, VC_2^+, and VC_4^+ was 100%.

The temperature range for the two chromium experiments was from 2083 to 2176°K. In the first chromium experiment ion intensities were measured at 11 temperatures and in the second experiment intensities were measured at 7 temperatures. The high and low limits of the temperature range studied were dictated by the same factors that prevailed in the vanadium experiment. The shutter effect for Cr^+ was 100% but for CrC_2^+ the shutter effect was between 80 and 100%. Ion intensity values were derived by making measurements with the shutter "open" and "closed" and taking differences. We were not able to identify the nonshutterable background peak at m/e 76 that interfered with the CrC_2^+ peak and the resolution of the mass spectrometer was not high enough to separate it from the CrC_2^+.

Ionization efficiency curves could only be obtained for V^+ and VC_2^+ because the other ion intensities were too low to obtain meaningful results. The measured appearance potential for VC_2^+ was 8.6 ± 0.5 eV, with the 6.74 eV value for V^+ being used as the internal standard.[15] All carbide ion intensities, I_i, were too low to measure absolute multiplier gains, and therefore the relative gains, γ_i, for the various species were taken to be the same as those measured in previous work[12] on the titanium–carbon system.

The factor, E_i, used to convert from the 20-eV point on the ionization efficiency curve to the maximum, was measured directly for V^+ and VC_2^+, but for VC_4^+ we assumed $E_{VC_4^+} = E_{VC_2^+}$. For the chromium–carbon

Table I: Third-Law Enthalpies $\Delta H_0°$ for the Reaction V(g) + 2C(s) = VC_2(g)

Temp, °K	K_p	log K_p	$-\Delta[(G_T° - H_0°)/T]$, J deg^{-1} mol^{-1}	$\Delta H_0°$, kJ mol^{-1}
2503	1.21×10^{-3}	−2.917	45.97	254.8
2568	1.80×10^{-3}	−2.745	45.72	252.4
2539	1.37×10^{-3}	−2.863	45.83	255.5
2547	1.69×10^{-3}	−2.785	45.80	252.5
2580	1.95×10^{-3}	−2.710	45.68	251.7
2549	1.59×10^{-3}	−2.799	45.79	253.3
2503	1.33×10^{-3}	−2.876	45.97	252.9
2488	1.22×10^{-3}	−2.914	46.02	253.3
2470	1.18×10^{-3}	−2.928	46.09	252.3
2452	8.41×10^{-4}	−3.075	46.15	257 5
2417	7.28×10^{-4}	−3.138	46.27	257.0
2557	1.50×10^{-3}	−2.824	45.76	255.2
2603	1.84×10^{-3}	−2.735	45.59	255.0
			Av =	254.1 ± 1.9[a]

[a] The error quoted is the standard deviation of the points. See text for overall estimated uncertainty.

Table II: Third-Law Enthalpies $\Delta H_0°$ for the Reaction V(g) + 4C(s) = VC_4(g)

Temp, °K	$K_p \times 10^6$	log K_p	$-\Delta[(G_T° - H_0°)/T]$, J deg^{-1} mol^{-1}	$\Delta H_0°$, kJ mol^{-1}
2503	3.16	−5.500	73.93	448.6
2568	3 18	−5 498	73.72	459.6
2539	3.45	−5.462	73.82	452.9
2547	3.00	−5.523	73.79	457.2
2580	4.61	−5.336	73.68	453.7
2549	3.12	−5.506	73.78	456.8
2503	2.48	−5.606	73.93	453.7
2557	3.32	−5.479	73.76	456.8
2603	3.97	−5.401	73.61	460.8
			Av =	455.6 ± 3.7[a]

[a] The error quoted is the standard deviation of the points. See text for overall estimated uncertainty.

(15) R. W. Kiser, "Introduction to Mass Spectrometry and Its Applications," Prentice-Hall, Englewood Cliffs, N. J., 1965, Appendix IV.

system we assumed $E_{CrC_2^+} = E_{VC_2^+}$. Measured values of E_{V^+} and $E_{VC_2^+}$ are 1.00 and 1.36, respectively.

Relative maximum ionization cross sections σ_i, for atoms were taken from Mann[16] and the cross sections for VC_2, VC_4, and CrC_2 were calculated by summing the respective metal atom cross section with the cross section of the appropriate number of carbon atoms. Ion intensity ratios corrected for γ_i, σ_i, and E_i are listed in Tables I to III for each measurement temperature.

Table III: Third-Law Enthalpies $\Delta H_0°$ for the Reaction $Cr(g) + 2C(s) = CrC_2(g)$

Temp., °K	K_p	log K_p	$-\Delta[(G_T° - H_0°)/T]$, J deg^{-1} mol^{-1}	$\Delta H_0°$, kJ mol^{-1}
Expt I				
2083	$4.1_8 \times 10^{-7}$	−6.379	62.32	384
2119	$7.6_1 \times 10^{-7}$	−6.119	62.24	380
2133	$9.2_8 \times 10^{-7}$	−6.032	62.21	379
2111	$6.8_9 \times 10^{-7}$	−6.162	62.26	381
2116	$7.6_3 \times 10^{-7}$	−6.117	62.25	380
2154	$1.0_2 \times 10^{-6}$	−5.991	62.17	381
2125	$1.0_5 \times 10^{-6}$	−5.979	62.23	376
2124	$6.5_5 \times 10^{-7}$	−6.184	62.23	384
2146	$1.0_1 \times 10^{-6}$	−5.996	62.18	380
2166	$1.2_3 \times 10^{-6}$	−5.910	62.14	380
2100	$1.0_4 \times 10^{-6}$	−5.983	62.28	371
Expt II				
2101	$9.2_7 \times 10^{-7}$	−6.033	62.28	374
2132	$1.4_1 \times 10^{-6}$	−5.851	62.21	371
2154	$9.2_0 \times 10^{-7}$	−6.036	62.17	383
2188	$1.7_9 \times 10^{-6}$	−5.747	62.10	377
2121	$8.2_5 \times 10^{-7}$	−6.084	62.24	379
2147	$1.3_4 \times 10^{-6}$	−5.873	62.18	375
2176	$1.2_5 \times 10^{-6}$	−5.903	62.11	381
				Av = 379 ± 4[a]

[a] The error quoted is the standard deviation of the points. See text for overall estimated uncertainty.

Three pressure independent reactions were considered. These reactions and the corresponding calculated third-law heats are

$$V(g) + 2C(s) = VC_2(g)$$
$$\Delta H_0° = 254.1 \pm 18.0 \text{ kJ mol}^{-1} \quad (1)$$
$$V(g) + 4C(s) = VC_4(g)$$
$$\Delta H_0° = 455.6 \pm 18.8 \text{ kJ mol}^{-1} \quad (2)$$
$$Cr(g) + 2C(s) = CrC_2(g)$$
$$\Delta H_0° = 379 \pm 16 \text{ kJ mol}^{-1} \quad (3)$$

The value for chromium was obtained by combining the results of experiments I and II. We assumed unit activity for C(s) because the graphite liner always assured an excess of carbon. Third-law heats were calculated according to the relation

$$\Delta H_0° = -2.303\, RT \log_{10} K_p - T\Delta\left(\frac{G_T° - H_0°}{T}\right) \quad (4)$$

where R is the gas constant, $\Delta[(G_T° - H_0°)/T]$ is the change of the Gibbs free-energy function for the reaction under consideration and the equilibrium constant is given by

$$K_p = \frac{I_1}{I_2}\frac{E_1}{E_2}\frac{\sigma_2}{\sigma_1}\frac{\gamma_2}{\gamma_1}\frac{n_2}{n_1} \quad (5)$$

where n_i is the isotopic abundance of species i. The values of K_p and $\Delta[(G_T° - H_0°)/T]$ are presented in Tables I to III, together with the calculated third-law heats.

The values of the free-energy functions used for V(g) and Cr(g) were taken from Hultgren, *et al.*,[17] and those used for C(s) were taken from the JANAF tables.[18] The free-energy functions for $VC_2(g)$ and $CrC_2(g)$ were calculated on the basis of estimated molecular parameters for an assumed linear asymmetric M–C–C molecule. For $VC_4(g)$ a linear symmetric C–C–V–C–C structure was assumed and the method of Engler and Kohlrausch[19] was used to estimate fundamental vibration frequencies. All thermodynamic functions were calculated with a computer program[20] using the rigid rotator–harmonic oscillator approximation. Pertinent molecular parameters are listed in Table IV and free energy functions are tabulated in Table V. The estimated total errors associated with the third-law heats, $\Delta H_0°$, were obtained by combining the standard deviations from the mean of all data points listed in Tables I through III with estimated uncertainties in values of K_p, ±50%; T, ±10° K; and $\Delta[(G_T° - H_0°)/T]$, ±6.3 J deg^{-1} mol^{-1}. The uncertainties in the free energy functions for the molecules are based on assumed errors of ±50 cm^{-1} in the estimated vibrational frequencies. The uncertainty does not take into account the possibility of low-lying multiplet electronic states or alternate ground state possibilities.

The heat of formation[18] of $C_2(g)$, $\Delta H_{f°} = 824.2 \pm 8.4$ kJ mol^{-1} was combined with the third-law heats of reactions 1 and 3, respectively, to give the dissociation energies

(16) J. B. Mann, *J. Chem. Phys.*, **46**, 1646 (1967).

(17) R. Hultgren, R. L. Orr, P. D. Anderson, and K. K. Kelley, "Selected Values of Thermodynamic Properties of Metals and Alloys," University of California, Department of Mineral Technology, 1967, supplement.

(18) D. R. Stull, Ed., "JANAF Thermochemical Tables," Dow Chemical Co., Midland, Mich., 1961.

(19) W. Engler and K. W. F. Kohlrausch, *Z. Phys. Chem. (Leipzig)*, **B34**, 214 (1936).

(20) B. J. McBride and S. Gordon, NASA TN D-4097, 1967.

Table IV: Estimated Molecular Parameters for VC_2, VC_4, and CrC_2

Molecule		VC_2	VC_4	CrC_2
Internuclear separation, pm	V–C	162[a]	162	...
	Cr–C	...	...	168[a]
	C–C	131[b]	131	131
Moment of inertia, g-cm^2		15.74×10^{-39}	44.71×10^{-39}	16.59×10^{-39}
Force constants, N/m	k_{V-C}[c]	7.36×10^2	7.36×10^2	...
	k_{Cr-C}[c]	...	...	5.82×10^2
	k_{C-C}[b]	9.25×10^2	9.25×10^2	9.25×10^2
	k_δ, N, m/rad[d]	0.67×10^{-18}	...	0.67×10^{-18}
	$f_{13,22}$[e]	...	1.30×10^2	...
Frequencies, cm^{-1} (degeracy)	ω_1	780 (1)	812 (1)	709 (1)
	ω_2	494 (2)	1883 (1)	488 (2)
	ω_3	1814 (1)	1013 (1)	1767 (1)
	ω_4	...	1841 (1)	...
	ω_5	...	136 (2)	...
	ω_6	...	570 (2)	...
	ω_7	...	468 (2)	...
Symmetry number		1	2	1
Ground state statistical weight		4[f]	4[f]	5[g]

[a] Calculated by the use of a modified Badger's rule. D. R. Herschbach and V. W. Laurie, *J. Chem. Phys.*, **35**, 458 (1961). [b] From C_2. G. H. Herzberg, "Molecular Spectra and Molecular Structure, I, Spectra of Diatomic Molecules," Van Nostrand, Princeton, N. J., 1950, Appendix. [c] The force constants for V–C and Cr–C were assumed to be the same as those of the corresponding oxides. G. H. Herzberg, "Molecular Spectra and Molecular Structure. I. Spectra of Diatomic Molecules," Van Nostrand, Princeton, N. J., 1950, Appendix. [d] See G. H. Herzberg, "Molecular Spectra and Molecular Structure. II. Infrared Spectra of Polyatomic Molecules," Van Nostrand, Princeton, N. J., 1945, pp 173–174. [e] See ref 19. [f] The ground state of $^4\Sigma$ was assumed for VC_2 by analogy to VO. C. J. Cheetham and R. F. Barrow in "Advances in High Temperature Chemistry," Vol. I, L. Eyring, Ed., Academic Press, New York, N. Y., 1967, pp 7–41. The same electronic contribution was assumed for VC_4. [g] A ground state of $^5\Sigma$ was assumed for CrC_2 by analogy with the apparent ground state for CrO (private communication, K. D. Carlson).

Table V: Free Energy Functions $-(G_T^\circ - H_0^\circ)/T$, J deg^{-1} mol^{-1}, for $VC_2(g)$, $VC_4(g)$ and $CrC_2(g)$

Temp, °K	$VC_2(g)$	$VC_4(g)$	$CrC_2(g)$
298.15	213.83	233.74	216.43
1800	...	...	294.89
1900	...	...	297.75
2000	297.14	369.51	300.49
2100	299.75	374.02	303.10
2200	302.25	378.36	305.62
2300	304.65	382.53	308.03
2400	306.96	386.56	310.36
2500	309.19	390.45	312.60
2600	311.35	394.21	...
2700	313.43	397.84	...
2800	315.44	401.37	...
2900	317.39	404.78	...
3000	319.29	408.10	...

$$VC_2(g) = V(g) + C_2(g)$$

$$D_0^\circ(V\text{–}C_2) = 570.1 \pm 19.9 \text{ kJ mol}^{-1} \quad (6)$$

$$CrC_2(g) = Cr(g) + C_2(g)$$

$$D_0^\circ(Cr\text{–}C_2) = 445 \pm 18 \text{ kJ mol}^{-1} \quad (7)$$

The atomization energies, $D_0^\circ{}_{atom}$ of V–C–C and Cr–C–C, were obtained by combining, respectively, the heats of reaction 1 and 3 with the heat of formation[18] of C(g) which is 709.5 ± 1.9 kJ mol^{-1}

$$VC_2(g) = V(g) + 2C(g)$$

$$D_0^\circ{}_{atom} = 1164.9 \pm 18.2 \text{ kJ mol}^{-1} \quad (8)$$

$$CrC_2(g) = Cr(g) + 2C(g)$$

$$D_0^\circ{}_{atom} = 1040 \pm 16 \text{ kJ mol}^{-1} \quad (9)$$

The heat of formation of $C_2(g)$ was combined with the third-law heat of reaction 2 to give the dissociation energy of C_2–V–C_2

$$VC_4(g) = V(g) + 2C_2(g)$$

$$D_0^\circ(C_2\text{–}V\text{–}C_2) = 1192.8 \pm 22.2 \text{ kJ mol}^{-1} \quad (10)$$

The atomization energy of $VC_4(g)$ was calculated by combining the heat of reaction 2 with the heat of formation of C(g)

$$VC_4(g) = V(g) + 4C(g)$$

$$D_0^\circ{}_{atom} = 2382.4 \pm 19.2 \text{ kJ mol}^{-1} \quad (11)$$

Discussion

Second-law treatments of the experimental data were not attempted because of the relatively short temperature ranges covered in each experiment. However, the absence of any severe trend with temperature in the third-law heats serves to indicate that no large systematic temperature error existed.

Our value for the atomization energy of $VC_2(g)$, 1165 ± 18 kJ mol^{-1}, is in excellent agreement with that

reported by Drowart, *et al.*,[1] 1167 ± 21 kJ mol^{-1}. Our results for the Cr–C system, however, differ in two respects from findings reported by Doan.[2] First, we were unable to detect any monocarbide and, secondly, our ratio of CrC_2^+ to Cr^+ is a factor of 10^{-2} to 10^{-3} smaller than that reported by Doan. These differences in results are not particularly disturbing because Doan's results were obtained by sparking, a process which is complex and not well understood. The mechanism of vaporization and ion production by sparking is complex. The energy dissipated by the spark vaporizes, ionizes, and physically removes material from the electrodes. The netural and ionic species formed do not necessarily represent an equilibrium vaporization process. On the other hand, our results are derived from the Knudsen method which samples an equilibrium process.

The comparisons of M–C_2 and M–O bond strengths that have previously been made for rare earth, group IIIa, group IVa,[6-11,21,22] and transition metal carbon systems[12] can now be extended to include the dicarbides of vanadium and chromium. The comparison of M–C_2 with M–O bond strengths is made because it has been postulated that the bonding of the C_2^{2-} group is similar (isoelectronic) to that of the O^{2-} ion.[21,22] The V–C_2 bond energy (570 ± 20 kJ) follows the apparent trend that the oxide bond energy,[23] $D_0°$(V–O) = 617 ± 11 kJ, is somewhat higher than the bond energy of the corresponding dicarbide. However, the difference between $D_0°$(V–C_2) and $D_0°$(V–O) is not as large as that of some of the other metal oxides and dicarbides, notably titanium[12] and some of the rare earths.[6,21] In the case of chromium we seem to have an exception because the dicarbide bond energy (445 ± 18 kJ) is slightly higher than that of the oxide,[23] $D_0°$(Cr–O) = 423 ± 29 kJ. However, the overlaping uncertainties make the situation nebulous enough that no positive conclusion can be made.

It is interesting to note that the bond energies for C_2–V–C_2, $D_0°$ = 1193 ± 22 kJ, and O–V–O,[23] $D_0°$ = 1213 ± 42 kJ, are comparable. This is in contrast to the case of titanium[24] where the O–Ti–O species, $D_0°$ = 1311 ± 21 kJ, is markedly more stable than C_2–Ti–C_2[12], $D_0°$ = 1214 ± 23 kJ.

The value of the atomization energy for VC_4(g) obtained in this study indicates that this is a reasonably stable molecule. The stabilities of VC_2 and VC_4 and the existence of stable oxides of niobium and tantalum[23] suggests that the corresponding carbides of Nb and Ta might be stable molecules. The fact that the NbC_2 molecule has recently been observed[25] in relatively high concentrations in the equilibrium vapor over NbC + C lends credence to our speculation.

(21) G. DeMaria, G. Balducci, A. Capalbi, and M. Guido, *Proc. Brit. Cer. Soc.*, 8, 127 (1967).

(22) W. A. Chupka, J. Berkowitz, C. F. Giese, and M. G. Inghram, *J. Phys. Chem.*, 62, 611 (1958).

(23) J. Drowart and P. Goldfinger, *Angew. Chem., Int. Ed. Engl.*, 6, 581 (1967).

(24) J. Drowart, P. Coppens, and S. Smoes, *J. Chem. Phys.*, 50, 1046 (1969).

(25) E. Storms, B. Calkin, and A. Yencha, *High Temp. Sci.*, 1, 430 (1969).

NOTES

Transference Numbers for Aqueous Potassium Chloride at 10 and 1° and the Temperature Coefficient of Ionic Conductances

by Robert L. Kay and George A. Vidulich

Mellon Institute, Carnegie-Mellon University, Pittsburgh, Pennsylvania 15213 *(Received July 14, 1969)*

Cation transference numbers for aqueous solutions of 0.01 *M* KCl were measured by means of the moving-boundary method. Boundary movement was detected by probe electrodes and an electrometer by a method that has recently been described in detail.[1] Autogenic cells with Cd anodes and with boundary tubes of internal diameters 3.0 and 4.5 mm were employed for all measurements. Temperatures were regulated to 0.005° and set by a platinum resistance thermometer. The volume calibration of the moving-boundary tube was based on Longsworth's[2] value of t^+(0.01 *M* KCl, 25°)$_{aq}$ = 0.4902. A correction amounting to less than 0.03% was made for thermal contraction of the calibrated tubes between 25 and 1°.

The results are given in Table I. The observed transference numbers t^+_{obsd} were independent of current

(1) R. L. Kay, G. A. Vidulich, and A. Fratiello, *Chem. Instrum.*, 1, 361 (1969).

(2) L. G. Longsworth, *J. Amer. Chem. Soc.*, 54, 2741 (1932).

Table I: Transference Numbers for KCl in Aqueous Solutions at 0.01 *M*

Temp, °C	No. of runs	t^+_{obsd}	$10^4\sigma$	t^+	t_0^+
1	16	0.4963	2.1	0.4965	0.4966
10	6	0.4936	2.6	0.4938	0.4940

for a change in current of 75%. The current range used was 0.2–0.8 mA depending on the cell. The standard deviation is given in the fourth column of Table I and the transference numbers, corrected for the solvent conductance and the volume change between the anode and the boundary,[2] are given in the fifth column. The Kay–Dye equation[3] was used to extrapolate the data to infinite dilution with an $\mathring{a} = 3.1$. Since the transference numbers are almost equal to 0.5, this extrapolation results in little change and, therefore, introduces a negligible error.

$$t_0^+ = t^+ + \frac{0.5 - t^+}{\Lambda_0} \times \frac{\beta C^{1/2}}{1 + \kappa\mathring{a}} \qquad (1)$$

The results are plotted in Figure 1 and extrapolate to $t_0^+(\mathrm{KCl}, 0°)_{aq} = 0.4970$. This is significantly higher than the value 0.4954 recently reported by Steel[4] with the rather high standard deviation of 7×10^{-4}. Steel used a modified Hittorf method in which analyses of electrode compartment contents were carried out essentially *in situ* by conductance measurements. On the other hand, our results compare favorably with a smooth curve extrapolation of the moving boundary data at higher temperatures of Allgood, LeRoy, and Gordon[5] but are somewhat lower than the value of 0.4959 quoted by Harned and Owen[6] for 5° obtained from an extrapolation of data at 10° and higher by means of an equation which was a cubic in the temperature. It should be noted that a further extrapolation of their equation to 0° predicts 0.4986 for the limiting transference number for KCl compared to our extrapolated value of 0.4970. This is possibly a good indication of the magnitude of the errors to be expected from an extrapolation of this cubic equation.

A referee has suggested that it would be more pertinent to compare our results with existing data for 0°. For example, using $\Lambda_0(\mathrm{KCl}) = 81.7$,[7] $\Lambda_0(\mathrm{HCl}) = 265.2$,[8] and $t_0^+(\mathrm{HCl}) = 0.8441$,[9] a value of $t_0^+(\mathrm{KCl}) = 0.4945$ can be calculated for 0°. However, a reextrapolation of the conductance data for HCl[8] shows that $\Lambda_0(\mathrm{HCl}) = 263.5 \pm 0.3$ would be more nearly correct and this produces $t^+(\mathrm{KCl}) = 0.4972$. Although this is in excellent agreement with our value of 0.4970, the agreement is somewhat fortuitous since the cation transference data[9] for HCl cannot be extrapolated even with eq 1 without introducing an error approaching 0.1% since the lowest concentration measured was 0.02 *M*. Since this error is magnified fivefold in calculating $t_0^-(\mathrm{HCl})$, there must be an uncertainty of about 0.002 in $t_0^+(\mathrm{KCl})$ as calculated from these earlier data.

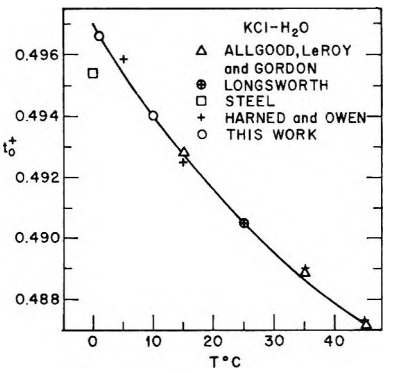

Figure 1. A comparison of the limiting cation transference numbers for KCl in aqueous solution at various temperatures as reported by various workers.

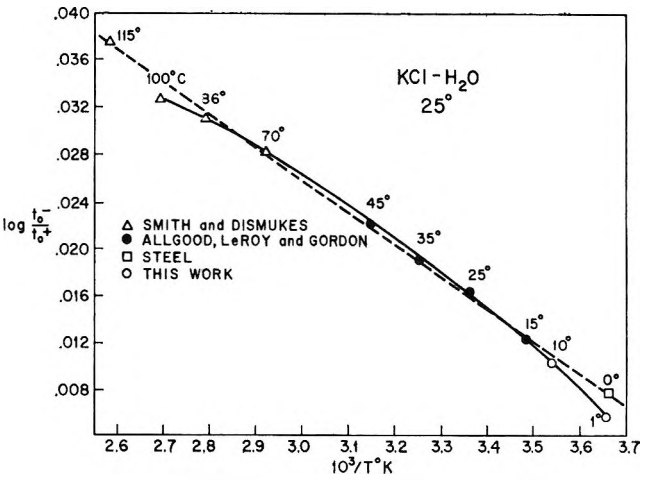

Figure 2. A plot of log of the ratio of anion to cation transference numbers *vs.* the reciprocal absolute temperature for KCl in water. The temperatures in °C are included in the plot.

Of particular interest is a comparison of our data with those of Smith and Dismukes[10] for high temperatures. They used essentially the same method as is reported here. The data can be seen in Figure 2 where the log of the ratio of anion to cation transference numbers is plotted *vs.* the reciprocal of the absolute temperature. The small corrections to their data required for extrapolation to infinite dilution [eq 1] and for the volume

(3) R. L. Kay and J. L. Dye, *Proc. Nat. Acad. Sci.*, **49**, 5 (1963).

(4) B. J. Steel, *J. Phys. Chem.*, **69**, 3208 (1965).

(5) R. W. Allgood, D. J. LeRoy, and A. R. Gordon, *J. Chem. Phys.*, **8**, 418 (1940).

(6) H. S. Harned and B. B. Owen, "The Physical Chemistry of Electrolyte Solutions," 3rd ed, Reinhold Publishing Corp., New York, N. Y., 1958, p 234.

(7) J. Lange, *Z. Phys. Chem.*, **A188**, 384 (1941).

(8) M. Randall and A. P. Vanselow, *J. Amer. Chem. Soc.*, **46**, 2418 (1924).

(9) A. K. Covington and J. E. Prue, *J. Chem. Soc.*, 1930 (1957).

(10) J. E. Smith, Jr., and E. B. Dismukes, *J. Phys. Chem.*, **67**, 1160 (1963).

changes due to electrolysis in the closed side of the cell are opposite in sign and tend to cancel. Originally, these authors had drawn a straight line through their points (missing the point for 100°) and those of Allgood, *et al.*, and calculated an activation energy for the chloride ion of 120 cal/mol greater than that for potassium ion at all temperatures. Steel found that his point for 0° was also on an extension of this line.

However, our new data at lower temperatures confirm Allgood, LeRoy, and Gordon's original finding that the plot in Figure 2 should be concave downward indicating an increasingly smaller difference in activation energy for the two ions as the temperature increases. Also, it should be noted that Smith and Dismukes' straight line plot gave great weight to the point at 115° although it was the result of only one run in a series of measurements of dubious value at that temperature owing to electrode gassing.

It has already been pointed out[5] that the experimental activation energy difference has a sign opposite to that predicted by the Eyring theory of transport processes in solution which states that the slower and presumably larger ion should have the greater activation energy since it requires the formation of a larger "hole" for its motion.

The increased mobility of the chloride ion relative to the potassium as the temperature increases could be due to the solvent dipole relaxation effect which results from the finite relaxation time required for solvent dipoles to reorient after passage of an ion. This theory in its final form[11] can be expressed as a correction to Stokes law by what has become known as the Zwanzig equation

$$\lambda_0\eta_0 = 10^8Fe/1800\Pi(\mathring{r} + B/\mathring{r}^3) \qquad (2)$$

where $B = (10^{24}e^2/9\Pi)(\tau/\eta)[(\epsilon_0 - \epsilon_\alpha)/\epsilon_0^2]$. Here, τ is the dielectric relaxation time of the solvent and ϵ_0 and ϵ_α are the low and infinite frequency dielectric constants, respectively. Inability of this equation to account for the variation of ionic mobilities with ionic size for aqueous[12] and nonaqueous solutions[13] has already been illustrated.

With the recent very precise measurements of τ and ϵ_α by Pottel and Lossen[14] and with the most recent dielectric constant data,[15] $\partial B/\partial T$ can be shown to have the value 0.28 ± 0.07. Since $\partial B/\partial T$ is positive, inspection of eq 2 shows that $\lambda_0\eta_0$ should decrease with increased temperature but the decrease should be the greater the smaller the ion. Consequently, in contrast with experimental observations, the faster, and presumably smaller, chloride ion should become slower relative to the hydrodynamically slower K^+ ion as the temperature increases.

We believe the data presented here can best be accounted for by considering the possible effects the ions can have on the solvent molecules in their vicinity. On the basis of the temperature dependence of ionic mobilities in aqueous solutions, ions have been classified as structure breakers and hydrophilic and hydrophobic structure makers.[16] This classification is in agreement with the conclusion reached from a wide variety of thermodynamic and other transport data. The increased mobility of the Cl^- ion relative to that for the K^+ ion could result primarily from changes in the relative structure-breaking properties of these two ions as the temperature increases. Little more can be said than this since no quantitative theory exists that takes into account the changes in the microscopic properties of the solvent near an ion. Other evidence that the Cl^- ion loses its structure-breaking properties slower than the K^+ ion in aqueous solutions would be most welcomed but unfortunately, transference numbers are the only precise data available that permit a comparison of cations and anions, particularly at different temperatures. There is some possibility now of separating partial molal volumes into ionic values using vibration potentials[17] but partial molal volumes and their temperature derivatives are difficult to interpret.

Acknowledgment. This work was supported by Contract No. 14-01-0001-1729 with the Office of Saline Water, U. S. Department of the Interior.

(11) R. Zwanzig, *J. Chem. Phys.*, **38**, 1603 (1963).

(12) H. S. Frank, "Chemical Physics of Ionic Solutions," B. E. Conway and R. G. Barrodas, Ed., Wiley, New York, N. Y., 1966, p 61.

(13) R. L. Kay, G. P. Cunningham, and D. F. Evans, "Hydrogen-Bonded Solvent Systems," A. K. Covington and P. Jones, Ed., Taylor and Francis, Ltd., London, 1968.

(14) R. Pottel and O. Lossen, *Ber. Bunsenges. Phys. Chem.*, **71**, 135 (1967).

(15) R. L. Kay, G. A. Vidulich, and K. S. Pribadi, *J. Phys. Chem.*, **73**, 445 (1969).

(16) R. L. Kay and D. F. Evans, *ibid.*, **70**, 2325 (1966).

(17) R. Zana and E. Yeager, *ibid.*, **71**, 521 (1967).

A Comparison of the Zero-Field Pulsing Technique and the ICR Technique for Studying Ion–Molecule Reactions

by A. A. Herod, A. G. Harrison,

Department of Chemistry, University of Toronto, Toronto 181, Ontario, Canada

Rebecca M. O'Malley, A. J. Ferrer-Correia, and K. R. Jennings

Department of Chemistry, Sheffield University, Sheffield S3 7HF, England *(Received December 10, 1969)*

The zero-field pulsing technique originally developed by Tal'rose and Frankevich[1] has been used exten-

(1) V. L. Tal'rose and E. L. Frankevich, *Zh. Fiz. Khim.*, **34**, 2709 (1960).

sively[2-6] to study ion–molecule reactions at ion energies assumed to be thermal. More recently, the technique of ion cyclotron resonance (ICR) has been developed and applied extensively to the study of reactions at thermal energies.[7-10] No direct comparison of the two techniques has been made, nor has it been shown conclusively that the zero-field technique, particularly, does provide results characteristic of thermal energy ions. Recently, two of us,[11] from pressure studies using a conventional medium pressure mass spectrometer, have shown that the relative product yields in the reaction $C_3H_6^+ + C_3H_6$, for both the propylene and cyclopropane systems, are strongly dependent on the ion exit energy (and thus the average reactant ion kinetic energy) over the range 0.6–6.3 eV exit energy. Because of this strong dependence of the relative yields on the ion energy, a study of this reaction appeared particularly suitable for a comparison of the two techniques as well as for an estimation of the kinetic energy of the reactant ions.

Table I records the fractional product yields measured by the zero-field and ICR techniques for the $C_3H_6^+ + C_3H_6$ reaction in the propylene and cyclopropane systems. The mass spectrometer[3] and the pulsing techniques[2,3] used in the zero-field method have been described previously and we need only observe that in the present work (carried out at $\sim 1\ \mu$ pressure) the total ion current remained constant for 1 to 1.5 μsec and had decreased by $\sim 10\%$ at 2 μsec, indicating that discrimination effects arising from differing thermal velocities of the ions should be negligible. In the ICR study of ion–molecule reactions relative ion currents can be obtained from rf (radio frequency) power absorption measurements at low rf field strengths, or from a reduction in total ion current (TIC) at high rf field strengths. Peak heights are normalized by dividing by either m or m^2 (where m is the mass number of the ion under observation), depending on the experimental conditions.[12] In all cases, conversions were kept as low as possible (<10%).

Table I: Product Distribution in the Thermal Energy Reaction $C_3H_6^+ + C_3H_6$

Technique	Fractional yields $C_3H_7^+$	$C_4H_7^+$	$C_4H_8^+$	$C_5H_9^+$
	Propylene			
Zero-field	0.21	0.11	0.42	0.26
TIC (low)	0.18	0.12	0.43	0.27[a]
ICR (low)[d]	0.22	0.12	0.41	0.26[b]
ICR (high)	0.20	0.10	0.43	0.27[c]
	Cyclopropane			
Zero-field	0.08	0.13	0.75	0.04
ICR(high)[d]	0.07	0.17	0.68	0.09[c]

[a] Normalized by dividing by m. [b] Normalized by dividing by m^2. [c] Normalized by dividing by m. [d] Low = low-ion densities; high = high ion densities. See ref 12 for normalization of ICR data.

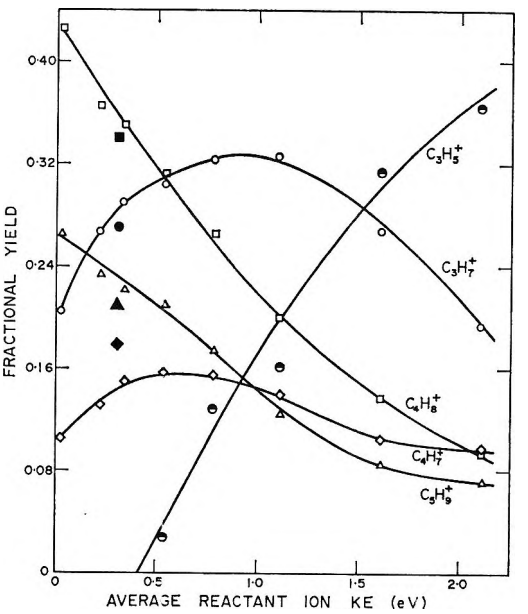

Figure 1. Fractional yields as a function of average reactant ion kinetic energy, propylene system.

The results obtained by the two techniques for the propylene system are in unbelievably good agreement. In addition, the recent ICR study of the propylene system by Henis[10] gives the fractional yields $C_3H_7^+ : C_4H_7^+ : C_4H_8^+ : C_5H_9^+ = 0.19 : 0.12 : 0.42 : 0.27$, in excellent agreement with the present results. The study of the cyclopropane system by both techniques was more difficult because of the lower reactivity and the greater difficulty in eliminating the reactive $C_3H_5^+$ fragment ion. Consequently, the agreement between the zero-field and ICR results is not as spectacular but is still quite satisfactory. The results clearly show that comparable results can be obtained by the zero-field and ICR techniques.

The average fractional yields obtained in the present

(2) A. G. Harrison, J. J. Myher, and J. C. J. Thynne, Advances in Chemistry Series, No. 58, American Chemical Society, Washington, D. C., 1966, p 150.

(3) S. K. Gupta, E. G. Jones, A. G. Harrison, and J. J. Myher, *Can. J. Chem.*, **45**, 3107 (1967).

(4) K. R. Ryan and J. H. Futrell, *J. Chem. Phys.*, **42**, 824 (1965).

(5) C. W. Hand and H. von Weyssenhoff, *Can. J. Chem.*, **42**, 195, 2385 (1964).

(6) J. L. Franklin, Y. Wada, P. Natalis, and P. M. Hierl, *J. Phys. Chem.*, **70**, 2353 (1966).

(7) J. Baldeschwieler, *Science*, **159**, 263 (1968).

(8) M. T. Bowers, D. D. Elleman, and J. L. Beauchamp, *J. Phys. Chem.*, **72**, 3599 (1968).

(9) R. M. O'Malley and K. R. Jennings, *J. Mass Spectrom. Ion Phys.*, **2**, 441 (1969).

(10) J. M. S. Henis, *J. Chem. Phys.*, **52**, 282 (1970).

(11) A. A. Herod and A. G. Harrison, *J. Phys. Chem.*, **73**, 3189 (1969).

(12) G. C. Goode, R. M. O'Malley, A. J. Ferrer-Correia, J. H. Futrell, K. R. Jennings, P. A. Llewellyn, and R. I. Massey, to be published.

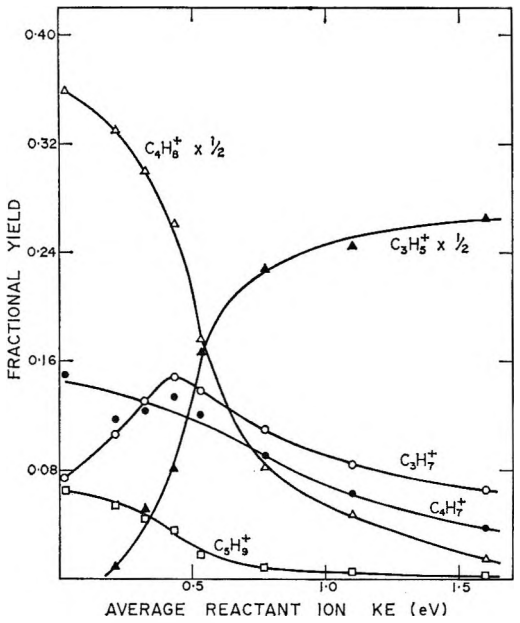

Figure 2. Fractional yields as a function of average reactant ion kinetic energy, cyclopropane system.

study and those measured in the earlier pressure studies[11] are combined in Figures 1 and 2 as a plot of the fractional yields *vs.* average reactant ion kinetic energy. The results from the pressure studies represent the appropriately weighted average for reactions of ions with energies ranging from zero to the final exit energy, E_e, and we have taken as the average reactant ion kinetic energy $\bar{E} = E_e/3$, which has been shown[13] to be valid for the low conversions attained. The solid points in Figure 1 represent the results obtained (using a tandem instrument) by Abramson and Futrell[14] for reaction of ions of 0.3 eV energy. The plots in Figures 1 and 2 clearly show that the reactant ion kinetic energy in the present study is quite low; indeed, the present data fit quite well with the higher energy data if we assume that the reactant ions in the zero-field and ICR experiments have thermal energies. This is to be expected for the ICR experiments and the good agreement between the ICR and zero-field results confirms that the latter also refer to thermal energy ions.

Finally, we would point out that, as the results in Figures 1 and 2 clearly show, the relative product yields are strongly dependent on the ion kinetic energy, at least for unsaturated hydrocarbons. Clearly, this effect must be considered when results obtained by different techniques are to be compared.

Acknowledgments. The work at the University of Toronto was supported by the National Research Council of Canada and that at the University of Sheffield by grants from the Science Research Council and from NATO.

(13) P. Warneck, *J. Chem. Phys.*, **46**, 513 (1967).

(14) F. P. Abramson and J. H. Futrell, *J. Phys. Chem.*, **72**, 1994 (1968).

Interaction of *n*-Butylamine with Tetracyanoethylene and Chloranil

by William J. Lautenberger and John G. Miller

John Harrison Laboratory of Chemistry and the Laboratory for Research on the Structure of Matter, University of Pennsylvania, Philadelphia, Pennsylvania 19104 *(Received January 14, 1970)*

The role of π and σ (outer and inner) complexes in the nucleophilic substitution reactions of amines with tetracyanoethylene (TCNE) and chloranil (CA) has been studied at several laboratories recently.[1-5] Evidence for the participation of the complexes has been obtained for the reactions of the aromatic amines, dimethylaniline[1,3] and aniline,[5] with TCNE and CA. A major part of the evidence for the participation of σ complexes as intermediates in the reactions has been based on kinetic measurements. The large difference between the rate of disappearance of the acceptor (TCNE or CA) or its π complex with the amine and the rate of formation of the product of reaction has indicated the existence of such intermediates in the reactions.

No kinetic study has been made heretofore of the reaction of aliphatic amines with these acceptors, although it has been known that primary and secondary aliphatic amines form both mono- and disubstituted products readily with TCNE[6] and CA.[4,7-9] Working with a large excess of amine, a condition used in the kinetic studies of the aromatic amines,[1,5] we have made an ultraviolet-absorption spectroscopic rate study of the reactions of the *n*-butylamine with both acceptors. The results show that the formation of the monosubstituted product is practically immediate and that, although the subsequent formation of the disubstituted product has a smaller rate, no evidence for an intermediate of appreciable stability exists even in that second reaction since the rate of disappearance of the monosubstituted product is the same as the rate of formation of the disubstituted product.

The ultraviolet absorption spectra of *n*-butylamine, TCNE, and a solution of the two with the amine in large excess, all in cyclohexane at 25°, are shown in

(1) Z. Rappoport, *J. Chem. Soc.*, 4498 (1963).

(2) R. Foster, *Rec. Trav. Chim. Pays-Bas*, **83**, 711 (1964).

(3) P. G. Farrell, J. Newton, and R. F. M. White, *J. Chem. Soc., B*, 637 (1967).

(4) B. K. Das and B. Majee, *J. Indian Chem. Soc.*, **45**, 1054 (1968).

(5) T. Nogami, K. Yoshihara, H. Hosoya, and S. Nagakura, *J. Phys. Chem.*, **73**, 2670 (1969).

(6) B. C. McKusick, R. E. Heckert, T. L. Cairns, D. D. Coffman, and H. F. Mower, *J. Amer. Chem. Soc.*, **80**, 2806 (1958).

(7) L. F. Fieser, *ibid.*, **48**, 2936 (1926).

(8) N. P. Buu-hoi, R. Royer, and B. Eckert, *Rec. Trav. Chim. Pays-Bas*, **71**, 1059 (1952).

(9) D. Buckley, H. B. Henbest, and P. Slade, *J. Chem. Soc.*, 4891 (1957).

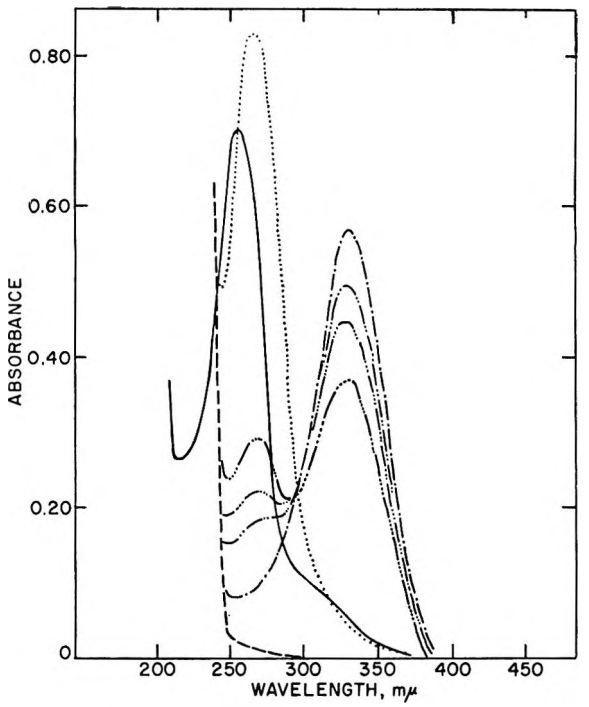

Figure 1. The ultraviolet absorption spectra of *n*-butylamine, TCNE, and their mixture in cyclohexane at 25°; 1.69×10^{-1} *M* amine, – – –; 7.16×10^{-5} *M* TCNE, —. Solution of 1.69×10^{-1} *M* amine and 7.16×10^{-5} *M* TCNE at different times after mixing: —·—, 1 min; —··—, 35 min; —···—, 55 min; —····—, 96 min; ·····, 2 days.

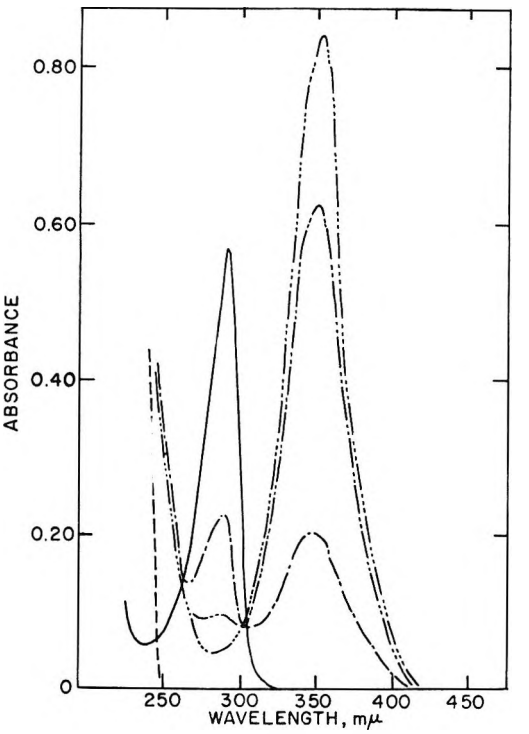

Figure 3. The ultraviolet absorption spectra of *n*-butylamine, CA, and their mixture in cyclohexane at 25°: 6.76×10^{-2} *M* amine, — — —; 2.71×10^{-5} *M* CA, —. Solution of 6.76×10^{-2} *M* amine and 2.71×10^{-5} *M* CA at different times after mixing: —·—, 1 min; —··—, 6 min; —···—, 25 min.

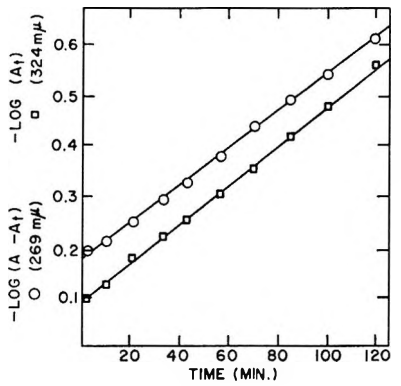

Figure 2. Pseudo-first-order rate plots of 1.69×10^{-1} *M* *n*-butylamine and 7.16×10^{-5} *M* TCNE in cyclohexane: □, $k = 0.00893 \pm 0.00015$ min^{-1}; ○, $k = 0.00846 \pm 0.00015$ min^{-1}.

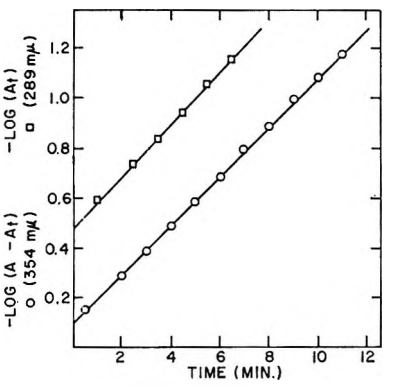

Figure 4. Pseudo-first-order rate plots of 6.76×10^{-2} *M* *n*-butylamine and 2.71×10^{-5} *M* chloranil in cyclohexane. □, $k = 0.2388 \pm 0.0039$ min.$^{-1}$; ○, $k = 0.2276 \pm 0.0002$ min.$^{-1}$

Figure 1. In 1 min after mixing, the prominent TCNE band has disappeared and an intense new band has appeared at 324 mμ. This new band is due to the monosubstituted product, N-tricyanovinyl-*n*-butylamine,[6] and not to a complex. Apparently, the replacement of one cyanide group of TCNE by the amine is extremely rapid. A new band has started to form at 269 mμ and grows as the band at 324 mμ diminishes. We have synthesized the disubstituted product, 1,1-bis(*n*-butylamino)-2,2-dicyanoethylene (*Anal.* Calcd for $C_{12}H_{20}N_4$: C, 65.4; H, 9.2; N, 25.4. Found: C, 65.1; H, 9.5; N, 25.4), and have found that its absorption band in cyclohexane is at 269 mμ.

First-order rate constants for the disappearance of the monosubstituted product and for the formation of the disubstituted product were obtained from the rates of change of the absorbance values at 324 and 269 mμ by plotting the quantities $-\log A_t$ and $-\log (A_\infty - A_t)$, respectively, against time, where A_t is the absorbance at time t and A_∞ is the value at the end of reaction. The absorbance values were corrected for overlap of the bands. Figure 2 shows the results obtained.

The k values and their standard errors were computed by a least-squares procedure. Over the period studied, the reaction went two-thirds to completion and the rates of the two processes were closely the same, showing no evidence for the existence of any intermediate of appreciable stability.

Similar results were obtained with n-butylamine and CA, as shown in Figures 3 and 4. The monosubstituted product has its maximum absorption at 289 mμ, the same as for CA itself, but with a smaller extinction coefficient. The growing band at 354 mμ is caused by the disubstituted product, 2,5-dichloro-3,6-bis(n-butylamino)-p-benzoquinone, which was identified as the final product of reaction (mp 200–202°, lit.[9] mp 201–202°; *Anal.* Calcd for $C_{14}H_{20}N_2Cl_2O_2$: C, 52.7; H, 6.3; N, 8.8; Cl, 22.2; O, 10.0. Found: C, 52.7; H, 6.3; N, 8.2; Cl, 20.7; O, 9.6. Uv and visible maxima (cyclohexane) 225, 354, 525 mμ; lit.[9] (dioxane) 224, 355, 520 mμ).

The near equality of the rates given in Figure 4 indicates that there is no stable intermediate in the reaction. The reaction is remarkably rapid, production of the disubstituted compound being 92% complete in 11 min. Foster[2] earlier found that ethylamine also reacts rapidly with CA in aqueous ethanol. Although he did not evaluate the rates, the spectral changes observed resembled closely those shown in Figure 3. The band of the monosubstituted product occurred at 303 mμ and replaced the CA band (285 mμ) practically instantly and then decayed rapidly. The disubstituted product had its growing band at 356 mμ. Due to the high speed of these reactions, Slifkin[10] was probably unaware of the reactions of ethylamine and diethylamine with CA and for that reason misinterpreted the spectra he obtained for those systems.

Acknowledgments. This research was supported in part by the Advanced Research Projects Agency, Office of the Secretary of Defense, and by a Public Health Service Fellowship (5-F1-GM-32, 638-02, awarded to W. J. L.) from the National Institute of General Medical Sciences. We also wish to acknowledge the assistance given by Mr. John W. Schulhoff.

(10) M. A. Slifkin, *Nature*, **195**, 635 (1962); J. B. Birks and M. A. Slifkin, *ibid.*, **197**, 42 (1963); M. A. Slifkin, *ibid.*, **198**, 1301 (1963).

The Determination of the Pressure Dependence of Transference Numbers

by Robert L. Kay, K. S. Pribadi, and B. Watson

Mellon Institute of Carnegie-Mellon University, Pittsburgh, Pennsylvania 15213 *(Received February 27, 1970)*

Recently, an electrical detection system for moving boundaries was described[1] that permits transference numbers to be measured precisely without the limitations imposed by the traditional optical system.[2] In this new system, the boundary is timed, as it passes probe electrodes sealed into the moving boundary tube, by the increase in the potential across adjacent probes as the boundary enters the volume between the probes. The method therefore makes use of the fact that the potential drop in the following solution behind a stable two-salt boundary must be different from that of the leading solution in front of the boundary. The potential change at each event can be detected by various electrometer circuits[1] and recorded.

The method is ideally suited to remote control operation and has been used with considerable success for high-temperature measurements.[3] In this paper we describe the adaptation of the method to measurements at high pressures.

Experimental Section

The adaptation of this method to pressure work has necessitated two substantial modifications in the conventional moving boundary apparatus. The cell was redesigned to reduce the dimensions to those imposed by the pressure vessel and the type of electrical connection to the cell and the detector itself was modified to overcome current leakage problems encountered at high pressures.

The essential features of the autogenic cell are shown in Figure 1. This type of cell was used since it imposes none of the difficulties involved in generating a boundary prior to pressurizing. A constant current is passed between the cadmium anode, situated at the bottom of the calibrated uranium glass tube (3.5-mm i.d.) containing the probe electrodes, and the Ag, AgCl cathode situated in the side arm. A flexible Teflon extension of the side arm provided a simple and effective method of transmitting pressure to the system without contaminating the electrolyte solution with the pressurizing oil. This design resulted in a cell that could fit into a 1.2-in. bore, thereby reducing the pressure vessel to one of manageable size and weight.

The electrical probes were grouped in two sets of three about 5 cm apart with a separation of 1 cm between individual probes. The cadmium anode was held firmly to a glass flange at the end of the calibrated tube by a Lucite clamp. A leak-proof seal was effected by a small rubber O-ring. The current range required for these measurements was supplied by a commerical 1500-V power supply wired for constant-current operation.[1]

(1) R. L. Kay, G. A. Vidulich, and A. Fratiello, *Chem. Instrum.*, **1**, 361 (1969).

(2) D. A. MacInnes and L. G. Longsworth, *Chem. Rev.*, **11**, 17 (1932).

(3) J. E. Smith, Jr., and E. B. Dismukes, *J. Phys. Chem.*, **67**, 1160 (1963).

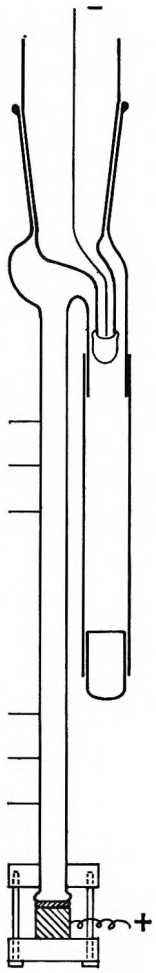

Figure 1. The high-pressure autogenic cell.

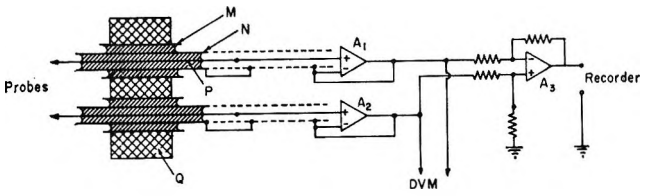

Figure 2. Schematic of the electrical system.

The main difficulty encountered in adapting the method to high-pressure work was that of connecting the probes to the electrometer through the high-pressure vessel so that a resistance to ground of greater than 10^{10} ohms was maintained, since a smaller resistance results in excessive electrode polarization at the probe electrodes owing to current leakage. The best available electrical connectors for high-pressure vessels have a resistance of about 10^8 ohms or two orders of magnitude too small. This problem was solved by using a driven-guard circuit as shown in Figure 2. The connections to the probes pass through the top of the pressure vessel Q by triaxial leads (1.5-mm o.d.) that consist of the concentric stainless steel sheaths M and N and a copper inner conductor P, the conductors being separated from each other by powdered MgO (Continental Sensing Inc.). The inner conductor is connected directly to the probes and to the inputs of FET operational amplifiers A_1 and A_2 (Burr-Brown 3038/25). These amplifiers have a gain of 1 and are used to drive the sheath N at the same voltage as the inner conductor P. Since both these leads are at the same potential, no current can flow between them and, consequently, effectively all leakage to ground from the inner conductor is eliminated. The outer sheath M is grounded and is soldered into the pressure vessel closure plug. The connections between the amplifiers and the various probe positions were made by means of small magnetic reed switches which permitted a continuously driven guard between the cell probes and the amplifier input terminals. The third amplifier A_3 in Figure 2 acts as a differential amplifier, the output from which can be recorded and the exact time of the boundary events noted. It is also possible to read the probe potentials directly across the amplifiers A_1 and A_2 with a digital voltmeter (input impedance about 10^8 ohms).

The cylindrical pressure vessel was machined from Type 17-4PH stainless steel with an O-ring closure and was pressurized from the side. It had an overall length of 18 in., with walls 0.65 in. and a working space of 1.2-in. diameter, 10-in. long. The pressurizing oil was Marcol 52 (Humble Oil). An air-driven pump was used to pressurize the vessel initially with the final adjustment being made by a hand generator. The exact pressure was read from a calibrated Heise gauge. Temperature control was maintained by keeping the pressure vessel in an oil bath regulated to 0.003°. It was necessary to allow the cell to stand for 1 hr after the initial pressurizing in order to permit the heat developed in this adiabatic process to dissipate.

Data reported here are restricted to a maximum pressure of 2 kbars although our pressure system can be carried to over 3 kbars. At higher pressures, the platinum probe electrodes developed small leaks and the method had to be abandoned.

Results

The volumes between the probe electrodes in the transference cell were obtained from six calibration runs at 1 atm assuming the value[4] of T^+(0.02 M aqueous KCl, 25°) = 0.4901.

The observed transference numbers for KCl in aqueous solutions of KCl at 0.02 M and 25° are given in the second column of Table I as a function of pressure. The values of T_P^+ in the third column result after a correction for the compressibility of glass[5] and of water.[6] At pressures above 1 kbar, the Tait

(4) L. G. Longsworth, *J. Amer. Chem. Soc.*, **54**, 2741 (1932).
(5) J. Adams, *ibid.*, **53**, 3769 (1931).

Table I: Observed and Corrected Cation Transference Numbers for 0.02 *M* Aqueous KCl

Pressure, bar	T_{obsd}^+	T_P^+
500	0.4757	0.4852 (4)
1000	0.4636	0.4811 (1)
1500	0.4548	0.4793 (5)
2000	0.4464	0.4770 (2)

equation as given by Owen[7] was used to obtain the density of water. At 0.02 *M* the difference between the compressibility of water and the solution can be neglected. Also, no volume or solvent conductance corrections were made since they both should be negligible.[4] Two runs were carried out at each pressure. Each number in parentheses in the last column of Table I gives the total difference in the 4th decimal place in T_P^+ obtained in the two runs. These results are compared to the only other data[8] with comparable precision in Figure 3.

Discussion

The results summarized in Figure 3 clearly confirm the previous measurements of Wall and Berkowitz[8] which extend only to 1 kbar, although our reproducibility appears to be much better. Wall and Berkowitz determined the boundary velocity be measuring the fractional change in the ac resistance with time between electrodes situated at the top and bottom of the cell, a method that required the current to be interrupted during the resistance measurements. They estimate the total error in their method to be 0.6%, whereas we claim at most 0.1%. The true accuracy of the data will best be decided when both transference and conductance data are available for two salts with a common ion.

The most significant difference in the two sets of data is the fact that T_P^+ does not show a continuous linear decrease with pressure as the previous results[8] indicated. Our data indicate that the change in T_P^+ levels off at higher pressures. It should be noted that T^+(KCl, aq) decreases both with increased pressure and increased temperature[3,9] and under both these circumstances the degree of hydrogen bonding in water is known to decrease. These high-pressure data confirm our previous conclusions[9] that the structural excess mobility of the potassium ion is greater than that for the chloride ion. Consequently, as the degree of hydrogen bonding or structure in the water decreases with increased temperature and pressure, the potassium ion becomes progressively slower with respect to the chloride ion.

Since water does not begin to act like other liquids until pressures above 2 kbars are reached, we wished to extend these transference measurements above this pressure limit of our present cells. For this purpose, we are designing a cell in which the moving boundary will be detected by impedance changes detected at metal film electrodes fused onto the outside of the glass walls.

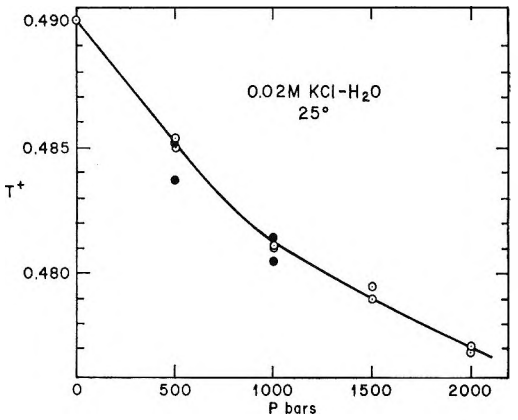

Figure 3. Cation transference numbers for 0.02 *M* KCl in aqueous solution at pressures up to 2 kbars: ○, this work; ●, ref 8.

Acknowledgments. We wish to acknowledge the considerable help of Dr. Harro Lentz with the design and construction of the pressure apparatus. The work was supported by Contract 14-01-0001-1729 with the Office of Saline Water, U. S. Department of the Interior.

(6) G. S. Kell and E. Whalley, *Phil. Trans. Roy. Soc. London, Ser. A*, **258**, 565 (1965).
(7) B. B. Owen, *J. Chem. Educ.*, **27**, 59 (1944).
(8) F. T. Wall and J. Berkowitz, *J. Phys. Chem.*, **62**, 87 (1958).
(9) R. L. Kay and G. A. Vidulich, *ibid.*, **74**, 2718 (1970).

Sodium Bicarbonate and Carbonate Ion Pairs and Their Relation to the Estimation of the First and Second Dissociation Constants of Carbonic Acid

by F. S. Nakayama

Soil and Water Conservation Research Division, Agricultural Research Service, U. S. Department of Agriculture, U. S. Water Conservation Laboratory, Phoenix, Arizona 85040
(Received January 23, 1970)

Recent reports[1] indicate that the forms $NaHCO_3^0$ and $NaCO_3^-$ are present in sodium carbonate solu-

(1) (a) A. Distèche and S. Distèche, *J. Electrochem. Soc.*, **114**, 330 (1967); (b) R. M. Garrels, M. E. Thompson, and R. Siever, *Amer. J. Sci.*, **259**, 24 (1961); (c) R. M. Garrels and M. E. Thompson, *ibid.*, **260**, 57 (1962); (d) J. N. Butler and R. Huston, Abstracts, 158th National Meeting of the American Chemical Society, Division of Water, Air, and Waste Chemistry, New York, N. Y., Sept 1969, p 113.

tions and, therefore, if these species are not accounted for, the computed dissociation constants of other carbonate species in such solutions may be in error. For example, Harned and coworkers[2] used the following relations to obtain the first [$K_{1A} = (H^+)(HCO_3^-)/(H_2CO_3)$] and second [$K_{2A} = (H^+)(CO_3^{2-})/(HCO_3^-)$] dissociation constants of carbonic acid in sodium bicarbonate and carbonate solutions

$$[-\log K_{1A}]_{\mu=0} = \frac{(E + E_c - E^0)F}{2.303RT} + \log \gamma_{CO_2} SP_{CO_2} + \log \frac{[Cl^-]}{[HCO_3^-]} + \log \frac{\gamma_H \gamma_{Cl}}{\gamma_H \gamma_{HCO_3}} \quad (1)$$

$$[-\log K_{2A}]_{\mu=0} = \frac{(E - E^0)F}{2.303RT} + \log \frac{[HCO_3^-][Cl^-]}{[CO_3^{2-}]} + \log \frac{\gamma_{HCO_3}\gamma_{Cl}}{\gamma_{CO_3}} \quad (2)$$

where E = emf of the cell, $E_c = (-RT/2F) \ln P_{H_2}$, E^0 = standard potential of reference electrode, R = gas constant, T = Kelvin temperature, F = Faraday, S = Henry's law constant, P = partial pressure, γ = activity coefficient, [ ] = concentration.

If $NaCO_3^0$ and $NaCO_3^-$ are indeed in solution, the ratios $[Cl^-]/[HCO_3^-]$ in eq 1 and $[HCO_3^-]/[CO_3^{2-}]$ in eq 2 are not necessarily equal to the stoichiometric ratio and instead related to one governed by the degree of association of Na^+ with HCO_3^- and CO_3^{2-}, and furthermore, extrapolation to zero ionic strength for getting the thermodynamic K's may not be adequate. This paper presents a method for estimating simultaneously the dissociation constants of $NaHCO_3^0$ [$K_{NaHCO_3^0} = (Na^+)(HCO_3^-)/(NaHCO_3^0)$], $NaCO_3^-$ [$K_{NaCO_3^-} = (Na^+)(CO_3^{2-})/(NaCO_3^-)$], H_2CO_3 and HCO_3^- without an *a priori* knowledge of any of these constants.

Dissociation Constants K_{1A} and $K_{NaHCO_3^0}$. The mass and charge balance relations for sodium and bicarbonate describing eq 1 which includes $NaHCO_3^0$ and $K_{NaHCO_3^0}$ are

$$[Na]_{total} = [Na^+] + \gamma_{Na}[Na^+]\gamma_{HCO_3}[HCO_3^-]/K_{NaHCO_3^0} \quad (3)$$

$$[HCO_3]_{total} = [HCO_3^-] + \gamma_{Na}[Na^+]\gamma_{HCO_3}[HCO_3^-]/K_{NaHCO_3^0} \quad (4)$$

$$[H^+] + [Na^+] = [Cl^-] + [HCO_3^-] \quad (5)$$

The OH^- and CO_3^{2-} forms are neglected since the pH of this system can be adjusted to levels where these are insignificant. The activity coefficients are derived from one form of the extended Debye–Hückel theory

$$-\log \gamma_i = Az_i^2\mu^{1/2}/(1 + Ba_i\mu^{1/2}) \quad (6)$$

where i is the specified ion, μ the ionic strength, z_i the valence, and A, B, and a_i are constants. Using computed H^+ activities for the different $NaHCO_3$–NaCl–CO_2 combinations, and by systematically selecting values for $K_{NaHCO_3^0}$ eq 3, 4, and 5 are solved simultaneously for the concentrations of the constituent parts and K_{1A} obtained from eq 1. When the proper value of $K_{NaHCO_3^0}$ is chosen, the computed K_{1A}'s should then be the same at the different ionic strength, sodium, and bicarbonate concentration combinations.

Dissociation Constants K_{2A} and $K_{NaCO_3^-}$. The mass and electroneutrality relations for this system are

$$[Na]_{total} = [Na^+] + \gamma_{Na}[Na^+]\gamma_{HCO_3}[HCO_3^-]/K_{NaHCO_3^0} + \gamma_{Na}[Na^+]\gamma_{CO_3}[CO_3^{2-}]/K_{NaCO_3^-}\gamma_{NaCO_3} \quad (7)$$

$$[carbonate]_{total} = [HCO_3^-] + [CO_3^{2-}] + \gamma_{Na}[Na^+]\gamma_{HCO_3}[HCO_3^-]/K_{NaHCO_3^0} + \gamma_{Na}[Na^+]\gamma_{CO_3}[CO_3^{2-}]/K_{NaCO_3^-}\gamma_{NaCO_3} \quad (8)$$

$$[Na^+] + [H^+] = [HCO_3^-] + 2[CO_3^{2-}] + [OH^-] + [NaCO_3^-] + [Cl^-] \quad (9)$$

Equation 2 is solved for K_{2A} in a manner similar to K_{1A} by making selections of $K_{NaCO_3^-}$ and using eq 7, 8, 9, and the previously computed $K_{NaHCO_3^0}$. If the same K_{2A}'s are obtained for a specified $K_{NaCO_3^-}$ value at the different Na^+, HCO_3^-, and CO_3^{2-} concentrations and ionic strength combinations, the supposition that the $NaHCO_3^0$ and $NaCO_3^-$ forms are present is essentially substantiated, and this K_{2A} is equivalent to a thermodynamic value derived without extrapolation to zero ionic strength.

Experimental Section

The excellent experimental electrometric data of Harned and coworkers[2] for the $NaHCO_3$–NaCl–CO_2 and $NaHCO_3$–NaCl–Na_2CO_3 mixtures with the H_2 | Ag || AgCl electrode system (E^0 = 0.22234 V) without liquid junction were used to test for the presence of $NaHCO_3^0$ and $NaCO_3^-$. pH's were computed for the Harned cell described by Bates[3] which is applicable to these experimental measurements. Henry's law constant relation, $S = 0.0344 - 0.00805\mu + 0.000192\mu^2$, for CO_2 solubility in NaCl solutions was computed from Harned and Davis'[2b] original data.

A digital computer was programmed to make systematic selections of $K_{NaHCO_3^0}$ and $K_{NaCO_3^-}$, to solve the simultaneous equations, and to test for the constancy of K_{1A} and K_{2A}. The $NaHCO_3^0$ and $NaCO_3^-$ forms were taken into account in the ionic strength computation. The activity coefficients for the undisso-

(2) (a) H. S. Harned and F. T. Bonner, *J. Amer. Chem. Soc.*, **67**, 1026 (1945); (b) H. S. Harned and R. Davis, Jr., *ibid.*, **65**, 2030 (1943); (c) H. S. Harned and S. R. Scholes, Jr., *ibid.*, **63**, 1706 (1941).

(3) R. G. Bates, "Electrometric pH Determination," Wiley, New York, N. Y., 1965, p 24.

ciated CO_2 and $NaHCO_3^0$ species were assumed to be unity and that for $NaCO_3^-$ equal to HCO_3^-. The constants for the Debye–Hückel relation were obtained from Kielland.[4]

Results and Discussion

An example of recomputed first dissociation constants of carbonic acid at 25° for the $NaHCO_3$–NaCl–CO_2 system is presented in Table I. The sample calculations show that the use of the "true" $[Cl^-]/[HCO_3^-]$ ratio instead of the stoichiometric ratio gives K_{1A}'s (column 4) that are independent of HCO_3^- concentration or ionic strength. In this example $K_{NaHCO_3^0} = 0.677$, and the inclusion of all applicable data of Harned and Davis[2b] resulted in $K_{NaHCO_3^0} = 0.690 \pm 0.096$ and $K_{1A} = (4.41 \pm 0.04) \times 10^{-7}$. This latter value substantiates the extrapolated K_{1A} of 4.45×10^{-7} obtained by Harned and Davis.[2b] A $K_{NaHCO_3^0}$ of 1.70 was reported by Garrels and Thompson,[1c] but a critical evaluation could not be made because their experimental data and technique were not available.

Table I: First Dissociation Constant of Carbonic Acid at 25° Computed on Basis of the Presence of $NaHCO_3^0$ Species at Different Bicarbonate Concentrations and Ionic Strengths in Equilibrium with 78.8% CO_2–21.2% H_2 Gas Mixture[a]

$[NaHCO_3] = [NaCl]$, $M \times 10^2$	E, V	$\mu \times 10^2$	$-\log K_{1A}$	$-\log K_S$[b]
0.2182	0.67236	0.436	6.356	6.354
0.3951	0.67271	0.787	6.364	6.360
0.7177	0.67243	1.424	6.361	6.355
2.859	0.67209	5.572	6.363	6.350
3.687	0.67192	7.144	6.362	6.347
10.391	0.67106	19.42	6.360	6.332

[a] $K_{NaHCO_3^0} = 0.677$; results in columns 3 and 4 based on raw data of columns 1 and 2 from Harned and Davis.[2b] [b] R. Davis Jr., Ph.D. Thesis, Yale University, New Haven, Conn., 1942.

Table II: Dissociation Constant of HCO_3^- at 25° Computed on Basis of the Presence of $NaHCO_3^0$ and $NaCO_3^-$ Species at Different Carbonate Concentrations and Ionic Strengths[a]

$[NaCl] = [Na_2CO_3]$, $M \times 10^2$	$[NaHCO_3]$, $M \times 10^2$	E, V	$\mu \times 10^1$	$-\log K_{2A}$
0.3940	0.3956	0.96680	0.1926	10.335
0.5606	0.5628	0.95746	0.2733	10.338
0.5821	0.5843	0.95647	0.2837	10.339
1.156	1.160	0.93700	0.5571	10.335
1.660	1.666	0.92693	0.7930	10.341
2.230	2.239	0.91302	1.056	10.250
2.620	2.630	0.91808	1.233	10.417
3.241	2.254	0.90620	1.514	10.321

[a] $K_{NaHCO_3^0} = 0.690$; $K_{NaCO_3^-} = 0.282$; computational results in columns 4 and 5 based on raw data of columns 1 to 3 from Harned and Scholes.[2c]

The computed K_{2A} values (column 5, Table II) were essentially independent of either ionic strength, Na or carbonate concentrations when a suitable value for $K_{NaCO_3^-}$ was used. The K_{2A} of $(4.65 \pm 0.48) \times 10^{-11}$ also compares favorably with the extrapolated K_{2A} of 4.69×10^{-11} reported by Harned and Scholes.[2c] The hydrolysis of CO_3^{2-} to form HCO_3^- and OH^- is automatically accounted for in this computational procedure (eq 9 and pH calculations), whereas Harned and Scholes[2c] and MacInnes and Belcher[5] had to treat it separately by resorting to additional extrapolations which sometimes were made from curvilinear portions of their graphs.

The dissociation constant $K_{NaCO_3^-} = 0.282$ is midway between those of 0.054 listed by Garrels, *et al.*,[1b] and 0.45 presented by Butler and Huston.[1d] Although significantly different K values are obtained in these three experiments, they strongly support the presence of sodium carbonate ion pairs, and more studies are needed to resolve the differences.

(4) J. Kielland, *J. Amer. Chem. Soc.*, **59**, 1675 (1937).
(5) D. A. MacInnes and D. Belcher, *ibid.*, **55**, 2630 (1933).

The Photoperoxidation of Unsaturated Organic Molecules. V. The Consequences of $O_2{}^1\Sigma_g{}^+$ Intervention

by B. E. Algar
Pilkington Brothers, Lancashire, England
and B. Stevens
University of South Florida, Tampa, Florida 33620

An analysis of the oxygen-concentration dependence of photoperoxidation quantum yields γ_{MO_2} in terms of an O_2 $^1\Delta_g$ reaction intermediate has shown[1] that this is generated solely by energy transfer from the sensitizer triplet state; this in turn is a product of both intersystem crossing from, and oxygen quenching of, the sensitizer singlet state. The overall quantum yield of peroxide formation may therefore be expressed as

$$\gamma_{MO_2} = \phi_T \phi_\Delta \phi_M \qquad (I)$$

where $\phi_M(M)$, the O_2 $^1\Delta_g$, substrate addition efficiency, depends on the reactivity and concentration of the substrate or acceptor M; $\phi_\Delta(O_2)$, the efficiency of O_2 $^1\Delta_g$ production from the sensitizer triplet state, is dependent on oxygen concentration when this is

(1) Part IV: B. Stevens and B. E. Algar, *J. Phys. Chem.*, **73**, 1711 (1969).

insufficient for effectively complete quenching of the triplet state; and

$$\phi_T(O_2) = \gamma_{IS} + (1 - F/F_0)(1 - \gamma_{IS})$$

is the overall yield of sensitiser triplet state from intersystem crossing (with efficiency γ_{IS}) and oxygen quenching of the sensitizer singlet state measured independently as the relative fluorescence yield F/F_0 of sensitiser at the prevailing oxygen concentration. Thus equation I may be arranged to

$$\gamma_{MO_2}F_0/F = \{\gamma_{IS} + F_0/F - 1\}\phi_\Delta\phi_M \qquad (II)$$

to obtain

$$\phi_\Delta\phi_M = d(\gamma_{MO_2}F_0/F)/d(F_0/F - 1) \qquad (III)$$

from the appropriate treatment of experimental quantities γ_{MO_2}, F_0, and F.

Of the possible triplet-state quenching processes

$$^3S^* + O_2\ ^3\Sigma_g^- \begin{cases} \longrightarrow {}^1S + O_2\ ^1\Delta_g & (1) \\ \longrightarrow {}^1S + O_2\ ^3\Sigma_g^- & (2) \\ \longrightarrow {}^1S + O_2\ ^1\Sigma_g^+ & (3) \end{cases}$$

1–3, the latter is endothermic if the sensitiser triplet state energy E_T is less than that of $O_2\ ^1\Sigma_g^+$ at 13,000 cm^{-1}; accordingly, at higher oxygen concentrations $\phi_\Delta(E_T < 13{,}000\ cm^{-1}) = k_1/(k_1 + k_2)$. On the other hand, Kearns and associates have presented theoretical arguments[2] and experimental evidence[3] in support of the preferred oxygen quenching process 3 when $E_T >$ 13,000 cm^{-1}. Subsequent relaxation[4] of $O_2\ ^1\Sigma_g^+$ to both $O_2\ ^1\Delta_g$ (at 8000 cm^{-1}) and $O_2\ ^3\Sigma_g^-$ (processes 4 and 5) should therefore reduce ϕ_Δ to ϕ_Δ ($E_T >$ 13,000

$$O_2\ ^1\Sigma_g^+ \begin{cases} \longrightarrow O_2\ ^1\Delta_g & (4) \\ \longrightarrow O_2\ ^3\Sigma_g^- & (5) \end{cases}$$

cm^{-1}) $= k_1/(k_1 + k_2 + k_3) + k_3k_1/(k_1 + k_2 + k_3)\cdot(k_4 + k_5)$ and introduce a dependence of ϕ_Δ (and of γ_{MO_2}) on the sensitizer triplet-state energy in the region of 13,000 cm^{-1}.

Values of $\phi_M\phi_\Delta$ (from eq III) are tabulated (Table I)[5-7] for sensitizers with triplet-state energies above and below that of $O_2\ ^1\Sigma_g^+$ in the presence of a common substrate at the same concentration in benzene at 25°. Since $\phi_M\phi_\Delta$, ϕ_M, and hence ϕ_Δ are independent of sensitizer it is concluded that with ϕ_Δ ($E_T <$ 13000 cm^{-1}) = ϕ_Δ ($E_T >$ 13000 cm^{-1}) either (a) $O_2\ ^1\Sigma_g^+$ is not an oxygen quenching product of these triplet states[8] ($k_3 \ll k_1 + k_2$) or (b) 1 and 3 are the dominant quenching processes ($k_3 \gg k_2 \ll k_1$) and $O_2\ ^1\Sigma_g^+$ relaxes quantitatively to $O_2\ ^1\Delta_g$ ($k_5 \ll k_4$).

Table I: Values of $\phi_M\phi_\Delta$ for Sensitized Photoperoxidation of 9,10-Dimethylanthracene (DMA) and 9,10-Dimethyl-1,2-benzanthracene (DMBA) in Benzene at 25° [a]

Sensitizer	E_T, cm^{-1}	Substrate M: DMA, 3.3×10^{-4} M	Substrate M: DMBA, 1.0×10^{-4} M
DMBA	15500[b]	...	0.11
DMA	~14700[c]	0.51	...
Anthanthrene	<13000[d]	0.52	0.12
Perylene	~12400[e]	0.52	0.12

[a] From equation III.[1] [b] See ref 5. [c] Value for anthracene.[7] [d] Assumed limit. [e] See ref 6.

Of these alternatives (b) is consistent both with the theoretical argument[2] that $k_3 > k_1 \gg k_2$ if $E_T >$ 13,000 cm^{-1} and with the kinetic conclusion[1] that $\phi_\Delta \simeq 1$ at higher oxygen concentrations. Foote and coworkers[9] have previously suggested that $O_2\ ^1\Sigma_g^+$ decays exclusively to $O_2\ ^1\Delta_g$ if formed on the grounds that the maximum quantum yield of peroxidation sensitized by rose bengale ($E_T \sim$ 16,000 cm^{-1}) is equal to γ_{IS} for this dye, indicating that no intermediate is lost. This argument is valid if the sensitizer triplet state is populated only by intersystem crossing ($\phi_T = \gamma_{IS}$) which is contrary to the observation that γ_{MO_2} (and hence ϕ_Δ) exceeds γ_{IS} for certain sensitizers (rubrene and 9,10-dimethylanthracene) which exhibit fluorescence quantum yields of virtually unity ($\gamma_{IS} \simeq 0$) and which must rely[1] on oxygen quenching of the singlet state for significant production of the triplet precursor of $O_2\ ^1\Delta_g$. For these sensitizers, the limiting peroxidation yield given by $\phi_T = (F_0 - F)/F_0$ varies with oxygen concentration.

(2) K. Kawaoka, A. U. Khan, and D. R. Kearns, *J. Chem. Phys.*, **46**, 1842 (1967); **47**, 1883 (1967).

(3) D. R. Kearns, R. A. Hollins, A. U. Khan, R. W. Chambers, and P. Radlick, *J. Amer. Chem. Soc.*, **89**, 5455, 5456 (1967).

(4) Quenching of $O_2\ ^1\Sigma_g^+$ by the substrate would lead to a nonlinear dependence of $\gamma_{MO_2}^{-1}$ on $[M]^{-1}$ contrary to observation.[1,9]

(5) M. Moodie and C. Reid, *J. Chem. Phys.*, **22**, 252 (1954).

(6) R. H. Clarke and R. M. Hochstrasser, *J. Mol. Spectrosc.*, **32**, 309 (1969).

(7) D. P. Craig and I. G. Ross, *J. Chem. Soc.* (London), 1589 (1954).

(8) The triplet states of DMA and DMBA lie in the "intermediate" region 37 > E_T < 50 kcal/mol defining[3] a transition from $k_1 > k_3$ to $k_1 < k_3$.

(9) R. Higgins, C. S. Foote, and H. Cheng, Advances in Chemistry Series, No. 73, American Chemical Society, Washington, D. C., 1968, p 102.

COMMUNICATIONS TO THE EDITOR

The Biradical Intermediate in the Addition of the Ground State Oxygen Atoms, O(^{3}P), to Olefins[1]

Sir: The main and probably the exclusive initial step in the reaction of the ground state oxygen atoms, O(^{3}P), with a number of simple olefins[2] is[2b,c] the addition of the oxygen atom to the olefinic double bond. Various features of these reactions have been investigated in considerable detail[2-5] and a general reaction mechanism has been formulated.[2b,c,g] The addition products formed are epoxides and carbonyl compounds. The molecular rearrangements (migration of an atom or a radical group) in the formation of carbonyl compounds have been explained[2c] in a consistent manner by postulating a triplet biradical intermediate as the initial adduct. However, in a recent study of the addition of O(^{3}P) atoms to condensed olefins at cryogenic temperatures (77 to 113°K) Scheer and Klein[6] observed the same addition products but were unable to reconcile their distribution with a biradical intermediate and proposed instead the following nonclassical "transition state" structures, formed from *cis*- and *trans*-2-butene, respectively

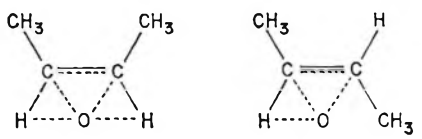

In these structures oxygen atom was assumed to be in the plane of the molecule, "interacting loosely" and "immobilizing" both vinylic H atoms in the *cis* (A) and only one in the *trans* structure (B). Migration of H was thus permitted in the *trans* structure, to give methyl ethyl ketone, but not in the *cis* structure, in which only CH_3 migrated, to give isobutanal. The ketone was actually a very important product of *cis*-2-butene and it had therefore to be assumed also that at temperatures as low as −196° rotation about the (only slightly perturbed) double bond occurred in the *cis* "transition state" to convert it to the *trans* "transition state" but was forbidden in the opposite direction.

In view of the great importance of the finer details of the mechanism of addition of O(^{3}P) atoms to olefins, it is imperative that the postulates of Scheer and Klein be subjected to close scrutiny. In the present communication it is shown that (1) they are entirely incompatible with the previous experimental observations and with several new experimental results now obtained, and (2) they are unnecessary since product distributions at cryogenic temperatures can be explained simply by conformational effects in the "triplet biradical" intermediates. Somewhat similar conformational effects have been observed in some types of Wagner–Meerwein rearrangements.[7]

The term "triplet biradical"[2] was not intended to convey the notion of two entirely independent free radicals. Spin conservation requires that the two are antibonding in the initial adduct but some overall electronic interaction is to be expected and perhaps a partial transfer of negative charge to the oxygen atom with acquisition of some zwitterion character.[2e] However, such interactions should not affect basically the following arguments, which are mainly based on the effects of nonbonded repulsions. With these qualifications, the term "triplet biradical" may be retained until detailed electronic and structural descriptions become available.[8] The biradical may therefore be portrayed as having a free radical associated with the oxygen atom, which is bonded to a tetragonal carbon, while the other planar alkyl free radical is centered on a trigonal carbon. The original double bond is now a single bond and rotation about it is possible but it requires an activation energy. Nonbonded repulsions between bulky alkyl substituents, when present, contribute substantially to the establishment of potential energy minima corresponding to the most stable conformations.

The conformers invoked here are restricted rotors and their structure is of course *not static*[9] since the internal motions are not frozen even at 77°K: the molecules do not by any means spend all their time in their most stable conformations. The explanation of the strongly stereoselective addition to *trans*-2-

(1) Issued as N.R.C. No. 11441.

(2) (a) R. J. Cvetanović, *J. Chem. Phys.*, **23**, 1375 (1955); (b) *ibid.*, **25**, 376 (1956); (c) *Can. J. Chem.*, **36**, 623 (1958); (d) *J. Chem. Phys.*, **30**, 19 (1959); (e) *Can. J. Chem.*, **38**, 1678 (1960); (f) *J. Chem. Phys.*, **33**, 1063 (1960); (g) *Advan. Photochem.*, **1**, 115 (1963).

(3) S. Sato and R. J. Cvetanović, *Can. J. Chem.*, **36**, 279 (1958); **36**, 970 (1958); **36**, 1668 (1958); **37**, 953 (1959).

(4) J. M. S. Jarvie and R. J. Cvetanović, *Can. J. Chem.*, **37**, 529 (1959).

(5) R. J. Cvetanović and L. C. Doyle, *ibid.*, **38**, 2187 (1960).

(6) (a) M. D. Scheer and R. Klein, *J. Phys. Chem.*, **73**, 597 (1969); (b) R. Klein and M. D. Scheer, *ibid.*, **73**, 1598 (1969).

(7) (a) P. I. Pollak and D. Y. Curtin, *J. Amer. Chem. Soc.*, **72**, 961 (1950); (b) C. K. Ingold, "Structure and Mechanism in Organic Chemistry," Cornell University Press, Ithaca, N. Y., 1953, pp 506–508; (c) "Steric Effects in Organic Chemistry," M. S. Newman, Ed., Wiley, New York, N. Y., 1956, pp 10, 270.

(8) Use of alternative names for this species is of questionable value at this time.

(9) M. D. Scheer and R. Klein, *J. Phys. Chem.* **74**, 2732 (1970).

butene at 77°K (predominant formation of *trans*-β-butene oxide and methyl ethyl ketone[6]) is simple. In the *trans* conformer of the intermediate, as shown by the Newman projection formula, the nonbonded interactions between CH_3 and H are relatively weak (*i.e.*, the potential energy minimum in the restricted

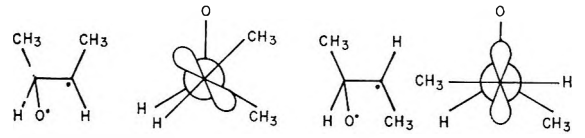

CIS-2-BUTENE ADDUCT TRANS-2-BUTENE ADDUCT

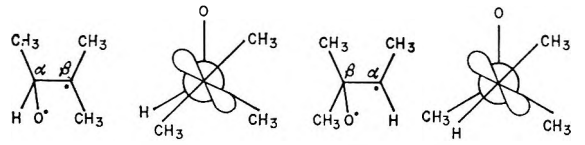

α and β 2-METHYL-2-BUTENE ADDUCTS

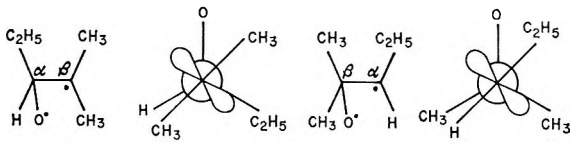

α and β 2-METHYL-2-PENTENE ADDUCTS

rotor is very broad) and the necessary geometrical alignments for H and CH_3 migration and for the ring closure can all be attained relatively easily. However, the inherently faster H migration and ring closure occur preferentially (to give the ketone and the *trans* epoxide) and are also much faster at this low temperature than rotation into the less stable *cis* conformer. As the temperature is raised to 300°K, on the other hand, the slower processes (CH_3 migration and rotation into the *cis* conformer) are accelerated relatively more than the faster processes and the reaction therefore becomes much less selective.[2c] (The "pressure independent fragmentation"[2] also becomes more important.)

In the case of *cis*-2-butene, the Newman projection formula shows that, because of repulsion between the bulky CH_3 groups, the orientation of the p orbital of the free alkyl radical favors CH_3 migration. As a result, this inherently slower process and the equally slow rotation to the *trans* conformer are able to compete with the inherently much faster H migration and ring closure. All the four addition products (*cis* and *trans* epoxide, methyl ethyl ketone, and isobutanal) are therefore important even at 77°K.[6] At 300°K all the processes are accelerated and product distribution is affected only little.[2]

With 2-methyl-2-butene two adducts are possible, α and β, as indicated, and CH_3 migration is sterically favored in both. Predominant addition at the less substituted α position[2c] explains predominant formation of pivalaldehyde at 90°K.[6a] At 298°K, on the other hand, the yield of methyl isopropyl ketone (27%) actually exceeds that of pivalaldehyde (17%).[10] The products from 2-methyl-2-pentene at 90°K[6b] can be explained in similar manner. In the α adduct C_2H_5 migration is sterically favored but it is inherently slow and therefore the less favorable H migration occurs also to some extent. In the β adduct CH_3 migration is sterically favored and, although slow, can compete with the ring closure.

Conformational effects evidently provide simple and logical explanation of product distribution both at room temperature and at cryogenic temperatures. It is therefore not necessary to invoke the "transition states" postulated by Scheer and Klein. Their postulate has also other serious shortcomings. It implies a concerted addition which however is inconsistent with the very fast reaction rates in a spin forbidden process (requiring in some cases only a few collisions). Moreover, the physical nature of the "loose interactions" of oxygen atoms with H atoms and with the double bond, completely immobilizing the H atoms in some cases and only partially in others and at the same time permitting rotation around a CC double bond at cryogenic temperatures, is difficult to understand. However, the most serious difficulty arises with the tetrasubstituted ethylenes, for example tetramethylethylene. In this molecule the four bulky methyl groups preclude a "transition state" of the type postulated by Scheer and Klein, yet its reaction with $O(^3P)$ atoms at 25°, 100 times faster than that of ethylene, is in fact the fastest reaction of $O(^3P)$ atoms studied so far, occurring at approximately each collision. Furthermore, the rates of oxygen atom addition to olefins[2d,g] show a continuous increase with the number of alkyl substituents on the double bond with little dependence on what the substituents are. All these results are entirely incompatible with Scheer and Klein's "transition states" with oxygen atoms in the plane of the olefin molecule, which, moreover, for uncertain reasons has to be exclusively on the side where vinylic H atoms are (*e.g.* in *cis*-2-butene).

Scheer and Klein assume that no H migration can occur *via* their "transition" state A for *cis*-2-butene because the two vinylic H atoms are "immobilized" and that methyl ethyl ketone is formed only when A isomerizes into B by rotation about the CC double bond. Such an "isomerization" is evidently impossible in cycloolefins and the mechanism of Scheer and Klein dictates therefore that, for example, cyclopentanone should not be a product of addition of $O(^3P)$ atoms to cyclopentene. This is in complete contradiction with our experimental results[11] (Table I).

Formation of cyclopentanone as an important product shows that Scheer and Klein's mechanism is untenable both at room temperature and at 77°K. It

(10) R. J. Cvetanović and L. C. Doyle, unpublished results.

Table I

Temp, °K	Addition products, % Cyclopentene oxide	Cyclopentanone	Cyclobutanecarboxaldehyde	PIF/total reaction
298	54	24	22	0.26
77	62	32	6	<0.01

is, however, readily explainable by simple conformational effects in the intermediate biradical, which favor H migration and epoxide ring closure.

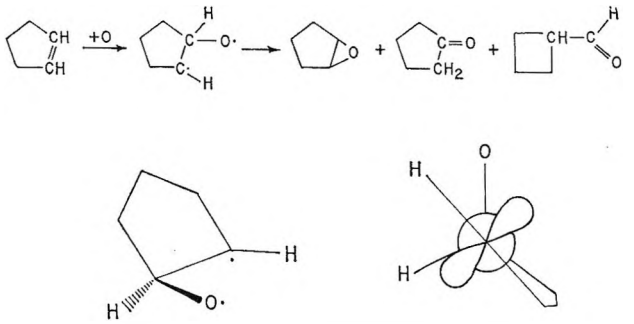

The greater part of the cyclobutanecarboxaldehyde formation (ring contraction) is probably preceded by ring opening, as is the pressure independent fragmentation, PIF, *i.e.*, the molecular split into C_2H_4 and $CH_2{=}CH{\cdot}CHO$. It must also be pointed out that cyclohexene (studied only at 298°K[2c]) gives large yields of cyclohexanone, and Scheer and Klein report in the following communication[9] that cycloheptene gives 28% cycloheptanone at 77°K. Evidently, the notion of an "immobilization" of vinylic H atoms by "loose interaction" with oxygen atoms in the "transition state" must be abandoned.

The assertion in the following communication[9] that increased stereospecificity[12] of O atom addition at low temperatures to straight chain internal olefins as the molecule increases from C_4 to C_8 is difficult to reconcile with a biradical intermediate is not correct. As explained above, stereospecificity is simply a reflection of slow rotation in the biradical relative to other competing processes (ring closure, atom and group migrations) and it will, in general, tend to be greater the slower the rotation. It is not surprising to find slower rotation when the substituents are larger, especially so at very low temperatures. With this in mind, it is obvious that the explanations given above for *trans*- and *cis*-2-butene are also applicable to other internal straight-chain olefins.[12]

(11) The author is grateful to Mr. L. C. Doyle for assistance with these experiments. The reaction products have been analyzed mainly on a 300-ft β,β'-thiodipropionitrile capillary column at 25°, with hydrogen flame detector and helium as the carrier gas. Some confirming analyses were done on packed and capillary dinonylphthalate columns. Experiments at 300°K have been done using the standard N_2O technique[2-6] and those at 77°K using the cryogenic technique.[6]

(12) R. Klein and M. Scheer, *J. Phys. Chem.*, **74**, 613 (1970).

DIVISION OF CHEMISTRY
NATIONAL RESEARCH COUNCIL OF CANADA
OTTAWA, CANADA
R. J. CVETANOVIĆ

RECEIVED SEPTEMBER 3, 1969

The Addition of O(^{3}P) to Olefins. The Nature of the Intermediate

Sir: The "triplet biradical" postulated by Cvetanović[1] as the intermediate in the O(^{3}P) addition to olefins requires a number of *ad hoc* conformational restrictions in order to account for the low-temperature results of Klein and Scheer.[2] For the O-atom adducts of *cis*-2-butane, 2-methyl-2-butene, and 2-methyl-2-pentene, these restrictions are presumed to be due to a repulsion between alkyl groups bonded to the two olefinic carbon atoms. Such a repulsion would geometrically favor the migration of one of the alkyl groups to the unpaired p orbital, resulting in a disproportionately high yield of the appropriate carbonyl compound. This *static* conformational effect is difficult to understand since rotation about the newly formed carbon–carbon single bond must also occur in order to account for the observed product yields. For the *trans*-2-butene adduct, on the other hand, rotation cannot be allowed at low temperatures since only epoxide ring closure and H-atom migration occur under these conditions.

It was inconsistencies such as this, arising out of attempts to reconcile a biradical intermediate with the product yields observed at low temperatures, that led Klein and Scheer to adopt an alternate model for the intermediate state.[2] It was assumed that the O-atom adduct retained the planarity of the original olefin and allowed for a loose (O---H) interaction between the oxygen and those H atoms bonded to the same side of the olefinic carbon atoms. Rotation was assumed to be possible in all cases and H-atom migration, when unrestricted, was presumed to be faster than that of an alkyl group. For the *cis*- and *trans*-2-butenes, two intermediates were assumed, namely

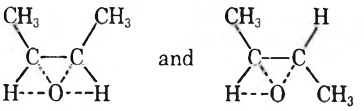

with interconversion between the two forms made possible by rotation through 180°. At low temperatures the stability of the *trans* relative to the *cis* configuration provided the rationale for the product

(1) R. J. Cvetanović, *Advan. Photochem.*, **1**, 115 (1963).

(2) M. D. Scheer and R. Klein, *J. Phys. Chem.*, **73**, 597 (1969).

ratios. In the case of 2-methyl-2-butene the intermediate was written as

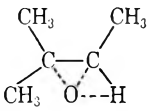

so that the relatively large yields of epoxide and aldehyde at 90°K are readily understood. The reaction of 2-methyl-2-pentene provided further evidence[3] that where the (O---H) interaction is possible, H migration is inhibited relative to that of the alkyl group.

Further, it was shown recently[4] that the stereospecificity of O-atom addition at low temperatures, first noted in the case of *trans*-2-butene at 90°K, increases significantly as the straight-chain, internal olefin increases in size from C_4 to C_8. The *cis* as well as the *trans* compounds exhibit this effect and can be readily understood when it is recognized that the rate of rotation is inversely related to the moment of inertia, and hence, the mass and size of the rotating group. It is difficult, on the other hand, to reconcile these observations with a biradical intermediate despite the conformational effects proposed by Cvetanović. For example, it would be necessary to assume that the migration rate of the most favorably oriented alkyl group in the *cis*-olefin biradical adduct increase with increasing size and mass.

In the previous note Cvetanović reports the fractional product yields obtained at 298 and 77°K for the reaction of $O(^3P)$ and cyclopentene. Besides epoxide formation and H atom migration yielding cyclopentanone, only ring rupture of the *c*-C_5 adduct followed by ring closure to a *c*-C_4 aldehyde is possible. The latter is analogous to alkyl migration in the straight-chain adducts but is severely limited by having to surmount a larger energy barrier. Such a process can hardly be expected to compete with the migration of the H atoms despite the loose interaction with oxygen postulated in the Klein–Scheer structure for the intermediate. This is particularly so in the case of cyclopentene where the product *c*-C_4 has more inherent ring strain than does the *c*-C_5 adduct. As a matter of fact, the formation at 77°K of even as much as 6% of the product yield as cyclobutylmethanol is a rather surprising result. This suggests an investigation of the reaction of $O(^3P)$ with a *c*-C_7 olefin. In this case the product aldehyde would be a *c*-C_6 with far less ring strain than the *c*-C_7 adduct. Table I gives the fractional product yields obtained for this reaction at 77°K. As expected, the relative yield of the *c*-C_6 aldehyde is greater than that of the *c*-C_4 aldehyde in the cyclopentane reaction reported by Cvetanović. This effect is probably assisted by the (O---H) interaction postulated to occur in the intermediate.

Table I: Fractional Product Yields for the Reaction of $O(^3P)$ and Cycloheptane at 77°K

Epoxycycloheptane	Cycloheptanone	Cyclohexylmethanal
0.58	0.28	0.14

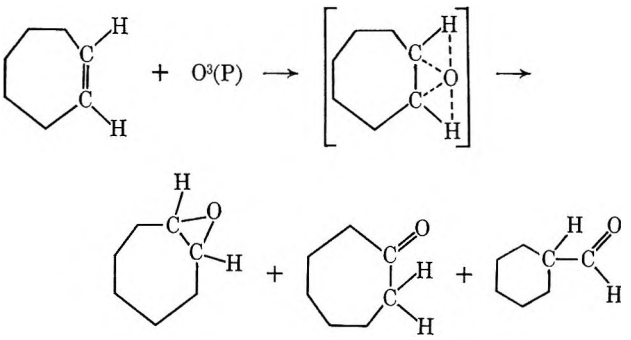

It would therefore appear that the currently available evidence, particularly that obtained at low temperatures, tends to support the Klein–Scheer planar intermediate for the reaction of ground-state O atoms with olefins. This structure subsequently undergoes a set of concerted rearrangements[4] in which a given group migration and oxygen atom localization occurs simultaneously to produce the final reaction products. Since electron spin is *not* conserved in the total reaction, the argument that a "triplet biradical" must first be formed before rearranging to singlet products is not compelling. The path by which the intermediate for this process rearranges to form the final products probably involves both energy and steric effects whose details have yet to be entirely elucidated. The spin relaxation process may ultimately prove to be only a minor barrier to the successful completion of these complex intramolecular rearrangements.

(3) R. Klein and M. D. Scheer, *J. Phys. Chem.*, **73**, 1598 (1969).
(4) R. Klein and M. D. Scheer, *ibid.*, **74**, 613 (1970).

PHYSICAL CHEMISTRY DIVISION
NATIONAL BUREAU OF STANDARDS
WASHINGTON, D. C. 20234

MILTON D. SCHEER
RALPH KLEIN

RECEIVED FEBRUARY 6, 1970

Nonexcitonic Energy Transfer in Crystalline Charge-Transfer Complexes[1]

Sir: The efficient long-range transfer of excitation energy in molecular crystals has been a well-known phenomenon ever since Bowen[2] showed that the emission of crystalline anthracene containing small amounts

(1) This work was supported by the National Research Council of Canada.

(2) E. J. Bowen, *Nature*, **142**, 1081 (1938); *J. Chem. Phys.*, **13**, 306 (1945).

of tetracene consists exclusively of tetracene fluorescence. According to the exciton theory,[3] a packet of excitation can hop from one lattice position to another, visiting many thousands of lattice sites during its lifetime. In a mixed crystal containing a "guest" molecule whose emitting state is below that of the "host" crystal lattice, the excitons produced initially by excitation of the host are trapped at the guest sites, resulting in selective emission from guest molecules. Exciton transfer is generally considered to be the mechanism of sensitized fluorescence in molecular crystals and similarly ordered aggregates.

We have found an apparent exception to this behavior in mixed crystals of a more complicated type, wherein two kinds of charge-transfer complexes are incorporated into a single crystal lattice. In a hydrocarbon–trinitrobenzene (TNB) mixed-donor[4] complex, some of the hydrocarbon lattice positions are occupied by guest hydrocarbon molecules of another species. Such a system, exemplified by phenanthrene–TNB containing small amounts of anthracene–TNB, is formally equivalent to a mixed crystal of the two charge-transfer complexes and furnishes a useful means of studying excitation transfer between two different charge-transfer states, in this case, from phenanthrene–TNB to anthracene–TNB.

The fluorescence of pure phenanthrene–TNB is most efficiently excited at 430 nm, and extends over a broad region between 15,000 and 21,000 cm^{-1} at room temperature. If 1% of the phenanthrene molecules in the lattice are replaced by anthracene, most of the emitted light still consists of host charge-transfer fluorescence. Only at guest-complex concentrations of 10 mol % and above is the crystal fluorescence exclusively that of anthracene–TNB.

Host and guest CT fluorescence intensities are about equal at 4 mol % anthracene–TNB concentration; this corresponds to a mean separation of approximately 170 Å between neighboring guest complexes along the linear donor–acceptor stacks of the crystal. This distance is of the order of the distances usually associated with dipole–dipole resonance transfer,[5] suggesting that this process may account for most of the sensitized fluorescence that is observed here.

This behavior is in striking contrast to that of other crystalline systems such as tetracene-in-anthracene, where the similar transition between host and guest emission occurs over a guest concentration range of 10^{-4} to 10^{-2} mol %.[6] These results show that exciton migration is not an efficient energy transfer process in crystalline charge-transfer complexes.

This conclusion lends support to the view[7] that excitation of a crystalline charge-transfer complex results in the formation of "localized excitons" whose migration is limited by the molecular reorientation that must accompany the excited center as it travels through the crystal.

(3) For a brief and literate review, see the article by M. W. Windsor in D. Fox, M. W. Labes, and A. Weissberger, "Physics and Chemistry of the Organic Solid State," Vol. II, Interscience, New York, N. Y., 1965.

(4) S. K. Lower, *Mol. Cryst., Liq. Cryst.*, **5**, 363 (1969).

(5) Th. Förster, "Floreszenz Organischer Verbindungen," Göttingen, Vandenhoeck, and Ruprecht, 1951, Chapter 13.

(6) F. R. Lipsett and A. J. Dekker, *Can. J. Phys.*, **30**, 165 (1952); J. Ferguson, *Aust. J. Chem.*, **9**, 160 (1956).

(7) R. M. Hochstrasser, S. K. Lower, and C. Reid, *J. Chem. Phys.*, **41**, 1073 (1964).

DEPARTMENT OF CHEMISTRY
SIMON FRASER UNIVERSITY
BURNABY 2, B. C., CANADA

STEPHEN K. LOWER

RECEIVED FEBRUARY 4, 1970

Effect of pH on the Ultrasonic Absorption of Aqueous Solutions of Proteins

Sir: Recently, Kessler and Dunn[1] reported results of ultrasonic investigation on aqueous solutions of bovine serum albumin (BSA). They attributed the observed changes of absorption at pH below 4.3 and above 10, respectively, to conformal changes and expansion of the protein molecule. This note is to report new data, taken on BSA, β-lactoglobulin (βL), and lysozyme at pH ranging from 1 to 13.3, which suggest that proton transfer reactions contribute significantly to the absorption of dilute protein solutions at pH <4.5 and at pH >10.

Figure 1 shows that in the acid pH region the frequency-free absorption α/N^2 (α is the absorption coefficient and N the ultrasonic frequency) goes through a maximum for a value pH_M of the pH. Several facts seem to indicate that the absorption maxima cannot be explained by conformal change or dissociation of the protein in subunits. (1) Such reactions are characterized by pH's which depend upon the nature of the protein[2] while Figure 1 shows that within the accuracy of the experiments pH_M is independent of the nature of the protein. (2) Unlike BSA and βL, lysozyme does not exhibit any conformal change[2] or dissociation[3] for protein concentration c_p below 0.01 g/cm^3, as used in this work and for $2 < pH < 4.5$, that is, precisely the pH region in which curve 3 relative to lysozyme shows a maximum similar to the ones observed for βL and BSA. (3) The absorption of lysozyme solutions is practically constant in the pH range 4.5–8.5 in which dimerization[3] and conformal change[4] are known to

(1) L. Kessler and F. Dunn, *J. Phys. Chem.*, **73**, 4256 (1969).

(2) C. Tanford, *Advan. Protein Chem.*, **17**, 69 (1962).

(3) A. Sophianopoulos and K. Van Holde, *J. Biol. Chem.*, **239**, 2516 (1964).

(4) J. Owen, E. Eyring, and D. Cole, *J. Phys. Chem.*, **73**, 3918 (1969).

occur; the same remark holds for βL.[5,6] (4) If a conformal change were responsible for the absorption maxima, α/N^2 would vary linearly with c_p in the whole pH range;[7] we did observe that α/N^2 increases linearly with c_p but only for pH's outside the range in which the maxima occur, while in this pH region the curve $\alpha/N^2 = f(c_p)$ shows a curvature toward the c_p axis. (5) An absorption maximum is also found at lower pH for diglycine (curve 4) and acetyl glycine.

A more likely explanation for the absorption maxima of Figure 1 is the protonation reaction of protein side-chain carboxyl groups: $-CO_2^- + H^+ \rightleftarrows -CO_2H$. It has been shown that the excess absorption associated with such reaction tends toward a limiting value at high CO_2H concentrations[8] and goes through a maximum[9] for a value of the pH given by $pH_M = {}^1/_2(pK_a - \log c)$, where c is the CO_2H concentration. This expression indicates that pH_M should shift toward lower values when $c = nc_p/M_w$; that is, c_p is increased (M_w is the molecular weight of the protein and n its number of CO_2H groups). For BSA a small decrease of pH_M of about 0.2 pH unit was observed when c_p was increased by a factor 4. For diglycine, the above expression of pH_M yields a value 2.10 which agrees well with the experimental value 2.25 (Figure 1, curve 4). For BSA and βL the values 2.85 and 3.3, respectively, were calculated for pH_M using for pK_a the values of the intrinsic pK[2] and for n the number of titrable CO_2H groups.[2] These calculated values of pH_M depend mostly on the choice of the pK_a values.

Figure 1 shows that for proteins the α/N^2 value at pH 6 is different from that at pH 1.1. On the other hand, the width of the absorption maximum on curve 4 suggests that the absorption due to proton transfers is probably negligible at pH 6 and 1.1. Therefore when the pH is changed the contributions of the other mechanisms causing the absorption at pH 6 and 1.1 must also be modified. Possible mechanisms which may be involved are: solvation equilibria,[10] conformal changes[1] and keto–enol equilibria,[11] that is, processes of the type A ⇌ B with contributions to the absorption varying linearly with c_p.[7] Our results show that when c_p is increased, the absorption due to these processes becomes larger than the one due to proton transfer reactions. For the high BSA concentrations used by others[1] the absorption maximum may eventually have become hidden in the variation of the absorption due to the other processes with pH.

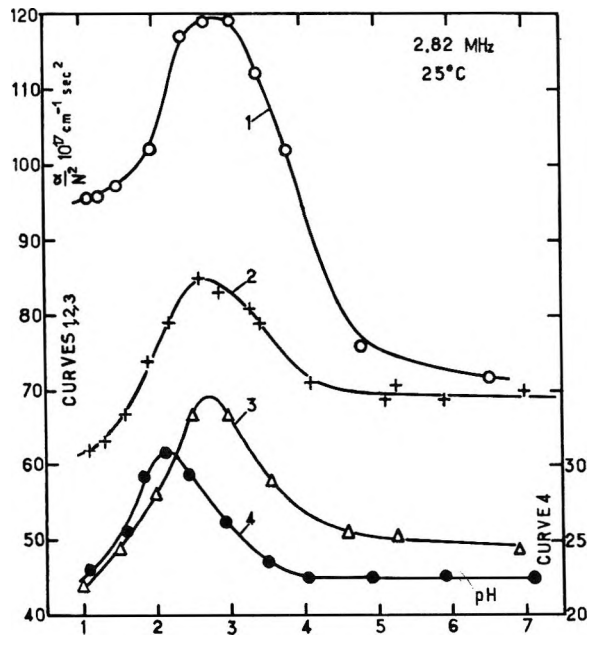

Figure 1. pH dependence of the ultrasonic absorption of solutions of proteins in H_2O–0.2 M NaCl; curve I, BSA, c_P = 0.0116 g/cm³; curve 2, βL, c_P = 0.0107 g/cm³; curve 3, lysozyme, c_P = 0.0104 g/cm³; curve 4, diglycine, c = 0.012 g/cm³. The right-side ordinate scale is relative to curve 4.

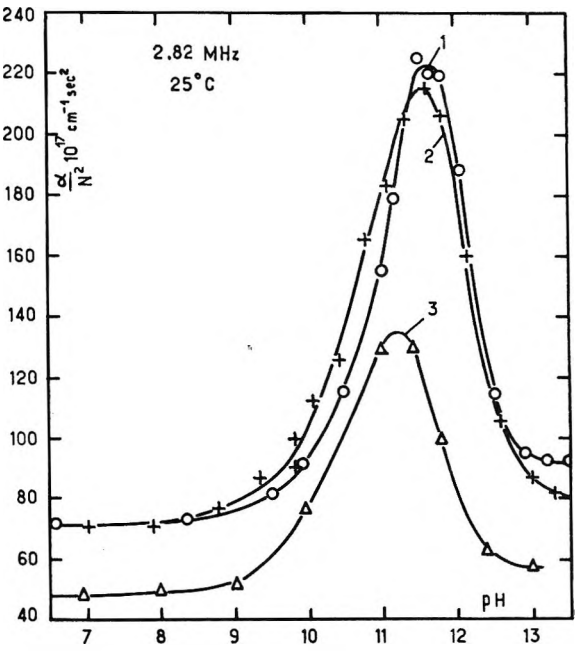

Figure 2. pH dependence of the ultrasonic absorption of solutions of proteins in H_2O–0.2 M NaCl: curve I, BSA, c_P = 0.0116 g/cm³; curve 2, β L, c_P = 0.0107 g/cm³; curve 3, lysozyme, c_P = 0.0104 g/cm³.

Figure 2 is relative to the three proteins in the alkaline pH region. It appears that the absorption maximum for BSA was not observed by Kessler, *et al.*,[1] because

(5) S. Timasheff, L. Mescanti, J. Basch, and R. Townend, *J. Biol. Chem.*, 241, 2496 (1966); C. Tanford and R. Taggart, *J. Amer. Chem. Soc.*, 83, 1634 (1961).

(6) T. Herskovits, R. Townend, and S. Timasheff, *ibid.*, 86, 4445 (1964).

(7) G. Schwarz, *J. Mol. Biol.*, 11, 64 (1965).

(8) B. Michels and R. Zana, *J. Chim. Phys. Physicochim. Biol.*, 72, 240 (1969).

(9) K. Applegate, L. Slutsky, and C. Parker, *J. Amer. Chem. Soc.*, 90, 6909 (1968).

(10) J. Burke, G. Hammes, and T. Lewis, *J. Chem. Phys.*, 42, 3520 (1965).

(11) A. Mayer and H. Vogel, *Z. Naturforsch. B*, 20, 85 (1965).

their measurements were not performed at pH >11.2. All the facts which were given above to explain our results in the acid pH region may be used to demonstrate that the absorption maxima on Figure 2 are due to proton-transfer reactions on protein side-chain amino groups: $-NH_3^+ + OH^- \rightleftharpoons -NH_2 + H_2O$. From our results on BSA, over the frequency range 1–150 MHz, we found that the standard volume change associated with this reaction is between 18.5 and 46.5 cm³/mol, according to the pK_a value used in the calculations. Applegate, *et al.*,[9] have obtained volume changes of 26 and 36 cm³/mol for diglycine and triglycine, respectively.

These preliminary results show that ultrasonic studies of the kinetics of conformal changes in protein solutions are made difficult by the existence of an absorption due to proton-transfer reactions which becomes significant precisely in the pH regions in which occur conformal changes and dissociation of proteins in subunits.

C.N.R.S. CENTRE DE RECHERCHES SUR LES MACROMOLECULES
STRASBOURG, FRANCE

RAOUL ZANA
JACQUES LANG

RECEIVED FEBRUARY 23, 1970

Further Remarks on the Ultrasonic Properties of Bovine Serum Albumin Solutions

Sir: Zana and Lang[1] have shown that the contribution of ultrasonic absorption in aqueous solutions of bovine serum albumin (BSA) resulting from proton transfer reactions in amino acids may be significant, particularly in the regions of the ultrasonic absorption peaks. Our recent findings[2] also have defined the absorption peak near pH 12. Unfortunately, there are insufficient data at this time to compare adequately the frequency dependence of the absorption peaks in BSA with those in the amino acids.[3]

Although there seems to be substantial agreement between some of our present conclusions and those of Zana and Lang, we wish to point out several unresolved difficulties in specifying the principal ultrasonic interaction mechanism in aqueous BSA solutions as proton transfer reactions. Comparison of the absorption peak in Figure 1 curve 1 of Zana and Lang[1] to those in Figures 2 to 4 of our paper,[4] which are at much higher BSA concentrations, shows a shift in the value of pH_M of approximately 0.8 pH unit in a direction opposite to that predicted by their equation, $pH_M = \frac{1}{2}(pK_a - \log c)$. Furthermore, over the concentration range 0.04 g/cm³ to 0.09 g/cm³ we did not observe a significant shift of pH_M, within the limit of our ability of measure pH, *viz.*, ±0.05 pH unit. That a process more complex than proton transfer is necessary to describe all of our data is indicated by the minimum in the normalized velocity of sound near pH 4.1 and displaced from pH_M, as shown in Figure 5 of our paper. This is not necessarily accounted for by chemical relaxation. The strong correlation of the velocity of sound minimum with the step increase in $[\eta]$, also at pH 4.1[5] and corresponding to the intermediate N–F′ transformation[6] suggests that perhaps ultrasonic velocity measurements may be less susceptible to masking by additional chemical relaxation processes than the absorption coefficient, and thus ultrasonic velocity may be a more reliable indicator of conformal change in the present case. It has been shown, for example, that a dip in the velocity of sound and a change in the viscosity can occur in the region of phase transition in certain liquid crystalline systems,[7] and the dependence of velocity and pH may be analogous for a solution in which a configurational equilibrium is perturbed by the sound wave.[8] Finally, some mechanism other than proton transfer is necessary to explain the change in absorption level from neutral pH to pH <1, *i.e.*, aside from the intervening peaking of the absorption. A similar remark pertains to the alkaline pH region.

(1) R. Zana and J. Lang, *J. Phys. Chem.*, **74**, 2734 (1970).
(2) L. W. Kessler and F. Dunn, unpublished data.
(3) K. Applegate, L. J. Slutsky, and R. C. Parker, *J. Amer. Chem. Soc.*, **90**, 6909 (1968).
(4) L. W. Kessler and F. Dunn, *J. Phys. Chem.*, **73**, 4256 (1969).
(5) C. Tanford, J. G. Buzzel, D. G. Rands, and S. A. Swanson, *J. Amer. Chem. Soc.*, **77**, 6421 (1955).
(6) J. F. Foster, "Plasma Proteins," F. W. Putnam, Ed., Academic Press, New York, N. Y., 1960, Chapter 6.
(7) J. F. Dyro and P. D. Edmonds, "Molecular Crystals and Liquid Crystals," Vol. 8, Gordon Breach, London, 1969, pp 141–156.
(8) P. D. Edmonds, private communication.

BIOACOUSTICS RESEARCH LABORATORY
UNIVERSITY OF ILLINOIS
URBANA, ILLINOIS 61801

F. DUNN

RESEARCH DEPARTMENT
ZENITH RADIO CORPORATION
CHICAGO, ILLINOIS 60639

L. W. KESSLER

RECEIVED MARCH 16, 1970